August 2017

Wireless Information and Power Transfer in Communication Networks: Performance Analysis and Optimal Resource Allocation

Tewodros Aklilu Zewde
Syracuse University

Abstract

Energy harvesting is considered as a prominent solution to supply the energy demand for low-power consuming devices and sensor nodes. This approach relinquishes the requirements of wired connections and regular battery replacements. This thesis analyzes the performance of energy harvesting communication networks under various operation protocols and multiple access schemes. Furthermore, since the radio frequency signal has energy, in addition to conveying information, it is also possible to power energy harvesting component while establishing data connectivity with information-decoding component. This leads to the concept of simultaneous wireless information and power transfer. The central goal of this thesis is to conduct a performance analysis in terms of throughput and energy efficiency, and determine optimal resource allocation strategies for wireless information and power transfer.

In the first part of the thesis, simultaneous transfer of information and power through wireless links to energy harvesting and information decoding components is studied considering finite alphabet inputs. The concept of non-uniform probability distribution is introduced for an arbitrary input, and mathematical formulations that relate probability distribution to the required harvested energy level are provided. In addition, impact of statistical quality of service (QoS) constraints on the overall performance is studied, and power control algorithms are provided.

Next, power allocation strategies that maximize the system energy efficiency subject to peak power constraints are determined for fading multiple access channels. The impact of channel characteristics, circuit power consumption and peak power level on the node selection, i.e., activation of user equipments, and the corresponding optimal transmit power level are addressed. Initially, wireless information transfer only is considered and subsequently wireless power transfer is taken into account. Assuming energy harvesting components, two scenarios are addressed based on the receiver architecture, i.e, having separated antenna or

common antenna for the information decoding and energy harvesting components. In both cases, optimal SWIPT power control policies are identified, and impact of the required harvested energy is analyzed.

The second line of research in this thesis focuses on wireless-powered communication devices that operate based on harvest-then-transmit protocol. Optimal time allocation for the downlink and uplink operation interval are identified formulating throughput maximization and energy-efficiency maximization problems. In addition, the performance gain among various types of downlink-uplink operation protocols is analyzed taking into account statistical QoS constraints.

Furthermore, the performance analysis of energy harvesting user equipments is extended to full-duplex wireless information and power transfer as well as cellular networks. In full-duplex operation, optimal power control policies are identified, and the significance of introducing non-zero mean component on the information-bearing signal is analyzed. Meanwhile, SINR coverage probabilities, average throughput and energy efficiency are explicitly characterized for wireless-powered cellular networks, and the impact of downlink SWIPT and uplink mmWave schemes are addressed.

In the final part of the thesis, energy efficiency is considered as the performance metric, and time allocation strategies that maximize energy efficiency for wireless powered communication networks with non-orthogonal multiple access scheme are determined. Low complex algorithms are proposed based on Dinkelbach's method. In addition, the impact of statistical QoS constraints imposed as limitations on the buffer violation probabilities is addressed.

WIRELESS INFORMATION AND POWER TRANSFER IN COMMUNICATION NETWORKS: PERFORMANCE ANALYSIS AND OPTIMAL RESOURCE ALLOCATION

By

Tewodros Aklilu Zewde

B.Sc., Bahir Dar University, Bahir Dar, Ethiopia, 2004

M.Sc., Addis Ababa University, Addis Ababa, Ethiopia, 2009

DISSERTATION

Submitted in partial fulfillment of the requirements for the degree of

Doctor of Philosophy in Electrical and Computer Engineering

Syracuse University

August 2017

Acknowledgment

Praise to the Almghty for His unspeakable mercy and blessings. Thanks to Theotokos, St. Virgin Mary, the bearer of our God.

Foremost, I would like to express my sincere gratitude to my advisor, Prof. Mustafa Cenk Gursoy, for his dedicated and sustained guidance, and I am eternally grateful for having such a humble, smart, and knowledgable advisor during my doctoral study. His patience, commitment, challenging questions, and critical comments were very helpful in all my research pieces. I am truly fortunate to work under his supervision.

Besides my advisor, I would like to thank the rest of my Ph.D. thesis committee: Prof. Senem Velipasalar, Prof. Jun (Brandon) Choi, Prof. Yingbin Liang, and Prof. Tomislav Bujanovic, for their time, for carefully reading my dissertation, and for their insightful comments. My sincere thanks also goes to Prof. Dawit Negussey, the chair of my dissertation committee, for his commitment reading my dissertation and his fatherly support as of my Ph.D. application at Syracuse University. Related to this, I would like to thank Dr. Elleni Kinfe, Dr. Kathleen Joyce, assistant dean, and Prof. Chilukuri K. Mohan, department chair, for their support and guidance during the admission process.

I thank my fellow labmates in Wireless Communication and Networking Lab. Dr. Gozde, Dr. Yi, Mustafa, Esma, Chuang, and Sheren, for the motivating discussions, and peaceful working environment. I learn a lot from the weekly meetings that we have with our advisor Prof. Mustafa Cenk Gursoy.

The moral support from the Syracuse Ethiopian community, and the prayers from G-Denagle St. Arsema and St. K-Semra Ethiopian Orthodox Tewahedo Church has been valuable inputs to successfully complet my Ph.D. study. Furthermore, I am blessed to have the support and prayers from my spiritual brothers and sisters in Mahibere Kidusan, more specifically NY subcenter. Also, I would like to recognize the prayers of my father-in-law, Wondimu Wuhib, and mother-in-law, Wosene Lenjiso, and their support by taking care of the family while I was compiling my dissertation.

Also, I would like to thank my family members: My mother Felekech Asegu, who taught me letters and numbers on a board she made by painting a black paint on a brocken bed frame, and my father Aklilu Zewde, who tirelessly challenged me with maths games whenever he was at home, played a major role for my academic success. Their life is a big lesson in many other ways, thank you mom and dad. I am always proud to be your son, I love you more than words can express. A special thanks goes to my uncle, Asnake Asegu, whose support and unconditional love during difficult times worth more than anything valuable. I am also grateful for the love and support of my brother, Biniyam A. Zewde, and my sister, Rahel A. Zewde; you are still the favorite ones!

Last but not least, this dissertation would not have been possible without the bright and cheerful smiles of my kids, Zemariam and Arsema; they have been my sunshine in the many long Syracuse winters. Also, the unconditional love and support from my strong, courageous, passionate, and kind wife, Dr. Frehiwot (BBYE) was my strength and inspiration to complete my study. With God's blessings, your enthusiasm, determination, positive attitude have been pillars of our strength and helped us to pass all the challenges of raising two kids and handling our social and spiritual responsibilities while attending our doctoral program at Syracuse University. As our son Zemariam said to you, I love you to Pluto and back to the Sun!

Table of Contents

List of Figures

List of Algorithms

Chapter 1

Introduction

1.1 Wireless Information and Power Transfer

With billions of low-power consuming devices, such as wireless sensors, connected to the internet within the frame work of Internet-of-Things (IoT), there is significant growth in the energy demand as well as data traffic. Hence, much attention has been given to effective utilization of available energy resources in the network while accomplishing reliable information exchange between the transmitter and receiver with certain quality of service guarantees. Inspiring scientific ideas have been providing promising solutions and approaches to the problem of ever increasing demand for scarce resources such as energy and bandwidth. These solutions help to reduce operating costs and the impact on the environment. In recent years, harvesting energy from the information-bearing signal has been proposed as one viable strategy. Theoretically, in wireless power transfer, energy can be harvested from either ambient radio-frequency (RF) electromagnetic signals or dedicated energy beamforming sources. Energy harvesting from RF signal is considered as a promising solution to power up low-power consuming devices such as sensors implanted in the human body to monitor certain activities [1]-[4], or those placed inside a physical structure, e.g. bridges [5], to continuously measure control parameters.

Advances in the technology lead to smaller devices with much better computational and communication capabilities. In such scenarios, using wired connection to supply energy from an external source may be infeasible if the number of devices is large as in sensor networks, or using built-in batteries could be challenging as these have limited-life span and replacing them becomes a rather difficult and very tedious procedure. This promotes energy harvesting before establishing data communication, and in the literature, the phenomenon is known as harvest-then-transmit protocol. It is mainly applicable to wireless-powered communication networks (WPCN) consisting of multiple nodes or remote user equipments (UEs) that harvest energy from abundant RF signals present in the surrounding environment or sent from dedicated wireless power sources. The latter method guarantees reliability of power supply, and it can be more efficient via energy-beamforming. Furthermore, the number of antennas as well as the spatial arrangement of wireless power source and information receiver can have an effect on the operation protocol, i.e., half-duplex mode or full-duplex mode, for wireless information and power transfer in WPCN. In half-duplex mode, uplink information transfer and downlink energy harvesting operations occur over non-overlapping time intervals, whereas in the full-duplex mode these operation can be carried out concurrently.

As mentioned above, energy harvesting enables the transfer of power to a wireless-powered device through a wireless link. On the other hand, conveying information on the signal that targets energizing the receiving end leads to simultaneous wireless information and power transfer (SWIPT). This enables the joint transfer of data as well as power to a destination where information-decoding (ID) component and energy-harvesting (EH) components are equipped with common or separated antenna architecture. In the first case, both ID and EH components employ a common antenna to collect the transmitted signals, whereas in the second case, both components have independent antenna architecture and hence EH component harvest energy opportunistically from the transmitted signal intended to the ID component. In the literature, there has been significant interest in exploring the feasibility, efficiency, and implementation of SWIPT strategies (see e.g., [6]−[10]).

1.2 Literature Overview

1.2.1 Power Allocation Strategies for Simultaneous Wireless Information and Power Transfer

Optimal resource allocation policies designed to benefit information transfer or to utilize available energy resources efficiently do not guarantee the same performance when energy transfer is incorporated along with the information-bearing signal. In principle, SWIPT requires modeling components and allocating resources at the transmitting and receiving ends taking into account of the additional constraint in SWIPT, i.e., harvested energy constraint. The authors in [11] designed a receiver architecture that employs SWIPT, but due to practical hardware limitations for co-located ID and EH components with common antenna setup, power splitting scheme was proposed to share the received signal power between these components proportionally and perform information decoding and energy harvesting tasks, concurrently [12]. Meanwhile, reconfigurable dual-antenna model was proposed in [13] to support uplink wireless information transfer (WIT) and downlink SWIPT at the user end operating in a broadband system. Related works are presented in references [14], and [15] considering multiple antennas at the transmitting and receiving ends. Furthermore, distributed antenna systems for SWIPT were introduced in [16], and power management strategy that maximizes information transfer was determined in the presence of stochastically distributed energy receivers while satisfying energy constraint. The authors in [17] considered a wireless network with nodes that can decode information and harvest energy simultaneously by applying the power splitting scheme. A similar setup but with multiple sources communicating with the destination through an energy-harvesting relay node is addressed in [18] and [19]. In these studies, the relay operates in half duplex mode in which it applies power splitting to the received signal during the first phase, and then forwards the decoded information to the destination in the second phase. Meanwhile, the authors in [20] considered sub-carrier partitioning for ID and EH components based on orthogonal

frequency division multiplexing (OFDM) instead of applying the power-splitting scheme. There are also several studies on the application of SWIPT in point-to-point communication systems and also in multiple-user model [12]−[21]. In addition, interesting observations can be found in various regards such as in cognitive-radio networks (CRN) and cooperative relay networks (see e.g., [22]−[26]).

In the above mentioned and related studies in the literature, optimization strategies and rate-energy tradeoffs are identified for time-switching and power-splitting schemes considering ideal Gaussian-distributed input signals. However, practical signals are generally selected from finite constellations, and hence it is appealing to study the performance of SWIPT with finite-alphabet input signals. Furthermore, it is important to study mutual information expression for SWIPT, and explore the significance of non-uniform input distributions to improve the rate-energy tradeoff characteristics.

On the other hand, in addition to having finite alphabet inputs, various nodes in wireless communication networks experience different channel characteristics due to path loss and small-scale multi-path fading. Hence, different nodes do not necessarily utilize available resources, e.g. operating intervals and transmit power, in the same way, and in such cases, allocating the resources optimally with the goal of maximizing the network throughput is an important and critical issue. More specifically, for delay-sensitive UEs, statistical queuing (or equivalently quality of service (QoS)) constraints such as limitations on buffer violation probabilities have significant impact on the throughput that is supported by each user, and this throughput is quantified by effective capacity (see e.g. [27]−[33] for comprehensive overview). Initially, the authors in [27] analyzed effective bandwidths of the time-varying departure processes. In [28], the maximum constant arrival rate that can be supported by a given service process under QoS constraints was investigated, whereas in [29], optimal power control policies that maximize the effective capacity were derived. Meanwhile, analysis of effective capacity for dual-hop network was conducted in [30]. More recently, the authors in [31] provided detailed characterizations of the statistical QoS-based throughput

and energy efficiency for various source models. Additional studies are conducted in [32] and [33] considering multiple-access fading channels and energy efficiency, respectively. These works provided interesting observations and insightful results focusing on the number of bits successfully transmitted over the wireless link. However, further investigation becomes necessary to comply with the design goals of future advanced green communication networks in which energy transfer along with information-bearing signals has gained more attention as a promising solution for low-power consuming devices.

1.2.2 Energy Efficiency in Fading Multiple Access Channels

In wireless networks, multiple access is a transmission scenario in which multiple nodes or user equipments (UE) transfer information uplink to an access point. There are various types of multiple access schemes including, e.g., time-division multiple access (TDMA), frequency-division multiple access (FDMA), and code-division multiple access (CDMA). In wireless channels, mobile UEs experience multipath fading and operate under different resource constraints, and hence in the above mentioned multiple access schemes, determining optimal resource allocation policies that maximize the system performance is required. With this motivation, fading multiple access channels have been extensively studied, generally considering throughput as the performance metric, and numerous publications in the literature provide concrete theoretical framework (see e.g., [33] – [39]).

Generally, throughput maximization in multiple access channels (MACs) encourages UEs to utilize their resources fully, i.e., transmit at the peak power level. However, due to increasing energy consumption and cost in communication systems, efficient utilization of available energy resources to transfer each bit of information is an important and a compelling performance indicator [34]. In particular, in energy-constrained wireless networks, energy-efficient operation leads to longer battery life and recharging cycle. In addition, this further enables the activation of more service nodes or UEs, and reduces the indirect impact on the environment due to carbon emission and related issues when considered at large. Despite these

motivating facts, as noted in [35], there were only limited works on the energy efficiency (EE) of MACs with respect to various multiple access methods, and in this work, the authors compared the impact of TDMA and spatial-division multiple access (SDMA) schemes on circuit power consumption and energy efficiency as well. They proposed energy aware algorithms that select either of these schemes to allocate time slots to multiple users on each sub-band. The tradeoff between EE and spectral efficiency (SE) for Gaussian MAC was investigated in [36] without circuit power consumption. Meanwhile, circuit power consumption was considered in [37], and the impact of transmission bandwidth and throughput were taken into account to model total circuit power consumption. In principle, EE and SE are conflicting performance metrics, i.e., one benefits at the cost of the other. Like spectral efficiency, quality-of-service (QoS) constraints also have significant impact on the EE of MAC as discussed in [38] in which the authors formulated energy minimization problem that determines optimal departure curves for each user given their arrivals characteristics. Related work was presented in [39] considering packet dropping as a QoS parameter.

All these studies provide interesting observations and new insights. However, only limited attention has been given to energy-efficient resource allocation in multi-user scenarios in which UEs communicate with a receiver through a MAC. However, this issue has gained more importance in the design of next-generation 5G wireless networks where energy efficient uplink/downlink operation (especially in small cells) is one of the primary goals [40] [41].

On the other hand, based on the fact that information-bearing signal also conveys energy, the feasibility and implementation of SWIPT have been intensively studied considering network throughput as a performance metric. However, energy-efficient resource allocation is another performance metric as noted earlier, and several recent studies have addressed this key parameter in the presence of wireless power and information transfer. The authors in [42] studied energy efficiency (EE) of multiple users that operate employing OFDMA under the assumption that each user has co-located ID and EH circuitries. In this work, harvested energy from a dedicated information-bearing signal and other nearby unknown interference

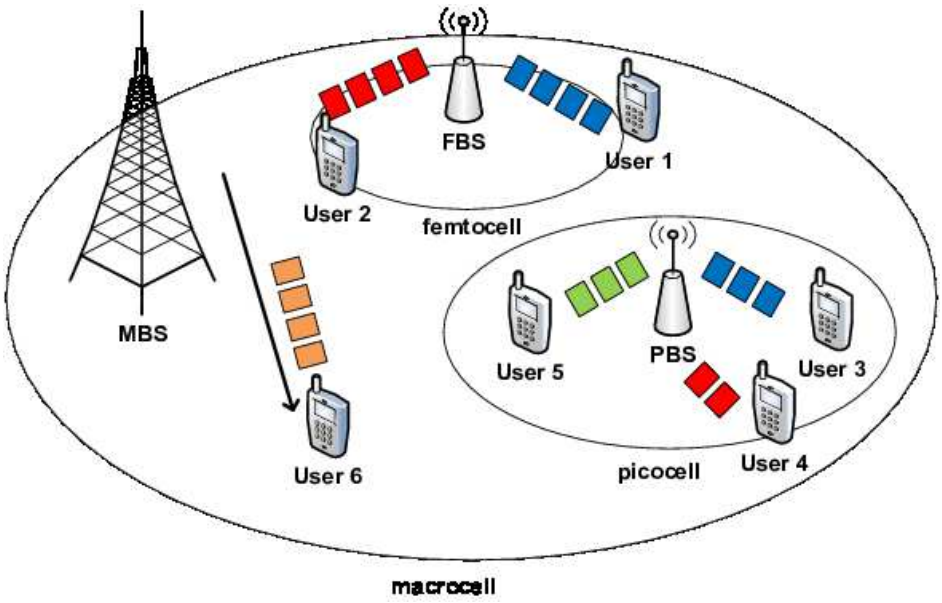

Figure 1.1: 5G wireless networks

was deducted from the consumption when evaluating the total number of bits successfully transferred per net consumed energy. A related work with similar EE definition was presented in reference [43] considering multiple-input single-output (MISO) models. Meanwhile, the conventional EE definition, i.e., achievable data rate per total consumed energy, was applied in [44] while studying energy-efficient OFDMA systems with non-overlapping uplink and downlink operation intervals. Unlike these approaches, the potential capacity produced by the transferred energy was added to the system capacity in reference [45] assuming that the harvested energy primarily contributes to future information transfer. In all these definitions, EE metrics measure successfully transferred bits of information per consumed energy. On the other hand, the authors in [46] introduced a new approach to evaluate the EE of SWIPT systems. They considered the EE of information transfer and EE of energy transfer separately, where the latter is defined as the amount of energy transferred per total consumption. As can be noted from these studies, incorporating SWIPT in wireless networks has direct impact on energy-efficient power control policies, but, as to the best of our knowledge, this has not been sufficiently addressed in MAC so far.

1.2.3 Throughput- and Energy-Efficient Transmission Strategies for Wireless Powered Communication Networks

As noted earlier, energy harvesting is a promising solution to the future energy-efficient WPCNs. It enables one to remotely energize low-power consuming devices that might not have an embedded power source or may be equipped with limited-size rechargeable batteries. In either case, wireless power transfer guarantees continuous power supply, and avoids disruption due to the need of battery replacement or recharging [47]. In fact, this newly emerging technique can be applied to a wide range of applications, but it has a direct impact on optimal resource allocation strategies among the network nodes, and the design of UEs [48]. Hence, the feasibility and implementation of WPCN have been intensively studied in recent years. (see e.g., [49] - [55]). The authors in [49] proposed harvest-then-transmit protocol in which an access point (AP) broadcasts wireless power to users that later transfer information to the AP through uplink channels. In this work, the downlink energy harvesting and uplink data transfer operations were assumed to take place over non-overlapping time intervals. In addition, each user transmitted an information-bearing signal based on TDMA scheme. The authors illustrated that sum-rate capacity maximization benefited nearby users, i.e., optimal solution encouraged to allocate more time for these users. A similar protocol was applied in [50] to operate remote devices considering a three-node system that consists of a single user with spatially separated wireless power source and information receiver. In this paper, average symbol error rate was introduced as a constraint while formulating an optimization problem to determine optimal time allocation strategy that maximize throughput. Related works were presented in [51] and [52] focusing on large-scale wireless-powered communication networks, and considering multiple antennas at the power station, respectively. A point-to-point WPCN with multiple antennas at the hybrid AP was presented in [53] taking into account delay-limited and delay-tolerant scenarios. In this work, energy beamforming was carried out using maximum ratio transmission. Meanwhile, multiple-user models having multiple antennas at the energy broadcasting and information decoding base

station (BS) were presented in [54] and [55] with the above-mentioned protocol.

In these references, downlink energy broadcast and uplink information transfer operations are carried out in half-duplex operation mode, i.e., over orthogonal time intervals. In fact, deploying multiple antennas at the AP/BS provides the opportunity to carry out these operations in full-duplex mode, i.e., base station or an access point broadcasts wireless power to energize the nearby users while decoding the information transmitted uplink by these or other users. Despite the possibility of having strong self-interference at AP/BS, recent studies demonstrate the feasibility of this approach in various settings. More specifically, the authors in [56] assumed that each user harvested energy until the beginning of its data transmission, and all the harvested energy was utilized during each symbol interval. Meanwhile, in [57] users were allowed to harvest downlink broadcast power except during their corresponding uplink information transfer interval. In such a case, any extra harvested energy which is not utilized for data transmission will be stored in the battery for the next block duration. Self-energy recycling in two-hop network with full-duplex operation was discussed in [58] under the assumption that the energy-constrained relay harvested energy while sending information. In this work, the authors considered MISO model, and proposed a two-phase AF protocol in which full-duplex operation occurs in the second phase.

All these WPCN studies provide detailed analysis and interesting results considering Shannon capacity formulation and outage capacity definition as measurement metrics for throughput. However, in practice, statistical queuing constraints have significant impact on the arrival rate that is supported by each user, and optimal resource allocation for WPCN under QoS constraints have not been addressed, to the best of our knowledge. On the other hand, designing resource allocation strategies which target energy efficiency of a WPCNs is necessary in these days. Recently, the authors in [59] investigated energy-efficient time allocation and power control strategy for WPCN considering a model that users harvest energy simultaneously and then transmit information uplink based on time-division protocol. However, it is possible for users to continuously harvest until scheduled for transmission

so long as WPS and AP are using independent antennas. Besides, users can also scavenge energy from an information-bearing signal transmitted by a user scheduled earlier for uplink data transfer, and this surely affects the energy-efficient time allocation for the operation intervals. Furthermore, considering the case in which energy harvesting UEs transmit information uplink through a multiple access channel, instead of time-division manner, could lead to better energy efficiency. Thus, it is much more interesting and relevant to study the energy efficiency of WPCNs considering various downlink-uplink operation protocols.

1.2.4 Performance Analysis of Energy Harvesting Cellular Networks

One of the main challenges in data gathering from randomly deployed sensor networks or user equipments is the need to have continuous energy supply, and energy harvesting can be one efficient solution, specially for low-power consuming devices. As mentioned earlier, this encourages wireless information and power transfer, and there are several publications in the literature which address the issue in cellular networks. The authors in [60] applied the concept of stochastic geometry, and provided analytical characterization and optimization of cellular mobile devices that are capable of harvesting energy and decoding information simultaneously. Related work was presented in [61] considering MIMO cellular networks. The authors in [62] modeled randomly located base stations of SWIPT-enabled cellular networks applying stochastic geometry, and they investigated the fundamental trade-offs using joint complementary cumulative distribution function (CCDF) of average rate and harvested energy. A related work was presented in [63] focusing on several diversity schemes for SWIPT-enabled cellular networks. It is shown that receiver diversity have the ability to improve both data rate and amount of harvested energy, simultaneously. Meanwhile, downlink SWIPT with power splitting at the receiving end and an uplink WIT using the downlink harvested energy was studied in [64] for heterogeneous cellular networks with K-tiers. In the paper, the authors considered both nearest base station cell association and

maximum received power cell association scenarios, and they evaluated the system performance considering outage probability and ergodic rate as performance metrics. Similarly, in reference [65], k-tier heterogeneous cellular network was considered with uplink information transfer, but the downlink was dedicated to power the mobile terminals, instead of SWIPT. The authors in [66] studied relay-based WPCNs where the relay node supports not only the uplink information transfer but also the downlink energy broadcasting. In this paper, iterative algorithms were proposed to determine optimal time and power allocation strategies. Related works are presented in [67] and [68] considering energy harvesting in K-Tier cellular networks.

When it comes to powering energy-limited cellular UEs, obtaining an energy-efficient resource allocation strategy is almost necessary and is a core point of research. In [69], energy-efficient beamforming was studied for heterogeneous cellular networks that have ID and EH users in the femto-cell co-channel overlaid with a macro-cell. The authors formulated optimization problems that maximize the information transmission efficiency of ID users and energy harvesting efficiency of EH users while satisfying QoS of all users. The authors in [70] have focused on energy efficiency, and addressed mmWave for relay-assisted cellular networks with non-cooperative mobile users and cooperative mobile users. Furthermore, analysis of bidirectional antenna for SWIPT in cellular networks were given in [71]. Yet, despite these works, the impact of allocating optimal downlink/uplink operating intervals on the system energy efficiency (EE) in the presence of randomly deployed wireless-powered UEs has not been investigated. In addition, using stochastic geometry as tools, it is necessary to investigate the influence of circuit power consumption as well as downlink transmit power level on the optimal operation intervals, and their impact on the overall system energy-efficiency.

Another key issue in cellular network the need to accommodate densely populated UEs with higher data rate, and in future green communication networks operating at higher frequencies, i.e., 28-30GHz, a.k.a. millimeter wave (mmWave) frequencies suggested as a prominent solution. Several studies in the literature have modeled the channel character-

istics for mmWave communications, and then investigated the performance gains. In [72], the authors modeled mmWave in cellular networks, and provided details focusing on coverage and rate analysis. They derived analytical expressions for the SINR coverage probabilities, and analyzed dense networks using an equivalent ball model. Related works were presented in [73]-[75]. Meanwhile, application of mmWave to wireless information and transfer was very recently studied in the literature. Specifically, the authors in [76] investigated the performance of harvesting energy from the signal transmitted in mmWave frequency bands, and derived closed-form expressions for energy coverage probability, and average harvested power. In addition, they formulated joint energy-information coverage probability for a wireless-powered network. A related work was presented in [77] considering harvest-then-transmit protocol in mmWave, i.e., downlink energy harvesting and uplink information transfer are carried out in mmWave frequency bands. They derived explicit expressions for the average harvested energy and average achievable uplink information transmission rate. Similarly, the authors in [78] analyzed joint CCDF of information rate and harvested power in mmWave cellular networks applying maximum ratio transmission and maximum ratio combining at the receiver and transmitter terminals, respectively. Despite these works, impact of operating time interval in mmWave wireless-powered cellular networks has not been investigated, to the best of our knowledge. For such models, hybrid approach, i.e., broadcasting an energy signal at lower microwave frequencies, instead of downlink mmWave, and then uplink information transfer in mmWave band, can provide better performance. This is because mmWave is sensitive to blockage and energy harvesting focuses only on the received power level. Moreover, energy efficiency analysis in energy harvesting cellular networks with mmWave uplink information transfer is a key issue to address, and it is important to analyze the impact of various parameters, such as operating intervals and circuit power consumption, as well.

1.2.5 Non-Orthogonal Multiple Access in WPCNs

The feasibility of wireless power transfer guarantees implementation of wireless-powered communications applying harvest-then-transmit protocol, and each node can transfer information uplink to the receiving end using time/frequency-division multiplexed transmission schemes, or in general orthogonal multiple access scheme, as mentioned in all the above and related studies. However, non-orthogonal multiple access (NOMA) has recently attracted much interest from both academia and industry as one of the prominent solutions for future 5G wireless networks as it enhances spectral efficiency. As discussed in the literature, NOMA is categorized into power-domain and code-domain NOMA based on how users' data multiplexing is achieved [79], and it can be applied to both downlink and uplink operations. In principle, power-domain NOMA utilizes superposition coding (SC) at the transmitter and successive interference cancellation (SIC) at the receiver, and this allows multiple users to transmit information on the same sub-carrier channel simultaneously. The decoding order for SIC depends on the channel characteristics of the wireless link between each transmitter-receiver pair, i.e., the main idea is that information transmitted to the receiver with the strongest wireless link is decoded without interference. In [80], the authors provided the basics of power-domain NOMA scheme and discussed possible solutions to address the challenges that could be experienced while applying this technique. Similarly, the authors in [81] focused on power-domain NOMA with downlink operation, i.e., SC at the transmitter and SIC at the receivers. Another related work was presented in [82] considering both power and channel allocation in a downlink cellular system. Meanwhile, the authors in [83] introduced and explicitly formulated the concept of power division multiple access (PDMA), and they proposed orthogonal PDMA protocol based on bit-orthogonality principle. In addition, they compared the energy efficiency of the proposed approach with conventional time/frequency division multiple access techniques. In fact, most of the above mentioned studies analyzed the throughput to characterize and compare the performances obtained using different approaches. However, in the presence of limited power resources, efficient utilization of the

available energy to transfer each bit of information is also necessary. Hence, several studies in the literature considered energy efficiency as a compelling performance metric to design optimal resource allocation strategies for future wireless networks [84]. More specifically, the authors in [85] considered heterogeneous radio access networks, and characterized the system energy efficiency in a setting in which the cloud center transferred information downlink to different types of base stations using NOMA scheme. In this work, it is argued that system energy efficiency under NOMA depends on the number of base stations in each type, and a heuristic algorithm is proposed to sequentially determine the optimal number of base stations for each type. Energy efficient resource allocation for downlink NOMA system were also presented in [86]. The authors in [87] proposed a low-complexity suboptimal algorithm for sub-channel assignment and power allocation. A related work was presented in [88] considering fading MIMO channels.

Meanwhile, several studies have addressed the issue in regard to WPCN. In [89], uplink NOMA is introduced for wireless powered communications where uplink and downlink operations are carried out over non-overlapping intervals, and the authors formulated optimization problems which maximize the throughput. The authors in [90] studied the joint design of time allocation, downlink energy beamforming and receiver beamforming in wireless powered communication networks employing uplink NOMA. In this work, the formulated optimization problem focused on obtaining a solution that maximizes the sum rate capacity, but because of the non-convexity of the problem, an iterative algorithm was proposed. Similarly, joint optimization of base station transmit power and operating intervals for uplink NOMA in WPCNs was considered in [91]. Yet, despite these works, the impact of NOMA on the system energy efficiency (EE) in the presence of wireless-powered users has not been investigated, to the best of our knowledge.

1.3 Main Contributions

We summarize the main contributions of the thesis below:

- In Chapter 3, we consider a point-to-point communication system in which a source transmits a SWIPT signal selected from finite alphabets. The receiver has ID and EH components, and power-splitting scheme is applied to carry out these operations concurrently. In order to improve the rate-energy tradeoff characteristics, we have introduced a novel approach that assigns probabilities non-uniformly to different signals in the constellation based on their energy level. According to the relationship between signal probabilities and energy consumption, these signal probabilities can be adjusted using two techniques, namely static slope characteristics and dynamic slope characteristics, given the minimum harvested energy constraint. Intuitively, advantage of one approach over the other depends on the improvement of the power-splitting factor when high energy input signals become more likely to be transmitted. In order to determine the optimal solution, we formulate an optimization problem and develop an algorithm taking into account the key parameters, e.g., splitting factor and signal probabilities.

- In addition, in Chapter 3, we consider a SWIPT model in which multiple-nodes with delay-limited sources transmit finite alphabet input signals. These nodes communicate through time-division multiple access channels, and the receiving node harvests energy from the received signal while decoding information by applying power splitting scheme. In addition, the transmitting nodes are subject to limitations on the buffer overflow probability, specified by the quality of service (QoS) exponent θ. Due to harvested energy constraint, we have applied the novel approach to assign probabilities non-uniformly to different signals in the constellation. We formulate optimization problems to maximize the effective capacity and effective EE while taking input signal probabilities, operating intervals, and splitting factor into account. Since obtaining

closed-form expressions for the optimization parameters are unlikely, we develop an algorithm to determine the solutions numerically.

- In Chapter 4, we consider multiple access channels, and focus on obtaining the optimal resource allocation schemes that maximize the system energy efficiency while satisfying energy and power constraints. In addition, we study the performance tradeoffs for energy-efficient transmission policies when SWIPT is incorporated in MACs. Usually, EE studies in the literature that consider SWIPT apply algorithms to obtain optimal solutions for given EE definitions, but in our work, we provide novel closed-form expressions for the optimal transmit power levels. More specifically, we, first, formulate concave-linear fractional optimization problems that maximize the instantaneous energy efficiency in a MAC, and identify the Karush-Kuhn-Tucker (KKT) conditions to determine optimal solutions. We provide novel closed-form expressions for the optimal transmit power levels, and characterize the impact of peak power constraint on the optimal resource allocation strategy. Then, we incorporate SWIPT and formulate optimization problems considering two types of receiver architectures, namely separated and common, for ID and EH components at the receiving node. We also address the impact of battery size on the optimal solution when energy demand is satisfied by the energy-efficiency maximizing input. We perform similar analysis when ID and EH components are supported by a common antenna. In this case, we incorporate power splitting scheme to share the received signal power between the decoding and harvesting operations, and hence we characterize power splitting factor in terms of the harvested energy requirement. In all the cases, we provide energy-efficient node selection policies and analytical expressions for the optimal transmit power level. In addition, we explicitly characterize optimal system EE, and the impact of harvested energy demand on the optimal EE and other critical parameters such as power splitting ratio.

- In Chapter 5, we study the performance of various wireless information and power transfer protocols for wireless-powered communication networks in the presence of delay-limited sources. We consider that UEs harvest energy from wireless power transmitter (WPT) and then transmit information uplink to AP either over orthogonal time slots using TDMA scheme or simultaneously using MAC. Each user is subject to limitations on the buffer overflow probability, and the time allocation for the downlink energy harvesting and uplink information decoding operations rely on these constraints in addition to the channel characteristics. Depending on whether the performance metric is throughput or energy efficiency, we formulate optimization problems to obtain the best resource allocation strategies while taking QoS constraints into account. Since the problems are concave/Pseudo-concave maximization problems, Karush-Kuhn-Tucker (KKT) conditions are necessary and sufficient for global optimality. Applying these conditions, we provide analytical expressions for the optimal operating intervals. However, in some cases, it is difficult to obtain closed-form expressions, and hence, we develop an algorithm to solve the problems numerically. Furthermore, we determine the special conditions where optimal solutions become independent of the QoS exponent.

- In Chapter 6, we introduce non-zero mean-information bearing signals, and study optimal resource allocation strategies for wireless information transfer (WIT) as well as SWIPT focusing on the throughput and system's energy efficiency. We consider multiple user settings with energy harvesting and non-energy harvesting UEs, and we derive explicit expressions for the throughput maximizing power control policies. In addition, we provide an iterative algorithm to obtain the optimal solution using the formulated expressions. Besides, we explicitly characterize energy-efficient strategies considering a two-user model, and then generalize to multiple users settings. We also characterize impact of harvested energy constraint on the optimal system energy efficiency and significance of introducing non-zero mean input signal.

- In Chapter 7, we consider a wireless-powered cellular network in which UEs do not have embedded power sources, but harvest energy from densely deployed APs. Using tools from stochastic geometry, we first characterize SINR coverage probabilities and achievable data rates as a function of the system parameters, i.e., uplink and downlink operating intervals. We also provide expressions to analyze the system energy efficiency (measured by throughput per total consumed energy). Furthermore, we study the performance characteristics incorporating SWIPT, instead of WPT, in the downlink channel while having WIT over the uplink channel. In such scenarios, we derive coverage probabilities as a function of an additional parameter, i.e., power splitting factor. Furthermore, we study mmWave based energy harvesting cellular networks where UEs harvest energy using signals in the lower frequency bands, but send information uplink using mmWave frequency bands. For this case, we provide the cellular network model, and explicitly characterize the average harvested energy, SINR coverage probability and achievable rate as a function of network parameters, such as directivity gains and APs density.

- In Chapter 8, we study the energy-efficient time allocation strategies for WPCN with uplink power-domain NOMA. More specifically, we consider two scenarios, namely half duplex and asynchronous transmission, based on the coordination of uplink and downlink operations, and we compare the performance gains achieved by these approaches with the conventional TDMA scheme. More specifically, energy-efficient resource allocation strategies are investigated for wireless information and power transfer considering two types of uplink-downlink coordination scenarios, namely half-duplex and asynchronous transmission. In both cases, we formulate optimization problems focusing on the system energy efficiency while UEs are allowed to transmit information-bearing signals simultaneously on the same frequency band based on the non-orthogonal multiple access scheme. We show that the optimization problems satisfy pseudo-concavity, and subsequently derive the necessary optimality conditions for each scenario. Due

to the difficulty in obtaining analytical expressions for the optimal solution, we provide iterative algorithms using the Dinkelbach's method. Furthermore, we consider delay-limited data sources, and address the impact of statistical queuing constraints on energy-efficient time allocation policies. In this case, we define and derive the system effective energy efficiency with downlink power transfer and uplink NOMA. We formulate optimization problems that maximize the system effective energy efficiency in the presence of constraints on buffer violation probabilities at UEs. We prove the presence of unique allocation of the optimal operating intervals, and propose an algorithm based on the bisection method.

1.4 Outline of Thesis

The thesis mainly addresses on the performance analysis of wireless information and power transfer focusing on throughput and energy-efficient resource allocation schemes. The remainder of the thesis is organized as follows: Chapter 2 provides the necessary preliminary background on statistical queuing constraints studied in the subsequent chapters of the thesis. Chapter 3 introduces novel schemes that assign non-uniform probabilities to finite alphabet input signals for SWIPT, and presents optimal resource allocation policies that maximize throughput and energy efficiency considering buffer violation probability as a quality-of-service (QoS) constraint. Chapter 4 mainly characterizes energy-efficient resource allocation strategies for fading multiple access channels both in the presence and absence of SWIPT, and analytical expressions are derived for each scenario. In Chapter 5, optimal time allocation policies are analyzed for delay-sensitive wireless-powered communication networks considering various downlink-uplink operation protocols. In chapter 6, energy-efficient transmission with non-zero mean input is characterized under full-duplex downlink energy transfer and uplink information transfer. Chapter 7 presents performance analysis for energy-harvesting cellular networks using stochastic geometry. In Chapter 8, non-orthogonal multiple access is

introduced for WPCNs, and energy-efficient time allocation strategies are characterized.

1.4.1 Bibliographic Note

- The results in Chapter 3 appeared in part in the following conference papers:
  - T. Zewde and M. Cenk Gursoy, "Simultaneous wireless information and power transfer with finite-alphabet input signals," in *Proc. of the IEEE 82nd Vehicular Technology Conference (VTC)- Fall*, Boston, MA, 2015.
  - T. Zewde and M. Cenk Gursoy, "QoS-driven resource allocation for SWIPT with finite-alphabet input signals," in *Proc. of the IEEE IEEE Wireless Communications and Networking Conference (WCNC)*, Sanfransico, CA, 2017
- The results in Chapter 4 appeared in part in the conference paper:
  - T. Zewde and M. Cenk Gursoy, "Energy-efficient resource allocation for SWIPT in multiple access channels," in *Proc. of the 50th Annual Conference on Information Sciences and Systems (CISS)*, Princeton, NJ, Mar. 2016.

  and is also submitted as a journal paper:
  - T. Zewde and M. Cenk Gursoy, "Energy-efficient information and power transfer in fading multiple access channels," submitted to *IEEE Trans. Commun.*, 2017.
- The results in Chapter 5 appeared in part in the following conference papers:
  - T. Zewde and M. Cenk Gursoy, "Energy-efficient time allocation for wireless energy harvesting communication networks," in *Proc. of the IEEE Globecom Workshop*, Washington, D.C., Dec. 8, 2016.
  - T. Zewde and M. Cenk Gursoy, "Wireless-powered communication under QoS constraints," in Proc. of the IEEE International Communication Conference, Kuala Lampur, Malaysia, May 23-27, 2016.

- The results in Chapter 6 appeared in part in the conference paper:
  - T. Zewde and M. Cenk Gursoy, "Energy-efficient full-duplex wireless information and power transfer," in *Proc. of the IEEE 84th Vehicular Technology Conference*, Montreal, Canada, Sep. 18-21, 2016.
- The results in Chapter 7 appeared in part in the conference paper:
  - T. Zewde and M. Cenk Gursoy, "Energy-efficient resource allocation for wireless powered cellular networks," in *Proc. of the 51th Annual Conference on Information Sciences and Systems (CISS)*, Baltimore, MD, 2017.
- The results in Chapter 8 is accepted in part in the VTC Fall 2017 conference:
  - T. Zewde and M. Cenk Gursoy, "NOMA-based energy-efficient wireless powered communications," to appear in *Proc. of the IEEE 86th Vehicular Technology Conference*, Toronto, Canada, Sep. 2017.

  and is also submitted as a journal paper:
  - T. Zewde and M. Cenk Gursoy, "NOMA-based energy-efficient wireless powered communications," submitted to *IEEE Trans. on Green Commun. and Networking*, 2017.

Chapter 2

Preliminaries

In this chapter, we discuss the basic concept of energy harvesting, and the main components of the receiving structure. In addition, mathematical models and preliminaries of statistical queuing constraints are presented briefly.

2.1 Energy Harvesting

As mentioned earlier in the first chapter, energy harvesting is a prominent solution for future green communication networks, and it is a phenomenon by which a power consuming electronic device harnesses energy from an external source. There are different types of energy sources such as as solar, wind, thermal, biochemical and wireless as illustrated in Fig. 2.1. Except for wireless/RF sources energy is obtained in other forms, and additional device is necessary to convert it into a usable form, i.e., electric energy. In the case of wireless power source, energy harvesting is about utilizing the electric as well as magnetic energy in the electromagnetic waves that are transmitted at certain frequencies. In fact, the distance between RF energy source and the receiver determines the type of harvesting technique as well as the amount of harvested energy. In the case of near-field harvesting, electric energy can be harvested based on inductive coupling principle, on the other hand in the case of far-field harvesting, the receiving component usually is equipped with antenna to scavenge

the abundant RF signals from radio broadcasting, WiFi communications, or a dedicated wireless power source.

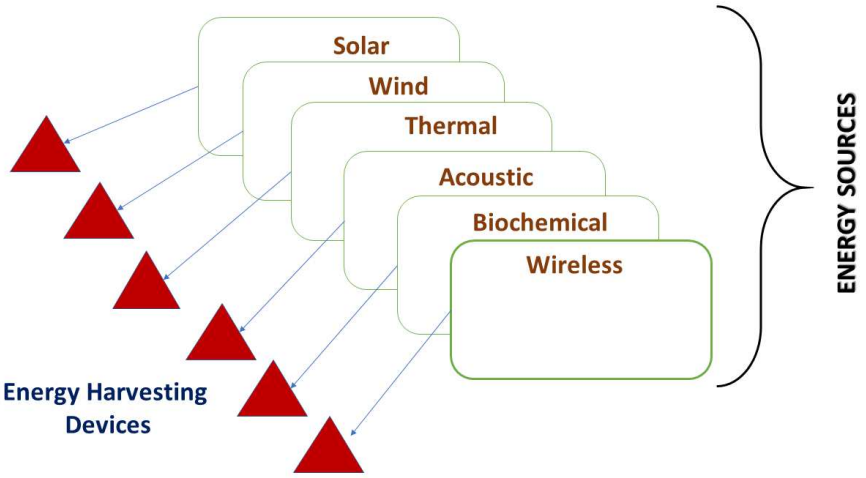

Figure 2.1: Energy sources block model

Architecturally, the main component of an energy harvesting device is known as a rectenna which is a rectifying circuit which is shown in Fig. 2.2. The diode is used to convert the AC signal into pulsating DC, and the low pass filter removes the high frequency components. In addition, the DC-to-DC converter allows the generation of approximately constant output voltage with very small ripple. The design of energy harvesting could be in such a way that the harnessed energy is directly utilized or stored in a large size capacitor/ rechargeable battery.

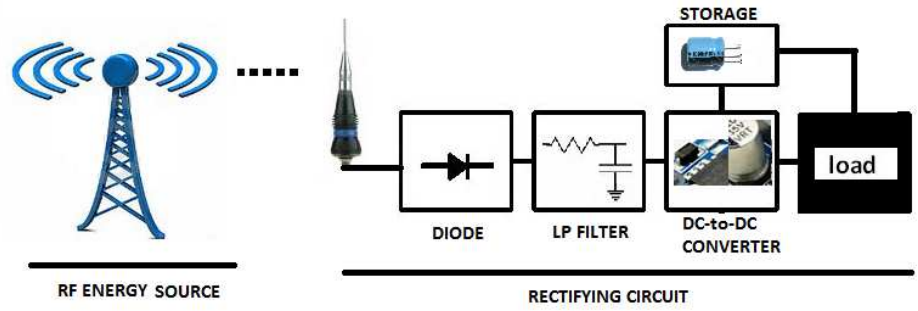

Figure 2.2: Rectenna model

2.2 Statistical Queuing Constraints

In our studies addressing delay-sensitive traffic, we consider that each user equipment stores received data packets generated by a delay-sensitive source that requires certain statistical QoS guarantees described by the QoS exponent θ. More specifically, the tail distribution of the buffer is required to have an exponential decay with rate controlled by the exponent θ, and the buffer violation or overflow probability is described as

$$\Pr\left\{Q_i \geq Q_{max}\right\} \approx \varsigma e^{-\theta_i Q_{max}} \tag{2.1}$$

where Q_i denotes the stationary queue length in the i^{th} user buffer, Q_{max} is the buffer overflow threshold, and $\varsigma = \Pr\{Q > 0\}$ is the probability of non-empty buffer. More rigorously, QoS exponent θ is defined as

$$\theta = \lim_{Q_{max}\to\infty} \frac{-\log \Pr\{Q_i \geq Q_{max}\}}{Q_{max}}. \tag{2.2}$$

2.3 Effective Capacity

Instantaneous channel capacity provides the maximum achievable data rate at which information can be transmitted through wireless medium based on the availability of channel state information. However, data arrival rates at which data packets are received from the source may be further limited by the buffering requirements such as the presence of statistical queuing constraints, as mentioned above. This buffer constraint determines the arrival rates that can be supported by the wireless link. Let $r_i[n]$ and $R_i[n]$ denote i^{th} user random arrival and instantaneous service rates, respectively, in the n^{th} time slot. The corresponding asymptotic logarithmic moment generating functions (LMGF) Λ_A and Λ_C, are given as

follows [27]:

$$\Lambda_A = \lim_{t\to\infty} \frac{\log\left(\mathbb{E}\left\{e^{\theta\sum_{n=1}^{t} r_i[n]}\right\}\right)}{t}$$
$$\Lambda_C = \lim_{t\to\infty} \frac{\log\left(\mathbb{E}\left\{e^{\theta\sum_{n=1}^{t} R_i[n]}\right\}\right)}{t}. \tag{2.3}$$

Having the buffer overflow probability to decay exponentially with rate θ as in (2.1) requires $\Lambda_A(\theta^*) + \Lambda_C(-\theta^*) = 0$. The work in [27] provides a mathematical formulation for the maximum arrival rate, also termed as effective capacity, with a certain QoS exponent θ as follows:

$$C_i^e(\theta_i) = -\lim_{t\to\infty} \frac{1}{t\theta_i} \log\left(\mathbb{E}\left\{e^{-\theta_i\sum_{n=1}^{t} R_i[n]}\right\}\right) \text{ bps/Hz.} \tag{2.4}$$

Assuming block fading scenario with frame duration T, this can be further simplified as

$$C_i^e(\theta_i) = -\frac{1}{T\theta_i} \log\left(\mathbb{E}\left\{e^{-\theta_i T R_i[n]}\right\}\right) \text{ bps/Hz.} \tag{2.5}$$

As the buffer constraint is relaxed, effective capacity approaches ergodic capacity, i.e., $\lim_{\theta_i\to 0} C_i^e = \mathbb{E}\{R_i\}$, whereas for increasingly strict constraints, i.e., as $\theta_i \to \infty$, effective capacity converges converges to the delay-limited capacity with zero outage.

Chapter 3

Simultaneous Wireless Information and Power Transfer with Finite-Alphabet Input Signals

This chapter mainly studies throughput optimization for SWIPT in the presence of finite-alphabet input signals. Two novel schemes are proposed in order to assign probabilities to the alphabets in the constellation set based on their energy levels. Then, using the non-uniform probability distributions, optimal solutions are determined using iterative procedure focusing on the throughput with arbitrary input signaling. Section 3.1 considers point-to-point transmitter receiver pair, and an optimization problem that maximizes mutual information subject to harvested energy constraint is formulated. Despite the complexity of getting analytical expression for power-splitting factor, an algorithm is provided to determine globally optimal solution. In Section 3.2, multiple users with delay-limited sources are taken into account. In these cases, optimization problems are formulated to determine throughput maximizing and energy-efficient transmission policies. Numerical results are presented and discussed at the end of each section.

3.1 Rate-Energy tradeoff for a Single User

In this section, the optimal power control scheme that maximizes the throughput for SWIPT with arbitrary input distributions subject to harvested energy constraint is presented. We introduce novel non-uniform probability assignment using two approaches, namely static slope and dynamic slope characteristics, to modify the input probability distribution based on the required harvested energy at the receiving end. We provide mathematical formulations for these probabilities according to the constraints on the minimum harvested energy level.

3.1.1 Preliminaries

System Model

We consider a communication system where a transmitter-receiver pair communicates over a wireless link as shown in Fig. 3.1. The source transmits a signal, $X[i]$, during i^{th} symbol duration selected from a finite set of alphabets denoted by $\mathcal{S} = \{X_1, X_2, \dots X_M\}$ with $|\mathcal{S}| = M$ indicating the cardinality of the signal set. In general, these alphabets could be one-dimensional as in pulse-amplitude modulation (PAM) signals

$$X_i = a_i \tag{3.1}$$

or two-dimensional such as phase-shift keying or quadrature-amplitude modulation (QAM) signals

$$X_i = a_i + jb_i \tag{3.2}$$

where a_i and b_i denote the distance of the constellation point from the origin on the respective axis. We assume that the input signal is limited by a peak energy constraint i.e., $|X[i]|^2 \leq E_{pk}$. The transmitted signal $X[i]$ targets transferring not only information but also energy to the receiving end, and hence we have simultaneous information and power transfer using the information-bearing signal. The receiver has both information-decoding (ID) and energy-

harvesting (EH) components, and it applies power splitting scheme to the received signal to support decoding and harvesting operations, concurrently. We denote ρ for the fraction of received power allocated to the ID component, and hence $1-\rho$ to the EH component.

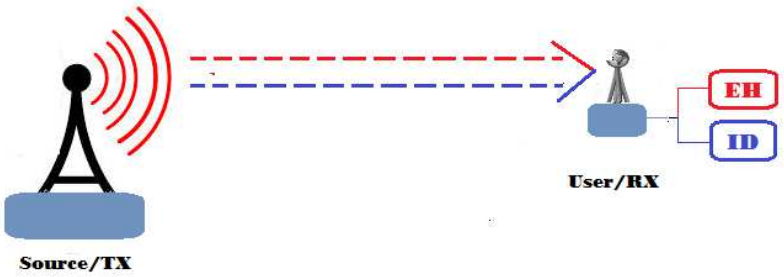

Figure 3.1: SWIPT model for a transmitter-receiver pair

The wireless link experiences frequency flat-fading and the channel fading coefficient in the i^{th} symbol period is denoted by $g[i]$. We assume that both the receiver and transmitter are equipped with a single antenna, and perfect channel state information is available on each side. Hence, under these assumptions, the discrete-time channel input-output relation is given by

$$Y[i] = g[i]X[i] + N[i] \quad i = 1, 2, \cdots \tag{3.3}$$

where i represents the time index, $Y[i]$ denote the received signal, and $N[i]$ is a zero-mean circularly symmetric, additive complex Gaussian noise with variance $\sigma^2 = N_0$, i.e., $N \sim \mathcal{CN}(0, N_0)$. Hereafter, time index i is omitted for brevity of notation. Once the signal is received, it will be processed to decode the information and/or replenish the energy according to operation policy priorities that depend on the received power level.

Information Transfer

It is well-known from information-theoretic results that input distribution has a direct impact on the achievable rates at which data can be reliably transmitted, and Gaussian input distribution maximizes the capacity for Gaussian channels [92]. On the other hand, practical input signals are generally selected from finite constellations. In such cases, achievable rate

expressions are determined by considering the input-output mutual information [92]:

$$\begin{aligned} R = &\ I(X;Y) \\ = &\ h(Y) - h(Y \mid X) \\ = &\ \sum_{k=1}^{M} p_k \int_{-\infty}^{\infty} f_{Y|X_k,g} \log \left[\frac{f_{Y|X_k,g}}{\sum_{j=1}^{M} p_j f_{Y|X_j,g}} \right] dy \end{aligned} \tag{3.4}$$

where $f_{Y|X_k,g} = \frac{1}{\pi N_0} e^{-\frac{|Y-gX_k|^2}{N_0}}$ is the probability density function of Y given X_k as well as the fading coefficient g, and $p_k = \Pr\{X = X_k\}$ is the probability that the transmitted signal takes the input signal X_k. After substitution and some rearrangements

$$I(X;Y) = -\sum_{k=1}^{M} \frac{p_k}{\pi N_0} \int_{-\infty}^{\infty} \int_{-\infty}^{\infty} e^{-|\boldsymbol{v}|^2} \log \left[\sum_{j=1}^{M} p_j e^{\left[-|\boldsymbol{v}+\gamma_d|^2+|\boldsymbol{v}|^2\right]} \right] dv_1 dv_2 \tag{3.5}$$

where $\boldsymbol{v} = \frac{Y-gX_k}{\sqrt{N_0}}$, $\gamma_d = \frac{g}{\sqrt{N_0}}(X_k - X_j)$, and v_1 and v_2 are real and imaginary component of v assuming that the alphabets are distributed on a two-dimensional constellation space.

Remark 3.1.1 *When only data transmission is considered, uniformly distributed input is in general optimal in the sense of maximizing the average achievable rate expressions.*

Energy Harvesting

In our model, the receiver harvests energy transferred from a source through the wireless medium so as to meet, at least, the minimum required energy, denoted by χ. Given that the source transmit signals selected from a finite constellation size, the instantaneous, $\mathcal{E}_{hv}[i]$, and average, $\mathcal{E}_{hv}$, harvested energy can be determined as follows:

$$\mathcal{E}_{hv}[i] = z[i]\left|X_j[i]\right|^2 + \sigma^2 \tag{3.6a}$$

$$\mathcal{E}_{hv} = \mathbb{E}\{\mathcal{E}_{hv}(z)\} \tag{3.6b}$$

where $z = |g|^2$ and the expectation in (3.6b) is with respect to both z and the distribution of the input signal in the constellation. As can be seen from (3.6a) and (3.6b), average harvested energy is directly proportional to each signal energy level as well as its assigned probability, and this fact encourages to assign higher probabilities to those with higher energy levels among the input signals.

Remark 3.1.2 *Unlike in the case of information transfer, optimal input probability distribution that maximizes the level of harvested energy is the one when the source transmits the highest-energy signal almost surely, i.e.,* $\Pr(X = X_m) = 1$ *where* $|X_m|^2 > |X_i|^2 \; \forall i, m \in \{1, 2, \ldots, M\}$ *and* $i \neq m$.

3.1.2 Non-Uniform Input Distribution

Finite-alphabet inputs can be geometrically described in the signal space by their coordinate points and the corresponding probabilities. In fact, the optimal choice of the probability distribution depends on the overall objective, and as stated in Remarks 3.1.1 and 3.1.2, the goals of maximizing the information transfer and harvested energy lead to uniformly distributed and deterministic inputs, respectively. However, each of these input characterizations may not be optimal when SWIPT is considered. Rather, non-uniform probability distribution can result better overall performance, i.e., improves rate-energy tradeoff, since signals in a given constellation, e.g., PAM with $M > 2$ and QAM with $M > 4$, do not necessarily have equal energy levels. Intuitively speaking, these unequal energy levels have direct impact on the information and power transfer strategies. For instance, assigning higher probabilities to those signals with higher energy level benefit harvested energy while sacrificing data rate. Note that this is not applicable to BPSK or QPSK as all the signals in these cases have equal energy level, and no extra benefit is attained with unequal input distribution in terms of harvested energy while achievable rates are reduced.

Theorem 3.1.1 *For a rectangular/square QAM constellation with size* $M = 2^n$ *where n denotes the number of bits per symbol, there are* $N \in \{N_s, N_r\}$ *different energy levels with*

$N < M$ *where*

$$N_s = \sum_{i=0}^{\sqrt{\frac{M}{4}}-1} \left(\sqrt{\frac{M}{4}} - i \right) \tag{3.7a}$$

$$N_r = \frac{M}{8} + \sum_{i=0}^{\sqrt{\frac{M}{8}}-1} \left(\sqrt{\frac{M}{8}} - i \right). \tag{3.7b}$$

N_s and N_r denote total number of different energy levels when the constellation has square and rectangular geometries, respectively.

Proof: See Appendix A.

As we can conclude from this theorem, constellation size is always greater than the number of unequal energy levels, and this implies that there exist some signals that have equal energy levels. Let us define a set which consists of all the signals but in terms of disjoint subsets, $\mathcal{S}_i$, where each includes signals with equal energy level as follows:

$$\mathcal{S}_{sc} \triangleq \bigcup_{i=1}^{N} \left\{ \mathcal{S}_i : X_a \in \mathcal{S}_i;\, X_b \in \mathcal{S}_{i+1};\, |X_a|^2 > |X_b|^2 \right\} \tag{3.8}$$

$\forall a = \{1, 2, \ldots, |\mathcal{S}_i|\}$ and $\forall b = \{1, 2, \ldots, |\mathcal{S}_{i+1}|\}$. For each subset $|\mathcal{S}_i| > 1$ where $i \in \{1, 2, \cdots, N\}$, it is obvious that unequal probability assignment for two signals that have equal energy levels benefits neither information transfer nor energy-harvesting. In such a case, signals probabilities in that subset are uniformly distributed i.e., $p_a = \Pr\{X = X_a\} = \frac{p_{s_i}}{|\mathcal{S}_i|}$, where p_{s_i} denote the probability assigned to the i^{th} subset. However, it is meaningful to optimally adjust probabilities assigned to each subset $\mathcal{S}_i \in \mathcal{S}_{sc}$ in consonance with the harvesting constraint while maximizing information rate.

Proposition 3.1.1 *For finite constellations, signal probabilities can be non-uniformly distributed based on their energy levels to improve SWIPT performance as long as the required harvested energy is bounded, $0 \leq \mathcal{X} \leq E_{mx}$, and hence the corresponding feasible set of signals probabilities, denoted as $\mathcal{S}_p$, becomes,*

$$\mathcal{S}_p \triangleq \bigcup_{j=1}^{M} \left\{ (p_j): \begin{array}{l} |\mathcal{S}|^{-1} < p_j < |\mathcal{S}_N|^{-1}, \;\; if \; X_j \in S_N; \\ |\mathcal{S}|^{-1} < p_j < 0, \;\; otherwise. \end{array} \right\} \tag{3.9}$$

Proof: See Appendix B.

According to Proposition 3.1.1, probability assigned to each subset, as well as signal, changes for any increment in $\mathcal{X}$, and this can be characterized by developing probability-energy relation. Thus, we consider two novel approaches, namely static slope characteristics and dynamic slope characteristics, that help to adjust probabilities given the harvested energy constraint.

Static slope characteristics

In this scenario, probabilities assigned to subsets, $p_{s_i} \triangleq \Pr\{s = \mathcal{S}_i\}$, are updated with constant slope for each increment in the minimum required harvested energy. The slope depends only on the gross harvested energy constraint boundaries and the corresponding input probability distributions, both of which are known priori. Hence, energy level probabilities, p_{s_i}, change linearly with static slope as shown in Fig.3.2. Mathematically, this probability-energy characteristic can be expressed as follows:

$$p_{s_i}(\mathcal{X}) = \delta\mathcal{X} + p_i(\mathcal{X})\Big|_{\mathcal{X}=0} \tag{3.10}$$

where $\mathcal{X} = \frac{\chi}{z-\rho z}$ is the scaled or gross harvested energy and $p_i(\mathcal{X})|_{\mathcal{X}=0} = \frac{1}{|\mathcal{S}|}$ defines the signal probability in the absence of harvested energy constraint. In addition, $\delta = \frac{|\mathcal{S}|-|\mathcal{S}_m|}{\mathcal{E}_\Delta(|\mathcal{S}_m||\mathcal{S}|)}$ if $X_i \in \mathcal{S}_N$, otherwise $\delta = -\frac{1}{(\mathcal{E}_\Delta|\mathcal{S}|)}$ where $\mathcal{E}_\Delta = \mathcal{E}_{mx} - \mathcal{E}_{mn}$. Note that $\mathcal{E}_{mn}$ and $\mathcal{E}_{mx}$ denote the minimum required gross harvested energy and the maximum available energy, respectively. As can be seen from (3.10) and Fig. 3.2, each subset probability changes with the same slope which implies $p_{s_i} = p_{s_j}$, except those of $\mathcal{S}_N$, and constellation size remains $|\mathcal{S}|$ until $\mathcal{X} = \mathcal{E}_{mx}$ at which it becomes $|\mathcal{S}_N$.

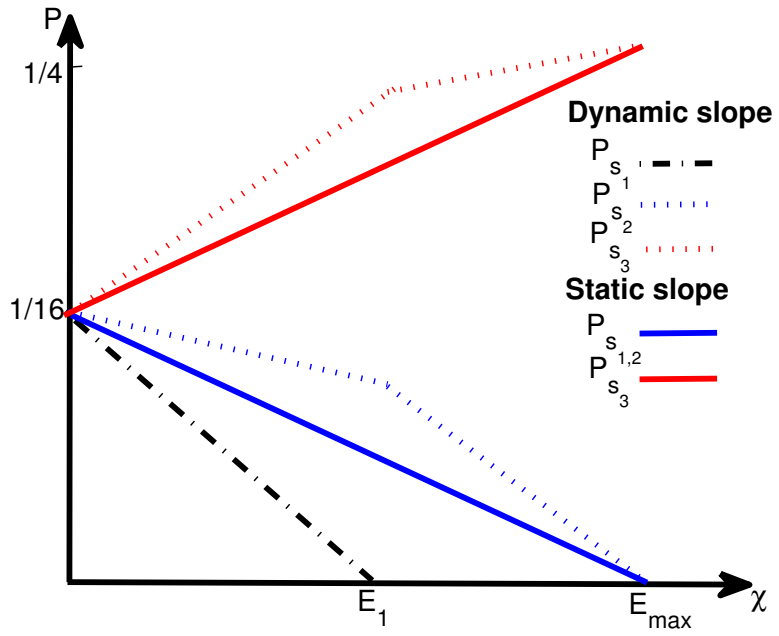

Figure 3.2: Probability-Energy characteristics for 16-QAM

Dynamic slope characteristics

The basic principle of this approach is that a subset having the lowest-energy signals is assigned the smallest probability i.e., $p_{s_i} < p_{s_{i+k}}$ for $k = \{1, 2, \ldots, N-i\}$, given the harvested energy requirements. When this energy exceeds a certain threshold, subset $\mathcal{S}_i$ is discarded from $\mathcal{S}_{sc}$, for instance $\mathcal{S}_1$ at E_1 as shown in Fig. 3.2, and the process continues successively until $\mathcal{X} = \mathcal{E}_{mx}$. Let the required gross harvested energy change with some increment, $\mathcal{X}_{\Delta_k} = \mathcal{X}^k_{mx} - \mathcal{X}^k_{mn}$, and the number of increments depend on the number of different energy levels in the constellation set. Then, the probability-energy relation during k^{th} increment is mathematically given as follows:

$$p_{s_i}(\mathcal{X}) = \delta^k_{s_i}\mathcal{X} + p^k_{s_i}\Big|_{\mathcal{X}=\mathcal{X}^k_{mn}} \tag{3.11}$$

where $k \leq i$ and $\delta^j_{s_i}$ defines the slope of the probability of subset $\mathcal{S}_i$ in the interval $\mathcal{X}^k_{mn} \leq \mathcal{X} \leq \mathcal{X}^k_{mx}$, and the last term in (3.11) denotes this subset probability when $\mathcal{X}$ takes the lowest value in the k^{th} increment. In order to determine $\delta^j_{s_i}$, we begin with the lowest energy

level as follows:

$$\delta_{s_1}^1 = \frac{\frac{1}{|\mathcal{S}|} - 0}{\mathcal{E}_{mn}^1 - \mathcal{E}_{mx}^1}, \tag{3.12}$$

and hence at $\mathcal{E} = \mathcal{X}_{mx}^1$, $p_{s_1} = 0$. Meanwhile, the probability for the lowest energy alphabet at this energy level for the static slop is determined as

$$p_{s_1} = \frac{\frac{1}{|\mathcal{S}|} - 0}{\mathcal{E}_{mn}^1 - \mathcal{E}_{mx}} \mathcal{E}_{mx}^1 + \frac{1}{|\mathcal{S}|}. \tag{3.13}$$

Thus, the difference for the probability assignment between static and dynamic slop schemes at $\mathcal{E} = \mathcal{X}_{mx}^1$ becomes

$$\Delta p_{s_1} = p_{s_1} - 0 = \frac{1}{|\mathcal{S}|} \left[1 - \frac{\mathcal{E}_{mx}^1}{\mathcal{E}_{mx} - \mathcal{E}_{mn}^1} \right]. \tag{3.14}$$

Then, the slope for the next (e.g., the second, the third and so on) lowest energy level in the first increment is given as

$$\begin{aligned} p_{s_j}^1 \Big|_{\mathcal{X}=\mathcal{X}_{mn}^2} &= \frac{\Delta p_{s_1}}{N-1} + p_{s_j} \\ \delta_{s_j}^1 &= \frac{\frac{1}{|\mathcal{S}|} - p_{s_j}^1 \Big|_{\mathcal{X}=\mathcal{X}_{mn}^2}}{\mathcal{E}_{mn}^1 - \mathcal{E}_{mx}^1}, \end{aligned} \tag{3.15}$$

Note that $P_{s_j} = p_{s_1}$ for $j \in \{2, 3, \cdots, N-1\}$ in the static slope characteristics. Similarly, for the highest energy level in the first increment is given as

$$\delta_{s_N}^1 = \frac{\frac{1}{|\mathcal{S}|} - \left[\frac{\Delta p_{s_1}}{N-1} + p_{s_N}^1 \right]}{\mathcal{E}_{mn}^1 - \mathcal{E}_{mx}^1}, \tag{3.16}$$

where

$$p_{s_N}^1 = \frac{\frac{1}{|\mathcal{S}|} - \frac{1}{|\mathcal{S}_N|}}{\mathcal{E}_{mn}^1 - \mathcal{E}_{mx}} \mathcal{E}_{mx}^1 + \frac{1}{|\mathcal{S}|}. \tag{3.17}$$

The details for other incremental ranges are omitted for brevity, but this procedure continues until the probability-energy relationship is derived over the entire feasible harvested energy region.

Compared to the earlier approach, the slope for any subset changes according to the harvested energy demand in this case. In addition, the slope does not change in the same way for different subsets. Moreover, constellation size consequently reduces in each increment $\mathcal{X}_{\Delta_k}$ and the probabilities for the available $N-k$ subsets increase where k indicates the number of subsets that are successively removed earlier based on the value of $\mathcal{X}$. The main benefit of this approach is that it enables the receiver to harvest more energy because higher energy level input signals have higher probabilities compared to the static slope technique as deduced from Fig. 3.2.

Remark 3.1.3 *Once p_{s_i} is known, the corresponding signal probability can easily be determined using $p_i = \frac{p_{s_i}}{|\mathcal{S}_i|}$. Hence, for any two signals $X_i \in \mathcal{S}_i$, $X_j \in \mathcal{S}_j$ and $\mathcal{S}_i, \mathcal{S}_j \neq \mathcal{S}_N$, $p_i \neq p_j$ in the first approach, i.e., where $p_{s_i} = p_{s_j}$.*

3.1.3 Throughput-Efficient SWIPT Policies

Performing information-decoding and energy-harvesting operations simultaneously while maintaining maximum achievable output, i.e., ($\mathcal{R}_{mx}$, $\mathcal{E}_{mx}$), is ideal whether these are carried out at co-located or separated receivers. Hence, it is important to determine the appropriate scheme and optimal way of allocating resources to improve the rate-energy tradeoff. In the literature, time-switching and power-splitting schemes are proposed to carry out these operations both in single and multiple user settings [12] [14] [21]. Here, we consider power-splitting scheme due to the fact that time-switching strategy would simply require us to characterize information maximizing and energy maximizing inputs separately over orthogonal time intervals. Hence, in such a case, non-uniform probability distribution for finite constellation inputs would not provide any benefits.

Power splitting scheme divides the received signal power to ID and EH components with a certain power-splitting fraction $\rho : 1-\rho$. Basically, when information decoding and energy harvesting components have a common antenna architecture at the receiving end, the performance of SWIPT with finite-alphabet inputs depends on the input probability distri-

bution at the transmitter and splitting factor at the receiver. These parameters need to be optimally adjusted to determine the best operating point for the system. Intuitively, when highest-energy level signals become more likely to be transmitted, the amount of power allocated to the ID component increases given the harvested energy constraint. However, the impact on the information rate is determined by the balance between the reduction and gain due to unequal probabilities and increased in power splitting factor, respectively.

Therefore, in order to investigate the tradeoff between information rate and harvested energy and determine the solution for the optimal probability distribution and splitting factor, we formulate an optimization problem as follows:

$$\text{(PR:3.1)} \quad \max_{\substack{p_i \in \mathcal{S}_p \\ \rho \in [0,1]}} \quad I(X;Y) \tag{3.18a}$$

$$\text{subject to } (1-\rho)\mathcal{E}_{hv} \;\geq\; \mathcal{X} \tag{3.18b}$$

$$0 \leq \rho \leq 1 \tag{3.18c}$$

$$0 \leq p_i \leq \frac{1}{|\mathcal{S}_N|} \tag{3.18d}$$

where the achievable data rate $I(X,Y)$ for SWIPT with finite-alphabet input is given as:

$$R(\rho, \mathbf{p}) = -\sum_{k=1}^{M} \frac{p_k}{\pi N_0} \int_{-\infty}^{\infty} \int_{-\infty}^{\infty} e^{-|v|^2} \log \left[\sum_{j=1}^{M} p_j e^{\left[\rho(-|v+\gamma_d|^2+|v|^2)\right]} \right] dv_1 dv_2 \tag{3.19}$$

where γ_d and $\mathcal{S}_p$ are as defined in (3.5) and (3.9), respectively. The last two constraints specify the domain set of the optimization parameters.

Proposition 3.1.2 *Given the probability distribution of the finite-alphabet inputs, the achievable rate expression in 3.19 is concave with respect to the power splitting factor, ρ.*

Proof: See Appendix C.

According to Proposition 3.1.2, there exists a global optimal solution which maximizes the achievable rate when the probabilities of the finite-alphabet inputs are fixed. On the

other hand, if the power splitting factor ρ is given, the mutual information expression in (3.18a) is concave in the marginal probability distribution of the finite-alphabet input p_i [92]. Since there is always a tradeoff between improving information transfer rate and satisfying the required harvested energy, it is necessary to adjust the probabilities accordingly. As mentioned above, these are determined using the static or dynamic slope characteristics curves. Hence, once those are determined, the optimization problem (PR:3.1) equivalently becomes minimization of a convex problem since $I(X,Y)$ is concave function of ρ and the constraints are convex. Thus, Kahun-Kurush-Tucker (KKT) conditions are necessary and sufficient for global optimality, and hence we have

$$\frac{\partial \mathcal{L}(\rho)}{\partial \rho} = -\sum_{k=1}^{M} \frac{p_k}{\pi N_0} \int_{-\infty}^{\infty}\int_{-\infty}^{\infty} e^{-|v|^2} \frac{\partial \log h(\rho, v_1, v_2)}{\partial \rho} dv_1 dv_2 + \mu_x \mathcal{E}_{hv} + \mu_\rho(1-2\rho) = 0 \quad (3.20)$$

where

$$\mathcal{L}(\rho) = R(\rho) - \mu_x\Big(\chi - (1-\rho)\mathcal{E}_{hv}\Big) - \mu_\rho \rho(1-\rho) - \sum_{i=1}^{N} \mu_i p_i \left(\frac{1}{|\mathcal{S}_N|} - p_i\right) \quad (3.21)$$

and

$$h(\rho, v_1, v_2) = \sum_{j=1}^{M} p_j e^{\left[\rho(-|v+\gamma_d|^2 + |v|^2)\right]}. \quad (3.22)$$

From the complementary slackness conditions, i.e.,

$$\begin{aligned} \mu_x^*\Big(\chi - (1-\rho^*)\mathcal{E}_{hv}\Big) &= 0 \\ \mu_\rho^* \rho^*(1-\rho^*) &= 0 \\ \mu_i^* p_i^* \left(\frac{1}{|\mathcal{S}_N|} - p_i^*\right) &= 0, \end{aligned} \quad (3.23)$$

it is clear that $\mu_\rho = 0$ and $\mu_i = 0$ since the feasible solution lies $0 < \rho < 1$ and $0 < p_i < \frac{1}{|\mathcal{S}_N|}$ for $\chi < \chi^{mx}$. When the demand reaches the maximum achievable harvested energy, the solution is $\rho^* = 1$, and $p_i = 0\ \forall i = \{1, 2, \cdots, N-1\}$ and $P_N = \frac{1}{|\mathcal{S}_N|}$. Therefore, for $\chi < \chi^{mx}$,

after several arrangements (3.20) is simplified as

$$\mathbb{E}\left\{\frac{e^{-|v|^2}}{h(\rho,v_1,v_2)}\left[\sum_{j=1}^{M}p_j(-|v+\gamma_d|^2+|v|^2)e^{\left[\rho(-|v+\gamma_d|^2+|v|^2)\right]}\right]\right\}=C \tag{3.24}$$

where $C=\pi N_0\mu_x\mathcal{E}_{hv}$ is a scaler quantity. Despite the difficulty in formulating closed-form expression for the optimum splitting factor, ρ^*, it can be easily obtained using standard numerical tools.

Algorithm 1 SWIPT with finite alphabets input

Given: $\mathcal{X}$, M
Require: $\max I(X;Y)$
Determine the number of energy levels using (3.7)
Initialize $\rho^u=1$ and $\rho^l=0$, $\boldsymbol{p}(0)=\frac{1}{M}[1\ 1\cdots 1]_{1\times M}$
$\rho(0)=0.5(\rho^u+\rho^l)$
$n\leftarrow 0$
repeat
  repeat
    Determine $I(X;Y)$ for $\rho(n)$ using $\boldsymbol{p}(n)$, and $R^n=I(X;Y)$
    Determine $\mathcal{X}=\frac{\chi}{z-z\rho(n)}$
    Determine signal probabilities based on $\mathcal{X}$
    if Static Slope **then**
      Apply the relation given in (3.10)
    else
      Use (3.11) for dynamic slope characteristics
    end if
    Solve (3.24) for ρ
    Determine $I(X,Y)$ using (3.19)
    $n\leftarrow n+1$
    Update $\rho(n)$ using bisection method
  until $|I(X;Y)-R^n|<\epsilon$
  Update μ_x using gradient method
until $|\mu_x(n)-\mu_x(n-1)|<\epsilon$
Determine the optimal signal probabilities at the transmitter and power-splitting factor at the receiver

3.1.4 Numerical Analysis

In this section, we provide numerical results considering 16-QAM constellation where the transmitted signal energy per second is limited by the peak value, $2W$. As we can clearly see from Fig. 3.3, there are three different energy levels, denoted as $p_C \in \mathcal{S}_1$, $p_B \in \mathcal{S}_2$, $p_A \in \mathcal{S}_3$, and hence there are two increments, $k = 2$, for the harvested energy level with $\mathcal{X}_\Delta = 0.5E_{mx}$.

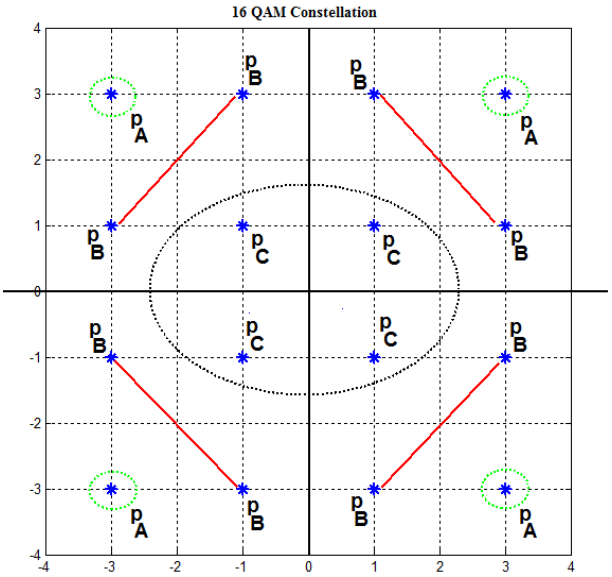

Figure 3.3: 16-QAM Constellation

Figure 3.4, illustrates that non-uniform probability distribution using either static or dynamic slope characteristics outperforms time-sharing and uniform probability distribution, and this becomes more significant for higher $\mathcal{X}$ values. In the absence of harvested energy constraint, i.e., $\chi = 0$, uniform probability distribution among the finite alphabet input signals is optimal, and hence selecting only the highest energy alphabets hurts the achievable rate without any benefit. In addition, for time-sharing scheme, each incremental demand for harvested energy degrades the data rate linearly. This is because, this scheme shares the operation time interval for the information-maximizing (uniform distribution) and energy-maximizing (highest energy alphabets) inputs, and as χ increases less time will be allocated to transfer the information. On the other hand, with uniform probability assign-

ment approach, the power splitting factor ρ is varied to satisfy the energy demand while tracing maximum information transfer rate. Despite its benefit to favor information transfer, lower splitting ratio for higher $\mathcal{X}$values hurts the overall performance, and this leads to time-sharing scheme to achieve better data rate for certain ranges of harvested energies as can be seen from the figure.

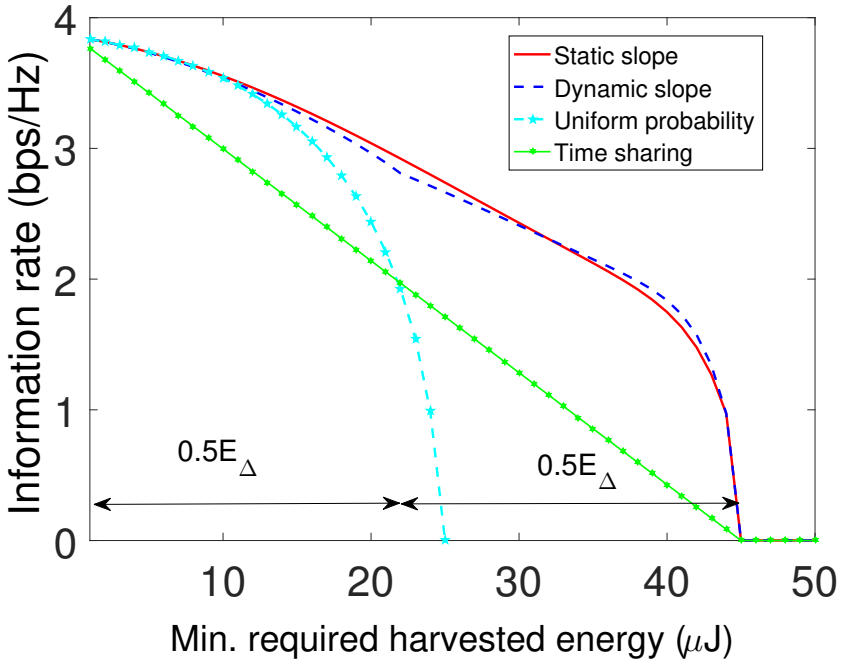

Figure 3.4: Rate-Energy tradeoff characteristics

Meanwhile, the significance of static over dynamic, or vice versa, depends on the net impact of signal probabilities and power-splitting factor. Intuitively, assigning higher probabilities to those alphabets with higher energy level allow to harvest more energy but hurts the achievable data rate. However, harvesting more energy in a given duration encourages to allocate more power to the ID component, i.e., higher ρ, which in turn benefits information transfer. Therefore, balance between the gain and the loss in data rate due to ρ and non-uniform probability assignment, respectively, determines the tradeoff characteristics. From Fig. 3.5a, we observe that as $\mathcal{X}$ increases, higher energy level signals become more likely for transmission in the dynamic slope approach as expected. This enables the receiver to

harvest more energy within a given duration compared to the probability distribution determined by static slope characteristics. As a result, the information-decoding circuitry shares the power more favorably, i.e., ρ increases as can be seen in Fig. 3.5b. The net effect of these parameters, i.e., probability distribution and power-splitting factor, is observed in Fig. 3.4. According to the numerical results, we can observe that the gain in ρ due to dynamic slope characteristics is not significant for lower harvested energy constraints, and this implies more weight should be given to information rate under these circumstances. However, as the energy demand exceeds a certain threshold, it is advantageous and efficient to ignore smaller energy level alphabets and adjust probability distribution accordingly.

3.2 QoS-Driven SWIPT with Multiple Users

In this section, the optimal power control scheme that maximizes the throughput as well as energy-efficiency for SWIPT with arbitrary input distributions in the presence of delay-limited sources are investigated. We apply the above-mentioned non-uniform probability assignment schemes to adjust the input probability distribution of each transmitting node based on the corresponding channel characteristics and harvested energy constraint.

3.2.1 Preliminaries

System Model

We consider a system where multiple delay-limited transmitting nodes communicate with a receiver over a wireless link as shown in Fig. 3.6. Assuming that each component is equipped with a single antenna, the transmitted signal from k^{th} source node during i^{th} symbol duration is selected from finite alphabets denoted by $\mathcal{S}_k = \{X_1^k, X_2^k, \dots X_M^k\}$ with $|\mathcal{S}_k| = M_k$ indicating the cardinality of the signal set. In addition, the input signal has a certain probability of occurrence denoted by $p_j = \Pr\{X = X_j^k\}$ where $j \in \{1, 2, \cdots, m_k\}$, and it is limited by a

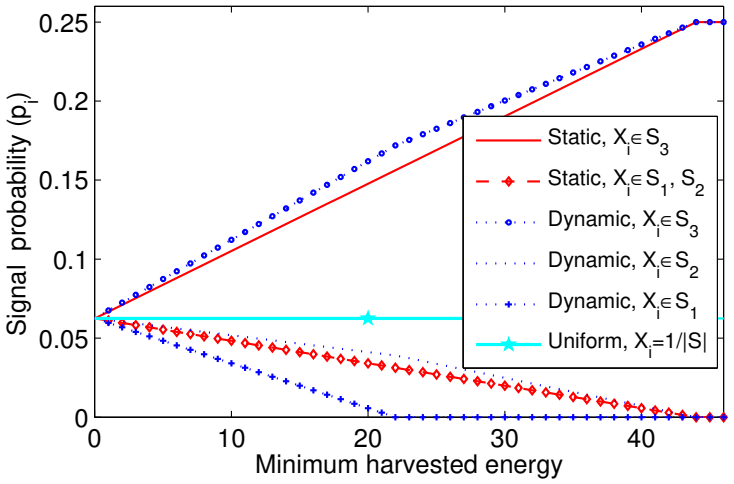

(a) Alphabets probabilities

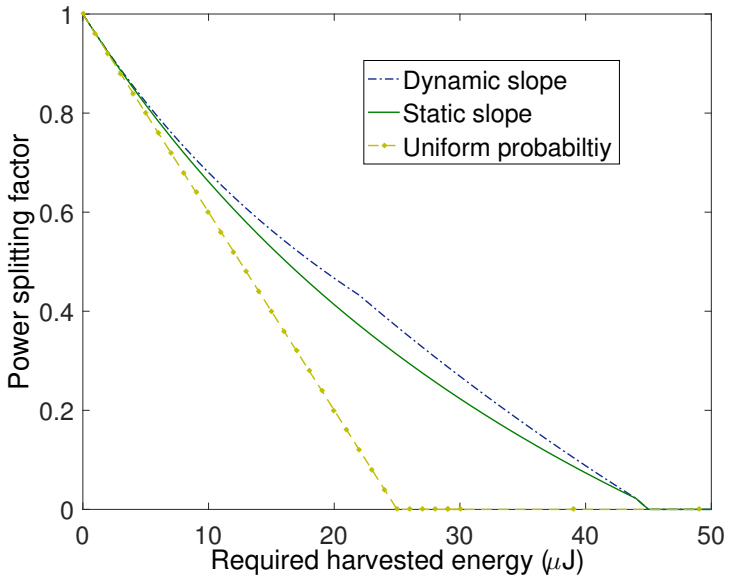

(b) Splitting factor

Figure 3.5: Effect of $\mathcal{X}$ on optimization parameters for 16-QAM

peak energy constraint i.e., $|X|^2 \leq E_{pk}$.

While harvesting energy, each user stores received data packets generated by a delay-sensitive source that requires certain statistical QoS guarantees described by the QoS exponent θ. More specifically, the tail distribution of the k^{th} source node buffer is required to have an exponential decay with the rate controlled by the exponent θ_k, and the buffer

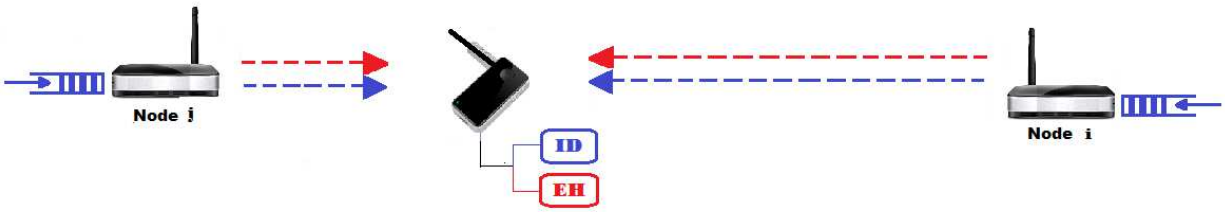

Figure 3.6: Multi-user SWIPT model with delay-limited sources

violation or overflow probability is described as

$$\Pr\left\{Q_i \geq Q_{max}\right\} \approx e^{-\theta_k Q_{max}} \tag{3.25}$$

where Q_k denotes the stationary queue length in the k^{th} source node buffer, and Q_{max} is the buffer overflow threshold. This buffer constraint dictates the arrival rates that can be supported by the wireless link. Each transmitter operates over non-overlapping time intervals such that

$$\sum_{k=1}^{N} \tau_k \leq 1 \tag{3.26}$$

where τ_k is the operation interval for node k. The wireless link between the k^{th} source node and the receiver experiences flat-fading and the channel fading coefficient in the i^{th} symbol period is denoted by $g_k[i]$. Hence, the received signal in this duration can be expressed as

$$Y_k[i] = g_k[i]W_k[i] + N[i] \tag{3.27}$$

where $W_k \in \mathcal{S}_k$ is the transmitted signal from source k and $N[i] \sim \mathcal{CN}(0, N_0)$ is the circularly symmetric complex Gaussian noise with zero mean and variance N_0. Furthermore, the receiver has ID and EH components, and it applies power splitting scheme, i.e., ρ fraction of the received energy is allocated to ID and $1-\rho$ to EH, in order to carry out the corresponding operations simultaneously.

Information Transfer

When multiple sources transmit their message to a common receiver over an orthogonal interval of duration τ_i with $i \in \{1, 2, \cdots, K\}$, the throughput can be expressed using input-output mutual information as follows:

$$\begin{aligned} R &= \sum_{i=1}^{K} \tau_i I(X_i; Y) \\ &= \sum_{i=1}^{K} \tau_i \left[\sum_{k=1}^{m_i} p_k \int_{-\infty}^{\infty} f_{Y|X_k,\mathbf{g}} \log \left[\frac{f_{Y|X_k,\mathbf{g}}}{\sum_{j=1}^{m_i} p_j f_{Y|X_j,\mathbf{g}}} \right] dy \right] \end{aligned} \tag{3.28}$$

which leads to

$$R = \sum_{i=1}^{K} \tau_i \left[-\sum_{k=1}^{m_i} \frac{p_k}{\pi N_0} \int_{-\infty}^{\infty} \int_{-\infty}^{\infty} e^{-|v|^2} \log \left[\sum_{j=1}^{m_i} p_j e^{\left[-|v+\gamma_d|^2 + |v|^2 \right]} \right] d\mathbf{v} \right] \tag{3.29}$$

where where $f_{Y|X_k,\mathbf{g}} = \frac{1}{\pi N_0} e^{-\frac{\left| Y - g_i X_k \right|^2}{N_0}}$ is the conditional probability density function of Y given X_k as well as fading coefficient $\mathbf{g} = (g_1, g_2, \ldots, g_n)$, $v = \frac{Y - g X_k}{\sqrt{N_0}}$, $\gamma_d = \frac{g}{\sqrt{N_0}}(X_k - X_j)$, and $\mathbf{v}$ is a vector consisting of real and imaginary component of v.

Energy Harvesting

Assuming that each source send information-bearing signal from a finite input signal constellations, the average harvested energy at the receiving end can be determined as follows:

$$\mathcal{E}_{hv} = \mathbb{E} \left\{ \sum_{j=1}^{N} \tau_j z_j[i] \left| X_j[i] \right|^2 + \sigma^2 \right\} \tag{3.30}$$

where $z_j = |g_j|^2$ and the expectation is with respect to both z_j and the distributions of the finite alphabet input signals from each source. Obviously, when energy harvesting is considered alone, it is more beneficial to assign higher probabilities to those with higher energy levels among the input signals.

3.2.2 Optimal Resource Allocation Strategies

Based on the remarks stated earlier, the choice of probability distribution for finite alphabet inputs depends on the overall objective. Thus, incorporating energy transfer along with information-bearing signal influences the optimal transmission policy, and in such a case, better performance, i.e., tradeoff, can be achieved with non-uniform probability distribution. In other words, alphabets that have different energy levels should have unequal probabilities for SWIPT. According to Theorem 3.1.1, the number of different energy levels in the finite-alphabets available for the k^{th} source node, assuming QAM constellation with size m_k, is given as

$$N_s^k = \sum_{i=0}^{\sqrt{\frac{m_k}{4}}-1} \left(\sqrt{\frac{m_k}{4}} - i \right) \tag{3.31a}$$

$$N_r^k = \frac{m_k}{8} + \sum_{i=0}^{\sqrt{\frac{m_k}{8}}-1} \left(\sqrt{\frac{m_k}{8}} - i \right) \tag{3.31b}$$

where N_s^k and N_r^k denote total number of different energy levels of k^{th} transmitting node when the constellation has square and rectangular geometries, respectively. Except 4-QAM, constellation size is always greater than the number of unequal energy levels, and this implies that there exist some signals that have equal energy levels as mentioned earlier. Hence, it is meaningful to optimally adjust probabilities assigned to each subset $\mathcal{S}_i^k$, where the superscript k denote the source node, in accordance with the harvested energy constraint. In Section 3.1, we introduced two novel approaches, but the way probabilities are adjusted are modified due to the presence of multiple users as follow:

Source dependent static slope characteristics

Probabilities assigned to subsets change linearly for each increment in the required harvested energy, but the slope which characterizes probability-energy relation is not necessarily the same for all transmitting nodes. This is because different nodes might experience different

channel characteristics, and hence the fraction of the total harvested energy obtained from each node should be determined accordingly. Thus, we have

$$\mathcal{X} = \sum_{i=1}^{K} b_i \mathcal{E}_i \tag{3.32}$$

where $\mathcal{X} = \frac{\chi}{1-\rho}$, $b_i = \tau_i z_i$ and $\mathcal{E}_i = \mathbb{E}\{|X_i|^2\}$. Therefore, in order to be fair among the transmitting nodes, the contribution from each node is determined based on its channel conditions as follows:

$$\mathcal{X}_k = \frac{\mathcal{X}|b_k|^2}{\sum_i^K |b_k|^2} \tag{3.33}$$

where

$$\mathcal{X} = \sum_{k=1}^{K} \mathcal{X}_k. \tag{3.34}$$

Therefore, the average energy level from the k^{th} source node becomes

$$\mathcal{E}_k = \frac{\mathcal{X}_k}{b_k}. \tag{3.35}$$

Then, based on (3.10), the probability-energy characteristic for the k^{th} transmitting nodes can be formulated as follows:

$$p_{s_i}^k(\mathcal{E}_k) = \delta_k \mathcal{E}_k + p_i^k(\mathcal{E}_k)\Big|_{\mathcal{X}=0} \tag{3.36}$$

where $p_i^k(\mathcal{X})|_{\mathcal{X}=0} = \frac{1}{|\mathcal{S}_k|}$ defines the signal probability for the k^{th} source node in the absence of energy constraints. In addition, $\delta_k = \frac{|\mathcal{S}^k| - |\mathcal{S}_m^k|}{\mathcal{E}_\Delta(|\mathcal{S}_m^k||\mathcal{S}^k|)}$ if $X_i \in \mathcal{S}_N^k$, otherwise $\delta_k = -\frac{1}{(\mathcal{E}_\Delta|\mathcal{S}^k|)}$ where $\mathcal{E}_\Delta = \mathcal{E}_{mx}^k - \mathcal{E}_{mn}^k$. As can be seen from (3.36), for a given transmitting node, each subset probability changes with the same slope which implies $p_{s_i}^k = p_{s_j}^k$, except those of $\mathcal{S}_N^k$, and constellation size remains the same, i.e., $|\mathcal{S}^k|$ until $\mathcal{E}_k = \mathcal{E}_{mx}^k$.

Source dependent dynamic slope characteristics

In this scenario, the probability assignment for the finite-alphabets of each transmitting node is in such a way that a subset with the lowest-energy signals in the k^{th} source node is assigned the smallest probability i.e., $p^k_{s_i} < p^k_{s_{i+j}}$ for $j = \{1, 2, \ldots, N-i\}$. In addition, as the fraction of the required harvested energy from node k increases, a subset with the lowest energy level from the available active alphabets is discarded, for instance $\mathcal{S}^k_i$ from $\mathcal{S}^k_{sc}$, and this process continues successively until $\mathcal{E}_k = \mathcal{E}^k_{mx}$. The probability-energy characteristic curve of each transmitting node depends on the ranges of harvested energy allocated to the corresponding source. Hence, various transmitting nodes might enforce different slope characteristics shown in the Fig. 3.7, and the likelihood of a certain subset (or alphabet) in one node could be different in the other for the same contribution of harvested energy level.

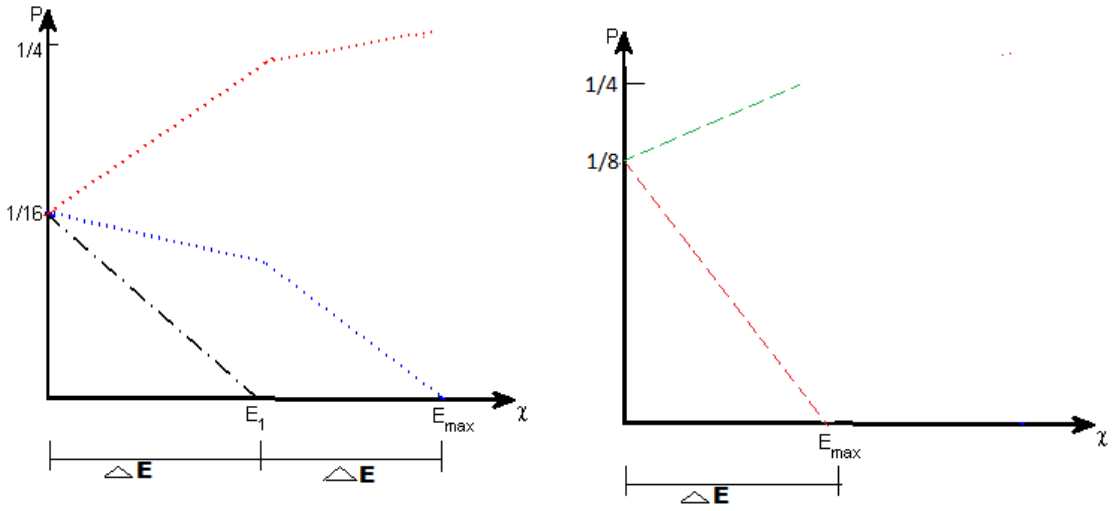

(a) Two-level increment for node i (b) One-level increment for node j

Figure 3.7: Probability-energy relation for multiple transmitting nodes with 16-QAM and 8-QAM finite alphabet inputs

Let us denote the required harvested energy in the j^{th} increment for the k^{th} source node as $\mathcal{X}^k_\Delta$. Then, the probability-energy relation for this node and increment is mathematically

given as follows:

$$p_{s_i}(\mathcal{E}_k) = \delta_{s_i}^{kj}\mathcal{E}_k + p_{s_i}^{kj}\Big|_{\mathcal{E}_k=\S_{mn}^k} \tag{3.37}$$

where $\delta_{s_i}^{kj}$ defines the slope of the probability of subset $\mathcal{S}_i^k$ in the interval $\mathcal{X}_{mn}^j \leq \mathcal{E}_k \leq \mathcal{X}_{mx}^j$, and the last term in (3.37) denotes this subset probability when $\mathcal{E}_k$ takes the lowest value during the j^{th} increment. The signal probabilities for each set of energy levels can be iteratively obtained as mentioned earlier in Section 3.1.2.

Throughput Maximization

In the presence of multiple UEs where information-decoding and energy-harvesting components are served by a common receiving antenna and RF chains, there are more variables to adjust in order to improve the rate-energy trade-off. The achievable data rate of users operating based on time-division multiple access scheme with finite alphabet input while applying power splitting at the receiving end can be modified as:

$$R_i(\boldsymbol{\tau}, \rho, \mathbf{p}) = -\sum_{i=1}^{N}\tau_i\sum_{k=1}^{M}\frac{p_k}{\pi N_0}\int_{-\infty}^{\infty} e^{-|v|^2}\log\left[\sum_{j=1}^{M} p_j e^{\left[\rho(-|v+\gamma_d^{kj}|^2+|v|^2)\right]}\right]d\mathbf{v} \tag{3.38}$$

where γ_d^{kj} is as defined earlier. Thus, the constant arrival rate for i^{th} delay-limited source node depends on the power splitting factor ρ as well as operating interval τ_i, and the explicit expression for the effective capacity is given as follows:

$$C_i^e(\theta_i, \tau_i, \rho, \mathbf{p}) = -\frac{1}{T\theta_i}\log\mathbb{E}\left\{e^{\frac{\theta_i\tau_i}{\pi N_0}\left[\sum_{k=1}^{m} p_k\mathbb{E}_v\left\{\log_2\left[\sum_{j=1}^{m} p_j e^{\left[-\rho|v+\gamma_d|^2+\rho|v|^2\right]}\right]\right\}\right]}\right\} \tag{3.39}$$

where $\mathbf{p} = [p_1, p_2, \cdots, p_N]$. Based on Proposition 3.1.2, it is obvious that the achievable data rate given in 3.38 is concave with ρ, and τ_i as well. This implies that $e^{\theta R_i(\tau_i,\rho)}$ is log-convex function, and hence the effective capacity given in 3.39 is jointly concave with the uplink operation interval τ_i and the power splitting factor ρ assuming that the probabilities for the finite-alphabet inputs are known apriori. Therefore, in order to investigate trade-off between effective capacity and harvested energy by optimally adjusting operating intervals and splitting factor for the given probability distribution, we formulate an optimization problem as follows:

$$\text{(PR:3.2)} \quad \max_{\tau,\rho} \quad \sum_{i=1}^{N} C_i^e \tag{3.40a}$$

$$\text{subject to } (1-\rho)\mathcal{E}_{hv} \;\geq\; \mathcal{X} \tag{3.40b}$$

$$\sum_{i=1} \tau_i \leq 1 \tag{3.40c}$$

$$\tau_i \geq 0, \quad \forall \; i \in \{1, 2, \cdots, N\} \tag{3.40d}$$

$$0 \leq \rho \leq 1 \tag{3.40e}$$

where χ denotes the required harvested energy at the EH component. The last three constraints specify the domain set of the optimization parameters. Given the probability distribution, the above problem is in general convex, and hence optimum splitting factor and operating intervals can be obtained numerically. We develop an algorithm that iteratively solve the problem as indicated in Algorithm 2.

Energy-Efficiency Maximization

In limited energy resource environment, total energy expenditure to transfer every bit of information is a critical issue. Basically, energy is consumed to power data processing circuitry and send the signal to the target destination through a wireless fading medium. Let P_{c_i} denote the circuit power consumption of node i, and assume that it is independent of

the transmitted power level P_i for $P_i > 0$. Hence, the total energy expense of multiple users over an uplink operation interval of T seconds becomes

$$E_{tot} = TP_c + \sum_{i=1}^{N} \tau_i P_i \quad \text{(Joules)} \tag{3.41}$$

where $P_c = \sum_{i=1}^{N} P_{c_i} = NP_{c_i}$, and without loss of generality, we assume each node consumes energy at the same rate. Since the information-bearing signal is used to energize the EH component, harvested energy should be subtracted from the total energy consumption in the formulation of the energy efficiency metric in order to reflect the net system energy consumption, as discussed in the literature [42] [43]. Thus, the effective energy efficiency of the system is expressed

$$\eta(\rho, \mathbf{p}, \boldsymbol{\tau}) = \frac{\sum_{i=1}^{N} C_i^e}{\mathbb{E}\Big\{TP_c + \sum_{i=1} \tau_i P_i - \chi\Big\}} \tag{3.42}$$

where $\boldsymbol{\tau} = [\tau_1, \tau_2, \cdots, \tau_N]$ is a vector consisting of each node operating interval. Note that $T = 1$ in the sequel for simplicity. Any increment in demand for harvested energy requires additional ΔP_i that could change the system efficiency by $\Delta\eta_s$. In addition, Remark 1 encourages uniform distribution in the absence of harvested energy constraint, but this might not be the optimal strategy when energy efficiency is considered, as will be discussed shortly. Hence, it is necessary to formulate optimization problems so as to trace the impact of harvested energy on the optimal operating points, and determine optimal transmit power

as well as system energy efficiency. Thus, we have

$$\begin{aligned} \text{(PR:3.3)} \quad & \max_{p_i,\rho,\tau} \ \eta \\ \text{subject to} \ & (1-\rho)\mathcal{E}_{hv} \ \geq \ \mathcal{X} \\ & \sum_{i=1} \tau_i \leq 1 \\ & \tau_i \geq 0, \quad \forall \ i \in \{1, 2, \cdots, N\} \\ & 0 \leq \rho \leq 1. \end{aligned} \tag{3.43}$$

Despite the difficulty in obtaining closed-form expressions for the optimizing parameters from the above problem (PR:3.3), standard numerical tools can easily be applied to determine the solution. We provide the procedure in Algorithm 2 to solve (PR:3.2) and (PR:3.3), but we skip the details for brevity.

Algorithm 2 QoS-Driven SWIPT with finite input constellations

```
Given: 𝒳
for i = 1 to N do
    Determine 𝒳_i using (3.35)
    Determine the number of energy levels for the node using (3.31)
    Determine corresponding signal probabilities
    if Static Slope then
        Apply the relation given in (3.36)
    else
        Use (3.37) for dynamic slope characteristics
    end if
end for
Decide the performance metric
if Throughput Max then
    Apply Gauss-Hermit approach to Solve (PR:2)
else
    Apply Dinkelbach method to solve (PR:3)
end if
Determine the optimal signal probabilities and power-splitting factor
```

3.2.3 Numerical Analysis

In this section, we provide numerical results considering 16-QAM constellation given in Fig. 3.3 where there are three different energy levels with probabilities denoted as p_1 for $\mathcal{S}_1$, p_2 for $\mathcal{S}_2$ and p_3 for $\mathcal{S}_3$. The transmitted signal energy per second is limited by the peak value, $2W$. In regard to the channel characteristics, we consider two scenarios, namely case X with $g_1 < g_2$ and case Y with $g_2 < g_1$. The QoS exponential decaying characteristics for user 1 and user 2 denoted by θ_1 and θ_2, respectively.

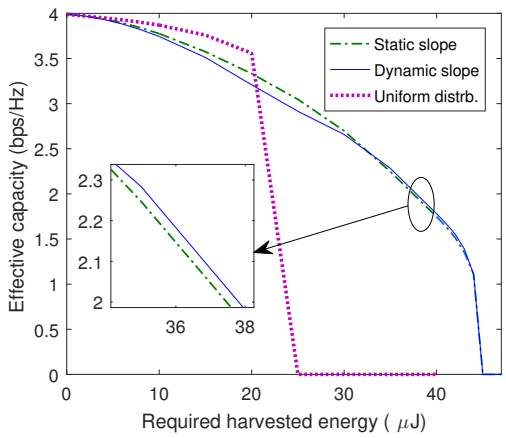

(a) C^e vs. required harvested energy

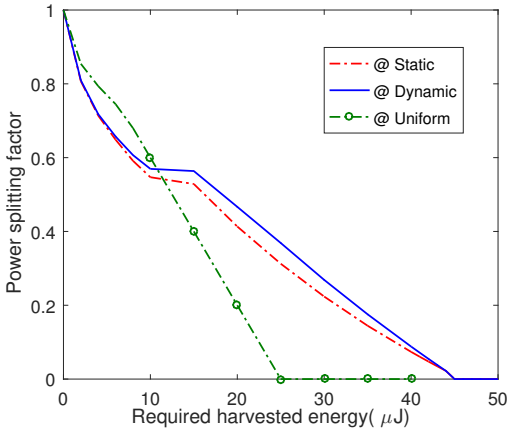

(b) Power splitting factor vs. χ

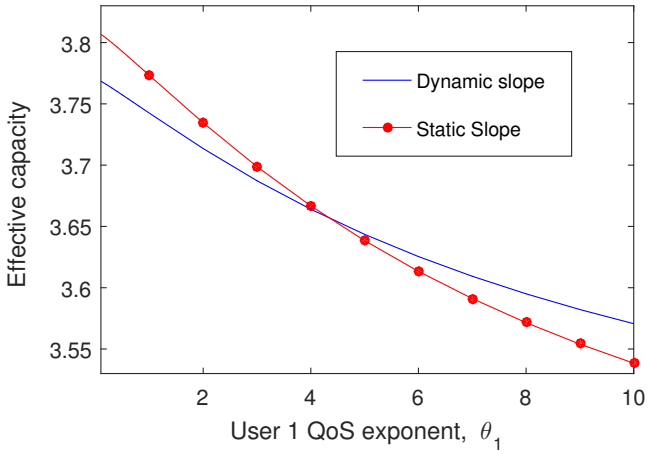

(c) C^e in (bps/Hz) vs. user 1 QoS exponent, θ_1

Figure 3.8: Throughput maximization for 16-QAM

Fig 3.8 illustrates the impact of harvested energy constraint and QoS exponent parameter on the overall throughput, i.e., sum effective capacity of the system. More specifically, Fig. 3.8a shows the tradeoff characteristics between required harvested energy and effective capacity, and from this figure, we observe that non-uniform probability distribution using either static or dynamic slope characteristics outperforms the uniform probability distribution as the demand hits higher values, and this encourages to harvest more energy by giving priority for high energy alphabets. Furthermore, the advantage of static scheme over the dynamic case is a function of harvested energy constraint. In any case, the power splitting factor is optimally adjusted accordingly, and Fig. 3.8b describes how the splitting factor ρ changes with χ. Meanwhile, Fig. 3.8c characterizes effect of changing θ_1 on the sum effective capacity, and as can be seen from the figure, strict QoS constraint hurts the throughput, i.e., effective capacity decreases with exponential decaying parameter θ. Besides, the performance of dynamic and static slope approaches depends on each node channel characteristics and their QoS constraint parameter. For instance, when user 1 has looser QoS constraint, i.e., $\theta_1 < \theta_2$, in scenario Y, static approach achieves better throughput.

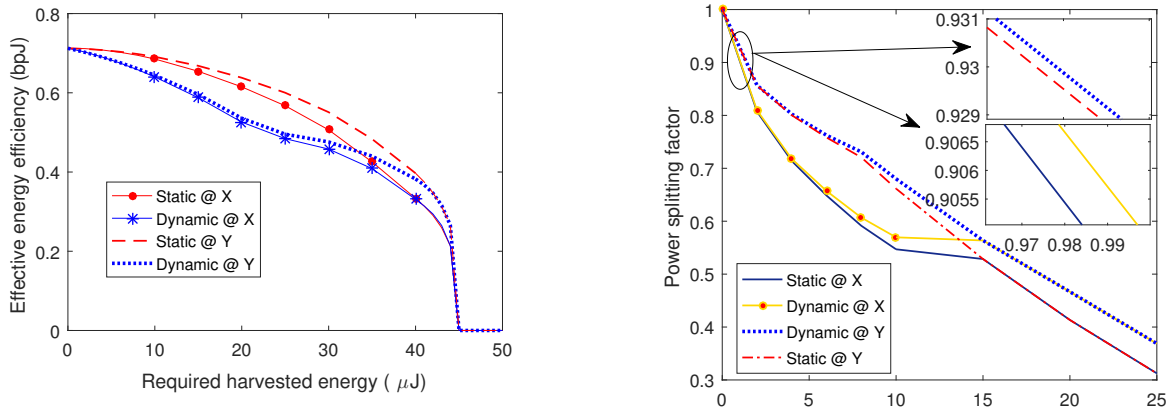

(a) Average energy efficiency in (bpJ/Hz) vs. required harvested energy

(b) Power splitting factor vs. minimum harvested energy (μ J)

Figure 3.9: EE-Maximization under $\theta_1 = 0.1$ and $\theta_2 = 1.0$

On the other hand, the tradeoff characteristics for the system energy efficiency and required harvested energy is plotted in Fig. 4.7. From the figure, we can see that en-

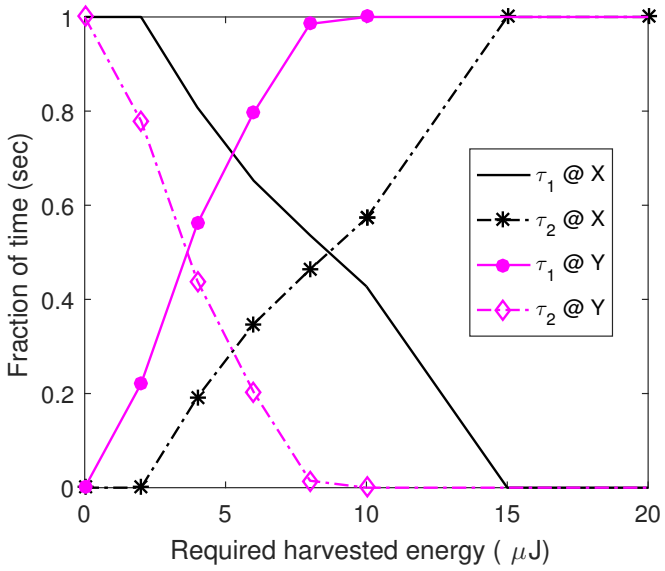

Figure 3.10: Operating interval vs. required harvested energy for EE-Max.

ergy efficiency is a non-increasing function and it reduces with χ despite harvested energy is subtracted in the denominator to reflect the net energy consumption. Comparing the non-uniform probability assignment approaches, static slope characteristics mostly leads to better energy efficiency in both cases, i.e., Case X and Case Y. The optimal time allocated for user 1 and user 2 while maximizing the system energy efficiency are illustrated in Fig. 3.10 as a function of harvested energy constraints. We observe that EE maximization gives more priority for less stringent QoS constraint under small harvested energy despite the user might experience smaller fading power, i.e., $\theta_1 < \theta_2$ and $g_1 < g_2$. However, as energy demand increases, more time is allocated for the node with better wireless link, ant this goes until χ forces only that node to transmit. Similar observation can be made from Fig. 3.10 under scenario Y with $\theta_1 > \theta_2$. Furthermore, better channel conditions result in more harvested energy over a smaller duration of time, which leads to higher power splitting factor at the receiving end.

Chapter 4

Energy-Efficient Resource Allocation in Fading Multiple Access Channels

This chapter presents energy-efficient power allocation schemes considering multiple users operating through fading MACs. First, novel expressions for the optimal power levels that maximize the instantaneous energy efficiency in a MAC are identified. Then, simultaneous wireless information and power transfer (SWIPT) is incorporated and optimization problems are formulated considering two types of antennas architecture, namely separated and common, for the ID and EH components at the receiving node. In all the cases, energy-efficient node selection policies and analytical expressions for the optimal transmit power level are derived. In addition, the performance tradeoffs for energy-efficient transmission policies when SWIPT is incorporated is studied, and the corresponding closed-form expressions for the optimal transmit power levels are derived focusing on the system energy efficiency while satisfying energy and power constraints. Furthermore, the impact of peak power constraint on the optimal resource allocation strategy is characterized. In addition, optimal system EE, and the impact of harvested energy demand on the optimal EE and other critical parameters such as power splitting ratio are identified.

Section 4.1 introduces the system model and illustrates the receiving architecture for

the SWIPT scenario. In Section 4.2, energy efficiency maximization problem is formulated for multiple access channels, and closed-form expressions for the optimal power allocation strategies are derived. In Section 4.3, wireless power transfer is incorporated with information transfer, and optimization problems are formulated considering harvested energy constraint. Numerical results are discussed at the end of Section 4.2 and 4.3.

4.1 System Model

We consider a wireless multiuser network in which N transmitting (TX) nodes send information-bearing signals on the same frequency band to a receiving (RX) node through a multiple access channel as shown in Fig. 4.1 Each TX node is equipped with a single antenna,

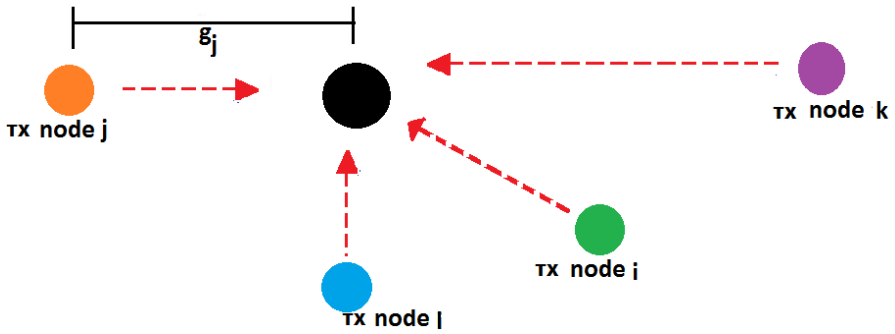

Figure 4.1: Multiuser model in multiple access channel

and the transmitted signal from node $i \in \mathcal{S} = \{1, 2, \cdots, N\}$ in the k^{th} symbol duration is $X_i[k] \sim \mathcal{CN}\big(0, P_i[k]\big)$ with instantaneous power $P_i[k] \in \mathcal{P}$ where

$$\mathcal{P} = \bigcup_{i \in \mathcal{S}} \Big\{ P_i : 0 \leq P_i \leq P_i^{mx} \Big\}. \tag{4.1}$$

The RX node has information decoding (ID) component and, if SWIPT is being considered, it has an energy harvesting (EH) component as well. The ID component applies successive interference cancellation to decode the information from the received signal. We first study energy-efficient resource allocation among the TX nodes focusing on information transfer

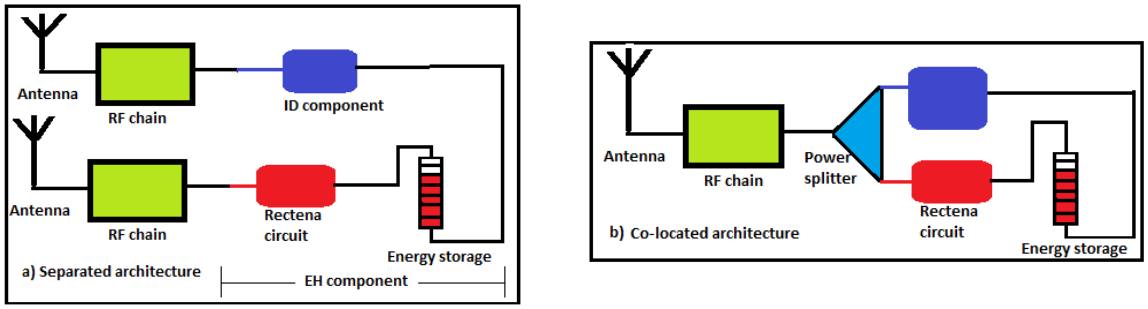

(a) Separated antenna architecture

(b) Common antenna architecture

Figure 4.2: RX architecture for SWIPT

only. Then, we analyze system's energy efficiency with SWIPT. In this case, we consider two scenarios as shown in Fig. 4.2. As can be seen, ID and EH components, in the separated architecture, have independent antenna and RF chains to collect the signals, whereas a single antenna is used in the common antenna architecture. In the latter model, power splitting scheme is applied to share the received signal proportionally, e.g., $\sqrt{\rho} : \sqrt{1-\rho}$ to ID and EH components where ρ denotes the fraction of power allocated to the ID component.

In regard to the wireless channel, we assume that the link between any TX node and the receiver experiences frequency-flat fading. The complex fading coefficient for the channel between i^{th} node and an information-receiving antenna during k^{th} symbol duration is denoted by $r_i[k]$, and the channel power gain, $h_i[k] = |r_i[k]|^2$, is constant over a block length T and changes independently to a new value based on its probability distribution. Similarly, $g_i[k] = |z_i[k]|^2$ is the normalized channel power gain for the link between i^{th} source and the EH receiving antenna in the case of separated architecture, while $h_i[k]$ is again denotes the channel power gain for the ID component. Furthermore, it is assumed that channel side information is available at both ends. Therefore, the received signal at the destination in the k^{th} symbol duration is given as

$$Y[k] = \sum_{i=1}^{N} w_i X_i[k] + N[k] \tag{4.2}$$

where $w_i \in \{r_i, z_i\}$ depending on the ID-EH receiving antenna architecture, and $N[k] \sim \mathcal{CN}(0,1)$ is the complex Gaussian noise component at the receiving antenna with unit variance.

4.2 Energy Efficiency in MAC

In wireless communication systems, user energy efficiency (EE) can be quantitatively measured by bits of information reliably transferred to a receiver per unit consumed energy at the transmitter. In the presence of multiple users, it is also relevant and meaningful to consider the system EE. For instance, the consideration of the system energy efficiency enables us to allocate resources in such a way that the overall energy usage becomes more efficient. With this motivation, we consider the system energy efficiency, which is defined as

$$\eta = \frac{\text{Throughput}}{\text{Total consumed energy}} \qquad \text{(bits/Joule)}. \tag{4.3}$$

In this chapter, we focus on the instantaneous achievable data rate per unit consumed energy, and given the fading state realization, sum-rate capacity over a block interval of T seconds is

$$\mathcal{R}_{sum}[k] = T \log_2 \Big(1 + \sum_{i=1}^{N} \gamma_i[k]\Big) \qquad \text{(bits/Hz)} \tag{4.4}$$

where $\gamma_i[k] = h_i[k]P_i[k]$. For simplicity, we eliminate the index k of symbol duration in the sequel. Based on (4.4), sum-rate capacity is maximized when each source transmits at its peak power level in the absence of average power constraint. However, this might not be the optimal strategy for MAC when energy efficiency is considered, as will be discussed shortly.

Let's now consider energy consumption. Note that energy is consumed to power the data processing circuitry and send the signal to the target destination. Let P_{c_i} denote the circuit power consumption of node i, and assume that it is independent of the transmitted power level as long as $P_i > 0$. However, if no information is transmitted, there is no power

consumption, i.e., $P_i = 0$ implies $P_{c_i} = 0$. Hence, the total energy consumption of multiple users over an uplink operation interval of T seconds becomes

$$E_{tot}(\boldsymbol{P}) = T\sum_{i=1}^{N}\Big(P_{c_i} + P_i\Big) = T\Big(P_c + \sum_{i=1}^{N} P_i\Big) \qquad \text{(Joules)} \tag{4.5}$$

where $\boldsymbol{P} = [P_1, P_2, \cdots, P_N]$, and $P_c = \sum_{i=1}^{N} P_{c_i}$. We also denote the sum of the circuit powers of k users as $\sum_{i=1}^{k} P_{c_i} = P_c^k$. Thus, the system energy efficiency is expressed as

$$\eta(\boldsymbol{P}) = \frac{\log_2\Big(1 + \sum_{i=1}^{N}\gamma_i\Big)}{P_C + \sum_{i=1}^{N} P_i}. \tag{4.6}$$

It is obvious that the sum-rate capacity and total consumed energy are concave and affine functions of $\boldsymbol{P}$, respectively. Besides, both are differentiable. Hence, according to Proposition 2.9 stated in [93], the system energy efficiency given in (4.6) satisfies the criteria for pseudo-concavity.

As noted earlier, analytical characterizations of optimal transmission policies and the corresponding system efficiency have not been addressed in the literature to the best of our knowledge. Hence, we formulate an optimization problem to determine the energy-efficient power allocation strategy for fading multiple access channels as follows:

$$\text{(PR:4.1)}: \qquad \max_{\boldsymbol{P}} \;\; \eta(\boldsymbol{P}) \tag{4.7a}$$

$$\text{subject to} \quad P_i\big(P_i - P_i^{mx}\big) \leq 0 \quad \forall i \tag{4.7b}$$

where $\boldsymbol{P} = [P_1, P_2, \cdots, P_N]$ and $i \in \mathcal{S}$. The constraint given in (4.7b) guarantees that the transmitted signal power level from each source node is within the feasible set $\mathcal{P}$. Since the objective function is pseudo-concave, as noted above, and the constraint is convex, from Proposition 2.8 and 2.9 stated in [93], Karush-Kuhn-Tucker (KKT) conditions are necessary and sufficient to obtain the globally optimal solution. This implies that there is a unique

optimal solution for (PR:4.1).

Theorem 4.2.1 *The energy-efficient power allocation strategy for MAC is carried out based on channel power gain, i.e., priority is given to the strongest wireless link, and hence if we assume, without loss of generality that,* $h_N > h_{N-1} > \cdots > h_2 > h_1$*, the optimal transmit power level from the* i^{th} *node is given by the following:*

$$P_i^* = \min\left\{\tilde{P}_i, P_i^{mx}\right\} \tag{4.8}$$

where

$$\tilde{P}_i = \xi_i \frac{e^{\mathcal{W}\left(\frac{\Gamma_i}{e}\right)+1} - \Omega_i}{h_i}, \tag{4.9}$$

and

$$\xi_i = \begin{cases} 1 & P_{i+1}^* = P_{i+1}^{mx} \quad (4.10a) \\ 0 & \text{otherwise} \quad (4.10b) \end{cases}$$

with $\xi_N = 1$, $\Omega_N = 1$, $\Gamma_N = -1 + h_N P_c$. In addition, $\Gamma_i = \sum_{j=i+1}^{N}(h_i - h_j)P_j^{mx} - 1 + h_i P_c^i$, and $\Omega_i = 1 + \sum_{j=i+1}^{N} h_j P_j^{mx}$ for $i \in \{1, 2, \cdots, N-1\}$. Finally, $\mathcal{W}(\cdot)$ above denotes the Lambert function. *Proof:* See Appendix D.

From Theorem 4.2.1, we note that the selection of the energy-efficient transmitting node depends on the channel gain, total circuit power consumption and the peak power constraint. For instance, considering the case where only node N is transmitting and the transmission power is less than the peak P_N^{mx}, the corresponding optimal transmit power level is given as

$$P_N^* = \frac{e^{\mathcal{W}\left(\frac{h_N P_c - 1}{e}\right)+1} - 1}{h_N}. \tag{4.11}$$

Due to the fact that $\mathcal{W}(x)$ is a monotonically increasing function for $x > 0$, we notice that the transmitted power level reduces with lower circuit power consumption. Thus, energy

efficiency improves as the power is lowered further and further if the circuit power consumption decreases. In addition, the optimal strategy always requires the node that has a weaker channel gain to be silent unless the peak power constraint of the transmitting node is active. For instance, if the solution for the transmit power level of the node with the best wireless link exceeds the peak power constraint, i.e., $\tilde{P}_N > P_N^{mx}$, then this node operates at its peak power level and the node with the second best wireless link transmits an information-bearing signal to the receiver at power P_{N-1}^* and the rest of the nodes stay silent unless $\tilde{P}_{N-1} > P_{N-1}^{mx}$.

Meanwhile, if multiple nodes have the same channel gain as the link with the highest gain, i.e., $h_k = h_N$ where $k \in \mathcal{S}$, then there will be infinitely many solutions (transmission power levels) that lead to the same optimal energy efficiency. In such a case, these transmission power levels can be determined using

$$\sum_{k=1}^{|\mathcal{A}|} P_k = \frac{\omega^*}{h_N} \tag{4.12}$$

where ω^* is given in (D.6) in Appendix D, and $\mathcal{A} = \Big\{k : h_k = h_N \text{ for } k \in \mathcal{S}\Big\}$. For instance, considering two TX nodes, (4.12) becomes $P_1 + P_2 = P^*$ where P^* is the total optimal power level determined by $\frac{\omega^*}{h_N}$, and the above claims can be clearly observed in Fig.4.3, where we plot the energy-efficiency as a function of the power level of each TX node. In the first case, assuming one has higher channel gain compared with the other, say $h_1 > h_2$, the numerical results illustrate that the global solution is obtained on the P_1 edge of the $P_1 - P_2$ power plane, i.e., $P_1 = 1.89$ and $P_2 = 0$, or it is at the coordinate (0.46, 1.89, 0) on the $\eta - P_1 - P_2$ three dimensional space, i.e., lies on the surface of the $\eta - P_1$ plane. This justifies that the energy-efficient policy encourages node 1 to transmit, when $h_1 > h_2$, at power level P_1^* while node 2 is kept silent provided that P_1^* does not violate the peak power constraint. On the other hand, if both nodes have the same channel gain, i.e., $h_1 = h_2$, any point on the line $P_1 + P_2 = P^*$ achieves the optimal solution as can be seen from Fig. 4.3b. This supports the statement that there are infinitely many solutions that satisfy (4.12).

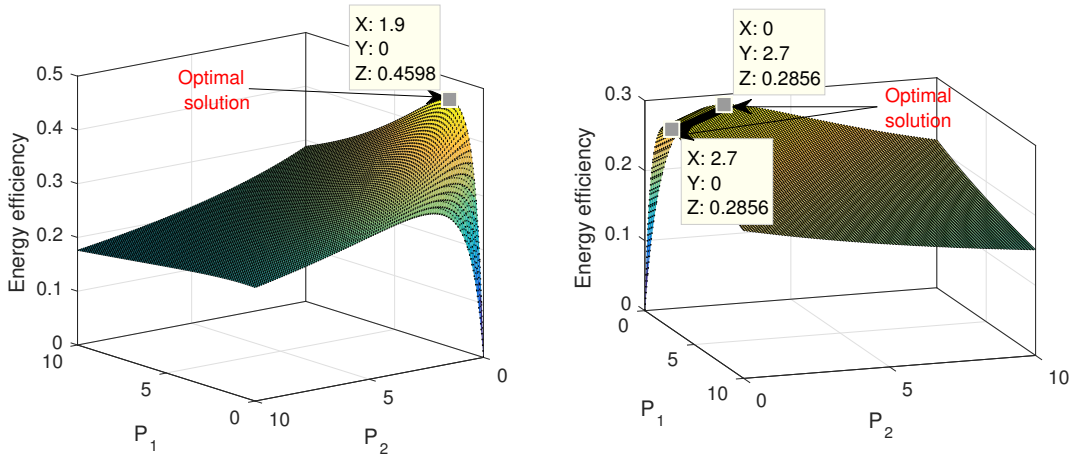

(a) For $h_1 > h_2$ (b) For $h_1 = h_2$

Figure 4.3: Energy efficiency (bpJ/Hz) plot for two-TX nodes over a multiple access channel

We also note from Theorem 1 that the optimal power allocation policy for the active node does not follow the water-filling strategy. Without loss of generality, let us consider the node with the highest channel gain, say h_N, and ignore the peak power constraint. Then, we analyze the asymptotic characteristics of the corresponding transmit power level, which is determined by (4.11), as channel gain goes to infinity and zero as follows.

$$\begin{aligned}\lim_{h_N\to\infty} P_N(h_N) &= \lim_{h_N\to\infty} \frac{e^{\mathcal{W}(\frac{h_N P_c - 1}{e})+1} - 1}{h_N} \\ &\approx e\Big[\lim_{h_N\to\infty} \frac{e^{\mathcal{W}(\frac{h_N P_c}{e})}}{h_N}\Big] \\ &= \frac{P_c}{\lim_{h_N\to\infty} \mathcal{W}(\frac{h_N P_c}{e})}\end{aligned} \tag{4.13}$$

where the last equality is obtained by substituting the identity property of Lambert function, i.e., $e^{\mathcal{W}(x)} = \frac{x}{\mathcal{W}(x)}$. Since $\mathcal{W}(x)$ is a monotonically increasing function for $x > 0$, we conclude that the optimal transmission power level is reduced as channel gain increases, unlike in the water-filling approach.

On the other hand, as $h_N \to 0$, we can apply L'Hopital's rule to determine the asymptotic

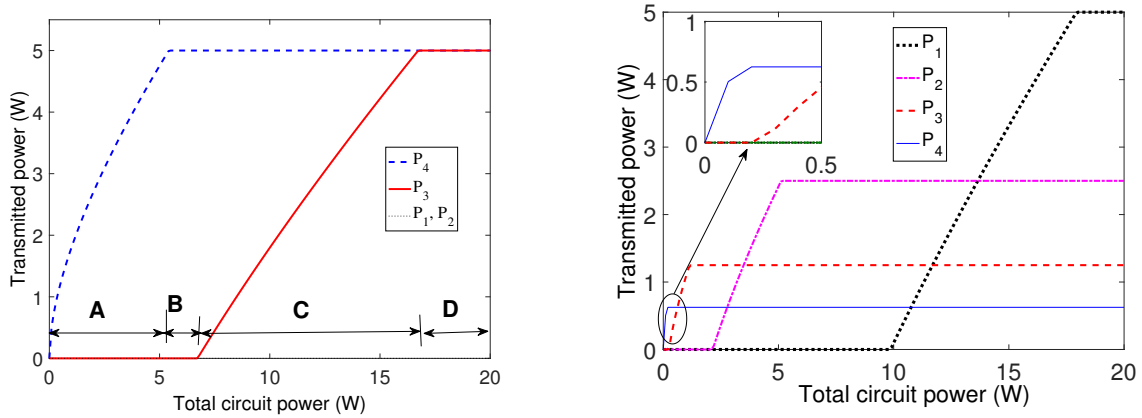

(a) All nodes have the same peak power limit, i.e., $P_i^{mx} = P^{mx}$ for $i \in \mathcal{Q}$

(b) Nodes have varying peak power levels, i.e., $P_i^{mx} = 2^{-i+1}P^{mx}$, for $i \in \mathcal{Q}$

Figure 4.4: Optimal power allocation with four TX nodes

value for very low h_N values as follows:

$$\begin{aligned}\lim_{h_N \to 0} P_N(h_N) &= \lim_{h_N \to 0} \frac{\frac{d}{dh_N}\left[e^{\mathcal{W}(\frac{h_N P_c - 1}{e})+1} - 1\right]}{\frac{d}{dh_N} h_N} \\ &= e \frac{\lim_{h_N \to 0} \mathcal{W}(\frac{h_N P_c - 1}{e})}{\lim_{h_N \to 0} \frac{h_N P_c - 1}{e}(1 + \mathcal{W}(\frac{h_N P_c - 1}{e}))} \\ &= \frac{\mathcal{W}(-\frac{1}{e})}{1 + \mathcal{W}(-\frac{1}{e})}\end{aligned} \tag{4.14}$$

Using the fact that $\mathcal{W}(-1/e) = -1$, we can clearly see that $\lim_{h_N \to 0} P_N(h_N) = \infty$. This implies more power is allocated as the channel gets worse similar to the channel inversion policy, and the required transmitted power level is unbounded for very small h_N.

As noted earlier, the transmitted power level from each TX node depends on the total circuit power consumption and peak power constraint, and we justify this using numerical results. It is assumed that there are four TX nodes with the peak power constraint $P_i^{pk} = 5$W or 37dBm where $i \in \mathcal{Q} = \{1, 2, 3, 4\}$. The bandwidth of the transmitted signal is assumed to be 10MHz, and the receiver noise is assumed to be white Gaussian with power spectral density -140dB/Hz. We assume that the channel fading gains are $h_1 = -44$dBm, $h_2 = -42$dBm, $h_3 = -41$dBm, and $h_4 = -40.5$dBm at the carrier frequency of $f_c = 900$ MHz.

Fig. 4.4 and Fig. 4.5 illustrate the effect of circuit power on the system energy efficiency and optimal power allocation strategy, respectively. More specifically, from Fig. 4.4a and Fig. 4.4b we observe that $P_i = 0$ for $i \in \mathcal{Q}$ when $P_c = 0$, i.e., if the circuit power is negligibly small, the strategy which benefits energy-efficiency encourages the TX nodes to transmit at lower and lower power levels. We also notice that, for $P_c \neq 0$, the node which has the best channel link, i.e., node 4, is always active, and its transmit power level increases with P_c. In addition, when the optimal transmitted power level of node 4 reaches to its peak, i.e., $P_4^* = P_4^{mx}$, the node with the next best channel link, i.e., node 3, could be allowed to transmit depending on the value of P_c as shown in both figures. For instance, in region B, node 4 is operating at its peak while node 3 is silent, whereas in region C node 3 becomes active. In region D, both node 4 and node 3 are at their peak power level, but node 2 and node 1 are still in silent mode. Furthermore, comparing Fig. 4.4a and Fig. 4.4b, we see that when those nodes with better channel links have limited peak power, energy-efficient power allocation strategy allows other nodes with weaker channel conditions, such as node 1 and 2 in this example, to transmit as P_c increases.

In regard to the energy efficiency, each increment in P_c hurts the average EE as shown in Fig. 4.5, and for very high circuit energy consumption per unit time, few bits of information will be transmitted per joule of total consumed energy. Moreover, when there are unequal power constraints and those with better channel gains, such as node 4 and node 3, have limited peak power as indicated in Fig. 4.4b, the system operates at a lower efficiency especially if the circuit power consumption is relatively large.

4.3 Energy Efficiency with SWIPT

Energy efficiency is essential in the presence of limited available resources, but this can be further challenging with SWIPT as there are additional optimization variables to control and constraints to satisfy. In this section, we study these issues and provide optimal resource

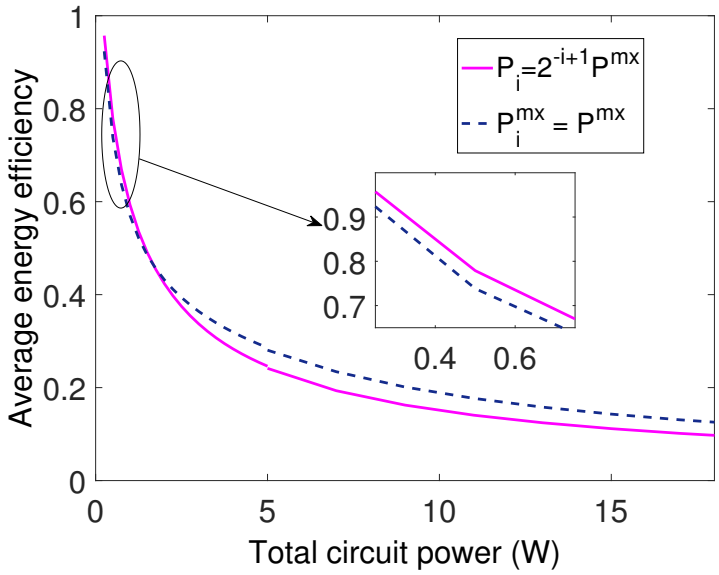

Figure 4.5: Energy efficiency (bpJ/Hz) vs. total circuit power consumption

allocation strategies while taking harvested energy constraints into account. Since the physical architecture of receiving antennas and RF chains have direct impact on the analysis of energy efficiency and the corresponding optimal parameters, we consider an architecture with separated antennas and an architecture with a common antenna for the ID and EH components in the following two subsections, respectively.

4.3.1 Separated Antenna Architecture

In this scenario, TX nodes broadcast information and power simultaneously to ID and EH components that have independent antennas and RF chains to collect the transmitted signal. Since the information-bearing signal is also used to energize the EH component, harvested energy should be subtracted from the total energy consumption in the formulation of the energy efficiency metric in order to reflect the net system energy consumption, as discussed in the literature [42] [43]. Based on this remark, the system energy efficiency for multiple

access channels is given as follows:

$$\eta_s(\boldsymbol{P}) = \frac{\log_2\left(1+\sum_{i=1}^{N}\gamma_i\right)}{\kappa+\sum_{i=1}^{N}P_i} \tag{4.15}$$

where $\kappa = P_C - \frac{\mathcal{E}_{hv}^s(\boldsymbol{P})}{T}$ denotes the total circuit power consumption minus the harvested energy per unit time, with the harvested energy expressed as

$$\mathcal{E}_{hv}^s(\boldsymbol{P}) = T\beta\sum_{i=1}^{N} g_i P_i \qquad \text{(Joules)} \tag{4.16}$$

where $\beta \in [0,1]$ denotes energy conversion efficiency. Without loss of generality, we assume that $T = 1$ in the sequel. Since it is not possible to harvest more than the transmitted amount, we have $\kappa + \sum P_i > 0$.

In SWIPT, each TX node transmits a signal not only to send information to the ID component but also to energize the harvesting device. Hence, it is necessary to formulate an optimization problem in order to trace the impact of energy demand at the EH component on the optimal operating points and system energy efficiency. Thus, we have

$$\text{(PR:4.2)} \qquad \max_{\boldsymbol{P}} \;\; \eta_s(\boldsymbol{P}) \tag{4.17a}$$

$$\text{subject to} \quad \mathcal{E}_{hv}^s(\boldsymbol{P}) \geq \chi \tag{4.17b}$$

$$P_i\big(P_i - P_i^{mx}\big) \leq 0 \quad \forall i \in \mathcal{S} \tag{4.17c}$$

where χ denotes the required harvested energy at the EH component, which is limited by the capacity of the energy storage device. (4.17b) describes an energy harvesting constraint that needs to be satisfied by the optimal solution in addition to the power constraint given in (4.17c). Any increment in demand for harvested energy requires additional transmitted power ΔP_i and this could change the system efficiency by $\Delta\eta_s$. For the ease of analysis, the above optimization problem is split into two cases based on the harvested energy constraint.

Energy constraint satisfied with strict inequality

When the constraint is satisfied with strict inequality at the optimal operating point, i.e., $\mathcal{E}_{hv}^{s}(\boldsymbol{P}^{*}) > \chi$, the information-bearing signal can be transmitted at the energy-efficiency-maximizing power level. In this case, harvesting more than the demand is feasible, if the battery has enough capacity to store any additional harvested energy. Otherwise, there is an energy overflow, and only portion of the available energy can be harvested. Hence, χ will be deducted instead of $\mathcal{E}_{hv}^{s}(\boldsymbol{P^*})$, and this in turn modifies κ. From these, we observe that the net energy consumption relies on the battery capacity, denoted as B, and hence we have

$$\kappa = \begin{cases} P_C - \mathcal{E}_{hv}^{s}(\boldsymbol{P^*}), & B > \chi \quad (4.18a) \\ P_C - \chi & B = \chi. \quad (4.18b) \end{cases}$$

In order to determine the energy-efficiency-maximizing input, optimization problem (PR:4.2) is reformulated as

$$\begin{aligned} (\text{PR:4.2a}): \quad & \max_{\boldsymbol{P}} \ \frac{\log_2\left(1+\sum_{i=1}^{N}\gamma_i\right)}{\kappa+\sum_{i=1}^{N}P_i} \\ & \text{subject to} \quad P_i\left(P_i - P_i^{mx}\right) \leq 0 \quad \forall i \end{aligned} \tag{4.19}$$

Regardless of whether κ takes the value in (4.18a) or (4.18b), the denominator is still convex, and hence the objective function maintains pseudo-concavity. Therefore, KKT conditions are still sufficient and necessary for global optimality. The following proposition provides an analytical expression for the optimal transmission power level when the energy constraint is satisfied with strict inequality.

Theorem 4.3.1 *We again assume, without loss of generality that, $h_N > h_{N-1} > \cdots > h_2 > h_1$. Then, for the separated architecture, the corresponding energy-efficient power allocation strategy under a loose energy harvesting constraint, i.e., when $0 \leq \chi \leq \chi^*$, is given by the following:*

$$P_i^* = \min\left\{\xi_i \frac{e^{\mathcal{W}\left(\frac{h_i\Phi_i - 1}{e}\right)+1} - 1}{h_i}, P_i^{mx}\right\} \tag{4.20}$$

where

$$\Phi_i = \begin{cases} \dfrac{P_c^i}{1-g_i} & B > \chi \quad (4.21a) \\ P_c^i - \chi & B = \chi, \quad (4.21b) \end{cases}$$

and ξ_i is the same as defined in (4.10a) and (4.10b) with now P_i^* given in (4.20) being applied. In addition, χ^* is the harvested energy level at which the constraint starts being active.

Proof: See Appendix E.

Under the given assumptions, Theorem 4.3.1 demonstrates that the user with better channel conditions has the priority to communicate with the ID receiver, and power the EH component as well, in order to maximize the system energy efficiency. Furthermore, it is interesting to observe that P_i^* decreases for each incremental $\Delta\chi$ in the case of $B = \chi$, and the reason is as follows. First, it is immediate that Φ decreases with increasing χ. Knowing that Lambert function $\mathcal{W}(x)$ is a non-negative and increasing function for $x > 0$, $e^{\mathcal{W}(\cdot)}$ is also an increasing function. Thus, incremental demand $\Delta\chi$ reduces $\mathcal{W}(\frac{h_i\Phi-1}{e})$. Therefore, we conclude that the optimal transmit power P_i^* reduces further until $\chi = \chi^*$ based on (4.20). Intuitively, an increase in χ reduces κ and this in turn shifts the energy-efficiency maximizing point to the left, i.e., towards the origin or zero. Note that the power allocation policy given in (4.20) is optimal provided that the demand for harvested energy is below the threshold χ^*, i.e., the harvested energy constraint given in (4.17b) is inactive. However, when the demand exceeds this threshold, the constraint becomes active and this case is treated next.

Active energy constraint

When the energy demand is beyond χ^*, the constraint in (4.17b) becomes active, and hence the constraint is satisfied with equality. Thus, we have

$$\text{(PR:4.2b)} \quad \max_{\boldsymbol{P}} \ \frac{\log_2\left(1+\sum_{i=1}^{N}\gamma_i\right)}{P_C+\sum_{i=1}^{N}(1-g_i)P_i} \tag{4.22a}$$

$$\text{subject to} \ \ \mathcal{E}_{hv}^{s}(\boldsymbol{P}) = \chi \tag{4.22b}$$

$$P_i \leq P_i^{mx} \tag{4.22c}$$

$$P_i \geq 0, \ i \ \in \{1,2,\cdots,N\}. \tag{4.22d}$$

Here, the constraint in (4.22b) enforces the power allocation strategy to meet the demand while maximizing the energy efficiency. As noted earlier, the objective function in (4.22a) satisfies pseudo-concavity, and the constraints given in (4.22b) and (4.22c) are affine and convex, respectively. Thus, the optimization problem (PR:4.2b) is a concave-linear fractional problem [93], and its Lagrangian is given by

$$\mathcal{L} = \eta_s^b + \mu\Big(\mathcal{E}_{hv}^{s} - \chi\Big) - \sum_{i=1}^{N}\kappa_i(P_i - P_i^{mx}) + \sum_{i=1}^{N}\phi_i P_i, \tag{4.23}$$

where μ, $\kappa_i \geq 0$, $\phi_i \geq 0$ denote Lagrange multipliers, and

$$\eta_s^b = \frac{\log_2\left(1+\sum_{i=1}^{N}\gamma_i\right)}{P_c+\sum_{i=1}^{N}(1-g_i)P_i}. \tag{4.24}$$

Since (PR:4.2b) is a concave-linear fractional programming optimization problem, the KKT conditions are both necessary and sufficient for global optimality, and are given by

$$\frac{\partial \eta_s^b}{\partial P_i} + \mu^* \frac{\partial \mathcal{E}_{hv}^{s}}{\partial P_i} + \kappa_i^* + \phi_i^* = 0, \tag{4.25a}$$

$$\mu^*\Big(\mathcal{E}_{hv}^{s} - \chi\Big) = 0, \ \ \kappa_i^*(P_i^* - P_i^{mx}) = 0, \ \ \phi_i^* P_i^* = 0. \tag{4.25b}$$

Incorporating the complementary slackness conditions, i.e., $\kappa_i^* = 0$ and $\phi_i^* = 0$ for $0 < P_i < P_i^{mx}$, into (4.25a) and applying the derivatives, we get

$$\Xi^{-1}(\boldsymbol{P})\mathbf{h} - \Psi(\boldsymbol{P})\mathbf{d} = \mu \ln(2)\mathbf{g} \tag{4.26}$$

where $\Xi(\boldsymbol{P}) = \left(1+\sum_{i=1}^{N}\gamma_i\right)\left(P_c+\sum_{i=1}^{N}(1-g_i)P_i\right)$ and $\Psi(\boldsymbol{P}) = \left(P_c+\sum_{i=1}^{N}(1-g)i)P_i\right)^{-1} \ln\left(1+\sum_{i=1}^{N}\gamma_i\right)$. In addition, $\mathbf{h} = [h_1, h_2, \cdots, N]$, $\mathbf{g} = [g_1, g_2, \cdots, g_N]$ and $\mathbf{d} = [1-g_1, 1-g_2, \cdots, 1-g_N]$. From (4.26), it is not easy to get a closed-form expression for the optimal transmit power level. Meanwhile, in the presence of two-nodes, the complexity is reduced and it is possible to derive analytical expressions for the optimal solution. Moreover, in this setup, the impact of χ on the energy-efficient transmit power level of the TX nodes can be explicitly characterized as stated in the following proposition.

Proposition 4.3.1 *The energy-efficient SWIPT power allocation strategy for two-user MAC with separated architecture in the presence of an active harvested energy constraint is given by the following:*

(a) If $h_i > h_j$ and $g_i > g_j$ for $i \in \{1, 2\}$, then

$$\chi \in [\chi^*, \chi_a'] \;\Rightarrow\; \begin{cases} P_i^* = \frac{\chi}{g_i} \\ P_j^* = 0 \end{cases} \tag{4.27a}$$

$$\chi \in (\chi_a', \chi^{mx}] \Rightarrow \begin{cases} P_i^* = P_i^{mx} \\ P_j^* = \min\left(\frac{\chi - g_i P_i^{mx}}{g_j}, P_j^{mx}\right) \end{cases} \tag{4.27b}$$

(b) If $h_i > h_j$ and $g_i < g_j$ for $i \in \{1, 2\}$, then

$$\chi \in [\chi^*, \chi_b'] \;\; \Rightarrow \;\; \begin{cases} P_i^* = \frac{\chi}{g_i} \\ P_j^* = 0 \end{cases} \tag{4.28a}$$

$$\chi \in (\chi_b', \chi''] \;\; \Rightarrow \;\; \begin{cases} P_i^* = \left(\frac{g_j e^{\mathcal{W}(\frac{A}{e})+1} - g_j - h_j \chi}{g_j h_i - g_i h_j} \right)^+ \\ P_j^* = \min\left(\frac{\chi - g_i P_i^*}{g_j}, P_j^{mx} \right) \end{cases} \tag{4.28b}$$

$$\chi \in (\chi'', \chi^{mx}] \;\; \Rightarrow \;\; \begin{cases} P_i^* = \min\left(\frac{\chi - g_j P_j^{mx}}{g_j}, P_i^{mx} \right) \\ P_j^* = P_j^{mx} \end{cases} \tag{4.28c}$$

where χ' and χ^{mx} denote the maximum energy that can be optimally harvested from user i and the maximum achievable harvested energy from both users, respectively. In addition, χ'' denotes the energy demand at which user j starts transmitting at the peak power level. Furthermore, $A = aP_c + \chi\left(\frac{1-g_j}{g_j}a - \frac{h_j}{g_j}\right) - 1$, and $a = \frac{h_i g_j - h_j g_i}{g_j - g_i}$.

Proof: See refer to Appendix F.

From Proposition 4.3.1, we observe that once the demand exceeds the threshold χ^*, the harvested energy constraint overrides the energy-efficiency-maximizing solution, and the transmitted power level changes linearly with χ. In addition, the optimal policies depend on the wireless link characteristics between each node and the ID and EH components. For instance, assuming $h_1 > h_2$, it is more energy-efficient to keep node 2 silent and allow node 1 to transmit until it reaches its peak power level provided $g_1 > g_2$. On the other hand, when $g_1 < g_2$ while $h_1 > h_2$, keeping node 2 silent is energy-efficient only if the demand for harvested energy is below χ_b'. However, once the energy constraint exceeds χ_b', it becomes more advantageous to utilize resources from both users according to the power allocation policy given in (4.28b). This implies that better energy efficiency can be achieved by introducing node 2 instead of increasing the transmitted power level of node 1 by an equivalent amount. For $\chi_b' < \chi < \chi''$, there is a tradeoff between choosing a node which has

better channel link with the ID, node 1 in this case, and a node which has better channel link with EH component, i.e., node 2. As can be seen from the power allocation policy in (4.28b), more weight is given to node 2 until it utilizes its full capacity so long as the demand increases within the range $\chi_b' < \chi < \chi''$. This is because, for a given increment $\Delta\chi$ in this range, allocating additional power ΔP to node 2 instead of node 1 in order to satisfy the demand results in a linear gain of $\delta_E = (g_2 - g_1)\Delta P$, and this becomes significant compared to the logarithmic loss $\log\big((h_1 - h_2)\Delta P\big)$. Based on the EE expressions given in (4.15) and (4.24), more will be subtracted in the denominator if ΔP is allocated to node 2 to instead of node 1, and this achieves higher energy efficiency despite the reduction in the rate (the numerator) since $h_2 < h_1$.

Corollary 4.3.1 *Given the harvested energy demand, the optimal system energy efficiency for a two-user MAC under separated antenna architecture for ID and EH components with $h_1 > h_2$ is given as*

$$\eta_s^*(\chi) = \begin{cases} \dfrac{h_1 \log_2(\omega^*)}{-1 + h_1(P_c - \chi) + \omega^*} & ; \chi < \chi^* \quad (4.29a) \\ \dfrac{\log_2\big(1 + (h_1 - a_2 g_1)P_1 + a_2\chi\big)}{P_c + \big(1 - \frac{g_1}{g_2}\big)P_1 + b_2\chi} & ; \chi^* < \chi < \chi^{mx} \quad (4.29b) \end{cases}$$

where $a_2 = \frac{h_2}{g_2}$, $b_2 = \frac{1}{g_2} - 1$, and

$$\omega^* = e^{\mathcal{W}\left(\frac{-1 + h_1(P_c - \chi)}{e}\right) + 1}. \quad (4.30)$$

Proof: The optimal energy efficiency can be easily obtained by substituting the expressions for P_1^* and P_2^* given in (4.27)-(4.28) into (4.15). ■

According to the above characterization stated in Corollary 1, we observe that $\eta_s^*(\chi)$ is always an increasing function of harvested energy demand for $\chi < \chi^*$. This is because the numerator in (4.29a) decreases logarithmically with ω^* (which decreases with increasing χ) while the denominator reduces only linearly with ω^*. Hence, the ratio becomes an increasing

function of χ. On the other hand, for $\chi^* < \chi < \chi^{mx}$, we can see that $\eta_s^*(\chi)$ is neither an increasing nor a decreasing function of χ, and in such instances energy efficiency is generally expressed in the form of $\frac{\log_2(ax+b)}{cx+d}$. This is clearly a pseudo-concave function, and there exists a point beyond which efficiency starts to decrease for each increment in χ. Therefore, energy efficiency is maximized when the harvested energy demand reaches a point at which

$$\frac{\partial \eta_s^*(\chi)}{\partial \chi}\Big|_{\chi=\chi_{pt}} = 0. \tag{4.31}$$

Applying (4.31) to (4.29b), we get

$$\frac{a_2}{a_2\chi + 1 + (h_1 - a_2 g_1)P_1} - \frac{b_2 \log(a_2\chi + 1 + (h_1 - a_2 g_1)P_1)}{b_2\chi + P_c + \left(1 - \frac{g_1}{g_2}\right)P_1} = 0 \tag{4.32}$$

which leads to

$$Z \ln Z - Z = \varkappa \tag{4.33}$$

where $Z = a_2\chi + 1 + (h_1 - a_2 g_1)P_1$ and $\varkappa = \frac{a_2}{b_2}(P_c + \left(1 - \frac{g_1}{g_2}\right)P_1) - (1 + (h_1 - a_2 g_1)P_1)$. Thus, the optimal solution for χ_{opt} can be expressed using the Lambert function as follows:

$$\chi_{opt} = \frac{1}{a_2}\left[\frac{\varkappa}{\mathcal{W}(\frac{\varkappa}{e})} + (h_1 - a_2 g_1)P_1 - 1\right]. \tag{4.34}$$

4.3.2 Common Receiving Antenna Architecture

In this scenario, each TX node transfers both information and power simultaneously to ID and EH components that are physically connected to a common receiving circuitry, i.e., common antenna and RF chains. Thus, for supporting harvesting and decoding operations at the same time, the received signal power is split between ID and EH components based on the ratio $\rho : 1 - \rho$ as noted earlier in Section 4.1. Hence, the energy efficiency depends

not only on the transmit power level, but also on the power splitting factor ρ, and we have

$$\eta_c(\rho, \boldsymbol{P}) = \frac{\mathcal{R}(\rho, P_i)}{P_C + \sum_{i=1}^{N} P_i - \mathcal{E}_{hv}^{c}(\rho, \boldsymbol{P})} \tag{4.35}$$

where

$$\mathcal{R} = \log_2\Big(1 + \rho \sum_{i=1}^{N} \gamma_i\Big) \qquad \text{(bps/Hz)} \tag{4.36a}$$

$$\mathcal{E}_{hv}^{c} = \beta(1-\rho)\Big(\sum_{i=1}^{N} h_i P_i\Big) \qquad \text{(Joules).} \tag{4.36b}$$

In the co-located architecture, each incremental value of the harvested energy demand is satisfied at the expense of information transfer, i.e., lower data rate, and this is due to the power splitting factor ρ. In such a case, allocating power so that EH harvests more than the demand is not energy-efficient. Therefore, the necessary as well as sufficient condition is to satisfy the energy harvesting constraint with equality, and hence, given the energy demand χ, the splitting factor during the k^{th} symbol duration can be determined as follows:

$$\rho = \left[1 - \frac{\chi}{\sum_{i=1}^{N} h_i P_i}\right]^{+} \tag{4.37}$$

where $[x]^{+} = \max(x, 0)$. The splitting factor is lower bounded by the condition at which the demand reaches to the maximum value, χ^{mx}, that can be supported by all the available resources. At this point, the received signal power is allocated to the EH component only, and if the desired harvested energy goes beyond this threshold, energy outage occurs.

Having said this, the energy efficiency formulation for MACs in this scenario can be simplified further by substituting (4.37) into (4.36a) as well as (4.36b), leading to

$$\eta_c(\boldsymbol{P}, \chi) = \frac{\log_2\Big(1 + \sum_{i=1}^{N} \gamma_i - \chi\Big)}{P_C + \sum_{i=1}^{N} P_i - \chi}. \tag{4.38}$$

Given the harvested energy demand, both the achievable rate and energy efficiency depend on the transmitted power level from each source, and as the demand changes by some increment, $\Delta\chi$, so does the optimal transmit power level. Thus, in order to analytically illustrate the impact of harvested energy on the system energy efficiency and provide the optimal strategy, we formulate an optimization problem as follows:

$$\text{(PR:4.3)} \qquad \max_{\boldsymbol{P}} \ \ \eta_c(\boldsymbol{P}, \chi) \tag{4.39a}$$

$$\text{subject to} \qquad P_i \leq P_i^{mx} \tag{4.39b}$$

$$P_i \geq 0. \tag{4.39c}$$

Indeed, the objective function is a pseudo-concave function for the same reason stated earlier. Note that the harvested energy constraint has already been taken into account in the objective function while substituting the splitting factor.

Theorem 4.3.2 *We assume, without loss of generality that, $h_N > h_{N-1} > \cdots > h_2 > h_1$. Then, the energy-efficient power allocation strategy for SWIPT in MAC when the ID and EH components are physically connected to a single receiving circuitry is given as*

$$P_i^* = \begin{cases} 0 & ; \chi < \chi_i^{mn} \\ \hat{P}_i & ; \chi_i^{mn} \leq \chi \leq \chi_i^{mx} \\ P_i^{mx} & ; \chi > \chi_i^{mx} \end{cases} \tag{4.40}$$

where

$$\hat{P}_i = \frac{e^{W\left(\frac{c_i + d_i\chi}{e}\right)+1} - 1 - \sum_{j=1, j\neq i}^{N} h_j P_j^* + \chi}{h_i}, \tag{4.41}$$

$c_i = h_i P_c^i + \sum_{j=1, j\neq i}^{N} \big(h_i - h_j\big) P_j^* - 1$, $d_i = 1 - h_i$. *In addition, χ_i^{mn} and χ_i^{mx} are the threshold harvested energy levels at which the transmitted power from node i reaches peak and node $i+1$ becomes active, respectively. Note that $\chi_N^{mn} = 0$ and χ_1^{mx} is the maximum energy which can be harvested from all source nodes.*

Proof: See AppendixG. ■

As can be seen from the explicit expressions given in (4.40), the optimal strategies for energy-efficient SWIPT with power splitting scheme at the receiving end is neither water-filling nor channel inversion. In addition, the node selection criteria and the corresponding optimal power allocation policies directly depend on the wireless channel conditions and harvested energy constraints. For instance, for lower energy demand, node with the best channel condition is prioritized to transmit while keeping those that experience poor conditions silent. However, after the demand for the harvested energy enforces the selected node to utilize its full capacity, i.e., the node starts transmitting the signal at its peak power, each incremental demand, $\Delta\chi$, can be satisfied either by allowing the node with the second best link to transmit or by optimally adjusting the power splitting factor at the receiving end without activating any other node. The latter approach is the optimal solution for a certain range of harvested energy. As the demand increases further, allowing the node with the second highest channel power gain to send information and power becomes the best strategy rather than adjusting ρ. In such instances, the transmitted power level of this node is optimally adjusted to maximize the system energy efficiency while complying with the energy demand. With an increase in χ, this procedure continues until the node with the weakest link is required to transmit at its peak power.

Note that the energy efficiency expression given in (4.38) is always a decreasing function of χ, and in the next corollary, we provide an explicit expression for the optimal energy efficiency using the power allocation strategies given in (4.40).

Corollary 4.3.2 *The optimal energy efficiency for the TX nodes with a receiver having ID*

and EH components that operate using the power splitting scheme is explicitly given as

$$\eta_c^* = \begin{cases} \dfrac{\frac{h_N}{\ln(2)}\left(W\left(\frac{c_i+d_i\chi}{e}\right)+1\right)}{\left(c_i+d_i\chi+e^{W\left(\frac{c_i+d_i\chi}{e}\right)+1}\right)} & ;\chi_i^{mn} \leq \chi \leq \chi_i^{mx} \\ \dfrac{\log_2\left(1+\sum_{j=i}^{N} h_j P_j^{mx}-\chi\right)}{\left(P_c^i+\sum_{j=i}^{N} P_j^{mx}-\chi\right)} & ;\chi_i^{mx} \leq \chi \leq \chi_{i-1}^{mn}. \end{cases} \tag{4.42}$$

Proof: Substituting (4.40) into (4.38) and simplifying the expressions completes the proof.■

4.3.3 Numerical Analysis

In this section, we provide numerical results considering four transmitting nodes (similarly as considered in Section III) for the co-located ID-EH setting. For the case of separated architecture, we assume two nodes since analytical expressions are explicitly derived for this setting. The transmitted power level from each node is upper bounded by $P^{mx} = 5W$. The corresponding normalized average channel gains for ID and EH components are $\mathbb{E}\{h_1\} = -41dBm$, $\mathbb{E}\{h_2\} = -44dBm$, and $\mathbb{E}\{g_1\} = -43dBm$. For the link between Node 2 and EH receiver, we have considered two cases: $\mathbb{E}\{g_2\} = -45dBm$ and $\mathbb{E}\{g_2\} = -41dBm$ in order to investigate impact of channel conditions on the optimal strategy and overall performance. In regard to the EH receiver model, we assume that the device is able to utilize the harvested energy with $\beta = 1$.

Energy Efficiency

Fig. 4.6 illustrates the quasi-concave characteristics of the optimal energy efficiency for the two-user MAC in the presence of the harvested energy constraint. As can be seen from Fig. 4.6a, for the separated ID and EH components with separate receiving antennas, system EE improves with the harvested energy demand so long as this demand is satisfied with the EE-maximizing input. The threshold or boundary for this condition depends on the peak power constraint and channel conditions. Further increase in harvested energy demand

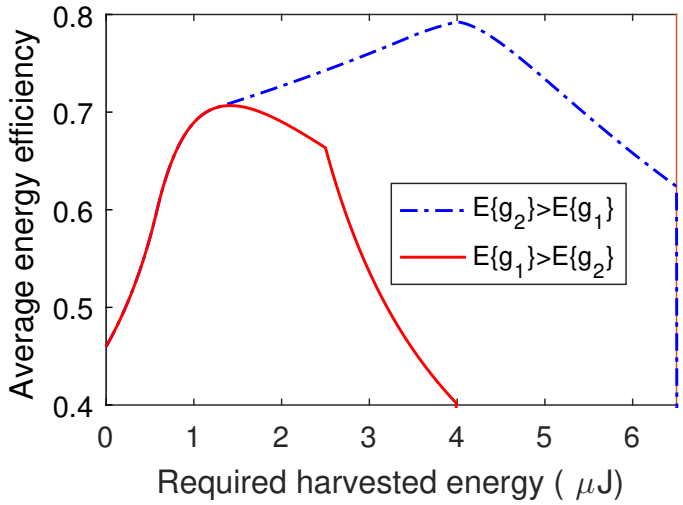

(a) Separated: η vs. χ

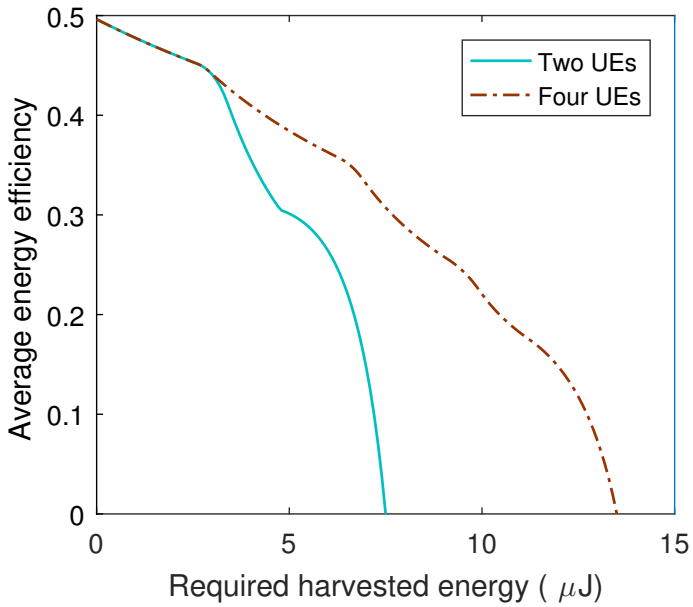

(b) Co-located: η vs. χ

Figure 4.6: Energy efficiency (bpJ/Hz) under two-user MACs with SWIPT

overrides EE optimality condition, i.e., the constraint forces the system to operate at a point below the most energy-efficient level. In the separated architecture, the overall performance depends on the corresponding channel gains of ID and EH components. For instance, when $h_1 > h_2$ and $g_1 > g_2$, activating user 2 always degrades the system efficiency, whereas if $g_1 < g_2$, allowing user 2 to transmit could lead to better efficiency for certain ranges of χ.

On the other hand, the system in the co-located scenario operates at the maximum energy efficiency point if no energy harvesting is required, and each incremental demand $\Delta\chi$ hurts the system EE. Hence, energy efficiency decreases with the increase in the harvested energy demand as shown in Fig. 4.6b. Similar characteristics are observed in the case of four-TX nodes except that more energy can be harvested when all the nodes are forced to utilize their peak power, at the cost of attaining lower energy efficiency levels, though. Furthermore, the impact of circuit power on the optimal energy efficiency is shown in Fig. 4.7 where the total circuit power is formulated as $P_C = P_{c_1} + P_{c_2} = \alpha P_{c1}$ for some $\alpha \geq 1$ when both users are active. As can be seen, when the second user becomes active, in region B, the additional circuit power consumption reduces the energy efficiency. Indeed, the upper most curve in region B corresponds to the case of $\alpha = 1.0$ in which P_{c_2} is negligible/ignored. Note that the second user circuit power consumption has no effect on the threshold at which this user starts transmission.

Transmit Power Level

As can be seen from Fig. 4.8 and Fig.4.9, transmitter and receiver parameters rely on the harvested energy demand in both separated and co-located architectures. Starting with the transmitted power level, we observe in Fig. 6.2a that P_1^* decreases as the EH component opportunistically harvests energy in the separated scenario. This achieves better efficiency for certain ranges of χ. Further increase in the energy demand leads to transmission at higher power levels, and this continues until the peak value is reached for node 1. The optimal transmit power level is slightly modified as shown in Fig. 6.2b when $h_1 > h_2$ but $g_1 < g_2$. In this case, P_1 first decreases and then increases with the harvested energy demand as in regions A and B, respectively. However, P_1 again starts to decrease in region C when additional energy obtained from user 2 becomes significant compared with the corresponding reduction in information rate. This continues until the harvested energy demand cannot be satisfied by user 2 as in region E where $P_2 = P^{mx}$ and $P_1 < P^{mx}$.

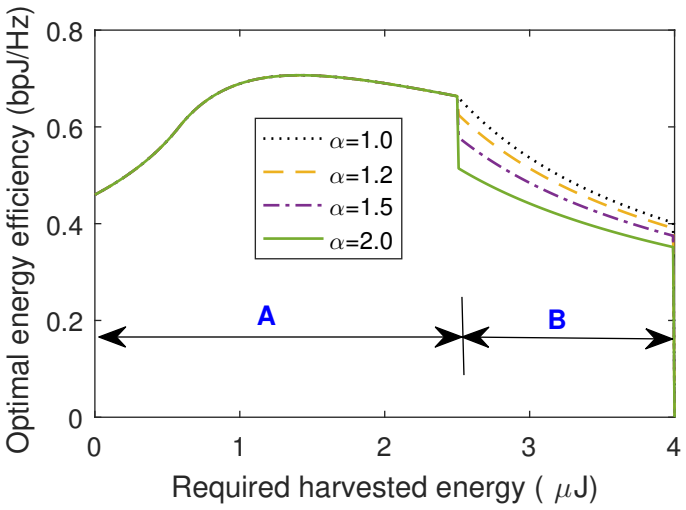

(a) Under $\mathbb{E}\{h_1\} > \mathbb{E}\{h_2\}$ and $\mathbb{E}\{g_1\} > \mathbb{E}\{g_2\}$

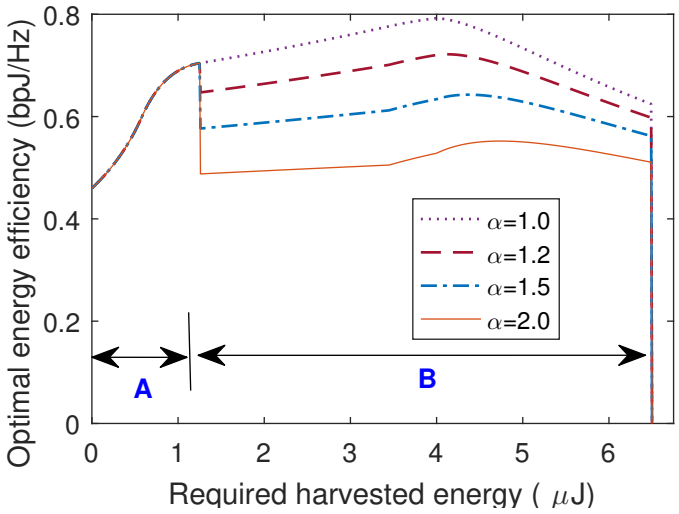

(b) Under $\mathbb{E}\{h_1\} > \mathbb{E}\{h_2\}$ and $\mathbb{E}\{g_1\} < \mathbb{E}\{g_2\}$

Figure 4.7: Effect of circuit power consumption

In regard to the co-located scenario, any increment in χ results in additional transmit power level regardless of the number of TX nodes. Besides, the node with the next better channel condition can only be triggered to transmit provided the other nodes that experience higher channel gain already transmit at their peak power level, and this is clearly shown in Fig. 4.9a and 4.9b. Furthermore, the effect of harvested energy constraint on the receiver power splitting parameter under the co-located architecture with a common receiving cir-

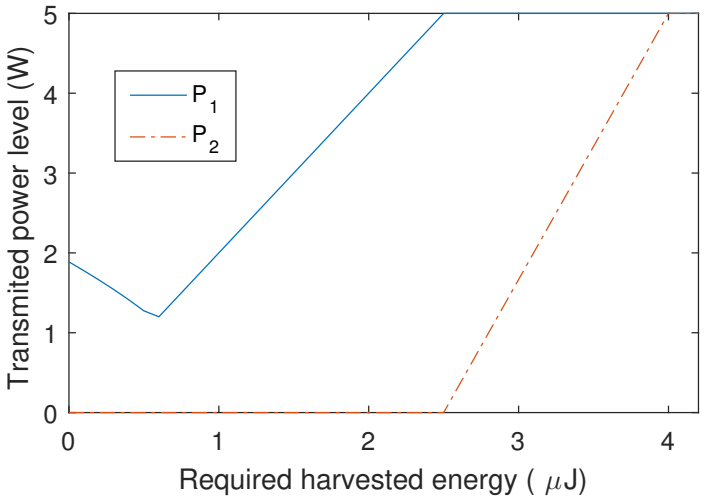

(a) $g_1 > g_2$

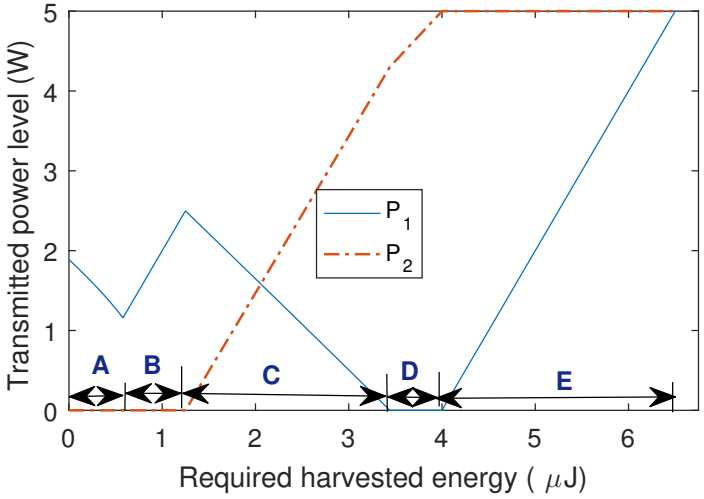

(b) $g_1 < g_2$

Figure 4.8: Optimal transmit power for two-TX nodes with SWIPT in the separated ID-EH scenario

---

cuitry is shown in Fig. 4.10. The figures illustrate how the optimal splitting factor varies when the demand χ increases, and we observe that ρ has mostly a decreasing, but sometime an increasing, characteristics. This is explained as follows. For instance in Fig. 4.10b, the power splitting factor decreases non-linearly in region A when the UE with highest channel gain is transmitting. The parabolic characteristics is due to the fact the ρ depends on both the harvested energy demand and the transmit power level, i.e., $\rho \propto \frac{\chi}{P}$. Then, in region B

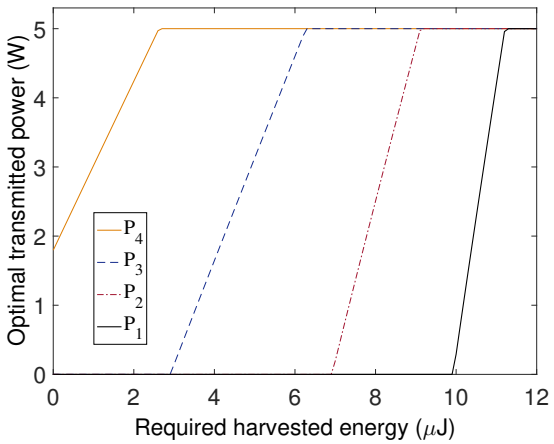

(a) In the four-TX nodes model

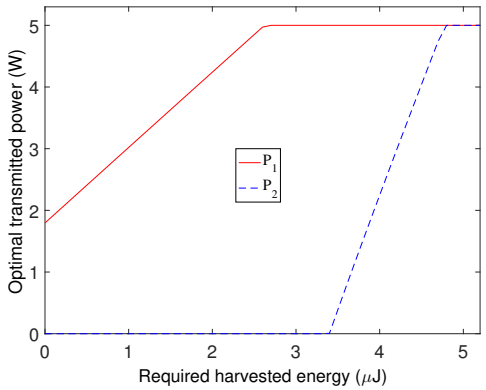

(b) In the two-TX nodes model

Figure 4.9: Optimal transmit power in the co-located ID-EH scenario

this UE is transmitting at its peak power, but the other UE is still silent, and hence the ρ decreases linearly. Meanwhile, as the demand increases further, the second UE becomes active and the additional energy is obtained from this user allows to allocate more power to the ID component. As a result, ρ increases with the harvested energy demand in region C. Once both users reach the peak, the splitting factor decreases linearly in region D until it is reach to the maximum energy level that can be harvested from the users.

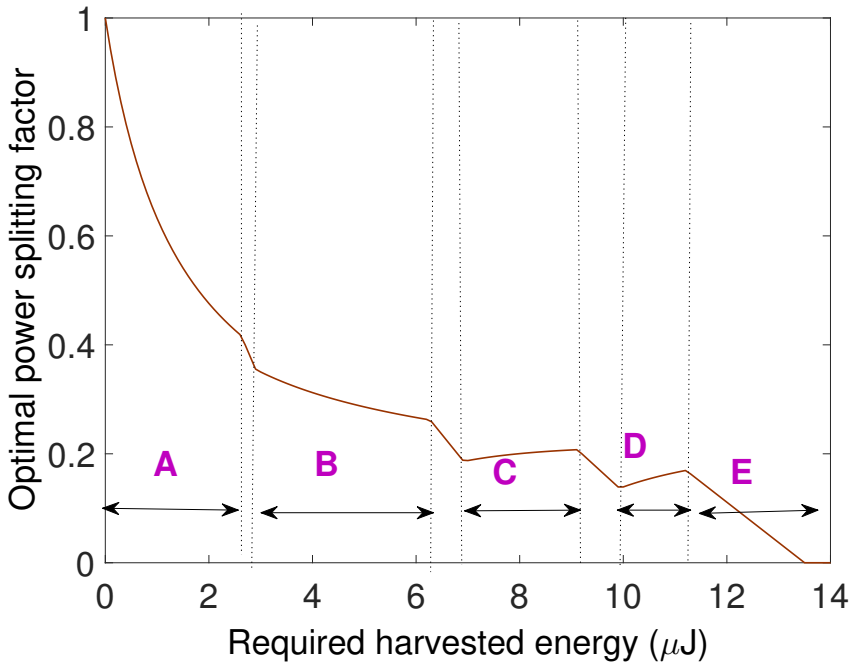

(a) In the four-TX nodes model

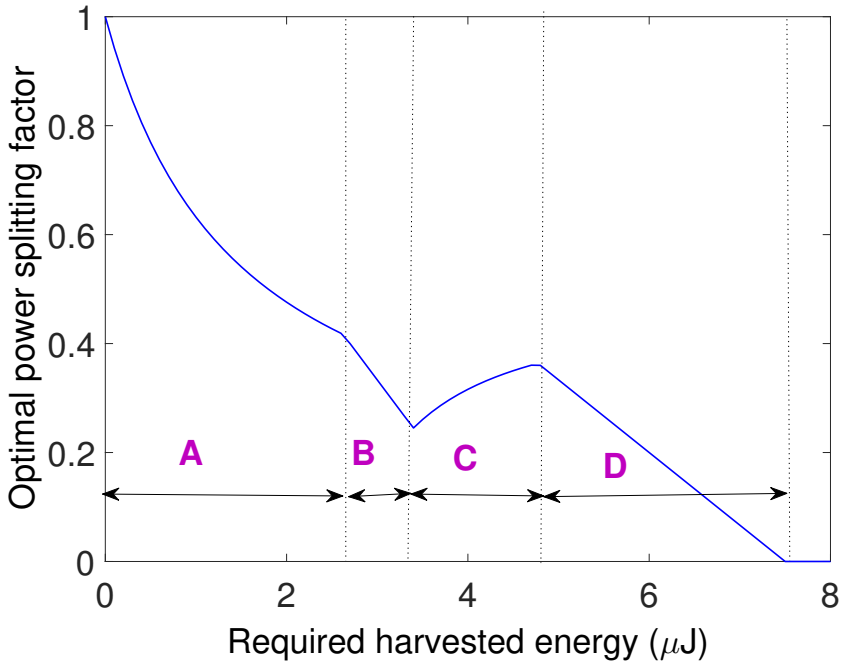

(b) In the two-TX nodes model

Figure 4.10: Optimal power splitting factor in the co-located ID-EH scenario

Chapter 5

Energy Harvesting Communication Networks Under Statistical QoS Constraints

In the previous chapters, simultaneous transmission of information and power to ID and EH components that are equipped with either a common or independent antenna architecture were considered, and throughput maximizing and energy-efficient power allocation strategies were determined while satisfying harvested energy constraints at the receiving node. In this chapter, the information receiver is assumed to have embedded power source, but transmitting nodes do not have battery or external power source, rather they harvest energy from a dedicated wireless power source. Based on the coordination of users to harvest energy and transfer information to the AP, three downlink-uplink wireless information and power transfer (WIPT) protocols are considered, and in all the cases, the influence of buffer overflow probabilities on the optimal operation intervals and their impact on the overall network performances, i.e., throughput and energy-efficiency are studied.

The remainder of the chapter is organized as follows: Section 5.1 introduces the system model and describes three types of WIPT operation strategies. In Section 5.2, throughput

maximization optimization problems are formulated for synchronous TDMA, asynchronous TDMA and simultaneous operation under statistical quality-of-service (QoS) constraints, and optimal solution are determined. In Section 5.3, energy-efficient time allocation strategies are obtained for each WIPT policy assuming delay-tolerant and delay-limited sources.

5.1 System Model and Preliminaries

5.1.1 System Model

In this chapter, we consider an energy harvesting communication networks in which an access point (AP) communicates with multiple users that do not have embedded energy sources. These users harvest energy from a dedicated wireless power transmitter (WPT) which broadcasts energy signal with power P_a over the downlink channel. Having equally divided time slots of T *sec*, wireless energy transfer occurs for a certain duration of each slot. Without loss of generality, we use a normalized unit for each cycle, i.e., $T = 1$. In addition, we assume that each user fully utilizes the harvested energy in each cycle (or time slot), as noted in [49] [56], to support data transmission and circuit power consumption.

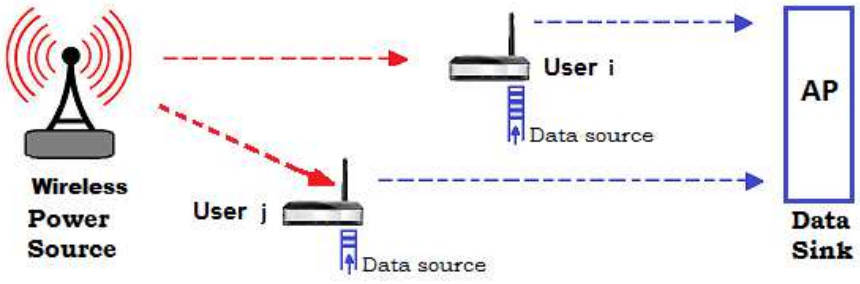

Figure 5.1: A delay-sensitive multiuser wireless-powered communication system

While harvesting energy, each user stores received data packets generated by a delay-sensitive source that requires certain statistical QoS guarantees described by the exponential QoS component θ. Moreover, the tail distribution of the buffer is required to have an exponential decay with rate controlled by the exponent θ, and this buffer constraint determines

the arrival rates that can be supported by the wireless link. Once energy is harvested, users send information-bearing signal over the remaining time of the slot to the AP. We assume that all the users transmit their data over the uplink channel in the same frequency band, and the transmitted signal from the i^{th} user is denoted by X_i where $i \in \mathcal{S} = \{1, 2, \cdots, N\}$. Note that the uplink power level P_i of this user directly depends on the amount of energy harvested. In regard to the channel, the link between an AP and any user experiences frequency flat-fading, and the channel fading coefficients changes from one block to another according to the distribution. Besides, the fading remains the same for both downlink and uplink operation of a given cycle.

5.1.2 WIPT Operation Strategies

As noted above, each user applies harvest-then-transmit protocol, and their coordination to carry out the downlink energy harvesting and uplink information transfer operations can be carried out using three difference schemes as will be discussed shortly. Namely, the scheme are synchronous energy harvesting with time-division multiple access (SH-TDMA) [49], synchronous harvesting with multiple access (SH-MAC), and asynchronous harvesting with time-division multiple access (ASH-TDMA) [56], and these are illustrated in Fig. 5.2 at the top of the next page. In the following sections, we will analyze and compare the performance gain achieved under each approach.

SH-TDMA

In this case, the downlink energy harvesting and each user uplink information transfer operations are carried out over non-overlapping time intervals, and WPT and AP are operating in half-duplex mode. Hence, all the users simultaneously harvest the downlink broadcast wireless power, but they transmit information uplink to the AP based on time-division multiple access scheme such that

$$\sum_{i=1}^{N} \tau_i \leq 1 - \tau_B \tag{5.1}$$

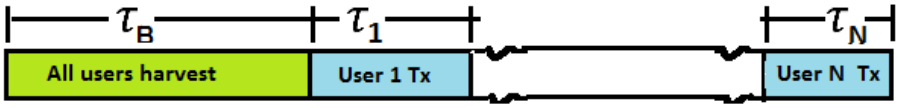

(a) SH-TDMA

(b) SH-MAC

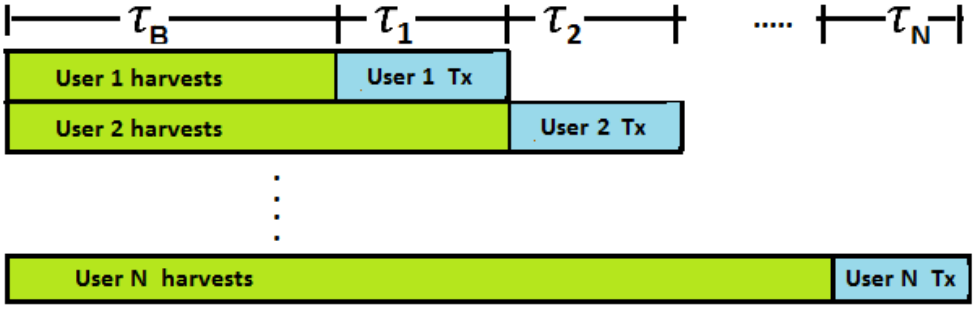

(c) ASH-TDMA

Figure 5.2: Various WIPT strategies

---

where τ_B denotes the fraction of the time for downlink operation, and τ_i is the time allocated for user i. Thus, the harvested energy at user i in one cycle can be expressed as

$$E_i^{hv} = \tau_B |g_i|^2 P_a \qquad \text{(Joules)} \tag{5.2}$$

where g_i denotes the channel fading coefficient between user i and WPT during downlink operation. Then, the transmitted signal power level from the i^{th} user is given as

$$P_i = \beta_i \frac{\tau_B}{\tau_i} |g_i|^2 P_a \tag{5.3}$$

where β_i denotes fraction of harvested energy utilized for data transfer while the remaining, i.e., $1 - \beta_i$, is consumed by the circuit.

Meanwhile, the uplink received signal at AP from the i^{th} user is given as

$$U_i = h_i X_i + N_i^u \tag{5.4}$$

where $N_i^U = \mathcal{CN}(0,1)$ is the circularly-symmetric complex Gaussian noise at the AP with unit variance, and h_i denotes the channel fading coefficient between user i and the AP the during uplink operation. Accordingly, the instantaneous achievable rate of user i becomes

$$R_i = \tau_i \log_2\left(1+\gamma_i\right) \quad \text{(bps/Hz)} \tag{5.5}$$

where $\gamma_i = |h_i|^2 P_i$ is the received SNR from user i in the k^{th} symbol duration. Substituting (5.3) into (5.5) and simplifying the expression, we get

$$R_i(\tau_B, \tau_i) = \tau_i \log_2\left(1 + a_i \frac{\tau_B}{\tau_i}\right) \tag{5.6}$$

where $a_i = \beta_i |g_i|^2 |h_i|^2 P_a$. Since the instantaneous service rate of each user is jointly concave with the downlink and uplink operating intervals as noted in [49], so does the average. Thus, the total average throughput,

$$\begin{aligned} R_{tot}(\boldsymbol{\tau}) &= \mathbb{E}\left\{\sum_{i=1}^{N} R_i(\tau_B, \tau_i)\right\} \\ &= \mathbb{E}_a\left\{\log_2 \prod_{i=1}^{N}\left(1 + a_i \frac{\tau_B}{\tau_i}\right)^{\tau_i}\right\} \end{aligned} \tag{5.7}$$

where $\boldsymbol{\tau} = [\tau_B, \tau_1, \cdots, \tau_N]$, is a jointly concave function of $\boldsymbol{\tau}$.

SH-MAC

Similar to the earlier case, wireless power broadcasting and information decoding operations occur over orthogonal time intervals, and harvested energy at user i can be determined from (5.2). However, users send information-bearing signals simultaneously over the uplink

channel throughout the interval $1-\tau_B$. Thus, the received signal at AP is written as follows:

$$V = \sum_{i=1}^{N} h_i X_i + N^v \tag{5.8}$$

where $N^v = \mathcal{CN}(0,1)$ is the circularly-symmetric complex Gaussian noise at the AP with unit variance. In order to decode each user's information, AP performs successive interference cancellation, and we consider fixed decoding order. Hence, the instantaneous service rate for the user whose signal is decoded in the i^{th} order can be determined as

$$R_i = (1-\tau_B)\log_2\left(1+\frac{|h_i|^2 P_i}{1+\sum_{j=i+1}^{N}|h_j|^2 P_j}\right) \text{ (bps/Hz)} \tag{5.9}$$

where the uplink transmitted power from user i in given as

$$P_i = \beta_i \frac{\tau_B}{1-\tau_B}|g_i|^2 P_a. \tag{5.10}$$

Substituting this into 5.9, the service rate is expressed in terms of harvesting interval τ_B as follows:

$$R_i(\tau_B) = (1-\tau_B)\log_2\left(1+\frac{a_i\tau_B}{1-\tau_B+a_i^*\tau_B}\right) \text{ (bps/Hz)} \tag{5.11}$$

here $a_i = \beta_i|g_i|^2|h_i|^2 P_a$ and $a_i^* = \sum_{j=i+1}^{N} a_j$.

Proposition 5.1.1 *The instantaneous service rate given in (5.11) is a concave function of harvesting interval τ_B.*

Proof: See Appendix H.

Thus, the total average throughput, i.e., average sum-rate capacity in this case, which is given as

$$R_{tot} = \mathbb{E}_a\left\{(1-\tau_B)\log_2\left(1+\sum_{i=1}^{N} a_i\frac{\tau_B}{1-\tau_B}\right)\right\}, \tag{5.12}$$

is a concave function of τ_B since concavity is preserved under summation.

ASH-TDMA

In this approach, users are allowed to harvest energy until they begin uplink data transfer as can be seen from Fig. 5.2c, and hence WPT and AP are no longer in half duplex mode. However, each energy harvesting and information transferring operations occur over non-overlapping time intervals. The harvested energy at user i becomes

$$E_i^{hv} = \Big(\tau_B + \sum_{j=1}^{i-1} \tau_j\Big) g_i P_a + E_i^{add} \qquad \text{(Joules)} \tag{5.13}$$

where τ_i denotes the time interval scheduled for this user to send information-bearing signal uplink to the AP, and E_i^{add} denotes the additional energy which can be harvested from the transmitted signal by other users. It is given as

$$E_i^{add} = \sum_{k=1}^{i-1} \tau_k |r_{ik}|^2 P_k \tag{5.14}$$

where r_{ik} is channel fading coefficient between user i and user k, and P_k is the transmitted signal from user k. As a result, the transmitted power level from user i is given as

$$P_i = \beta_i \frac{E_i^{hv}}{\tau_i} \tag{5.15}$$

which leads to

$$\begin{aligned} P_i &= \beta_i P_a \left[\frac{g_i\Big(\tau_B + \sum_{j=1}^{i-1} \tau_j\Big) + \sum_{u=1}^{i-1} r_{iu} g_u \Big(\tau_B + \sum_{v=1}^{u-1} \tau_v\Big)}{\tau_i} \right] \\ &= \beta_i P_a \left[\frac{\tau_B a_B^i + \sum_{j=1}^{i-1} \tau_j a_j^i}{\tau_i} \right] \end{aligned} \tag{5.16}$$

where a_B^i and a_j^i's are weighting coefficients while taking transmitted power level from user i, and they are obtained from the channels power gains. For instance, in a two-user model, we have $a_B^1 = g_1$ and $a_1^1 = 0$, $a_B^2 = g_2 + g_1 r_{12}$, and $a_1^2 = g_2$.

In regard to the uplink operation, users are operating based on time-division multiple access scheme, and hence the received signal at the AP and the corresponding achievable data rate during the time interval τ_i are as expressed in 5.4 and 5.5. Substituting (5.16) into (5.5), the instantaneous throughput of user i in terms of operating intervals becomes

$$R_i(\boldsymbol{\tau}_i) = \tau_i \log_2 \left(1 + \beta_i \frac{a_B^i \tau_B + \sum_{j=1}^{i-1} \tau_j a_j}{\tau_i} \right) \tag{5.17}$$

where $\boldsymbol{\tau}_i = [\tau_B, \tau_1, \cdots, \tau_i]$.

Proposition 5.1.2 *The instantaneous throughput of user i given in (5.17) is jointly concave with orthogonal operating intervals* $\tau_1, \tau_2, \cdots, \tau_i$.

Proof: See Appendix I.

Therefore, the total average throughput, which is given as

$$R_{tot}(\boldsymbol{\tau}) = \sum_{i=1}^{N} \mathbb{E}\big\{ R_i(\boldsymbol{\tau}_i) \big\}, \tag{5.18}$$

is a concave function of operating intervals.

5.2 Throughput Maximization under QoS constraints

In wireless-powered communication networks, the time intervals allocated for harvesting as well as decoding operation, and the power level of an energy-bearing signal transmitted downlink by WPT are important parameters that can be optimized to improve the throughput or service rate. In fact, broadcasting a signal at a higher power level enables users to harvest more energy within a shorter time interval, and this allows to transfer data over a

longer duration of each cycle. Since the AP is assumed to have a reliable external power source as mentioned in Section 5.1.1, it always transmits an energy-bearing signal at the peak power level. Thus, operation time intervals become the only parameters to control for maximum throughput, and in the following subsections, we analyze impact of QoS parameter on the optimal time allocation policies.

5.2.1 Optimal Harvesting Time in the MAC Protocol

In this case, energy-harvesting users send information bearing signal to AP through multiple access channels, and hence harvesting time becomes the only parameter to optimize for better performance. Knowing that each user harvests energy to support data transfer, the effective capacity expression of user i given in (2.5) is modified for SH-MAC scheme by incorporating the additional parameter τ_B, i.e., the harvesting interval, as follows:

$$C_i^e(\theta_i, \tau_B) = -\frac{1}{T\theta_i} \log_2 \left(\mathbb{E}\left\{ e^{-\Phi_i \log\left(1+\frac{a_i \tau_B}{1-\tau_B+a_i^* \tau_B}\right)} \right\} \right) \tag{5.19}$$

where $\Phi_i = (1-\tau_B)\theta_i$. The sum effective capacity of users transmitting through a multiple access channel can be determined by summing up the individual effective capacities:

$$C^e(\boldsymbol{\theta}, \tau_B) = \sum_{i=1}^{N} C_i^e(\theta_i, \tau_B) \tag{5.20}$$

where $\boldsymbol{\theta} = [\theta_1, \theta_2, \cdots, \theta_N]$.

Theorem 5.2.1 *Given the QoS exponent θ, the sum effective capacity of the considered wireless-powered communication network under SH-MAC operation protocol is concave in τ_B.*

Proof: See Appendix 5.2.1.

Intuitively, the QoS exponent θ has an impact on the optimal harvesting interval, and a strict QoS constraint requires higher service rates which can be provided if there is sufficient

time to harvest as well as transmit data. Since these are conflicting requirements, obtaining optimal duration in the presence of buffer violation constraints while improving the overall performance is a challenging task. Hence, we first formulate an optimization problem considering a single user case, and then extend it to multiple users.

Single User

In the presence of a single user setting, let us denote as user 1, and the optimal harvesting time can be obtained by formulating an optimization problem as follows:

$$\begin{aligned} \text{(PR:5.1)} \qquad & \max_{\tau_B} \; -\frac{1}{T\theta_1} \log\left(\mathbb{E}\left\{e^{-\theta_1 \mathcal{R}_1}\right\}\right) \\ & \text{subject to } \; \tau_B(-1+\tau_B) \leq 0. \end{aligned} \tag{5.21}$$

Proposition 5.2.1 *The optimal harvesting time for a single user scenario is independent of the statistical QoS exponential decaying parameter θ, and it is given as*

$$\tau_B^* = \frac{e^{\mathcal{W}\left(\frac{a_1-1}{e}\right)+1} - 1}{a_1 + e^{\mathcal{W}\left(\frac{a_1-1}{e}\right)+1} - 1}. \tag{5.22}$$

Proof: See Appendix K.

According to Proposition 5.2.1, it is interesting to see that the exponential decaying parameter θ_1 does not have an impact on the optimal harvesting time interval. On the other hand, if the harvesting interval is independent of the fading state realization, i.e., $\tau_B[k] = \tau_B[k+1]$, then (K.3) given in Appendix K becomes

$$\mathbb{E}\left\{e^{-\theta_1 \mathcal{R}_1}\left[\ln\left(1+\frac{a_1\tau_B}{1-\tau_B}\right) - \frac{a_1}{1-\tau_B+a_1\tau_B}\right]\right\} = 0. \tag{5.23}$$

Since the Qos exponential decay parameter θ_1 can not be taken out from the expectation, the optimal harvesting time depends on not only the channel characteristics but also θ_1. In

such a case, the solution is obtained by finding the root of the following function

$$f(\tau_B) = \mathbb{E}\Bigg\{ e^{-\theta_1(1-\tau_B)\ln(\Gamma)} \Big[\ln(\Gamma) - \frac{A}{\Gamma} \Big] \Bigg\} \tag{5.24}$$

where $\Gamma = 1 + \frac{a_1\tau_B}{1-\tau_B}$ and $A = \frac{a_1}{1-\tau_B}$. In order to guarantee the existence of a unique solution, we apply the first order derivative, i.e.,

$$\begin{aligned} \frac{\partial f(\tau_B)}{\partial \tau_B} &= \mathbb{E}\Bigg\{ \Bigg[\ln(\Gamma) - \frac{A}{\Gamma} \Bigg] \Bigg[\frac{\partial}{\partial \tau_B} e^{-\theta_1(1-\tau_B)\ln(\Gamma)} \Bigg] + \Bigg[e^{-\theta_1(1-\tau_B)\ln(\Gamma)} \Bigg] \Bigg[\frac{\partial}{\partial \tau_B} \Big(\ln(\Gamma) - \frac{A}{\Gamma} \Big) \Bigg] \Bigg\} \\ &= \mathbb{E}\Bigg\{ e^{-\theta_1(1-\tau_B)\ln(\Gamma)} \Bigg[\Big(\ln(\Gamma) - \frac{A}{\Gamma} \Big)^2 \theta_1 + \frac{a_1^2}{(1-\tau_B)^2 + (1-\tau_B)a_1\tau_B} \Bigg] \Bigg\} \geq 0, \end{aligned} \tag{5.25}$$

and it can be inferred from (5.25) that $f(\tau_B)$ is an increasing function for any feasible harvesting interval. Furthermore, taking the boundary conditions, $\tau_B = 0$ and $\tau_B = 1$, the functional values are $f(0) = -a_1$ and $f(1) \gg 0$, respectively. Therefore, based on intermediate value theorem, there exists a unique value of τ_B^* such that $0 < \tau^* < 1$ and $-a_1 < f(\tau^*) = 0 < f(1)$. It is obvious that $\Gamma \geq 1$ and $A > 0$ for $a_1 \neq 0$. Nevertheless, there is no guarantee whether $\log_e(\Gamma) - \frac{A}{\Gamma} > 0 \ \forall \tau_B \in (0,1)$ despite $\log_e(\Gamma)$ being monotonically increasing and $1/(\Gamma)$ decreasing functions of τ_B. Thus, (5.24) does not necessarily imply $\ln(\Gamma) = \frac{A}{\Gamma}$. Besides, it is unlikely to obtain closed-form expressions for the optimal harvesting interval. Hence, we provide an algorithm determine the optimal harvesting interval from (5.24) using bisection method as described in Algorithm 3.

Multiple Users

In this case, there are at least two or more users having buffer violation probabilities defined by the exponential decaying parameter θ_i. The goal is to determine the best time allocation strategy that benefit the total throughput, i.e., effective capacity, while satisfying the peak time constraint $\tau_B \leq 1$ over each fading state realization. Thus, the optimization problem

Algorithm 3 Harvesting interval independent of channel condition

Let: $f(\tau_B)$ as defined in (5.24).
Require: τ_B^* where $f(\tau_B^*) = 0$
Given ϵ, τ_B^u and τ_B^l
Initialize $\tau_B(0) = \tau_B^l$
$i \leftarrow 0$
repeat
  $\tau_B(i) = 0.5 * (\tau_B^u + \tau_B^l)$
  Calculate $f(\tau_B)$ using (5.24)
  if $f(\tau_B(i)) * f(\tau_B^l) > 0$ **then**
    update $\tau_B^l = \tau_B(i)$
  else
    update $\tau_B^u = \tau_B(i)$
  end if
  $i \leftarrow i + 1$
until $|\tau_B(i) - \tau_B(i-1)| < \epsilon$ and $|f(\tau_B(i))| < \epsilon$
$\tau_B^* = \tau_B(i)$

is formulated as

$$\text{(PR:5.2)} \qquad \max_{\tau_B} \; C^e(\theta, \tau_B) \tag{5.26a}$$

$$\text{subject to } \; \tau_B(-1 + \tau_B) \leq 0. \tag{5.26b}$$

The constraint is convex, and it guarantees that the harvesting interval does not exceed the peak or give infeasible solution, i.e., $\tau_B^* < 0$. From characterization in Theorem 5.2.1 and property of (5.26b), we note that (PR:5.2) is a convex optimization problem. This implies that KKT conditions guarantee global optimality, and hence

$$\frac{\partial \mathcal{L}}{\partial \tau_B} = 0 \tag{5.27a}$$

$$\lambda^*(\tau_B^* - {\tau_B^*}^2) = 0. \tag{5.27b}$$

can be applied where the Lagrange function $\mathcal{L}$ is now defined as

$$\mathcal{L} = C^e(\boldsymbol{\theta}, \tau_B) + \lambda(\tau_B[1 - \tau_B]). \tag{5.28}$$

Knowing that $0 < \tau_B^* < 1$ for the reason mentioned earlier, the first order optimality criteria becomes

$$\nabla C^e = \sum_{i=1}^{N} \frac{\partial C_i^e(\theta_i, \tau_B)}{\partial \tau_B} = 0. \tag{5.29}$$

where ∇C_i^e is further expressed as

$$\nabla C_i^e = \frac{e^{-\theta_i \mathcal{R}_i[k]}}{\mathbb{E}\big(e^{-\theta_i \mathcal{R}_i[k]}\big)} \left[\ln\Big(H_i(\tau_B)\Big) - \frac{\frac{a_i}{1-\tau_B}}{\Big(H_i(\tau_B) + \frac{a_i^* \tau_B}{1-\tau_B}\Big) H_i(\tau_B)} \right] \tag{5.30}$$

where $H_i(\tau_B) = 1 + \frac{a_i \tau_B}{1-\tau_B + a_i^* \tau_B}$. Here, we can clearly observe that QoS has a direct impact on the optimal harvesting interval, and each incremental $\Delta\theta_i$ changes the operation time allocation strategy. However, it is still not easy to explicitly characterize how an increase/decrease of θ_i affect τ_B and to provide a closed-form expression for the optimal harvesting time interval as well. Nevertheless, the global points of convex programming problems can be obtained using standard numerical tools.

We note that the uplink operating interval depends on the QoS exponents, and the upper boundary is achieved when each user does not have a buffer overflow limitation. In such a case, i.e., in the absence of statistical QoS constraints, throughput becomes average sum-rate capacity given in (5.12). In such a case, assuming $0 < \tau_B^* < 1$, the optimality criteria becomes

$$\frac{\partial}{\partial \tau_B} \mathbb{E}\left\{ (1-\tau_B) \log_2 \left(1 + \frac{\tau_B}{1-\tau_B} \gamma_T\right) \right\} = 0 \tag{5.31}$$

which leads to

$$\ln\left(1 + \frac{\gamma_T \tau_B}{1-\tau_B}\right) - \frac{\gamma_T}{1-\tau_B+\gamma_T \tau_B} = 0 \tag{5.32}$$

where $\gamma_T = \sum_{i=1}^{N} a_i$. Following similar procedure as in the proof of Proposition 3, the solution becomes

$$\tau_B^* = \frac{z^* - 1}{z^* - 1 + \gamma_T}. \tag{5.33}$$

where

$$z^* = e^{\mathcal{W}(\frac{-1+\gamma_T}{e})+1}. \tag{5.34}$$

Based on the above analytical result for wireless-powered users transmitting through multiple access channels, the optimal harvesting interval given in (5.33) decreases with increase in $\gamma_T[k]$. This in turn implies that higher $\gamma_T[k]$ value reduces $\tau_B^*[k]$ as shown in Fig. 5.3. Intuitively, better channel gain allows to harvest the required energy within shorter time interval, and this improves the throughput by encouraging users to transmit information for longer duration.

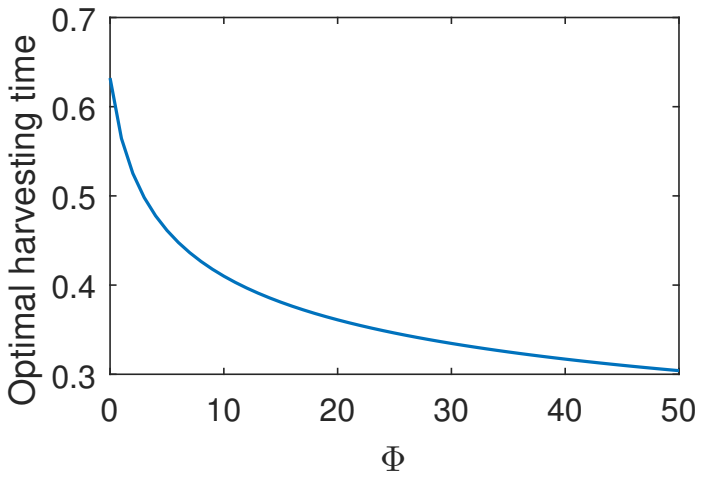

Figure 5.3: Optimal harvesting time τ_B^* (Sec.) versus $\Phi = -1 + \gamma_T$

5.2.2 Optimal Time Allocation in the TDMA Protocol

As noted in earlier for TDMA schemes, energy harvesting users transmit information uplink over non-overlapping time intervals that are governed by (5.1). The corresponding service rates can be determined using either (5.6) or (5.17) depending on how users are coordinated for the downlink operation. The relation between the wireless-powered user i effective capacity and operating intervals can be obtained by substituting the above mentioned service

rates into (2.5). The simplified expressions are given as

For SH-TDMA

$$C_i^e(\theta_i, \tau_B, \tau_i) = -\frac{1}{T\theta_i} \log\left(\mathbb{E}\left\{e^{-\theta_i \tau_i \log_2\left(1+a_i \frac{\tau_B}{\tau_i}\right)}\right\}\right) \tag{5.35a}$$

For ASH-TDMA

$$C_i^e(\theta_i, \tau_B, \boldsymbol{\tau}_i) = -\frac{1}{T\theta_i} \log\left(\mathbb{E}\left\{e^{-\theta_i \tau_i \log_2\left(1+\beta_i\left[\frac{a_B^i \tau_B + \sum_{k=1}^{i-1} \tau_k a_k}{\tau_i}\right]\right)}\right\}\right) \tag{5.35b}$$

where $\boldsymbol{\tau}_i = [\tau_B, \tau_1, \tau_2, \cdots, \tau_N]'$. Thus, the total effective capacity in either case is determined by

$$C_{tot}^e(\boldsymbol{\theta}, \boldsymbol{\tau}) = \sum_{i=1}^{N} C_i^e. \tag{5.36}$$

where $\boldsymbol{\tau} = [\tau_B, \tau_1, \cdots, \tau_N]'$.

Proposition 5.2.2 *The total effective capacity of wireless-powered users preserves concavity under TDMA.*

Proof: See Appendix L.

From Theorem 5.2.1 and Proposition 5.2.2, we observe that the throughput of wireless-powered users having delay-limited sources preserves concavity over the downlink and uplink operating time intervals. This implies obtaining effective capacity maximizing operating solution is feasible given the statistical QoS exponential parameters. In the previous scenario, since energy-harvesting users were simultaneously transferring data to AP, it was necessary and sufficient to optimize the harvesting time alone. Meanwhile, when these users transmit information-bearing signals based on TDMA scheme, resource allocation strategy requires obtaining the set of time intervals for the downlink energy broadcasting and uplink informa-

tion transfer operations. Thus, we formulate an optimization problem as follows:

$$\text{(PR:5.3)} \qquad \max_{\tau_B, \tau_i} \; C^e_{tot} \tag{5.37a}$$

$$\text{subject to } (5.1), \tau_i \geq 0, \tau_B \geq 0. \tag{5.37b}$$

The Lagrangian of (PR:5.3) is

$$\mathcal{L}(\boldsymbol{\tau}) = C^e_{tot} - \Theta\Big(\tau_B + \sum_{i=1}^{N} \tau_i - 1\Big) \tag{5.38}$$

where Θ is the Lagrange multiplier for the constraint. The solutions of (PR:5.3) can be obtained from the corresponding dual problem, which is given as

$$\max_{\Theta} \quad \min_{\boldsymbol{\tau}} \; \mathcal{L}(\boldsymbol{\tau}). \tag{5.39a}$$

$$\text{subject to } (5.37b). \tag{5.39b}$$

Knowing C^e_{tot} is a concave function and the time constraint is convex, (PR:5.3) is a convex optimization problem. Thus, the KKT conditions

$$\frac{\partial \mathcal{L}}{\partial \tau_B} = 0 \tag{5.40a}$$

$$\frac{\partial \mathcal{L}}{\partial \tau_i} = 0 \tag{5.40b}$$

$$\Theta^*\Big(\tau^*_B + \sum_{i=1}^{N} \tau^*_i - 1\Big) = 0 \tag{5.40c}$$

are necessary and sufficient for optimality. The complementary slackness condition implies $\Theta^* \neq 0$ if the optimal total duration is the same as the symbol interval. Intuitively, maximizing the throughput requires harvesting more energy and transferring information for longer

period of time, which in turn enforces

$$\tau_B^* + \sum_{i=1}^{N} \tau_i^* = 1. \tag{5.41}$$

Since first order optimality criteria given in (5.40) depend on the Lagrange function, or more specifically the objective function, we provide the details for synchronous and asynchronous TDMA schemes separately as follow.

SH-TDMA

Similarly as in [29] and [94], the maximization problem (PR:5.3) can be equivalently expressed as the following sub-optimal minimization problem,

$$\min_{\tau_B, \tau_i} \sum_{i=1}^{N} \mathbb{E}\left\{ \left(1 + a_i \frac{\tau_B}{\tau_i}\right)^{-\theta_i \tau_i} \right\} \tag{5.42a}$$

$$\text{subject to } (5.37b), \tag{5.42b}$$

and the corresponding Lagrange function given in (5.38) becomes

$$\mathcal{L} = \sum_{i=1}^{N} \mathbb{E}\left\{ \left(1 + a_i \frac{\tau_B}{\tau_i}\right)^{-\theta_i \tau_i} \right\} - \Theta\Big(\tau_B + \sum_{i=1}^{N} \tau_i - 1\Big). \tag{5.43}$$

Then, applying (5.40a) and (5.40b), we get

$$\nabla \mathcal{L}_{\tau_B} = \sum_{i=1}^{N} a_i \big(1 + a_i \frac{\tau_B}{\tau_i}\big)^{-\theta_i \tau_i - 1} - \Theta = 0 \tag{5.44a}$$

$$\nabla \mathcal{L}_{\tau_i} = \big(1 + a_i \frac{\tau_B}{\tau_i}\big)^{-\theta_i \tau_i} \left[\ln\big(1 + a_i \frac{\tau_B}{\tau_i}\big) - \frac{a_i \frac{\tau_B}{\tau_i}}{1 + a_i \frac{\tau_B}{\tau_i}} \right] - \Theta = 0, \tag{5.44b}$$

which leads to

$$z_i \ln(z_i) - z_i(1 + \Theta_i) = 1 \tag{5.45}$$

where $z_i = 1 + a_i \frac{\tau_B}{\tau_i}$ and $\Theta_i = \Theta T\big(1 + a_i \frac{\tau_B}{\tau_i}\big)^{\theta_i \tau_i}$. The above equations in (5.45) have a form $X \ln X - aX = b$, and after several manipulations as in the proof of Proposition 3, the corresponding solution to (5.45) is given as

$$z_i^* = \frac{1}{\mathcal{W}(\mathbf{e}^{-(1+\Theta_i)})}. \tag{5.46}$$

Hence, each user optimal uplink operating time interval is expressed as

$$\tau_i^* = \frac{a_i \tau_B}{z_i^* - 1}. \tag{5.47}$$

Substituting (5.47) into (5.41), and solving for τ_B^* we get

$$\tau_B^* = \frac{1}{1 + \sum_{i=1}^{N} \frac{a_i}{z_i^* - 1}} \tag{5.48}$$

ASH-TDMA

In this case, some users can harvest while others are transferring information to AP, and the corresponding the expression for each user's effective capacity and total throughput are determined using (5.35b) and (5.36), respectively. Substituting these into the objective function of (PR:5.3) gives us an optimization problem that maximizes total effective capacity for ASH-TDMA scheme. Following similar approach as to the earlier case, the equivalent sub-optimal minimization problem becomes

$$\min_{\tau_B, \tau_i} \sum_{i=1}^{N} \mathbb{E}\left\{ \left(1 + \beta_i \left[\frac{a_B^i \tau_B + \sum_{k=1}^{i-1} a_k^i \tau_k}{\tau_i} \right] \right)^{-\theta_i \tau_i} \right\} \tag{5.49a}$$

$$\text{subject to } (5.37b). \tag{5.49b}$$

From the first order optimality criteria given in (5.40a), where the Lagrangian function in this case is

$$\mathcal{L}(\boldsymbol{\tau}) = \sum_{i=1}^{N} \mathbb{E}\left\{\left(1+\beta_i\left[\frac{a_B^i\tau_B+\sum_{k=1}^{i-1}a_k^i\tau_k}{\tau_i}\right]\right)^{-\theta_i\tau_i}\right\} - \Theta\Big(\tau_B+\sum_{i=1}^{N}\tau_i-1\Big), \tag{5.50}$$

we have

$$\nabla\mathcal{L}_{\tau_B} = \sum_{i=1}^{N}\beta_i a_B^i\left(1+\beta_i\left[\frac{a_B^i\tau_B+\sum_{k=1}^{i-1}a_k^i\tau_k}{\tau_i}\right]\right)^{-\theta_i\tau_i-1} - \Theta. \tag{5.51}$$

Similarly, the explicit expression for (5.40b) using (5.50) becomes

$$\nabla\mathcal{L}_{\tau_i} = \big(1+\beta_i x_i\big)^{-\theta_i\tau_i}\left[\ln\big(1+\beta_i x_i\big) - \frac{\beta_i x_i}{1+\beta_i x_i}\right] + \sum_{j=i+1}^{N}\frac{\beta_i a_j^i}{\tau_j}\big(1+\beta_j x_j\big)^{-\theta_j\tau_j-1} - \Theta \tag{5.52}$$

where

$$x_i = \frac{a_B^i\tau_B + \sum_{k=1}^{i-1}a_k\tau_k}{\tau_i}.$$

After few manipulations, we have

$$(1+\beta_i x_i)\ln(1+\beta_i x_i) - (1+\beta_i x_i)(1+\Theta_i') = -1 \tag{5.53}$$

where

$$\Theta_i' = (1+\beta_i x_i)\left[\Theta - \sum_{j=i+1}^{N}\big(1+\beta_j x_j\big)^{-\theta_j\tau_j-1}\frac{a_j}{\tau_j}\right]. \tag{5.54}$$

This equation is similar to (5.45), and can be solved following the same procedure using Lambert function. Thus, the optimal uplink operation interval for each user can be implicitly expressed as

$$\tau_i^* = \frac{\beta_i\Big(a_B^i\tau_B + \sum_{k=1}^{i-1}a_k^i\tau_k\Big)\mathcal{W}(\mathbf{e}^{-(1+\Theta_i')})}{1-\mathcal{W}(\mathbf{e}^{-(1+\Theta_i')})} \tag{5.55}$$

Therefore, once the total time interval required for information transfer is known, the optimal initial harvesting time can be determined as

$$\tau_B^* = 1 - \sum_{i=1}^{N} \tau_i^*. \tag{5.56}$$

Since the expressions given for the optimal operating intervals in both SH-TDMA and ASH-TDMA cases are implicit functions, solution can only be obtained numerically using an iterative procedure. Note that the above downlink energy broadcasting and each user uplink data transfer time intervals are determined for the given the dual parameter, and sub-gradient approach can be applied to iteratively update Θ until the solution converges to the optimal value. We provide an iterative algorithm to solve (PR:5.3) as shown in Algorithm 4.

5.2.3 Numerical Analysis

In order to justify theoretical characterizations, we provide numerical results considering two energy harvesting users communicating with an AP. We assume that the uplink and downlink channel of a given user have the same characteristics, and the corresponding magnitude square of fading coefficients are exponentially distributed with means $\frac{1}{\varrho_1}$ and $\frac{1}{\varrho_2}$ for user 1 and user 2, respectively. For the asynchronous harvesting - TDMA scheme, we consider two cases, namely ASH-TDMA^A and ASH-TDMA^B, for comparison purpose. ASH-TDMA^A denotes the scenario discussed in Section 5.1.2 where the harvested energy at user i is governed by 5.13. On the other hand, ASH-TDMA^B considers the same situation as illustrated in Fig. 5.2c except that users harvest only from downlink broadcast signal as noted in [56], i.e., $E_i^{add} = 0$ in 5.13.

Fig. 5.4 illustrates the impact of downlink transmitted power level and user exponential QoS decaying parameter θ on the network throughput, i.e., sum effective capacity. As can be seen from 5.4a, broadcasting an energy-bearing signal at higher power level, in general,

Algorithm 4 Sub-optimal interval for TDMA under QoS

Require: τ_B^*, and τ_i^* $\forall i \in \{1, 2, \cdots, N\}$

Given ϵ, $a_1, a_2, \cdots, a_N$
Initialize $k = 0$, and $\tau_B(0), \tau_1(0), \cdots, \tau_N(0)$
Initialize $r = 0$, and $\beta(0)$
repeat
  repeat
    for $i = 1$ **to** $i = N$ **do**
      $\Theta_i = \Theta(k)T\left[1 + a_i \frac{\tau_B(k)}{\tau_i(k)}\right]^{\theta_i \tau_i(k)}$
      Θ_i' using 5.54
    end for
    if Nov-TDMA **then**
      Calculate $\tau_B(k+1)$, using 5.48
      for $i = 1$ **to** $i = N$ **do**
        Calculate $\tau_i(k+1)$ 5.47
      end for
    else
      for $i = 1$ **to** $i = N$ **do**
        Calculate $\tau_i(k+1)$ 5.55
      end for
      $\tau_B(k+1) = 1 - \sum_{i=1}^{N} \tau_i(k+1)^*$
    end if
  until $\left|\tau_i(k) - \tau_i(k-1)\right| < \epsilon$, and $\left|\tau_B(k) - \tau_B(k-1)\right| < \epsilon$
  $r = r + 1$
  Update $\Theta(r)$
until $\Theta(r) - \Theta(r-1) < \epsilon$
$\tau_i^* = \tau_i(k)$ and $\tau_B^* = \tau_B(k)$

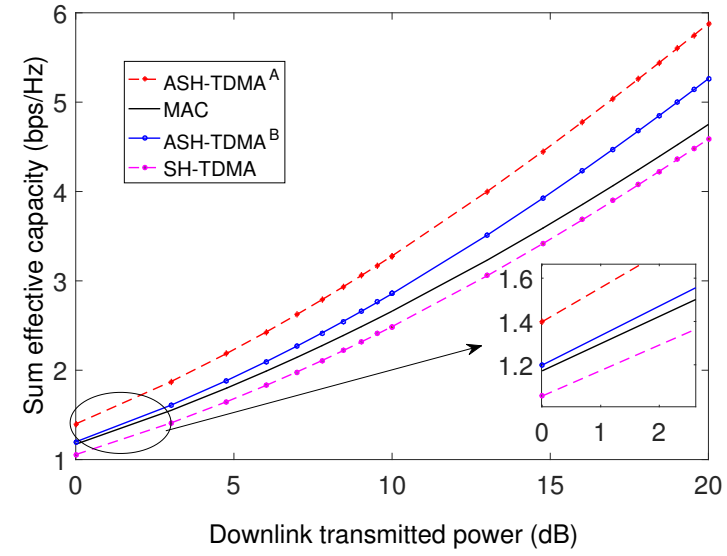

(a) C^e_{tot} vs. P @ $\theta_1 = 1$, $\theta_2 = 0.1$

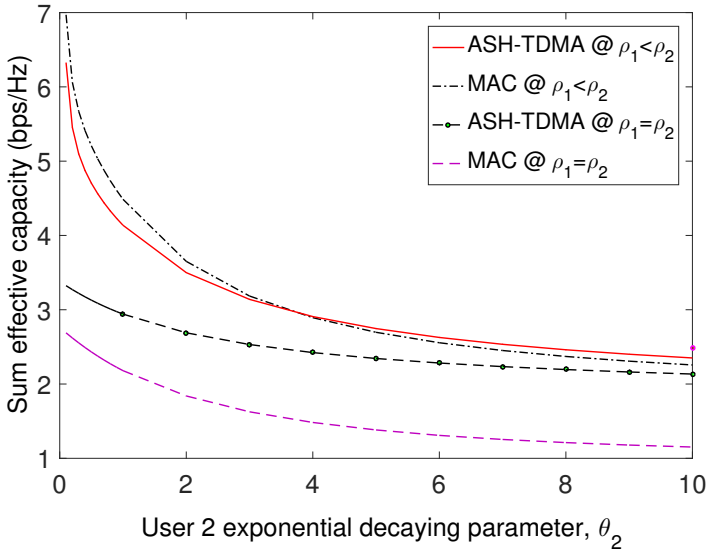

(b) C^e_{tot} vs. θ_2 @ $P = 10dB$, $\theta_1 = 1$

Figure 5.4: Impact of downlink transmitted power P and user 2 exponential decay parameter θ_2 on sum effective capacity C^e_{tot}

---

improves the network throughput as expected. This is because, if the received downlink signal at each user has relatively higher power level, sufficient amount of energy can be harvested in shorter duration which leaves more time for the uplink information transfer.

Comparing the various types of WIPT operation protocols, asynchronous energy harvesting is the best approach for throughput maximization of a wireless-powered communication network. In addition, we observe that allowing one user to opportunistically harvest energy from the uplink information-bearing signal transmitted by the other user to the AP provides additional energy and this increases the total number of bits that can be transferred as can be inferred from ASH-TDMA^B and ASH-TDMA^A. On the other hand, Fig. 5.4b shows impact of changing user 2's QoS parameter θ_2 on the sum-effective capacity while user 1's QoS parameter is kept constant at $\theta_1 = 1$. Generally speaking, higher θ values, i.e., stricter QoS constraint, hurts the throughput under fixed downlink transmit power. As can be seen from the figure, the performance gain of asynchronous harvesting with uplink TDMA over synchronous harvesting with uplink MAC is dependent on not only the users' buffer violation probabilities but also the channel characteristics experienced by each of them. For instance, assuming both users have the same average channel power gain, ASH-TDMA achieves better data rate than SH-MAC for any values of $\theta_2 > 0$. However, if user 2 experiences favorable situations compared with user 1, i.e., $\varrho_2 < \varrho_1$, then loose QoS constraint at user 2 encourages to apply SH-MAC in order to benefit for throughput maximization. This is because the channel characteristics improvement leads to allocating more time for the uplink information transfer which actually benefits both users. Meanwhile, each incremental reduces the performance difference in the two approaches, and at point P the same amount of bits is transferred using either scheme. Furthermore, Fig. 5.5 explains how the average optimal harvesting time changes with both channel conditions and user 2's exponential decaying QoS parameter θ_2. From the figure, we understand that better channel condition reduces the time allocated for energy harvesting which actually benefits the throughput. On the other hand, when the user experiences bad channel condition or transmits through worse wireless link, its buffer violation probability has little impact on the optimal harvesting time, and hence as θ_2 becomes more strict less change is observed in τ_B under the given channel condition.

Fig. 5.6 shows explicitly users' data arrival rates as a function of user 2's exponential de-

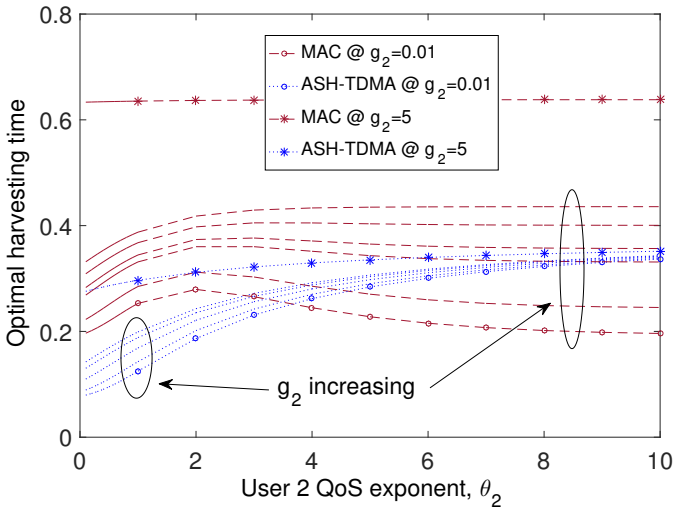

Figure 5.5: τ_B^{avg} in (Sec.) vs. θ_2 @ $P = 10$, $\theta_1 = 1$

caying parameter θ_2 under different channel conditions. From 5.6a, we can see that at lower θ_2 values user 2 achieves higher data arrival rates for both uplink TDMA and MAC schemes. More specifically, letting this user to harvest while user 1 transmits under ASH-TDMA case is advantageous. Despite the exponential decreases in effective capacity as θ_2 takes higher values, user 2 maintains better arrival rate compared with user 1 until θ_2 exceeds certain threshold, for instance i.e., $\theta_2 \approx 1$ for SH-TDAM or $\theta_2 = 3$ for ASH-TDMA. In regard to MAC, since both users operate simultaneously, strictness of θ_2 has little impact on user 1 achievable data rate, and both users achieves the same data arrival rate when $\theta_2 = 6.5$. This is due to the fixed decoding order applied at the receiving end. On the other hand, when user 2 experiences better channel condition, i.e., $\varrho_2 > \varrho_1$, users data arrival rates and the corresponding point at which both users attain the same throughput is also changed as shown in Fig. 5.6b. Intuitively, when $\varrho_2 > \varrho_1$, allocating more time to user 2 improves the network throughput, but this can hurt user 1's data arrival rate. From the figure, we observe that effective capacity of user 1 reduces slightly considering both SH-TDMA and ASH-TDMA WIPT protocols when user 2 has better channel gain. However, this condition does not reflect the same characteristics under SH-MAC. This is because, in synchronous

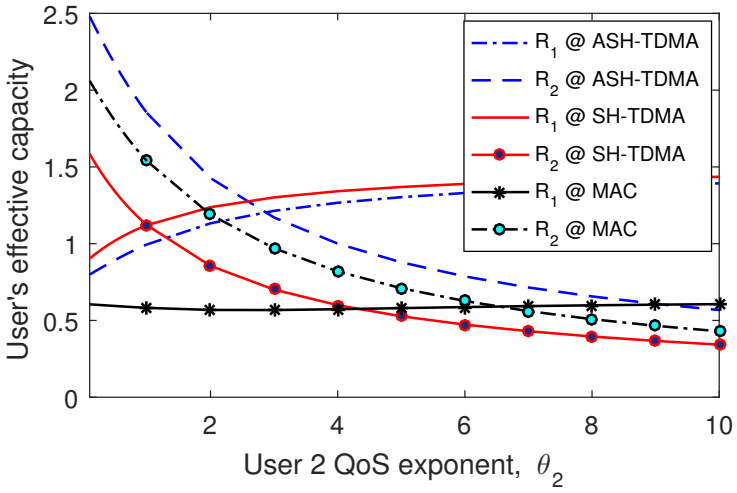

(a) User effective capacity vs. user 2 QoS parameter θ_2 under the same channel condition, i.e., $\varrho_1 = \varrho_2$

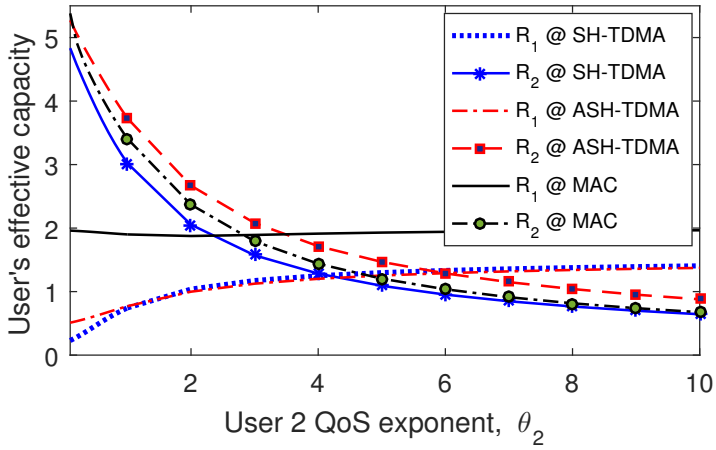

(b) User effective capacity vs. user 2 QoS parameter θ_2 under different channel conditions, i.e., $\varrho_1 > \varrho_2$

Figure 5.6: Impact of channel characteristics and exponential decay parameter θ on users' effective capacity given $\theta_1 = 1$

harvesting with uplink MAC, both users share the benefit of user 2's channel gain through the time allocated for energy harvesting and information transfer. Furthermore, comparing Fig. 5.6a and Fig. 5.6b, user 1 and user 2 data arrival rates improve simultaneously. However, the effective capacity of both users becomes the same at $\theta_2 = 2.8$ under MAC protocol, and each incremental value of θ_2 beyond this point degrades user 2 performance,

and as a result, user 1 achieves better arrival rate. Whereas, in the case of uplink SH-TDMA scheme, since user 2 benefits from the channel power gain significantly, higher value of θ_2 is expected in order to reach $R_1 = R_2$. In other words, the time allocated for each user to transfer information uplink to AP, more specifically for TDMA scheme, is highly affected by the buffer violation probability in the presence of delay-limited sources, and the doubly near-far problem mentioned in [49] depends on these parameters.

5.3 Energy-Efficient Time Allocation

Resource allocation for wireless-powered users considering throughput as a performance measuring metric benefits the uplink information transfer. Meanwhile, energy-efficiency is another compelling performance parameter mainly in energy-limited environment. In this section, we focus on obtaining optimal time allocation strategies that maximize the system energy efficiency of an energy harvesting communication networks. More specifically, we begin with instantaneous values and determine operating intervals without exponential decaying QoS constraints. Then, we investigate impact of these constraints on the system average performance, i.e., effective-EE.

5.3.1 Energy Efficiency without QoS Constraints

The system energy efficiency determines the total number of bits transferred to the AP per a joule of energy consumed by the system, and in subsequent subsections, we apply this metric to wireless-powered nodes considering uplink TDMA and uplink MAC protocols.

Under uplink TDMA protocol

In this protocol, wireless-powered users transfer data over non-overlapping time intervals, and their corresponding instantaneous service rates can be determined using (5.6) and (5.17) for synchronous and asynchronous energy harvesting operations, respectively. It is clear that

the system expends energy to transfer $\mathcal{R}$ bits of information to the AP, and this expenditure depends on the downlink transmitted power level P_a as well as the power consumption of the circuitry. Thus, the energy consumption rate during the downlink and uplink operations intervals are given as

$$\begin{aligned} P_D =& P_a + P_{cir}^{WPT} \\ P_U =& P_{cir}^{AP} \end{aligned} \tag{5.57}$$

where P_{cir}^{WPT} and P_{cir}^{AP} denote circuit power consumption at the WPT and AP, respectively. Note that since the wireless-powered nodes do not have embedded power source, their circuit power consumption is satisfied from the harvested energy. Hence, it does not need to be included in 5.57. Therefore, the system energy efficiency, which evaluates the amount of data transferred per joule of consumed energy in each fading realization, is mathematically expressed as

$$\eta_T^a(\boldsymbol{\tau}) = \begin{cases} \dfrac{\log_2 \prod_{i=1}^{N} \left(1+a_i \frac{\tau_B}{\tau_i}\right)^{\tau_i}}{P_D \tau_B + P_U(1-\tau_B)} & \text{SH-TDMA} \\ \dfrac{\sum_{i=1}^{N} \tau_i \log_2 \left(1+\beta_i \left[\frac{a_B^i \tau_B + \sum_{k=1}^{i-1} a_k^i \tau_k}{\tau_i}\right]\right)}{P_D(1-\tau_N) + P_U(1-\tau_B)} & \text{ASH-TDMA.} \end{cases} \tag{5.58}$$

Knowing that the throughput, which is the numerator of η_T^a, is a concave function of operating intervals in both types of TDMA scenarios as noted in Section 5.1.2 and the consumed energy is affine function, the system energy efficiency given in 5.58 is Pseudo-concave claiming Proposition 2.9 of [93]. This guarantees the existence of a stationary point that maximize the utility function, and in order to determine the optimal set of operation

time intervals, an optimization problem is formulated as follow:

$$\text{(PR:5.4)} \qquad \max_{\boldsymbol{\tau}} \ \eta_T^a(\boldsymbol{\tau}) \tag{5.59a}$$

$$\text{subject to } (5.37b). \tag{5.59b}$$

Since (PR:5.4) is a concave-linear fractional problem, Dinkelbach method can be applied to solve the optimization problem [93]. This method follows an iterative procedure until the optimal solution which maximizes the system energy efficiency is achieved. Each step involves solving another convex maximization problem which is defined as

$$\boldsymbol{x}^* = \arg\max_{\boldsymbol{X}\in\mathcal{S}} \ \Big[\mathcal{F}(\boldsymbol{x}) - \alpha_n g(\boldsymbol{x})\Big] \tag{5.60}$$

where $\mathcal{F}(\boldsymbol{x})$ is the numerator, and $g(\boldsymbol{x})$ is the denominator of system energy efficiency given in (5.58). In addition, the parameter α_n is a constant for the n^{th} iteration, and it is updated iteratively with $\alpha_{n+1} = \frac{\mathcal{F}(\boldsymbol{x})}{g(\boldsymbol{x})}$ until the solution converges to the optimal value. The convex maximization problem given in (5.60) is a.k.a. inner loop and it has different description for SH-TDMA and ASH-TDMA scenarios as will be discussed shortly.

i. Inner loop under SH-TDMA

From the characterization in (5.58), the inner loop maximization problem defined in (5.60) can be reformulated as

$$\min_{\boldsymbol{\tau}} -\ln \prod_{i=1}^{N} \left(1 + a_i \frac{\tau_B}{\tau_i}\right)^{\tau_i} + \alpha_n \Big((P_D - P_U)\tau_B + P_U\Big) \tag{5.61a}$$

$$\text{subject to } (5.37b). \tag{5.61b}$$

For the given α_n, the problem reflects throughput maximization formulated in [49] except the additional term $\alpha_n((P_D - P_U)\tau_B + P_U)$. The Lagrangian function $\mathcal{L}$ for the above optimization

problem is defined as

$$\mathcal{L}(\tau_B, \boldsymbol{\tau}, \beta) = -\ln \prod_{i=1}^{N} \Big(1 + a_i \frac{\tau_B}{\tau_i}\Big)^{\tau_i} + \alpha_n \Big((P_D - P_U)\tau_B + P_U\Big) - \Phi\Big(\tau_B + \sum_{i=1}^{N} \tau_i - 1\Big) \tag{5.62}$$

where Φ is the Lagrange multiplier for the constraint. Since $\ln \prod_{i=1}^{N} \left(1 + a_i \frac{\tau_B}{\tau_i}\right)^{\tau_i}$ is proved to be concave, it is straightforward to see that the above problem is convex with respect to the operating time intervals, and hence their optimal values can be determine applying KKT conditions,

$$\Phi^*\Big(\tau_B^* + \sum_{i=1}^{N} \tau_i^* - 1\Big) = 0. \tag{5.63a}$$

$$\frac{\partial \mathcal{L}}{\partial \tau_B} = 0 \quad \text{and} \quad \frac{\partial \mathcal{L}}{\partial \tau_i} = 0 \tag{5.63b}$$

Thus, we get

$$\sum_{i=1}^{N} \frac{a_i}{1 + a_i \frac{\tau_B}{\tau_i}} + \alpha_n (P_D - P_U) - \Phi = 0 \tag{5.64}$$

$$\ln\Big(1 + \frac{a_i \tau_B}{\tau_i}\Big) - \frac{\frac{a_i \tau_B}{\tau_i}}{1 + \frac{a_i \tau_B}{\tau_i}} - \Phi = 0. \tag{5.65}$$

Similarly as in [49], from (5.64) and (5.65), we have

$$\sum_{i=1}^{N} a_i - 1 = z \ln z - z(1 + \omega_i), \tag{5.66}$$

and the optimal time allocations are given as

$$\tau_B = \frac{z^* - 1}{\sum_i^N a_i + z^* - 1} \quad \text{and} \quad \tau_i = \frac{a_i}{\sum_i^N a_i + z^* - 1} \tag{5.67}$$

where $\omega_i = \alpha_n(P_D - P_U)$, $z = 1 + \frac{\tau_B}{K}$, and $K = \frac{1-\tau_B}{\sum_{i=1}^{N} a_i}$. Thus, the solution to (5.66) can be expressed as

$$z^* = \frac{a_i - 1}{\mathcal{W}\Big((a_i - 1)\mathbf{e}^{-(1+\omega_i)}\Big)}. \tag{5.68}$$

Substituting (5.68) into (5.67), solution of operating intervals while α_n is fixed are explicitly expressed as

$$\tau_B^* = \frac{\frac{a_i - 1}{\mathcal{W}\Big((a_i-1)\mathbf{e}^{-\left(1+\alpha_n(P_D-P_U)\right)}\Big)} - 1}{\sum_{i=1}^{N} a_i + \frac{a_i - 1}{\mathcal{W}\Big((a_i-1)\mathbf{e}^{-\left(1+\alpha_n(P_D-P_U)\right)}\Big)} - 1} \tag{5.69a}$$

$$\tau_i^* = \frac{a_i}{\sum_{i=1}^{N} a_i + \frac{a_i - 1}{\mathcal{W}\Big((a_i-1)\mathbf{e}^{-\left(1+\alpha_n(P_D-P_U)\right)}\Big)} - 1}. \tag{5.69b}$$

Therefore, the optimal time intervals for the downlink energy broadcasting and uplink information transfer can be determined by updating (5.69) iteratively. The procedure for solving the optimization problem (PR:5.4) considering synchronous harvesting with uplink TDMA is indicated in Algorithm 5.

Algorithm 5 EE maximization for SH-TDMA scheme using Dinkelbach's algorithm

1: Given: ϵ
2: Define: $\mathcal{F}(\boldsymbol{\tau}) = \ln \prod_{i=1}^{N} \left(1 + a_i \frac{\tau_B}{\tau_i}\right)^{\tau_i}$,
$g(\boldsymbol{\tau}) = (P_D - P_U)\tau_B + P_U$
3: $n \leftarrow 0$
4: Initialize τ_B, $\tau_1, \tau_2, \cdots, \tau_N$.
5: **repeat**
6: Update τ_B and τ_i using (5.69a) and (5.69b), respectively
7: Determine $\Delta_n = \mathcal{F}(\boldsymbol{\tau}) - \alpha_n g(\boldsymbol{\tau})$
8: $\alpha_{n+1} = \frac{\mathcal{F}(\boldsymbol{\tau})}{g(\boldsymbol{\tau})}$
9: $n \leftarrow n + 1$
10: **until** $|\Delta_n| > \epsilon$
11: Set $\tau_B^* = \tau_B$ and $\tau_i^* = \tau_i$.

ii. Inner loop under ASH-TDMA

In this case, the inner loop is expressed as follows:

$$\min_{\boldsymbol{\tau}} -\sum_{i=1}^{N}\tau_i \ln_2\left(1+\beta_i\frac{a_B^i\tau_B+\sum_{k=1}^{i-1}a_k^i\tau_k}{\tau_i}\right)+\alpha_n C(\tau_N,\tau_B) \tag{5.70a}$$

$$\text{subject to } (5.37b) \tag{5.70b}$$

where $C(\tau_N,\tau_B) = P_D + P_U - P_D\tau_N - P_U\tau_B$. The corresponding Lagrange function $\mathcal{L}$ is given as

$$\mathcal{L}(\tau_B,\boldsymbol{\tau},\beta) = \\ -\sum_{i=1}^{N}\tau_i \ln\left(1+\beta_i\frac{a_B^i\tau_B+\sum_{k=1}^{i-1}a_k^i\tau_k}{\tau_i}\right)+\alpha_n(P_D+P_U-P_D\tau_N-P_U\tau_B)-\Phi\Big(\tau_B+\sum_{i=1}^{N}\tau_i-1\Big) \tag{5.71}$$

where Φ is the Lagrange multiplier. As noted in the SH-TDMA case, this problem is also a concave throughput maximization apart from the additional term. Clearly, KKT conditions in (5.63) are necessary and sufficient for global optimality. Thus, applying the first order optimality criteria, we get

$$\frac{\partial\mathcal{L}}{\partial\tau_i} = \ln\Big(1+\beta_i x_i\Big)-\frac{\beta_i x_i}{1+\beta_i x_i}+\sum_{j=i+1}^{N}\frac{\beta_j a_i^j}{1+\beta_j x_j}-\Phi=0 \tag{5.72a}$$

$$\frac{\partial\mathcal{L}}{\partial\tau_N} = \ln\Big(1+\beta_N x_N\Big)-\frac{\beta_N x_N}{1+\beta_N x_N}-\alpha_n P_D-\Phi=0 \tag{5.72b}$$

$$\frac{\partial\mathcal{L}}{\partial\tau_B} = \sum_{i=1}^{N}\frac{\beta_i a_B^i}{1+\beta_i x_i}-\alpha_n P_U-\Phi=0 \tag{5.72c}$$

where $x_i = \frac{a_B^i\tau_B+\sum_{k=1}^{i-1}a_k^i\tau_k}{\tau_i^*}$. After several manipulations as in [56], we have

$$z_i\ln z_i - z_i\big(1+\phi_i(\boldsymbol{z}_i)\big) = \beta_i a_B^i - 1 \tag{5.73}$$

where $z_i = a_i x_i + 1$, $\boldsymbol{z}_i = [z_1, z_2, \cdots, z_{i-1}, z_{i+1}, \cdots, z_N]'$,

$$\phi_i(\boldsymbol{z}_i) = \sum_{j=i+1}^{N} \frac{\beta_j(-a_i^j + a_B^j)}{z_j} - \alpha_n P_U + \sum_{k=1}^{i-1} \frac{\beta_k a_B^k}{z_k} \tag{5.74}$$

$$\forall i \in \{1, \cdots, N-1\} \text{ and } \phi_N(\boldsymbol{z}_N) = \sum_{j=1}^{N-1} \frac{a_B^j \beta_j}{z_j} + \alpha_n(P_D - P_U). \tag{5.75}$$

Note that (5.73) is similar to (5.66), and hence the solution is given as

$$z_i^* = \frac{\beta_i a_B^i - 1}{\mathcal{W}\Big((\beta_i a_B^i - 1)\mathbf{e}^{-\left(1+\phi_i(\boldsymbol{z}_i)\right)}\Big)}. \tag{5.76}$$

However, since z_i depends on the z_j where $i, j \in \{1, 2, \cdots, N\}$ but $i \neq j$, it is required to apply an iterative procedure. Then, for a given α_n, the uplink operating intervals can be expressed as a function of τ_B using $x_i^* = \frac{a_B^i \tau_B^* + \sum_{k=1}^{i-1} a_k^i \tau_k^*}{\tau_i^*}$ and $z_i^* = a_i x_i^* + 1$ as follow:

$$\tau_1^* = \frac{a_B^1 a_1^1}{z_1^* - 1}\tau_B^* \tag{5.77a}$$

$$\tau_2^* = \frac{a_B^2 a_2}{z_2^* - 1}\tau_B^* + \frac{a_1^1 a_1^2 a_2 a_B^1}{(z_1^* - 1)(z_2^* - 1)}\tau_B^* \tag{5.77b}$$

$$\vdots \tag{5.77c}$$

$$\tau_N^* = \left[\frac{a_B^N \tau_B^* + \sum_{j=1}^{N-1} a_j^N \tau_j^*}{z_N^* - 1}\right] a_N. \tag{5.77d}$$

From the complementary slackness condition, recall that

$$\tau_1^* + \tau_2^* + \cdots + \tau_N^* + \tau_B = 1. \tag{5.78}$$

Substituting (5.77) into (5.78), we get

$$\sum_{i=1}^{N} \frac{a_B^i a_i}{z_i^* - 1}\tau_B^* + \sum_{i=1}^{N} \left[\frac{\sum_{j=1}^{i-1} a_j^i \tau_j^*}{z_i^* - 1}\right] a_i + \tau_B = 1. \tag{5.79}$$

which leads to

$$\tau_B^* = \frac{1}{\sum_{k=1}^{N} \frac{a_B^k a_k}{z_k^* - 1} + \mathcal{H}(\boldsymbol{a})} \tag{5.80}$$

where $\boldsymbol{a}$ is a set of a_B^l and $a_m^n \ \forall \ l, m, n \in \{1, 2, \cdots, N\}$, and $\mathcal{H}(\boldsymbol{a})$ is a scalar valued function which is obtained from (5.79). We provide an algorithm for energy-efficient time allocation strategy considering ASH-TDMA scheme as indicated in Algorithm 6.

Algorithm 6 Energy-efficient time allocation for ASH-TDMA scheme using Dinkelbach's algorithm

Given: ϵ
Define: $\mathcal{F}(\boldsymbol{\tau}) = \sum_{i=1}^{N} \tau_i \ln\left(1 + \beta_i \frac{a_B^i \tau_B + \sum_{k=1}^{i-1} a_k^i \tau_k}{\tau_i}\right)$
$g(\boldsymbol{\tau}) = P_D + P_U - P_D \tau_N - P_U \tau_B$
$n \leftarrow 0$
Initialize τ_B, $\tau_1, \tau_2, \cdots, \tau_N$.
repeat
  $r \leftarrow 0$
  repeat
    Determine $z_i(r) = a_i \left[\frac{a_B^i \tau_B + \sum_{k=1}^{i-1} a_k^i \tau_k}{\tau_i^*} + 1\right]$
    $r \leftarrow r + 1$
    Update $z_i(r)$ using (5.76)
  until $|z_i(r) - z_i(r-1)| < \epsilon$
  Calculate τ_B using (5.80)
  Update τ_i using (5.77)
  Determine $\Delta_n = \mathcal{F}(\boldsymbol{\tau}) - \alpha_n g(\boldsymbol{\tau})$
  $\alpha_{n+1} = \frac{\mathcal{F}(\boldsymbol{\tau})}{g(\boldsymbol{\tau})}$
  $n \leftarrow n + 1$
until $|\Delta_n| < \epsilon$
Set $\tau_B^* = \tau_B$ and $\tau_i^* = \tau_i$.

Under uplink MAC protocol

In this case, users are transmitting information-bearing signals through MAC after harvesting energy simultaneously from a dedicated wireless power source, and the energy-efficient time

allocation policy can be determined by formulating the following optimization problem:

$$\text{(PR:5.5)} \qquad \min_{\tau_B} \; -\frac{(1-\tau_B)\log_2\left(1+\frac{a_T\tau_B}{1-\tau_B}\right)}{(P_D-P_U)\tau_B+P_U} \tag{5.81a}$$

$$\text{subject to } (5.26b) \tag{5.81b}$$

where P_D and P_U are as defined in (5.57). Having a concave numerator and an affine denominator with respect to harvesting interval τ_B together with the convexity of the constraint in (5.26b), (PR:5.5) is proved to be a concave-linear fractional problem (CLFP). The corresponding Lagrange function is given as

$$\mathcal{L} = \frac{(-1+\tau_B)\log_2\left(1+\frac{a_T\tau_B}{1-\tau_B}\right)}{(P_D-P_U)\tau_B+P_U}) + \Omega\tau_B\big(1-\tau_B\big) \tag{5.82}$$

where Ω is the lagrange multiplier for the constraint in (5.81b). Since KKT conditions are necessary and sufficient to obtain global solution for concave-linear/convex fractional problems [93], (K.2a) and (K.2b) can be directly applied to the Lagrange function defined in (5.82). Thus, we have

$$\frac{\ln\left(1+\frac{a_T\tau_B}{1-\tau_B}\right) - \frac{\frac{a_T}{1-\tau_B}}{1+\frac{a_T\tau_B}{1-\tau_B}}}{\kappa\tau_B+P_U} - \frac{\kappa(1-\tau_B)\ln\left(1+\frac{a_T\tau_B}{1-\tau_B}\right)}{(\kappa\tau_B+P_U)^2} = 0 \tag{5.83}$$

where $\kappa = P_D - P_U$. Note that the optimal harvesting interval can neither be $\tau_B^* = 0$ nor $\tau_B^* = 1$ for the same reason mentioned earlier, and hence $\Omega^* = 0$. After several rearrangements on (5.83), we get

$$z\ln(z) - \varphi z = \xi \tag{5.84}$$

where $z = 1 + \frac{a_T\tau_B}{1-\tau_B}$, $\xi = \frac{a_T-1}{P_D}(\kappa\tau_B + P_U)$, and $\varphi = \xi * (a_T - 1)$. The solution to (5.84) can be simply expressed as

$$z^* = \frac{\xi}{\mathcal{W}(\xi * \mathbf{e}^{-\varphi})}. \tag{5.85}$$

Thus, the energy-efficient harvesting time under uplink MAC protocol with synchronous harvesting becomes

$$\tau_B^* = \frac{\frac{\xi}{\mathcal{W}(\xi * \mathbf{e}^{-\varphi})} - 1}{a_T + \frac{\xi}{\mathcal{W}(\xi * \mathbf{e}^{-\varphi})} - 1}. \tag{5.86}$$

Since ξ is dependent on τ_B, so does φ. This shows that (5.86) is an implicit equation, and it can only be solved using an iterative procedure. Therefore, we provide an algorithm to obtain the optimal harvesting interval for (PR:5.5) using (5.86) as detailed in Algorithm 7.

Algorithm 7 Energy-efficient harvesting interval for MAC

Require: τ_B^*

Given ϵ, a_T, P_D, P_U, and κ
Initialize $\tau_B(0)$
$r \leftarrow 0$
repeat
    $\xi = \frac{a_T - 1}{P_D}\big(\kappa \tau_B(r) + P_U\big)$
    $\varphi = \xi * (a_T - 1)$
    $r \leftarrow r + 1$
    Update $\tau_B(r)$, using 5.86
until $\big|\tau_B(r) - \tau_B(r-1)\big| < \epsilon$
$\tau_B^* = \tau_B(r)$

5.3.2 Effective Energy Efficiency

In this section, we analyze the impact of exponential decaying QoS parameter θ on the energy-efficient time allocation strategies. Since effective capacity measures the constant data arrival rate, i.e. throughput in the presence of delay-limited data sources, we focus on the effective-EE to determine the number of bits arrived per a joule of consumed energy by the system. Thus, we formulate an optimization problem considering the three WIPT operation protocols as follow:

$$\text{(PR:5.6)} \quad \max_{\boldsymbol{\tau}} \ \eta^e(\boldsymbol{\tau}) \tag{5.87a}$$

$$\text{subject to} \quad (5.26b) \quad \text{For MAC} \tag{5.87b}$$

$$(5.37b) \quad \text{For TDMA} \tag{5.87c}$$

where

$$\eta^e(\boldsymbol{\tau}) = \begin{cases} \dfrac{\sum_{i=1}^{N} -\frac{1}{T\theta_i} \log\left(\mathbb{E}\left\{ \left(1+\frac{a_i \tau_B}{1-\tau_B+a_* \tau_B} \right)^{\frac{-\theta_i(1-\tau_B)}{\ln(2)}} \right\} \right)}{\mathbb{E}\left\{ P_D \tau_B + P_U(1-\tau_B) \right\}} & \text{MAC} \\ \dfrac{\sum_{i=1}^{N} -\frac{1}{T\theta_i} \log\left(\mathbb{E}\left\{ e^{-\theta_i \tau_i \log_2\left(1+a_i \frac{\tau_B}{\tau_i}\right)} \right\} \right)}{\mathbb{E}\left\{ P_D \tau_B + P_U(1-\tau_B) \right\}} & \text{SH-TDMA} \\ \dfrac{\sum_{i=1}^{N} -\frac{1}{T\theta_i} \log\left(\mathbb{E}\left\{ \left(1+\beta_i \left[\frac{a_B^i \tau_B + \sum_{k=1}^{i-1} \tau_k a_k}{\tau_i} \right] \right)^{\frac{-\theta_i \tau_i}{\ln(2)}} \right\} \right)}{\mathbb{E}\left\{ P_D(1-\tau_N) + P_U(1-\tau_B) \right\}} & \text{ASH-TDMA} \end{cases} \tag{5.88}$$

Knowing that the sum effective capacity in each case is concave function of operating intervals as mentioned in Section 5.1.2 and the corresponding denominators of η^e are affine, the above optimization problem (PR:5.6) is generally a concave-linear fractional problem. Hence, optimal solution can be obtained by applying the Dinkelbach's method as indicated in Algorithm 8.

Algorithm 8 Effective-EE maximization using Dinkelbach's algorithm

1: Given: ϵ
2: Define: $\mathcal{C}_{tot} = \sum_{i=1}^{N} C_i(\theta_i, \boldsymbol{\tau})$
$g(\boldsymbol{\tau})$ =Total consumed energy
3: $n \leftarrow 0$
4: Initialize α_0
5: **repeat**
6: $\boldsymbol{\tau} = \arg\max_{\boldsymbol{\tau}} \{\mathcal{C}_{tot}(\boldsymbol{\tau}) - \alpha_n g(\boldsymbol{\tau})\}$ (Inner loop)
7: $F(\alpha_n) = \mathcal{C}_{tot}(\boldsymbol{\tau}) - \alpha_n g(\boldsymbol{\tau})$
8: $\alpha_{n+1} = \frac{\mathcal{C}_{tot}(\boldsymbol{\tau})}{g(\boldsymbol{\tau})}$
9: $n \leftarrow n+1$
10: **until** $|\mathcal{F}(\boldsymbol{\tau})| > \epsilon$
11: Set $\tau_B^* = \tau_B^n$ and $\tau_i^* = \tau_i^n$.

In regard to the inner loop, we have

$$\begin{aligned} \min_{\tau_B} \quad & -\sum_{i=1}^{N} C_i^e(\theta_i, \boldsymbol{\tau}) + \alpha_n g(\boldsymbol{\tau}) \\ \text{subject to} \quad & (5.26b) \quad \text{For MAC} \\ & (5.37b) \quad \text{For TDMA} \end{aligned} \tag{5.89}$$

where $C_i^e(\theta, \boldsymbol{\tau})$ is as defined in (5.19) for MAC, and (5.35a) and (5.35b) for SH-TDMA and ASH-TDMA, respectively. Thus, the corresponding Lagrange function becomes

$$\mathcal{L} = -\sum_{i=1}^{N} C_i^e(\theta, \boldsymbol{\tau}) + \alpha_n g(\boldsymbol{\tau}) + \mu h(\boldsymbol{\tau}) \tag{5.90}$$

where $h(\boldsymbol{\tau}) = \tau_B(1-\tau_B)$ for MAC, or $h(\boldsymbol{\tau}) = \tau_B + \sum_{i=1}^{N} \tau_i - 1$ otherwise. We note that the above problem is convex, and hence the KKT conditions are necessary and sufficient for global optimality. Thus, applying (K.2a) and (K.2b) on (5.90) considering MAC protocol, we have

$$\sum_{i=1}^{N} \frac{\partial C_i^e(\theta, \tau_B)}{\partial \tau_B}\bigg|_{\theta=\theta_i} = \alpha_n(P_D - P_U) \tag{5.91}$$

assuming that the optimal solution lies $0 < \tau_B^* < 1$. The explicit expression for $\nabla_{\tau_B} C_i^e$ is as given in (5.30). Similarly, applying the KKT conditions given in (5.40) considering TDMA protocol, we get

$$\begin{aligned} &\text{For SH-TDMA} \\ &\sum_{i=1}^{N} \frac{a_i z_i^{-\theta_i\tau_i - 1}}{\mathbb{E}\left\{z^{-\theta_i\tau_i - 1}\right\}} - \alpha_n(P_D - P_U) - \mu = 0 \\ &\frac{z_i^{-\theta_i\tau_i}}{\mathbb{E}\left\{z^{-\theta_i\tau_i - 1}\right\}} \left[\ln\left(z_i\right) - \frac{z_i - 1}{z_i}\right] - \mu = 0. \end{aligned} \tag{5.92}$$

where $z_i = 1 + a_i \frac{\tau_B}{\tau_i}$.

For ASH-TDMA

$$\begin{aligned}
&\sum_{i=1}^{N} \frac{\beta_i a_B^i \big(1+\beta_i x_i\big)^{-\theta_i \tau_i - 1}}{\mathbb{E}\Big\{(1+\beta_i x_i)^{-\theta_i \tau_i}\Big\}} + \alpha_n P_U - \mu = 0 \\
&\sum_{i=1}^{N} \frac{\partial C_i^e(\theta_i, \boldsymbol{\tau})}{\partial \tau_i} - \mu = 0, \quad i \in \{1, 2, \cdots, N-1\} \\
&\sum_{i=1}^{N} \frac{\partial C_i^e(\theta_i, \boldsymbol{\tau})}{\partial \tau_N} + \alpha_n P_D - \mu = 0
\end{aligned} \tag{5.93}$$

where $x_i = \frac{a_B^i \tau_B + \sum_{k=1}^{i-1} a_k \tau_k}{\tau_i}$ and

$$\nabla_{\tau_i} C_i^e = \frac{1}{\mathbb{E}\Big\{(1+\beta_i x_i)^{-\theta_i \tau_i}\Big\}} \big(1+\beta_i x_i\big)^{-\theta_i \tau_i} \left[\ln\big(1+\beta_i x_i\big) - \frac{\beta_i x_i}{1+\beta_i x_i}\right] + \sum_{j=i+1}^{N} \frac{\beta_i a_j^i}{\tau_j} \big(1+\beta_j x_j\big)^{-\theta_j \tau_j - 1}. \tag{5.94}$$

After making several rearrangements, the above expressions leads to

$$\sum_{i=1}^{N} \frac{\partial C_i^e(\theta_i, \boldsymbol{\tau})}{\partial \tau_B} - \sum_{i=1}^{N} \frac{\partial C_i^e(\theta, \boldsymbol{\tau})}{\partial \tau_k} = \alpha_n K \tag{5.95}$$

where

$$K = \begin{cases} P_D - P_U & \text{TDMA} \\ P_U & \text{MAC} \end{cases} \tag{5.96}$$

for $k \in \{1, 2. \cdots, N-1\}$. If $k = N$, then we have $K = P_D - P_U$ for both cases. As can be observed from the optimality criteria, it is difficult to obtain a closed-form expression for the operating time interval in all the three schemes. However, they can still be solved using standard numerical tools due to convexity of the inner loops.

5.3.3 Numerical Analysis

In this section, we provide numerical results to illustrate impact of channel characteristics and downlink transmitted power level on the system average energy efficiency both in the absence and presence of delay-limited sources. First, we consider two energy harvesting users for the ease of demonstration and discussion, but then extend to more number of users.

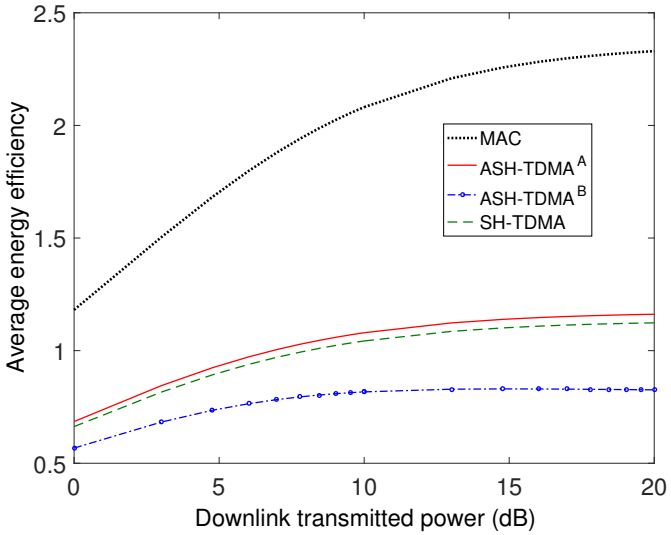

Figure 5.7: EE in (bpJ/Hz) vs. downlink transmit power level under $\varrho_1 = \varrho_2$

Fig. 5.7 and Fig. 5.8 illustrates the impact of downlink transmit power level on the average energy efficiency under various settings of statistical QoS constraints. According to Fig. 5.7, we observe that the performance curve has non-decreasing characteristics which implies broadcasting the energy-bearing signal with higher power level benefits the energy efficiency. Intuitively, increasing the downlink power reduces its operation interval which allows to allocate more time for the uplink information transfer. This benefits not only achievable data rate but also limits the downlink energy consumption, and overall there is a gain on the energy efficiency. However, the incremental gain becomes steady under each operation protocol for higher values of transmitted power P_a. Comparing the three WIPT protocols, we observe that SH-MAC is an energy-efficient approach, and it has much better performance regardless of channel characteristics and exponential decaying QoS parameter.

Furthermore, synchronous harvesting with uplink TDMA achieves higher energy efficiency than asynchronous harvesting with $E_{add} = 0$, but slightly smaller compared with ASH-TDMA^A.

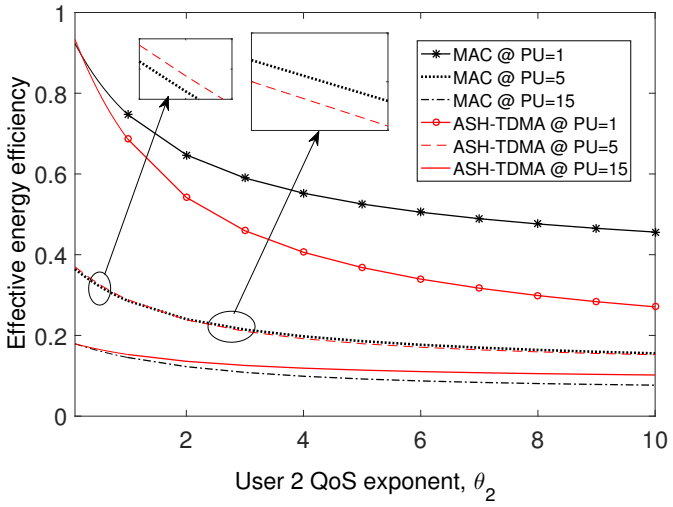

(a) EE_{eff} vs. θ_2 under various P_U values, given $\varrho_1 = \varrho_2$ and $\theta_1 = 1$

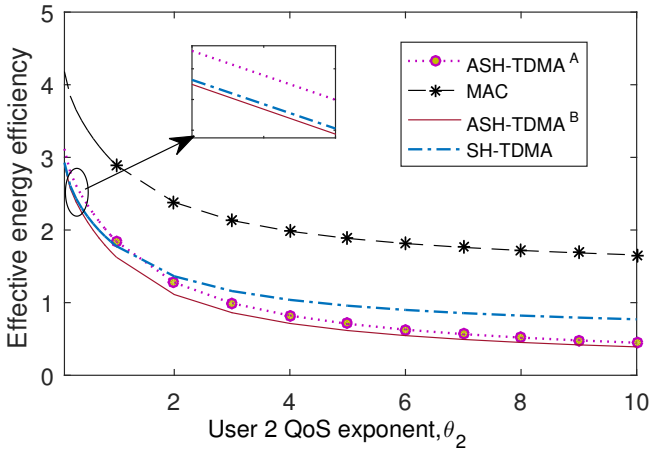

(b) EE_{eff} vs. θ_2 for $\varrho_1 > \varrho_2$ with $\theta_1 = 1$ and $P_U = 2$

Figure 5.8: EHCNs energy efficiency under different scenarios

---

In regard to the impact of statistical QoS constraint, Fig. 5.8a clearly illustrates that the system performance degrades with respect to the exponential decaying parameter θ. In general, each WIPT protocol performance depends on the exponential decay QoS parameter,

channel characteristics and AP energy consumption rates. For instance, assuming that both users have the same average channel condition, SH-MAC achieves better performance compared with ASH-TDMA^A for smaller power consumption as shown in Fig. 5.8a, and it becomes significant as user 2's exponential QoS decaying factor increases. Meanwhile, as the uplink energy consumption rate, P_U, takes higher values, the performance gap between the two approaches gets very small, and further increase in the power consumption at the AP favors ASH-TDMA instead of SH-MAC as an energy-efficient scheme. These can be explained using how the operating intervals are allocated based on circuit power consumption and user 2's exponential decaying parameter θ_2 as shown in Fig. 5.9a and Fig. 5.9b for ASH-TDMA and SH-MAC protocols, respectively. As can be seen in Fig. 5.9a, smaller values of P_U encourages to allocate more time for the uplink information transfer in order to reduce the energy consumed by WPT during the downlink energy broadcasting phase. Hence, τ_B and τ_1 are relatively very small compared with τ_2 for $P_U = 1$. On the other hand, for higher values of P_U, harvesting duration significantly increases with θ_2 while that of user 2 uplink interval decreases exponentially as expected. Similarly, in the case of MAC protocol, operating intervals are hardly affected by θ_2 for small value of P_U as illustrated in Fig. 5.9b. In such cases, the decreasing characteristics of effective energy efficiency shown in Fig. 5.8a is mainly due to user 2's stricter QoS constraint, i.e., θ_2. Furthermore, higher power consumption under MAC protocol results allocating more time for energy harvesting operation as shown in Fig. 5.9b, but less change is observed on the system energy efficiency.

On the other hand, Fig.5.10 illustrate impact of exponential decaying QoS parameter θ_2 on users' constant arrival rates while maximizing the system effective energy efficiency. As can be seen from the figures, User 1's data arrival rate is less affected by the change in θ_2 under MAC protocol regardless of the channel characteristics, but user 2's data rate is exponentially decreasing as its QoS constraint gets more strict. Meanwhile, user 2 achieves higher arrival rate for TDMA protocol for any θ_2 value as shown in the figure for $\varrho_1 < \varrho_2$.

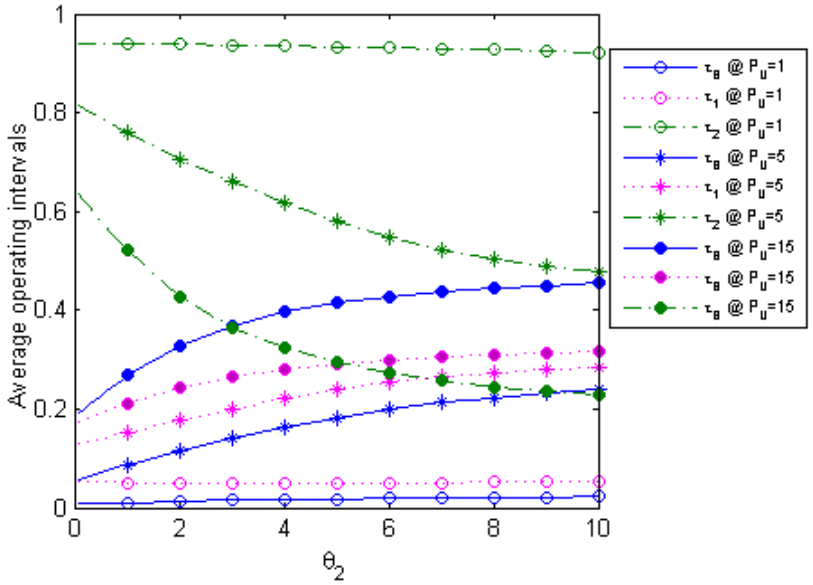

(a) Under ASH-TDMA protocol

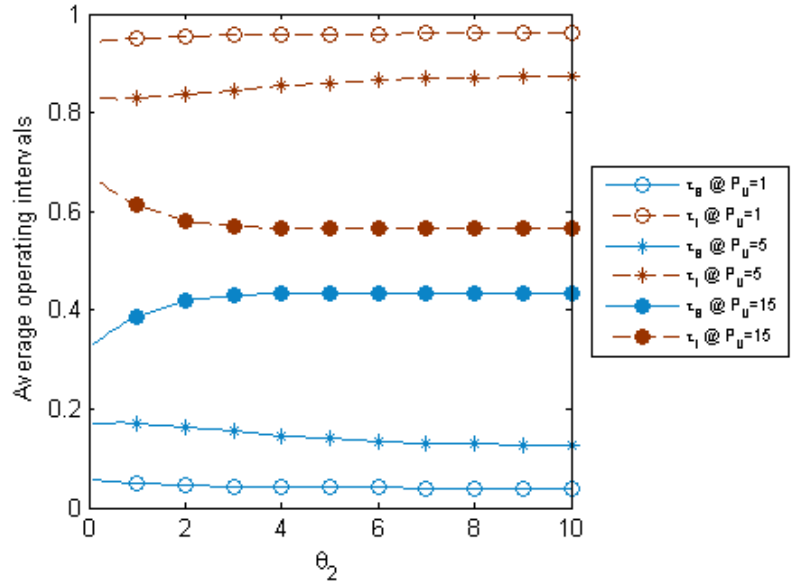

(b) Under SH-MAC protocol

Figure 5.9: Average operating interval in (Sec.) vs. user 2 decaying parameter θ_2 under $\varrho_1 = \varrho_2$

This is because user 2 experience much better channel gain.

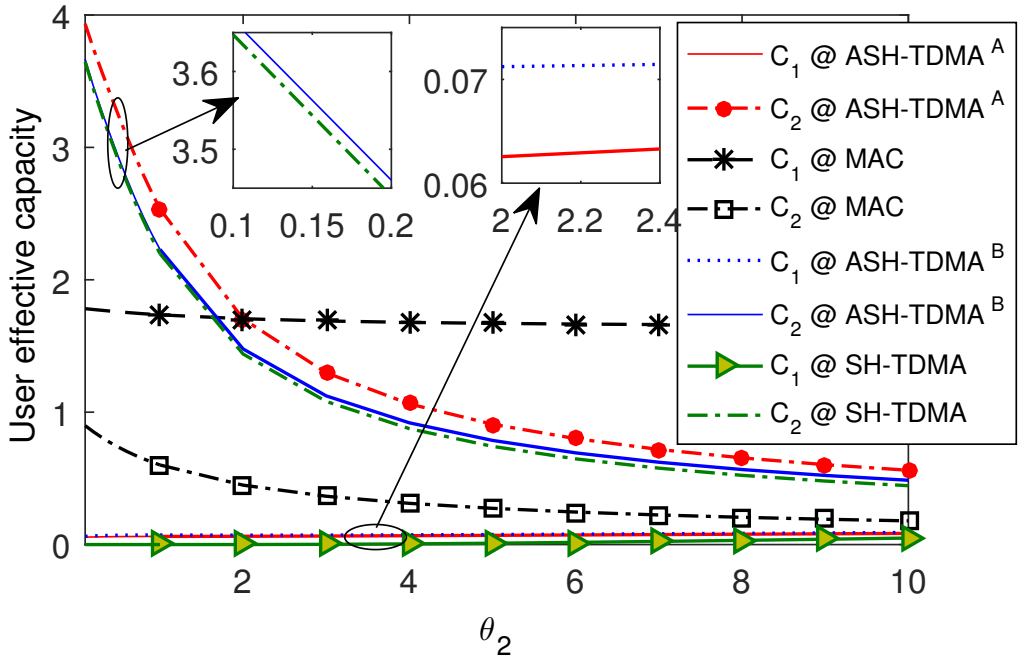

Figure 5.10: User effective capacity (bps/Hz) vs. user 2 exponential Qos parameter, θ_2 while maximizing effective energy efficiency under $\varrho_1 < \varrho_2$, i.e., $5\varrho_1 = \varrho_2$

Chapter 6

Full-Duplex Wireless Information and Power Transfer with Non-Zero Mean Input

This chapter mainly studies energy-efficiency optimization for WIPT considering a full-duplex uplink and downlink operations in a hybrid system that consists of energy harvesting and non-energy harvesting nodes. The significance of introducing non-zero mean component on the information-bearing signal is well investigated. The system model is presented in Section 6.1 and throughput maximizing and energy-efficient resource allocation strategies are studied in Section 6.2, and Section 6.3, respectively. Subsequently, numerical results are presented and discussed in Section 6.3.

6.1 System Model

We consider a hybrid wireless network that consists of an AP, an energy-harvesting user (EHU) and multiple non-energy harvesting users (NEHU) as shown in Fig. 6.1. The AP operates in full-duplex mode in the sense that it broadcasts a deterministic signal denoted as $X_A e^{j\theta_h}$ to the EHU while decoding received information transmitted uplink by the NEHUs.

Co-phasing is performed at the transmitter, offsetting the channel phase shifts, in order to harvest additional energy as will be discussed shortly. Each NEHU has embedded power source and transmits information continuously to the AP, whereas EHU harvests energy from the downlink wireless transferred power by the AP as well as the uplink transmitted signal by the NEHUs.

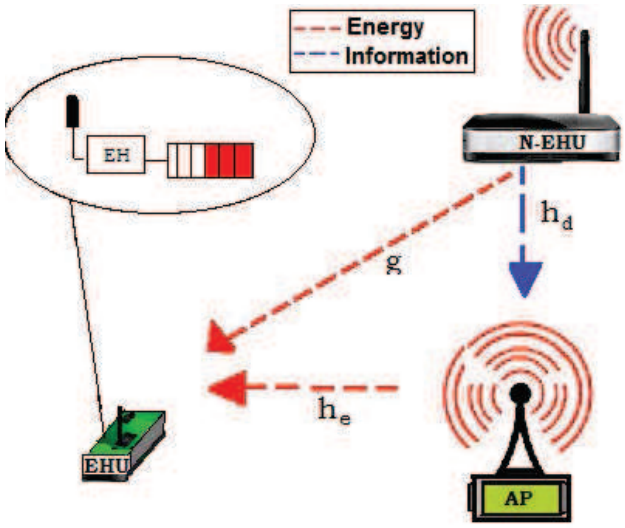

Figure 6.1: Wireless power and information transfer model

Assuming the channel state information is known both at the transmitter and receiver, each NEHU can introduce a pre-phase-shifted deterministic component in the information bearing-signal to benefit the harvested energy at EHU. Let us denote the transmitted signal from i^{th} NEHU in the k^{th} symbol duration by $X^i[k] \sim \mathcal{N}\big(\phi_i, \sigma_i^2[k]\big)$. Technically, this can be expressed as follows:

$$X^i[k] = X_I^i[k] + X_E^i[k] \tag{6.1}$$

where $X_I^i \sim \mathcal{N}\big(0, \sigma_i^2[k]\big)$ is an information-bearing component and $X_E^i = \phi_i$ is the deterministic component that targets energy transfer only. The transmitted signal power is upper bounded as $\mathbb{E}\big\{|X^i[k]|^2\big\} = \sigma_i^2 + \phi_i^2 = P_i[k] \leq P_i^{pk}$.

In regard to the wireless channel, we assume that the link between any transmitter and the receiver experiences frequency-flat fading. The complex fading coefficient for the channel between i^{th} NEHU and the AP is denoted by h_d^i, and $r_i = |h_d^i|^2$ is the channel power gain.

Similarly, h_e denotes the channel coefficient between the EHU and AP. The wireless channel link between the EHU and i^{th} NEHU is denoted by $g_i = |g_i|e^{j\theta_g}$, and $z_i = |g_i|^2$. Hence, the non-zero mean component of NEHU is shifted in phase by θ_g, i.e., $X_E^i = \phi_i e^{-j\theta_g}$, as noted in [95], to benefit the harvested energy. The deterministic component can easily be removed at AP, and hence the received information-bearing signal at the AP in the k^{th} symbol duration is given as

$$Y_D[k] = \sum_{i=1}^{N} h_d^i X_I^i[k] + N_d[k] \tag{6.2}$$

where $N_d[k] \sim \mathcal{CN}(0,1)$ is the complex symmetric Gaussian noise component with unit variance at the receiving antenna. Thus, the instantaneous achievable data rate at which the AP decodes the received information in full-duplex WIPT mode is given as

$$\mathcal{R}_T = \log_2\left(1 + \sum_{i=1}^{N} r_i \sigma_i^2\right) \qquad \text{(bps/Hz)}. \tag{6.3}$$

where σ_i^2 is the information-bearing component of the i^{th} NEHU .

Similarly, the received signal at the EHU is expressed as

$$Y_E = \sum_{i=1}^{N} g_i\Big(X_I^i + X_E^i\Big) + h_e X_A e^{-j\theta_h} + N_e \tag{6.4}$$

where N_e is the noise component at the energy harvesting receiver. For simplicity, we eliminate the time index 'k' in the sequel. Hence, the harvested energy at EHU can be determined as follows:

$$\begin{aligned}
\mathcal{E}_{hv} =& \mathbb{E}\{|Y_E|^2\} \\
=& \sum_{i=1}^{N} |g_i|^2 P_i + |h_e|^2 P_A + \sum_{i=1}^{N} 2|g_i||h_e|\mathbb{E}\big\{X_E^i X_A\big\} \\
=& \sum_{i=1}^{N} \Big(z_i P_i + \alpha_i \phi_i\Big) + C
\end{aligned} \tag{6.5}$$

where $\alpha_i = 2|g_i||h_e|\sqrt{P_A}$, and $C = |h_e|^2 P_A$ are constants for the given fading states. In addition, we assume that X_E and X_A are independent, i.e., $\mathbb{E}\{X_E^i X_A\} = \mathbb{E}\{X_E^i\}\mathbb{E}\{X_A\}$. The harvested energy given in (6.5) can be rewritten as follows:

$$\begin{aligned}\mathcal{E}_{hv}(\boldsymbol{\sigma^2}, \boldsymbol{\phi}) &= \sum_{i=1}^{N} \Big(z_i \sigma_i^2) + \sum_{i=1}^{N} z_i \phi_i^2 + \alpha_i \phi_i \Big) + C \\ &= f(\boldsymbol{\sigma}^2) + g(\boldsymbol{\phi}).\end{aligned} \tag{6.6}$$

where $\boldsymbol{\sigma}^2 = [\sigma_1^2, \sigma_2^2, \cdots, \sigma_N^2]$ and $\boldsymbol{\phi} = [\phi_1, \phi_2, \cdots, \phi_N]$.

Lemma 6.1.1 *If there are two convex functions $f(x)$ and $g(x)$, then their sum $f(x) + g(y)$ is also jointly convex with respect to the domain of $f(x)$ and $g(y)$.*

Proof: See Appendix M.

Based on Lemma 6.1.1, the following proposition guarantees that the harvested energy is a convex function in the domain set.

Proposition 6.1.1 *For the wireless-powered node, i.e., EHU, the harvested energy expression given in (6.6) is a convex function of information-bearing component and non-zero mean component of the transmitted signal from each NEHU.*

Proof: See Appendix N

Without loss of generality, we assume unit time intervals so that energy and power can be interchangeably used. Based on (6.3) and (6.5), we notice that introducing ϕ_i could hurt the throughput, but this might not necessarily be the case when energy efficiency is taken into account. In the following sections, we determine optimal power control strategies taking throughput and energy efficiency as performance metrics.

6.2 Throughput Maximizing Power Control Policy

In this case, the goal is to maximize the achievable data rate, and intuitively this can be achieved if all NEHU transmit at peak power level with zero mean gaussian input, i.e.,

$X_E^i = 0\ \forall i \in \{1, 2, \cdots, N\}$. However, this might not be the optimum allocation strategy when the harvested energy constraint at the EHU can not be satisfied with zero-mean input signal, and in such a case, it is required to introduce non-zero mean component on the transmitted signals from one or more NEHUs. Therefore, in order to trace the impact of harvested energy constraint on the throughput maximizing power control policy, the following optimization problem is formulated.

$$\begin{aligned} \text{(PR:6.1)} \qquad & \max_{P \in \mathcal{P}} \ \mathcal{R}_T \\ & \text{s.t.} \ \ \mathcal{E}_{hv} = \chi. \end{aligned} \tag{6.7}$$

Knowing that the sum-rate capacity is concave with respect to the information-bearing component, and the harvested energy is convex, the above formulated problem (PR:6.1) is a convex optimization problem, and hence the KKT conditions, i.e.,

$$\frac{\partial \mathcal{L}}{\partial \phi_i} = 0 \qquad \frac{\partial \mathcal{L}}{\partial \sigma^2} = 0 \tag{6.8a}$$

$$\mu^* \big(\mathcal{E}_{hv} - \chi\big) = 0 \qquad \kappa_i^* P_i \big(P_i^* - P_i^{pk}\big) = 0 \tag{6.8b}$$

guarantee global optimality where the Lagrange function is defined as

$$\mathcal{L} = \log_2 \Big(1 + \sum_{i=1}^{N} r_i \sigma_i^2\Big) + \mu \Big(\sum_{i=1}^{N} z_i (\sigma_i^2 + \phi_i^2) + \alpha_i \phi_i + C - \chi \Big) + \sum_{i=1}^{N} \kappa_i P_i \big(P_i - P_i^{pk}\big). \tag{6.9}$$

Intuitively, each NEHU should transmit at peak power level to maximize the throughput, and hence $P_i^* = P_i^{pk}$ which implies that $\kappa_i \neq 0$ according to the complementary slackness condition. Thus, $\sigma_i^2 + \phi_i^2 = P_i^{pk}$. If the harvested energy is satisfied with $\phi_i = 0\ \forall i \in \{1, 2 \cdots, N\}$, then the optimal solution is $\sigma_i^2 = P_i^{pk}$. In such a case, we have

$$\mathcal{E}'_{hv} = \sum_{i=1}^{N} z_i P_i^{pk} + C \tag{6.10}$$

and $\phi_i = 0$ holds as long as $\mathcal{E}'_{hv} \geq \chi$. However, if χ exceeds this threshold, then it becomes necessary to introduce non-zero mean component, i.e., $\phi_i^2 = P_i^{pk} - \sigma_i^2 \neq 0$. In this case, the optimal solution can be obtained using $\phi_i^2 + \sigma_i^2 = P_i^{pk}$ in the Lagrange function, and applying the first order derivative criteria given in (6.8a). From this, we get

$$\frac{\partial \mathcal{L}}{\partial \sigma_i^2} = \frac{r_i}{\ln(2)\Big(1 + \sum_{i=1}^{N} r_i \sigma_i^2\Big)} - \frac{\mu}{2\sqrt{P_i^{pk} - \sigma_i^2}} + \kappa_i = 0 \tag{6.11}$$

which leads to

$$\sigma_i^2 = P_i^{pk} - \frac{4}{\mu^2}\left(\frac{r_i}{A(\boldsymbol{\sigma}^2)} + \kappa_i\right)^2 \tag{6.12}$$

where $A(\boldsymbol{\sigma}^2) = \ln(2)\Big(1 + \sum_{i=1}^{N} r_i \sigma_i^2\Big)$. The power control policy given above is an implicit function, and it can be computed using iterative procedure. Furthermore, the lagrange multipliers μ and κ_i $\forall i \in \{1, 2, \cdots, N\}$ can be determined using subgradient method, and detail procedure is given in Algorithm 9.

Algorithm 9 Algorithm for throughput maximization of full duplex WIPT

Given: Tolerance ϵ
Compute $\mathcal{E}'_{hv}$
if $\mathbb{E}'_{hv} > \chi$ **then**
  $\phi_i = 0$, $\sigma_i^2 = P_i^{pk}$, $k \in \mathcal{S} = \{1, 2 \cdots, N\}$
else
  Assume $\boldsymbol{\sigma}_0^2 = [\sigma_{1_0}^2, \sigma_{2_0}^2, \cdots, \sigma_{N_0}^2]$
  repeat
    $j \leftarrow 0$
    repeat
      for i=1:N **do**
        Compute $\sigma_{i_j}^2$ using (6.12)
      end for
      $j \leftarrow j + 1$
    until $\sigma_{i_j}^2 - \sigma_{i(j-1)}^2$ $\forall j \in \mathcal{S}$
    update μ and κ_i using ellipsoid method
  until μ and κ_i converge to the accuracy ϵ
end if
Compute $\phi_i = \sqrt{P_i^{pk} - \sigma_i^2}$ $\forall i \in \mathcal{S}$

6.3 Energy-Efficient Resource Allocation

In this section, we provide energy-efficient resource allocation strategies for full-duplex operation of wireless information and power transfer. As noted earlier, EHU opportunistically harvests energy from the information-bearing signals transmitted by the NEHUs which are intended for the AP. This can lead to much better utilization of available energy resources and higher energy efficiency if the energy demand at the EHU can be satisfied with the energy-efficiency-maximizing input. Nevertheless, this cannot be guaranteed when the demand increases further. For the ease of analysis, we begin with two-users model and then generalize to multiple users settings.

6.3.1 Optimal Strategy for Two-Users

In principle, incorporating energy transfer along with information-bearing signal influences not only the optimal transmission policy but also the conventional definition of energy efficiency. Hence, when the information-bearing signal transmitted by NEHU is also used to energize the EHU, the harvested energy should be deducted while analyzing the system's net energy consumption as discussed in the literature [42] [43]. Based on this remark, the expression to determine the system energy efficiency for two-users model, i.e., one EHU and one NEHU, when transferring $\mathcal{R}_T$ bits of information to the destination while supporting the energy demand at EHU is given as

$$\eta_{EE} = \frac{\log_2\left(1 + r\sigma^2\right)}{P_c + P_A + P - \chi} \tag{6.13}$$

where χ denotes the required harvested energy at the EHU.

Proposition 6.3.1 *The system energy efficiency η_{EE} is a pseudo-concave function of the signal components transmitted by NEHU.*

Proof: See Appendix O.

It is clear that both $\mathcal{R}_T$ and $\mathcal{E}_{hv}$ depend on the transmitted power levels, and any increment in the harvested energy demand requires additional ΔP that could change the system efficiency by $\Delta\eta$. Thus, we formulate the following maximization problem in order to determine energy efficient solution given the harvested energy constraint.

$$\text{(PR:6.2)} \qquad \max_{\sigma^2,\phi} \ \eta_{EE} \tag{6.14a}$$

$$\text{subject to} \quad \mathcal{E}_{hv} \geq \chi \tag{6.14b}$$

$$P \leq P^{pk}. \tag{6.14c}$$

This is a non-convex problem, and cannot be easily solved using available convex optimization tools. However, since the energy efficiency is a pseudo-concave function according to Proposition 6.3.1 and the constraints are convex, Karush-Kuhn-Tucker conditions are necessary and sufficient to obtain the globally optimal solution. Hence, Lagrangian for the optimization problem (PR:6.2) can be expressed as follows:

$$\mathcal{L} = \eta_{EE} + \gamma(\mathcal{E}_{hv} - \chi) + \lambda(P - P^{pk}) \tag{6.15}$$

where γ and λ are the Lagrange multipliers associated with the energy constraint and transmitted power level given in (6.14b) and (6.14c), respectively. The corresponding optimality conditions are

$$\frac{\partial \mathcal{L}}{\partial \phi} = 0 \qquad \frac{\partial \mathcal{L}}{\partial \sigma^2} = 0 \tag{6.16a}$$

$$\gamma^*\big(\mathcal{E}_{hv} - \chi\big) = 0 \qquad \lambda^*\big(P^* - P^{pk}\big) = 0 \tag{6.16b}$$

Applying (6.16a) to (6.15), we get

$$\begin{aligned}\frac{\frac{h_d}{\ln(2)}}{(1+h_d\sigma^2)(K+P)} - \frac{\log_2(1+h_d\sigma^2)}{(K+P)^2} + \gamma h_e + \lambda = 0 \\ -\frac{2\phi\log_2(1+h_d\sigma^2)}{(K+P)^2} + \gamma(2\phi h_e + \alpha) + \lambda = 0\end{aligned} \tag{6.17}$$

where $K = P_c + P_A - \chi$. For the ease of analysis, we split the problem considering two scenarios based on the slackness condition given in (6.16b), i.e., for the harvested energy.

Constraint Satisfied with Strict Inequality

This case refers to the situation when the optimal solution satisfies the harvested energy in (6.14b) with strict inequality, $\mathcal{E}_{hv} > \chi$, while information-bearing signal is transmitted at the energy-efficiency-maximizing power level. However, we assume that only the demand can be harvested, and hence it would be fair to deduct χ instead of $\mathcal{E}_{hv}$ from the total energy consumption for energy efficiency analysis. Thus, problem (PR:6.2) can be equivalently expressed as

$$\text{(PR:6.2a)} \quad \max_{P\in\mathcal{P}} \ \eta_{EE}. \tag{6.18}$$

We know that $\gamma = 0$ according to the slackness condition, and hence substituting this into (6.17), we get

$$\begin{aligned}\frac{\frac{h_d}{\ln(2)}}{(1+h_d\sigma^2)(K+P)} - \frac{\log_2(1+h_d\sigma^2)}{(K+P)^2} + \lambda = 0 \\ -\frac{\log_2(1+h_d\sigma^2)}{(K+P)^2} + \lambda = 0\end{aligned} \tag{6.19}$$

However, this equation is not feasible for $\forall h_d \neq 0$ unless either $\phi = 0$, i.e. there is no non-zero mean component on the transmitted signal by N-EHU, or $\sigma^2 = 0$, i.e., the transmitted signal does not convey information. In fact, it is more energy-efficient to have $\sigma^2 \neq 0$ instead of $\phi \neq 0$ and $\sigma^2 = 0$. Thus, we conclude that transmission of information-bearing signal with non-zero mean is not needed when the required harvested energy at the EHU can be

satisfied with the energy-efficient input.

Theorem 6.3.1 *The analytical expression for the optimal transmit power when the energy demand at the EHU is satisfied with energy-efficiency-maximizing input level is given as*

$$\sigma^2 = \frac{e^{\mathcal{W}\left(\frac{h_d K-1}{e}\right)+1} - 1}{h_d} \qquad \forall \chi < \chi^*. \tag{6.20}$$

where $\mathcal{W}(\cdot)$ is Lambert function, and χ^* is the maximum demand at which efficiency-maximizing input satisfies the required harvested energy.

Proof: See Appendix P.

The above theorem explicitly shows how the transmitted power level from the NEHU changes with the harvested energy demand at the EHU. Accordingly, we observe that an increases in χ reduces K, or σ^2 in general, as the Lambert function is non-decreasing function. Hence, we claim that the power level decreases with χ, and this leads to the fact that opportunistically harvesting energy improves the system energy efficiency. Mathematically, let us first substitute (6.20) into (6.13). Then, the expression for the optimal energy efficiency becomes

$$\eta_{EE}^* = \frac{h_d}{\ln(2)} \left[\frac{\mathcal{W}\left(\frac{\Omega}{e}\right)+1}{\Omega + e^{\mathcal{W}\left(\frac{\Omega}{e}\right)+1}} \right] \tag{6.21}$$

where $\Omega = h_d K - 1$. Applying first order derivative on (6.21) with respect to the new parameter Ω, we get

$$\begin{aligned} \frac{\partial \eta_{EE}^*}{\partial \Omega} =& \frac{h_d}{\ln(2)} \frac{\partial}{\partial \Omega} \left[\frac{\mathcal{W}\left(\frac{\Omega}{e}\right)+1}{\Omega + e^{\mathcal{W}\left(\frac{\Omega}{e}\right)+1}} \right] \\ =& \left[\frac{1}{\Omega + e^{\mathcal{W}\left(\frac{\Omega}{e}\right)+1}} \right] \mathcal{W}'\left(\frac{\Omega}{e}\right) - \left[\mathcal{W}\left(\frac{\Omega}{e}\right)+1 \right] \frac{1+\mathcal{W}'\left(\frac{\Omega}{e}\right) e^{\mathcal{W}\left(\frac{\Omega}{e}\right)+1}}{(\Omega + e^{\mathcal{W}\left(\frac{\Omega}{e}\right)+1})^2}. \end{aligned} \tag{6.22}$$

After several manipulations, we have

$$\frac{\partial \eta_{EE}^*}{\partial \Omega} = -\frac{(1-\frac{1}{e})\Omega \mathcal{W}'\left(\frac{\Omega}{e}\right) + \mathcal{W}\left(\frac{\Omega}{e}\right)+1}{(\Omega + e^{\mathcal{W}\left(\frac{\Omega}{e}\right)+1})^2}. \tag{6.23}$$

Thus, it is obvious that $\frac{\partial \eta_{EE}^*}{\partial \Omega} < 0$ and hence optimal energy efficiency function decreases with each incremental value of Ω. However, Ω increases with a reduction in χ, which then implies EE is clearly an increasing function of the required harvested energy χ so long as it is below the threshold level χ^*. Within this range, the system energy efficiency improves with the demand while satisfying the harvested energy constraint with inequality, i.e., $\mathcal{E}_{hv} > \chi$. The threshold χ^*, i.e., the maximum demand which can be satisfied with the energy-efficiency-maximizing input, is at a point where $\mathcal{E}_{hv} = \chi^*$, and this can be obtained by substituting (6.20) into (6.5) with $\phi = 0$. This leads to the following equation:

$$h_d(\chi^* - rP_A) = z\left(e^{\mathcal{W}\left(\frac{h_d(P_c+P_A-\chi^*)-1}{e}\right)+1} - 1\right). \tag{6.24}$$

While this is an implicit equation and obtaining a closed-form expression is unlikely, (6.24) can be easily solved for χ^* using standard numerical tools.

Constraint Satisfied with Equality

When the required harvested energy exceeds the threshold χ^*, the constraint given in (6.14b) is active, and in such a case the optimal way is to satisfy the demand is with strict equality. In such a case, the optimization problem given in (PR:6.2) becomes

$$\begin{aligned} \text{(PR:6.2b)} \qquad & \max_{P\in\mathcal{P}} \ \eta_{EE} \\ & \text{s.t.} \ \ \mathcal{E}_{hv} = \chi. \end{aligned} \tag{6.25}$$

This is a concave-linear fractional problem, and (PR:6.2b) can be equivalently solved using its dual problem which is given as

$$\min_{\gamma,\lambda} \ G(\gamma, \lambda) \tag{6.26}$$

where $G(\gamma,\lambda) = \max_{\sigma^2,\phi} \mathcal{L}(\sigma^2,\phi,\gamma,\lambda)$ and the Lagrange function $\mathcal{L}$ is as defined in (6.15). We know that applying the KKT conditions in (6.16a) lead to (6.17), but now the solution for information-bearing component σ^2 and the mean ϕ of the signal from NEHU depends on its transmitted power level. Hence, we consider two possible scenarios as follows:

Case I - Inactive peak power constraint: In this case, the optimal transmitted power is beyond the energy-efficiency maximizing input with zero-mean but it still satisfies the peak power constraint with strict inequality, i.e., $P^* < P^{pk}$. This forces constraint in (6.14c) to be inactive, and hence the slackness conditions given in (6.16b) result in $\lambda = 0$. Thus, substituting this into (6.17), we have

$$\begin{aligned} \frac{h_d}{(1+h_d\sigma^2)(K+P)} &= \frac{\log(1+h_d\sigma^2)}{(K+P)^2} - \gamma h_e \\ \frac{\log(1+h_d\sigma^2)}{(K+P)^2} - \gamma h_e &= \frac{\gamma\alpha}{2\phi}. \end{aligned} \tag{6.27}$$

Despite the difficulty in getting analytical expression for the optimal solution of σ^2 and ϕ, the above equations in (6.27) can be easily solved using numerical tools, which then can be used to evaluate $G(\gamma,\lambda)$.

Case II - Active peak power constraint: In such a case, it is required to utilize all the available resource, i.e., the peak power, to satisfy the harvested energy constraint in (6.14b). Then, $K+P$ becomes a constant given the energy demand, and let us denote this with $k_a = K+P^{pk}$. Thus, simplifying the expressions in (6.17) according to the current scenario, we have

$$\frac{k_a h_d}{(1+h_d\sigma^2)} = \frac{\gamma\alpha k_a^2}{2\phi} \tag{6.28}$$

which leads to

$$\phi = \beta\left(\frac{1}{h_d} + \sigma^2\right) \tag{6.29}$$

where $\beta = 0.5\gamma\alpha k_a$. Substituting $\sigma^2 = P^k - \phi^2$ into (6.29), and solving for ϕ, we get

$$\phi = \frac{-b + \sqrt{b^2 + 4c}}{2} \tag{6.30}$$

where $b = \frac{1}{\beta}$ and $c = \frac{1}{h_d} + P^{pk}$. Note that these are solutions given the lagrange multiplies, and hence once σ^2 and ϕ are determined using either (6.27) or (6.30) depending the existing constraints, solutions are substituted into $\mathcal{L}$ to obtain $G(\gamma)$ and iteratively update the lagrange multipliers. The detail procedure is given in Algorithm 10, and sub-gradient method is applied to determine the optimal solution.

Algorithm 10 Algorithm for EE full-duplex WIPT

Given: Tolerance ϵ
Compute E'_{hv} at $\sigma^2 = P^{pk}$
if $E'_{hv} < \chi$ **then**
  $\lambda = 0$, $\phi = 0$
  Compute σ^2 using 6.20
else
  repeat
    Solve (6.30,) for ϕ,
    Compute $\sigma^2 = P^{pk} - \phi$
    update γ and λ using subgradient method
  until γ and λ converge to the accuracy ϵ
end if
update the solution for σ^2 and ϕ

6.3.2 Optimal Strategy for Multiuser Settings

Extending the discussion in the previous section to multiple NEHUs, the system energy efficiency is modified as

$$\eta = \frac{\log_2\left(1 + \sum_{i=1}^{N} r_i \sigma_i^2\right)}{\sum_{i=1}^{N} \sigma_i^2 + \phi_i^2 + P_A + P_C^{tot} - \chi} \tag{6.31}$$

where P_C^{tot} is the total circuit power consumption of the system. Here, the goal is to determine an optimal allocation of information-bearing and non-zero mean component to each transmitting node so that the system energy efficiency is maximized while the harvested en-

ergy constraint is satisfied. Except adding more parameters to control, neither the pseudo-concavity of the objective function nor the characteristics of the optimization problem given for two-users model are changed. Thus, the KKT conditions given in (6.16a) can be directly applied, and these result the following condition:

$$\begin{aligned} \frac{\frac{h_d^i}{\ln(2)}}{(1+h_d^i\sigma_i^2)(K+\sum_{i=1}^{N}P_i)} - \frac{\log_2(1+h_d^i\sigma_i^2)}{(K+\sum_{i=1}^{N}P_i)^2} + \gamma h_e + \lambda_i = 0 \\ -\frac{2\phi\log_2(1+h_d^i\sigma_i^2)}{(K+\sum_{i=1}^{N}P_i)^2} + \gamma(2\phi h_e + \alpha) + \lambda_i = 0 \end{aligned} \tag{6.32}$$

where λ_i is the lagrange multiplier for the i^{th} user peak power constraint. From the same argument stated in the proof of Theorem 4.2.1, an energy-efficient strategy allows the user with the best link to transmit and keep the rest silent. In fact, this is the true solution provided that the optimal solution satisfies the harvested energy constraint with inequality. Any incremental in the harvested energy demand could require to transmit at the peak, and beyond this point, the decision relies on whether to allow the NEHU with the second best link to transmit or introduce non-zero-mean at the previous NEHU. Similar approach is followed when the constraint is satisfied with equality, but details are omitted for brevity.

6.4 Numerical Results

In this section, we provide simulation results to justify the theoretical frameworks presented in previous sections. For the analysis, we consider that $h_d = 0.8$ and $h_e = 0.35$. In addition, $P_A = 10dB$ and $P_c = 1dB$. In order to compare the performance improvement and identify the effect of non-zero mean input, we consider two different values based on the channel characteristics, i.e., $\alpha \in \{0.1, 0.75\}$ and $g \in \{0.1, 0.75\}$ where $\alpha \neq g$ as indicated in the figures.

Fig. 6.2a and Fig. 6.3a illustrate the optimal power allocation strategies based on the required harvested energy. As can be seen in Fig. 6.2a, zero-mean input is optimal until

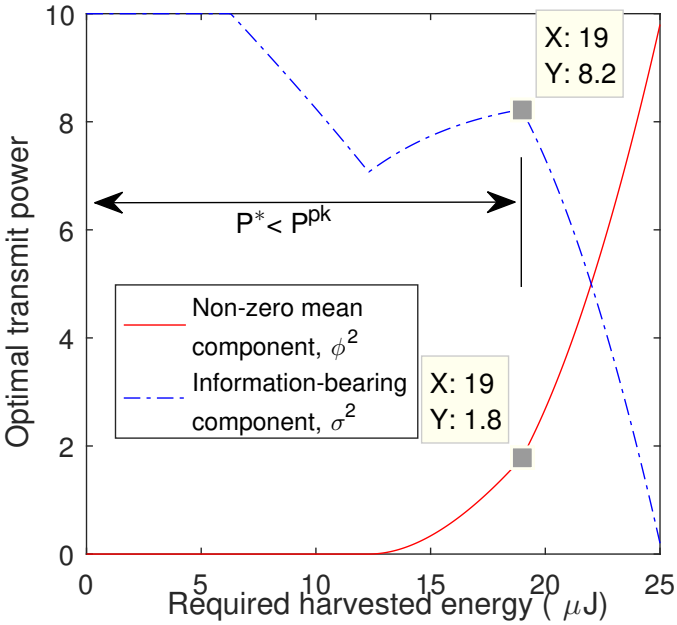

(a) variance and mean-square (W) vs. required harvested energy

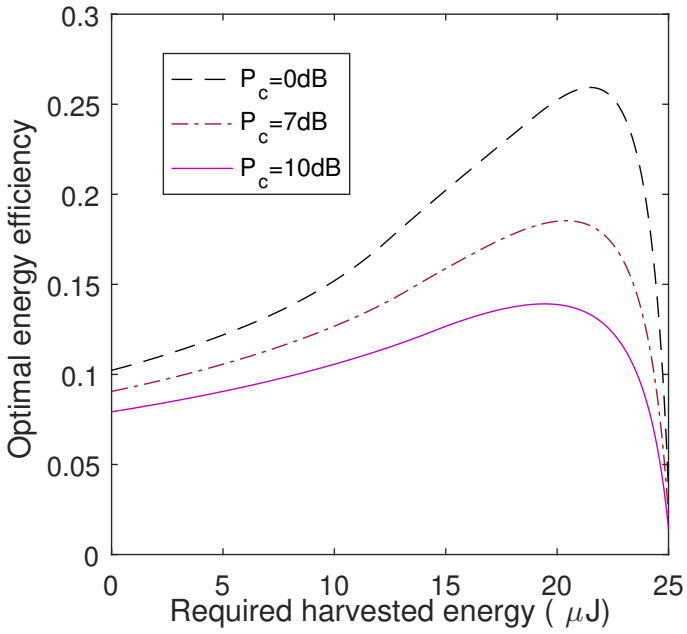

(b) Energy efficiency vs. required harvested energy, χ

Figure 6.2: Performance parameters under more favorable channel conditions between EHU and AP, i.e., $\alpha = 0.75$ and $g = 0.75$

---

the demand exceeds a certain threshold. In addition, in this region, the transmitted power level decreases with χ. However, once the demand exceeds the threshold, the transmitted

power level increases with the demand until the sum of information-bearing and non-zero mean components reaches the peak. Similar trends is observed in Fig. 6.3a except that, in this case, the optimal policy encourages to transmit with zero-mean. This is because the link between EH and NEHU experiences very bad channel condition. Hence, we observe that introducing non-zero mean into the information-bearing signal have significance impact when the wireless link from AP to each user has better channel gain compared with between the users, i.e., $\alpha \gg h_d$. Likewise, $\alpha \ll h_d$ encourages NEHU to transmit the signal with zero-mean as can be seen in Fig. 6.3a. On the other hand, the variance and non-zero mean component increases with χ until the total transmitted power reaches the peak. This is clearly shown in Fig. 6.2a, and once $P = P^{pk}$, any incremental energy demand is satisfied by sacrificing the data conveying component, i.e., by reducing σ^2.

On the other hand, Fig. 6.2b and Fig. 6.3b demonstrate how the system energy efficiency changes with the required harvested energy. We observe that the optimal energy efficiency improves as the demand increases. This is because when the demand is satisfied by the energy-efficiency maximizing input, opportunistic harvesting leads to smaller overall energy consumption, i.e., the net consumed energy is reduced. However, this depends on the channel characteristics, as noted earlier, and the circuit power consumption. This is due to the fact that each incremental energy demand $\Delta\chi$ is satisfied by the increasing transmitted power level or equivalently the variance of the data signal, and hence there is still a gain in the number of bits transferred. Whereas, since relatively higher α value encourages introducing the non-zero mean component when the energy demand increases beyond the threshold χ^* indicated in (6.20), this hurts the system energy efficiency as can be seen from Fig. 6.2b. Although it is difficult to observe the significance of the non-zero mean component on the overall energy efficiency in Fig. 6.3b, it is more clear to understand in Fig. 6.2b. In this figure, if NEHU transmits the information-bearing component only, the maximum harvested energy is much lower than that can be obtained with non-zero mean component. In addition, while η for the zero-mean input starts to decrease, i.e., the slope becomes negative, introduc-

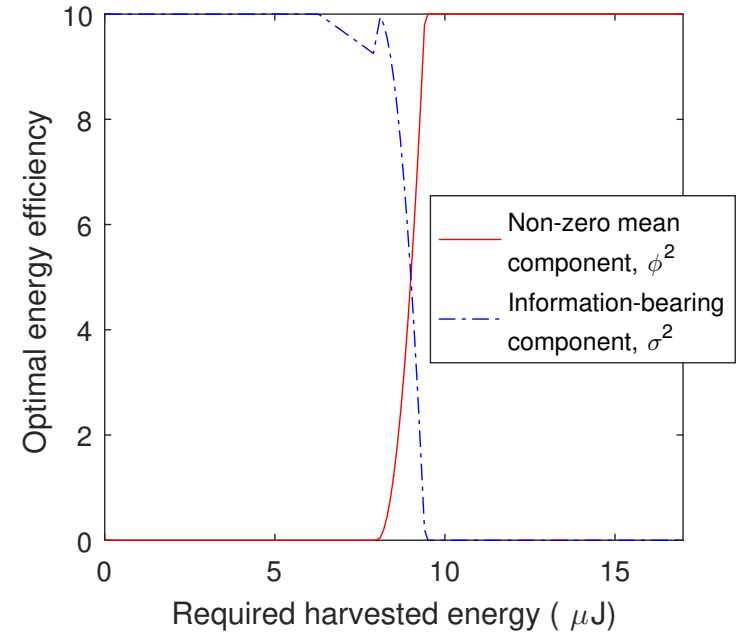

(a) variance and mean-square (W) vs. required harvested energy

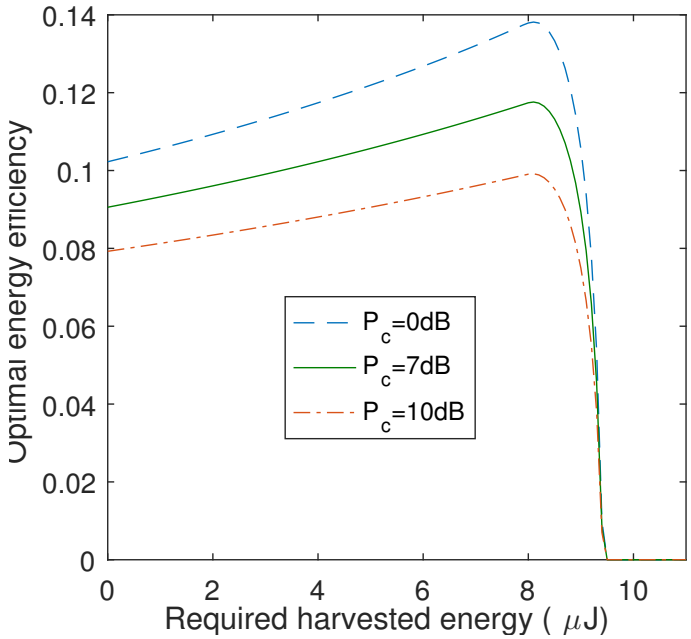

(b) Energy efficiency (bpJ/Hz) vs. required harvested energy, χ

Figure 6.3: Performance parameters under less favorable channel conditions between EHU and AP, i.e, $\alpha = 0.1$ and $g = 0.1$

---

ing a non-zero mean component achieves better efficiency with positive slope. Furthermore, it becomes possible to meet higher energy demand with better efficiency in the presence of

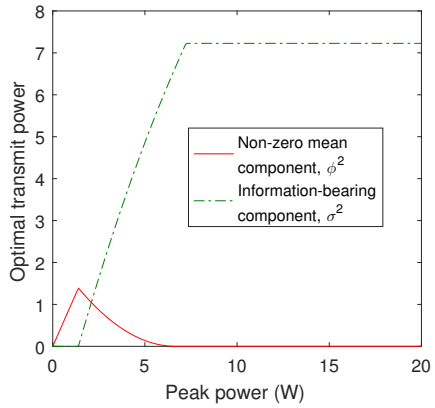

(a) Variance and mean-square (W) vs. peak power level at $\chi = 8\mu J$

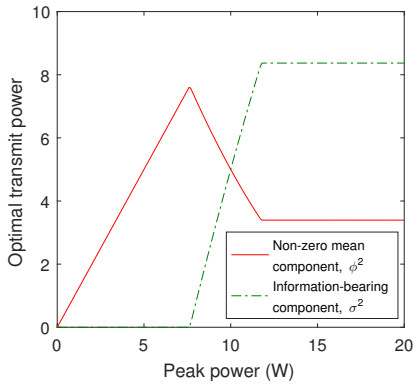

(b) Variance and mean-square (W) vs. peak power level at $\chi = 22\mu J$

Figure 6.4: Effect of peak power under $\alpha = 0.75$ and $g = 0.75$

non-zero mean compared with the input having zero mean.

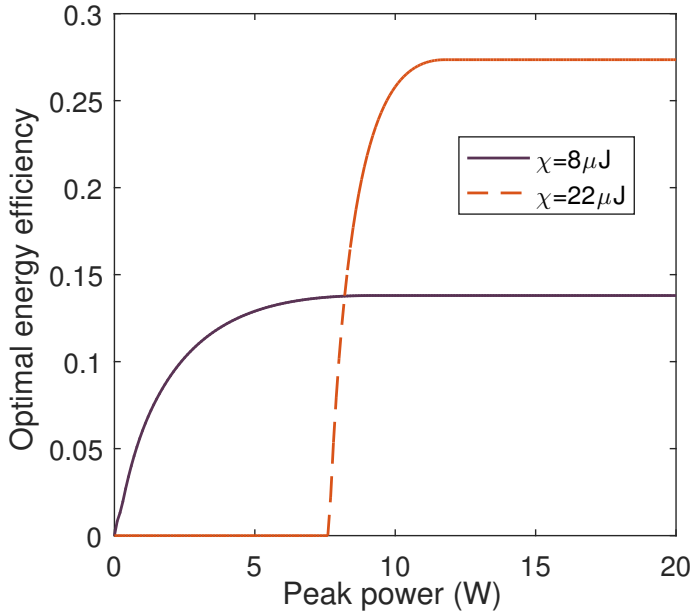

Figure 6.5: Energy efficiency (bpJ/Hz) vs. peak power level

We also demonstrate in Fig. 6.4a the impact of peak power level of the transmitted signal from the NEHU on the variance and non-zero mean component for a given required harvested energy χ. As can be seen from the figure, the optimal allocation policies for σ^2

and ϕ vary with P^{pk} depending on whether the transmitted power is fully utilized or not. When the available peak power is higher than the optimal transmitted power level for the given harvested energy constraint, i.e., $P^* < P^{pk}$, the solution of the variance and the mean become independent of the peak power constraint. In regard to system energy efficiency η_{EE}, we observe from Fig. 6.5 that there is an information transfer as long as the available resource is at least sufficient enough to satisfy the required harvested energy.

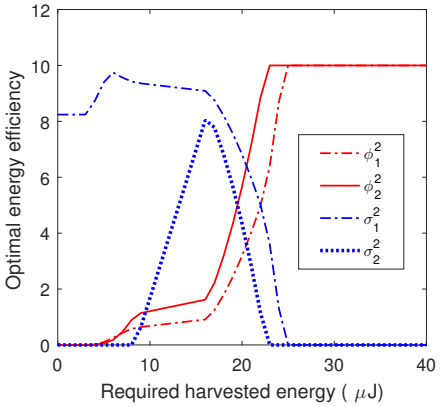

(a) Energy efficiency maximizing solution

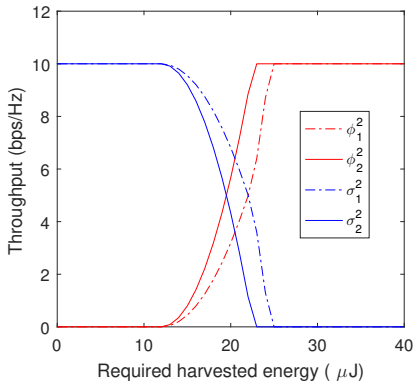

(b) Throughput maximizing solution

Figure 6.6: Transmit power level (W) vs. harvested energy constraint $\alpha 1 = 0.75$, $\alpha 2 = 0.5$, a and $g = 0.75$

In the presence of multiple NEHUs, the optimal power allocation strategy depends on their channel characteristics and the performance metric to maximize. For instance, in the case of energy efficiency maximization, since UE has higher channel gain both with the AP and EHU, it starts to transmit until the required harvested energy forces to UE 2 to introduce non-zero mean component as can be seen from Fig. 6.6a. Further increment in χ encourages to give more weight to the non-zero mean component, and the information-bearing component begins to decrease when the total transmitted power from the corresponding user reaches the peak. On the other hand, in 6.6b, both users transmit at peak power without having non-zero mean component so long as the harvested energy constraint is not binding. Once this constraint is active, the harvested energy constraint overrides the throughput-efficient solution, and hence non-zero mean becomes important to satisfy the additional

demand. Thus, the information-bearing components of both users decrease with incremental of χ until the demand reaches the maximum energy that can be supported by the users under the given channel condition.

Chapter 7

Analysis of Wireless-Powered Cellular Networks

In this chapter, performance analysis of energy harvesting communication networks with randomly distributed access points and user equipments is well studied considering three different scenarios, i.e., downlink WPT and uplink WIT, downlink SWIPT and uplink WIT, and downlink WPT and uplink WPT with mmWave. In all the three scenarios, average harvested energy, SINR coverage probabilities, average achievable rate, and system energy efficiency are characterized as a function of uplink and downlink operating intervals, and other relevant parameters such as AP density and directivity gain. We introduce system model and fundamental concepts in Section 7.1. Then, performance analysis is explicitly carried out for each scenario in Section 7.2, Section 7.3 and Section 7.4. Finally, numerical results are illustrated in Section 7.5.

7.1 System Model and Preliminaries

7.1.1 Cellular Networks Model

We consider a cellular wireless communication networks in which APs and energy-harvesting UEs are spatially distributed according to an independent and homogeneous Poisson point process (HPPP) Φ and Φ_{UE} with spatial density λ and λ_{UE}, respectively. We assume that these UEs are more densely deployed compared with the APs, i.e., $\lambda_{UE} > \lambda$, and hence in the cellular region partitioned into Voroni cells as shown in Fig. 7.1 every AP serves at least one UEs within its coverage area. Without loss of generality, due to Sylvinyak Theorem [96] and stationary property of HPPP, the analysis is performed for the typical UE located at the origin of coordinate system. The AP associated with the typical UE is denoted by AP_0, whereas the set containing interfering APs is denoted by $\Phi_{/0}$.

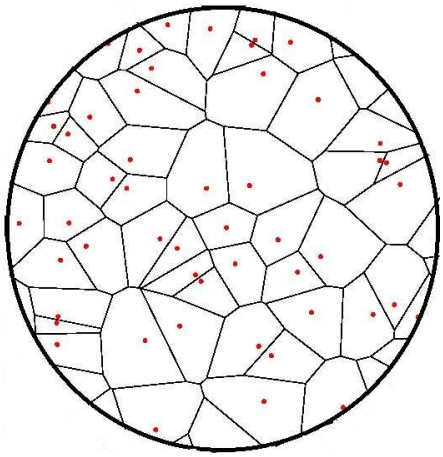

Figure 7.1: Voroni tessellation for the wireless-powered cellular network

Physically, UEs are designed without having an embedded power source, but they operate based on harvest-then-transmit protocol. We assume that APs are directly connected to external power supply, and every active AP operates in two sequential phases: In the first phase, it broadcasts a signal with power P_a over the downlink channel to energize the nearby UEs. Indeed, the typical UE harvests energy not only from the associated AP, but also from the interfering APs located outside the cell. In the case of wireless power transfer,

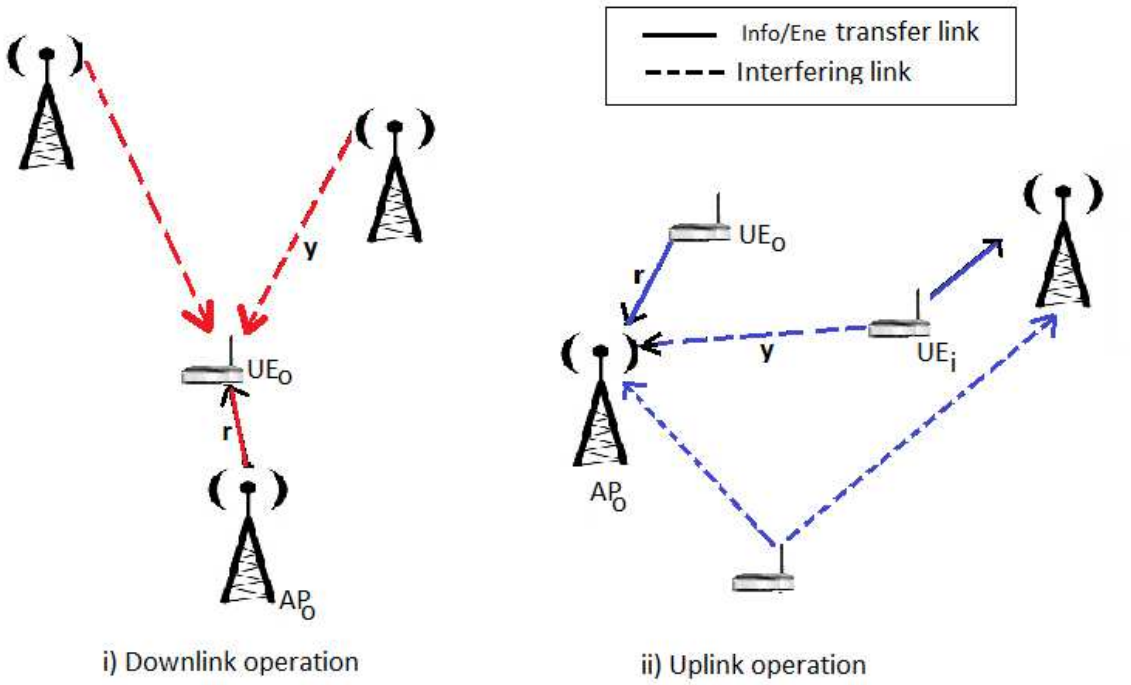

Figure 7.2: Downlink energy broadcasting and uplink information transfer

interference has a positive contribution to the performance of UE, i.e., additional energy can be harvested. All UEs harvest energy simultaneously during the downlink operation from all the APs located within and outside their cell. Then in the second phase, APs receive faded information-bearing signals transmitted uplink by these UEs. Since UEs are highly dense, multiple UEs can be located in a given cell coverage area. In such a case, we assume that the corresponding AP receives information-bearing signals from each UE over non-overlapping time intervals. This avoids any interference from the UEs in the same cell, i.e., intercell interference. However, depending on the distance and transmit power level, APs may still experience interference arising from the signals transmitted by UEs in the other cells as shown in Fig. 7.2. Symbolically, τ_B denotes the fraction of time allocated for the downlink operation, and hence $T - \tau_B$ becomes available for the uplink data transfer. We assume block fading scenario, and the downlink and uplink operation intervals remain the same over the consecutive fading state realizations. Without loss of generality, we use a normalized unit for each block, i.e., $T = 1$, in the sequel. Similar to

the remark in [64], UEs can store the harvested energy in a battery equipped with a super capacitor which eliminates the randomness of instantaneous received power and provides fixed transmit power. Furthermore, we assume that each wireless-powered user fully utilizes the harvested energy to support data transmission in one cycle or a communication block.

7.1.2 Channel Model

As noted above, we assume that fading state realizations, channel gain, and related channel characteristics parameters are constant over a block duration. In order to mathematically model the wireless link, we consider the distance dependent path loss and the small-scale multipath fading. More specifically, the path loss model between a UE and the corresponding AP is given by

$$g = [\max(d, r)]^{-\alpha} \tag{7.1}$$

where α is path loss exponent, r is the Euclidean distance between the UE and AP, and $d \geq 1$ is used to avoid model inaccuracy for a very short distance [13]. Similarly, g_i denotes the path loss for the i^{th} AP and its respective active UE. The probability density function (PDF) of the distance between a typical user and its serving AP is given as

$$f_r(r) = 2\pi\lambda r e^{-\pi\lambda r^2}. \tag{7.2}$$

In addition, the link between UE and serving AP experiences Rayleigh fading, and the magnitude square of the fading coefficient, which is exponentially distributed with mean μ, is denoted by $h_i \sim exp(\mu)$ where $i \in \Phi$. Note that $i = 0$ for the serving AP, i.e., associated to the typical user.

Assuming densely deployed UEs, we stated that each active AP serves at least one UE in its coverage area. However, how a typical UE is associated to a particular AP needs certain criteria. For instance, smallest path loss and highest received power are two ways among other cell association criterion. In this section, we consider that a single cell consists of all

the UEs that achieve the lowest path loss, which is formulated as

$$g_0 = \min_{i \in \Phi} \left\{ g(r^{(i)}) \right\} \tag{7.3}$$

where $r^{(i)}$ denotes the Euclidean distance between a typical UE and a serving AP.

7.1.3 Downlink Harvested Energy

As mentioned above, every AP operates in half-duplex mode, i.e., it broadcasts energy in the first phase and then decodes the received signals transmitted by wireless-powered UEs in the second phase. Depending on the distance and strength of the transmitted signal, there could be considerable interference due to the AP and UEs in the downlink and uplink operations, respectively. It is obvious that the interference in the second phase reduces the received SINR and degrades the performance, i.e., throughput. Nevertheless, wireless-powered UEs benefit from the interfering APs while harvesting energy from the AP within the associated cell, and this can support to transfer additional bits of information.

Thus, the amount of harvested energy at the typical UE during the downlink operation interval can be computed using

$$E_0^{hv} = \tau_B \mathbb{E} \left\{ P_a h_0 g_0 + \sum_{i \in \Phi \setminus 0} P_a h_i g_i \right\} \tag{7.4}$$

where the second term describes opportunistically harvested energy from all active interfering APs located outside the associated cell. The above equation can be simply rewritten as

$$\begin{aligned} E_0^{hv} &= \tau_B \big(P_0 + P_I \big) \\ &= \tau_B P_0^{hv} \end{aligned} \tag{7.5}$$

and the explicit expressions for P_0 and P_I are as follow:

$$\begin{aligned} P_0 &= \mathbb{E}\Big\{ P_a h_0 g_0 \Big\} \\ &= \mu P_a \mathbb{E}_r \left\{ \big[\max(r,d) \big]^{-\alpha} \right\} \\ &= \mu P_a \left[\int_0^d d^{-\alpha} f_r(r) dr + \int_d^\infty r^{-\alpha} f_r(r) dr \right] \\ &= \frac{\mu P_a}{2} \left[d^{-\alpha} \Big(- e^{-Cd^2} + 1 \Big) + C^{\frac{\alpha}{2}} \Gamma\Big(\frac{-\alpha+2}{2}, Cd^2 \Big) \right] \end{aligned} \tag{7.6}$$

where $\Gamma(a,x)$ is the incomplete gamma function, and $C = 2\pi\lambda$. In addition, the second equality above uses the fact that $\mathbb{E}\{h_0\} = \mu$. Similarly,

$$\begin{aligned} P_I &= \mathbb{E} \left\{ \sum_{i \in \Phi \setminus 0} P_a h_i g_i \right\} \\ &= \mathbb{E} \left\{ \sum_{i \in \Phi \setminus 0} P_a h_i \Big[\max(x_i, d) \Big]^{-\alpha} \right\} \end{aligned} \tag{7.7}$$

where x_i is the distance between the typical user and an interfering AP, and indeed $x_i > r$. Applying Campbell's theorem, which states that $\mathbb{E}\Big\{ \sum_{x \in N} f(x) \Big\} = \lambda \int_{R^d} f(x) dx$ where N denotes a stationary point process defined on the d-dimensional Euclidean space, (7.7) becomes

$$P_I = 2\pi\lambda\mu P_a \int_0^\infty \Big[\int_r^\infty \Big[\max(u,d) \Big]^{-\alpha} u du \Big] f_r(r) dr \tag{7.8}$$

which leads to

$$\begin{aligned} P_I &= 2\pi\lambda\mu P_a \left[\int_0^d \Big[.5d^{-\alpha+2} - 0.5 d^{-\alpha} r^2 - \frac{d^{-\alpha+2}}{2-\alpha} \Big] f_r(r) dr + \int_d^\infty \frac{r^{-\alpha+2}}{\alpha-2} f_r(r) dr \right] \\ &= \mu P_a \left[\frac{d^{-\alpha+2}}{2} \Big(\frac{1}{2} - \frac{1}{2-\alpha} \Big) \Big(- e^{-Cd^2} + 1 \Big) + \frac{d^{-\alpha}}{4C} \Big[(Cd^2+1) e^{-Cd^2} - 1 \Big] + \frac{C^{\frac{\alpha}{2}-1}}{2\alpha-4} \Gamma\Big(\frac{-\alpha+4}{2}, Cd^2 \Big) \right]. \end{aligned} \tag{7.9}$$

On the other hand, the amount of harvested energy at UEs which are not near the generic AP can be easily determined using

$$\begin{aligned} E_i^{hv} &= \tau_B \left[\sum_{k \in \Phi} P_a h_k [\max(y, d)]^{-\alpha} \right] \\ &= \tau_B P_i^{hv} \end{aligned} \tag{7.10}$$

where y denotes the distance between UE in the i^{th} cell and any active AP.

7.2 WP Cellular Networks with Harvest-then-Transmit Protocol

In this section, we analyze energy efficiency and throughput of the energy harvesting cellular networks as a function of the downlink-uplink operating intervals. In fact, there is always a tradeoff in allocating time for the downlink energy broadcasting and uplink information transfer since the performance of wireless-powered nodes rely on how much time is allocated for the energy harvesting operation. In addition, the transmit power level from the APs as well as their spatial density have an impact on the network throughput and energy consumption. Hence, in our performance analysis, we initially derive the expressions for SINR coverage probability and achievable data rate as a function of the parameters to be optimized such as harvesting interval.

7.2.1 Received Signal-to-Interference-Noise Ratio

In the uplink information transfer phase, each UE sends an information-bearing signal to the AP that has the lowest path loss link. In case there are multiple UEs associated to a given AP, they will transmit over orthogonal time intervals based on the time-division multiplexing scheme. As noted above, a typical AP in the uplink phase can experience interference from the UEs in the nearby cells. But, the overall impact depends on channel characteristics and

uplink transmitted signal power level of each UE. We assume that each UE utilizes β fraction of the harvested energy to transmit information while the rest is consumed by the circuitry to carry out the transmission process. Hence, the uplink transmitted signal power level by the UE that is associated with the k^{th} cell is given as

$$P_k^u = \zeta \beta_k \frac{\tau_B P_k^{hv}}{1 - \tau_B} \tag{7.11}$$

where $k \in \Phi$, and ζ is the RF-to-DC conversion efficiency, and without loss of generality, we assume that all UEs have the same conversion efficiency. Thus, the received signal-to-interference-noise ratio (SINR) at the typical AP over the uplink transmission interval is given as

$$SINR_0 = \frac{a_0 h_0 g_0}{\sigma_a^2 + \sum_{i \in \Phi \setminus 0} a_i h_i g_i} \tag{7.12}$$

where $\sigma_a^2 = \sigma^2 \frac{1-\tau_B}{\tau_B}$, $a_0 = \zeta \beta_0 P_0^{hv}$, and $a_i = \zeta \beta_i P_i^{hv}$ for $i \in \Phi \setminus 0$. In addition, $g_i = [\max(d, y)]^{-\alpha}$ denotes the pathloss for the link between generic AP and an interfering UE which is found at a distance y.

The interference from wireless-powered nodes might be small, specially when they are distant and transmit at low power level, and in such cases, noised-limited scenario is an approximately best model and further simplification can be done to carry out performance analysis. On the other hand, the higher density of UEs might result a significant interference compared with the noise power, and this leads to interference-limited scenario. In the following sections, we formulate mathematical expressions for the achievable ergodic rates and outage capacities considering noise-limited and interference-limited scenarios, and study the corresponding system performance. Thus, we begin with a generalized model considering both noise and interference simultaneously, and then we specifically analyze the characterization for each scenario.

7.2.2 Coverage Probability

For energy-harvesting UEs, the uplink transmission coverage probability describes the probability that the received signal from UEs at a randomly chosen AP exceeds a certain threshold. Given the target SINR, γ_T, the coverage probability is defined as

$$P_c = \int_0^\infty \Pr\Big\{ SINR > \gamma_T \big| r \Big\} f_r(r) dr. \tag{7.13}$$

Substituting (7.29) into (7.13), and simplifying the expression, we obtain

$$\begin{aligned} P_c &= \int_0^\infty \Pr\Big\{ h_0 > \frac{\gamma_T (I_{int} + \sigma_a^2) r^\alpha}{a_0} \big| r \Big\} f_r(r) dr \\ &= \int_0^\infty e^{-\frac{\gamma_T \mu \sigma_a^2}{a_0} r^\alpha} \mathbb{E}\Big\{ \exp(s I_{int}) \Big\} f_r(r) dr \end{aligned} \tag{7.14}$$

where $s = \frac{\mu \gamma_T r^\alpha}{a_0}$, $I_{int} = \sum_{i \in \Phi \setminus 0} a_i h_i g_i$. Applying Campbell's Theorem to $\mathbb{E}\Big\{ \exp(s I_{int}) \Big\}$ and computing the expectation over the variable h_i, we get

$$\begin{aligned} \mathbb{E}\Big\{ e^{s I_{int}} \Big\} &= \mathbb{E}\Big\{ e^{s \sum_{i \in \Phi/0} a_i h_i g_i} \Big\} \\ &= \mathbb{E}\left\{ \prod_{i \in \Phi/0} e^{-s a_i h_i y^{-\alpha}} \right\} \\ &\overset{\text{a}}{=} \exp\Big(-2\pi\lambda \int_r^\infty \Big[1 - \mathbb{E}\Big\{ e^{-s a_i h_i y^{-\alpha}} \Big\} \Big] y dy \Big) \\ &\overset{\text{b}}{=} \exp\Big(-2\pi\lambda \int_r^\infty \Big[\frac{s a_i y^{-\alpha}}{\mu + s a_i y^{-\alpha}} \Big] y dy \Big). \end{aligned} \tag{7.15}$$

Thus, the probability that the received SINR at a typical AP exceeds a given threshold γ_T in the uplink information transmission phase can be expressed as

$$\begin{aligned} P_c &= \int_0^{\infty} e^{-\frac{\gamma_T \mu \sigma_a^2}{a_0} r^{\alpha}} \exp\Big(-2\pi\lambda \int_r^{\infty} \frac{s a_i y^{-\alpha}}{\mu + s a_i y^{-\alpha}} y dy \Big) f_r(r) dr \\ &= \int_0^{\infty} e^{-\frac{\gamma_T \mu \sigma_a^2}{a_0} r^{\alpha}} \exp\left(-\frac{\pi\lambda r^{2-\alpha}}{\mu(-2+\alpha)} {}^2F_1\Big(\Big[1, \frac{-2+\alpha}{\alpha}\Big]; 2 - \frac{2}{\alpha}; -\frac{s a_i r^{-\alpha}}{\mu}\Big)\right) f_r(r) dr. \end{aligned} \tag{7.16}$$

Proposition 7.2.1 *In the energy-harvesting cellular communication network, coverage probability is an increasing function of the harvesting interval τ_B under noise-limited scenario.*

Proof: See Appendix Q

According to Lemma 7.2.1, we see that allocating more time for downlink energy broadcasting improves uplink SNR coverage probability, i.e., as $\tau_B \to 1$, we have $P_c \to 1$. However, this does not necessarily imply that the achievable data rate also increases with τ_B as will be discussed in the following section.

7.2.3 Achievable Data Rate

One of the performance parameter for the wireless-powered cellular network illustrated in Section 7.1.1 is the number of bits successfully received by a typical AP during the uplink transmission interval, and mathematically this can be formulated as

$$R = \int_0^{\infty} \mathbb{E}\Big\{ (1-\tau_B) \log_2\Big(1 + SINR\Big)\Big\} f_r(r) dr \tag{7.17}$$

which can be further expressed as

$$R = \int_0^{\infty} \Big[\int_0^{\infty} Pr\Big\{ SINR > \gamma_a \Big\} f_r(r) dr \Big] dt \tag{7.18}$$

where $\gamma_a = 2^{\frac{t}{1-\tau_B}} - 1$. The inner integral is indeed the SINR coverage probability for the threshold γ_a, and this can be computed using the explicit expression provided in (7.33) by replacing γ_T with γ_a. Thus, substituting (7.33) into (7.18), we have

$$R = \int_0^\infty \int_0^\infty \mathcal{K}(r,t) \exp\Big(\mathcal{H}(r)\ {}_2F_1\Big(\big[1,b\big];c;d\Big)\Big) f_r(r) dr dt \tag{7.19}$$

where $\mathcal{K}(r,t) = e^{-\frac{\mu\gamma_a\sigma_a^2}{a_o} r^\alpha}$, $\mathcal{H}(r) = -\frac{\pi\lambda r^{2-\alpha}}{\mu(-2+\alpha)}$, $b = \frac{-2+\alpha}{\alpha}$, $c = 2 - \frac{2}{\alpha}$, and $d = -\gamma_a \frac{a_i}{a_0}$. This is a general expression that takes into account of both noise and interference, and in the following subsections, we explicitly consider noise-limited and interference-limited scenarios.

Noise-limited scenario

In this scenario, the thermal noise at the receiving end is assumed to dominate the interference signal from other UEs outside the associated cell, and in such a case, the rate expression given in (7.19) becomes

$$R_{NL} = \int_0^\infty \mathbb{E}_r \left\{ e^{-\left[c_0 \frac{1-\tau_B}{\tau_B}\left(2^{\frac{t}{1-\tau_B}}-1\right) r^\alpha\right]} \right\} dt \tag{7.20}$$

where $c_o(r) = \frac{\mu\sigma^2 r^\alpha}{a_0}$. Since expectation preserves convexity/concavity and exponential function is convex, the characteristics of rate expression formulated above depends on the function on the exponent, i.e., $\mathcal{H} = \frac{1-\tau_B}{\tau_B}\left[2^{\frac{t}{1-\tau_B}} - 1\right]$. Applying first order derivative to $\mathcal{H}$, we have

$$\frac{d\mathcal{H}}{d\tau_B} = -\frac{(1-\tau_B)(2^{\frac{t}{1-\tau_B}} - 1)}{\tau_B^2} - \frac{2^{\frac{t}{1-\tau_B}} - 1}{\tau_B} + \frac{t\log(2) 2^{\frac{t}{1-\tau_B}}}{(1-\tau_B)\tau_B}. \tag{7.21}$$

This is neither an increasing nor a decreasing function of τ_B, and hence, unlike to the characteristics of SNR coverage probability described in Proposition7.2.1, it is obvious from (7.21) that the achievable data rate given in 7.20 is not a monotonically increasing function of harvesting interval.

Interference-limited scenario

Due to the highly dense network deployment, noise power could be negligible compare with the aggregated interference power. In this scenario, there is a very strong interference at a typical AP in the uplink transmission compared to the thermal noise, i.e., $\sigma_a^2 \ll I_{Int}$, and hence the signal-to-interference ratio (SIR) is derived from the SINR as follows:

$$\begin{aligned} SINR &= \frac{\frac{\tau_B}{1-\tau_B}\Big(\zeta\beta_0 P_0^{hv} h_0 g_0\Big)}{\sigma^2 + \sum_{i\in\Phi/0}\frac{\tau_B}{1-\tau_B}\Big(\zeta\beta_i P_i^{hv} h_i g_i\Big)} \\ &\approx \frac{a h_0 r^{-\alpha}}{\sum_{i\in\Phi/0} a_i h_i g_i} = SIR. \end{aligned} \tag{7.22}$$

Since both the information-bearing signal and the interference change by the same factor $\frac{\tau_B}{1-\tau_B}$ given the harvesting interval, it is interesting to observe from (7.22) that τ_B does not have an impact on the received SIR. Nevertheless, the achievable data rate, which is expressed as

$$R_{IL} = \int_0^\infty \left[\int_0^\infty Pr\Big\{\frac{a h_0 r^{-\alpha}}{\sum_{i\in\Phi/0} a_i h_i g_i} > \gamma_a\Big\} dt\right] f_r(r) dr, \tag{7.23}$$

still depends on the harvesting interval as the threshold γ_a is a function of τ_B. The expression given in (7.23) can be simplified as

$$R_{IL} = \int_0^\infty \mathbb{E}_r\left\{\exp\left(-\frac{\pi\lambda r^{2-\alpha}}{\mu(-2+\alpha)}{}_2F_1\Big(\big[1,b\big];c;-\gamma_a\frac{a_i}{a_0}\Big)\right)\right\} dt \tag{7.24}$$

where $b = \frac{-2+\alpha}{\alpha}$, and $c = 2 - \frac{2}{\alpha}$.

7.2.4 Energy Efficiency

An energy-efficient strategy is an essential in the presence of energy constrained nodes in wireless communication systems, and the system energy efficiency can be quantitatively

measured as the bits of information reliably transferred to a receiver per unit consumed energy at the transmitter as well as the receiver. Basically, energy is required in the system to transmit energy-bearing signal to the harvesting nodes as well as due to static power consumption including signal processing, cooling, and so on at the AP. Since the circuitry consumption at the users is supplied by the harvested energy, it will not be included in the net system energy consumption. Let P_T^D and P_T^U denote the total power consumption during downlink and uplink operation intervals, respectively. As mentioned above, the energy consumption during the harvesting interval τ_B is due to the transmitted energy-bearing signal and the required energy to carry out the signal process, i.e., $P_T^D = \zeta P_a + P_c^D$, where $\frac{1}{\zeta}$ is the efficiency of the power amplifier. On the other hand, energy is consumed at the APs during the uplink operation interval in order to decode the received information, and hence $P_T^U = P_c^U$. Thus, the average energy consumption of APs in the cellular network is given as

$$E_{tot} = \lambda\tau_B(P_c^D + \zeta P_a) + \lambda(1-\tau_B)P_c^U \tag{7.25}$$

where P_c^U and P_C^D denote the static power consumption of a typical AP. Thus, the system energy efficiency of a wireless-powered cellular network, denoted as η_{Cell}, can be defined as the ratio of network throughput to the average power consumption of the system, i.e.,

$$\eta_{Cell} = \frac{\text{Network throughput}}{P_{tot}}. \tag{7.26}$$

The expression for the cellular throughput of the energy-harvesting network modeled in Section 7.1.1 is given as λR where R is as defined in (7.19). Therefore, the system energy efficiency can be expressed as

$$\eta_{cell}(\tau_B) = \frac{\mathcal{R}(\tau_B)}{\tau_B P_T^D + (1-\tau_B)P_T^U} \tag{7.27}$$

where $\mathcal{R} \in \{R_{NL}, R_{IL}\}$. Based on the above characterizations, we understand that there is a trade-off between the time allocated for the downlink harvesting and uplink information transfer. Indeed, if UEs are allowed to scavenge energy over a longer time, they can harvest more energy, but there might not be enough time to support data transfer. Thus, it is necessary to investigate how operating intervals affect the network throughput as well as system energy efficiency.

7.3 WP Cellular Network with Downlink SWIPT

In this section, we consider that the randomly distributed APs jointly transfers information and power to the UEs during the downlink operation interval. These UEs are assumed to be equipped with information decoding and energy harvesting components, and hence the transmitted signal from the AP not only targets to power nearby UEs but also conveys information to establish data connectivity. In fact, these users also send their data uplink to their associated APs using the harvested energy. As mentioned earlier, the analysis is conducted for a typical UE located at the origin based on the Slivnyak theorem [96]. We address the performance analysis applying power-splitting scheme at the typical UE, and details are provided for the downlink and uplink operation intervals as follow.

Phase I: Downlink operation

A serving AP broadcasts a signal to the typical user for an interval of τ_B sec., and the harvested energy during this time can be computed as

$$E_0^{hv} = \tau_B(1-\rho_0)(P_0 + P_I) \tag{7.28}$$

where ρ denotes the fraction of power allocated to the ID component. Note that the explicit expression for P_0 and P_I are as given in (7.6) and (7.9), respectively. As can be seen from the equation, the presence of interference allows to harvest additional energy, and hence P_I

could help to allocate more power to the information decoding component which in turn support data rate. The received SINR at UE_0 during the downlink operation is given as

$$SINR_0^{DL} = \frac{P_a h_0 g_0}{\frac{\sigma_c^2}{\rho} + \sigma^2 + \sum_{i \in \Phi \setminus 0} P_a h_i g_i} \tag{7.29}$$

where σ_c^2 is the noise component introduced due to the conversion of the received bandpass signal to baseband, and in practice, this could be higher than the thermal noise component, i.e., $\sigma^2 \ll \sigma_c^2$. Intuitively, when the interference dominates the noise power, the SIR becomes independent of the splitting factor ρ, and this encourages to allocate more power to the energy harvesting component. Mathematically, the downlink ergodic rate can be expressed as

$$R_{erg}^{DL} = \int_0^\infty \mathbb{E}\Big\{ \tau_B \log_2 \Big(1 + SINR_0^{DL}\Big) \Big\} f_r(r) dr \tag{7.30}$$

which leads to

$$R_{erg}^{DL}(\rho, \tau_B) = \int_0^\infty \int_0^\infty e^{-\frac{\mu \gamma \sigma^2}{\rho P_a} r^\alpha} \exp\Big(- \frac{\pi \lambda r^{2-\alpha}}{\mu(-2+\alpha)} \; {}_2F_1\Big(\Big[1, \frac{-2+\alpha}{\alpha}\Big]; 2 - \frac{2}{\alpha}; -\gamma_a' \Big) \Big) f_r(r) dr dt \tag{7.31}$$

where $\gamma_a' = 2^{\frac{t}{\tau_B}} - 1$, and assuming that $\rho_i = \rho_0 = \rho$. It is clear that the downlink achievable data rate is a function of both the harvesting interval and the power splitting factor. Indeed, allocating more time for the downlink operation improves not only the harvested energy but also the downlink information transfer rate. However, performance for the uplink operation, i.e., uplink data rate, depends on the advantage of the additional harvested energy and the penalty due to less available time for information transfer.

Similarly, the outage capacity when the generic AP transmit data at a fixed rate during the downlink operation can be determined using

$$R_{out}^{DL}(\tau_B, \rho_0) = P_c^{DL}(\rho_0) \tau_B \log_2(1 + \gamma_T) \tag{7.32}$$

where P_c^{DL} is the coverage probability, which is given as

$$\begin{aligned} P_c^{DL} &= \int_0^\infty \Pr\left\{ \frac{P_a h_0 g_0}{\frac{\sigma_c^2}{\rho} + \sigma^2 + \sum_{i\in\Phi\setminus 0} P_a h_i g_i} > \gamma_T \middle| r \right\} f_r(r) dr \\ &= \int_0^\infty e^{-\frac{\gamma_T \mu \sigma^2}{\rho P_a} r^\alpha} \exp\left(-\frac{\pi\lambda r^{2-\alpha}}{\mu(-2+\alpha)} {}_2F_1\Big(\Big[1, \frac{-2+\alpha}{\alpha}\Big]; 2 - \frac{2}{\alpha}; -\gamma_T\Big)\right) f_r(r) dr. \end{aligned} \tag{7.33}$$

Note that the coverage probability depends only on the power splitting factor, but the outage capacity is still benefits from longer harvesting interval. Further simplification can be done considering noise-limited and interference-limited scenarios. For instance, the coverage probability expression in (7.14) under noise-limited scenario becomes

$$\begin{aligned} P_c^{DL}(\tau_B, \rho_0) &= \int_0^\infty \Pr\left\{ h_0 > \frac{\gamma_T \sigma_c^2 r^\alpha}{\rho_0 P_a} \middle| r \right\} f_r(r) dr \\ &= \int_0^\infty e^{-\frac{\gamma_T \mu \sigma_c^2}{\rho_0 P_a} r^\alpha} f_r(r) dr \end{aligned} \tag{7.34}$$

Now, the coverage probability is dependent on not only the downlink operating interval but also the power splitting factor at the UE. In addition to the coverage probability, we are also interested in the joint complementary cumulative distribution function (JCCDF) of harvested energy and achievable data rate, which is given as

$$F^{DL}(R_{mn}, \chi) = \Pr\Big\{ \mathbb{E}\Big\{ R_*^{DL} \geq R_{mn}, E_{hv}^{DL} \geq \chi \Big\} \tag{7.35}$$

where $* \in \{erg, out\}$.

Phase II: Uplink operation

In the second phase, UEs send information-bearing signal to their serving AP simultaneously over the entire uplink operation interval. The transmitted signal power level at the typical

UE depends on the amount of harvested energy, and it is expressed as

$$P_0^{UL} = \zeta\beta_0 \frac{(1-\rho_0)E_0^{hv}}{1-\tau_B} \tag{7.36}$$

where E_0^{hv} is as defined in (7.5). Hence, received SINR at the serving AP during the uplink interval is given as

$$SINR_0^{UL} = \frac{(1-\rho_0)a_0h_0g_0}{\sigma_a^2 + \sum_{i\in\Phi\setminus 0}(1-\rho_i)a_ih_ig_i}. \tag{7.37}$$

As can be seen from the above equation, the downlink power splitting factor affects the performance of uplink information transfer . More specifically, in noise-limited scenario, each incremental of ρ_0 at the typical user degrades the SNR_0^{UL} linearly, and this has an impact on the energy efficiency as well as throughput of the system. However, every additional bits of information transferred in the first phase counts toward the overall performance. Thus, following similar procedure as mentioned earlier in Section 7.2, the coverage probability and the ergodic capacity for the wireless-powered cellular network during the uplink operation interval can be explicitly expressed as follow:

$$P_c^{UL} = \int_0^\infty \Pr\left\{SINR_0^{UL} > \gamma_T \middle| r\right\} f_r(r)dr \tag{7.38a}$$

$$R_{erg}^{UL} = \int_0^\infty \mathbb{E}\left\{(1-\tau_B)\log_2\left(1+SINR_0^{UL}\right)\right\} f_r(r)dr \tag{7.38b}$$

which lead to

$$\begin{aligned} P_c^{UL} &= \int_0^\infty e^{-\frac{\gamma_T\mu\sigma_a^2}{(1-\rho_0)a_0}r^\alpha} \exp\Big(-2\pi\lambda\int_r^\infty \frac{s(1-\rho_i)a_iy^{-\alpha}}{\mu+s(1-\rho_i)a_iy^{-\alpha}}ydy\Big) f_r(r)dr \\ &= \int_0^\infty e^{-\frac{\gamma_T\mu\sigma_a^2}{(1-\rho_0)a_0}r^\alpha} \exp\left(-\frac{\pi\lambda r^{2-\alpha}}{\mu(-2+\alpha)}{}_2F_1\Big(\left[1,\frac{-2+\alpha}{\alpha}\right];2-\frac{2}{\alpha};-\frac{s(1-\rho_i)a_ir^{-\alpha}}{\mu}\Big)\right) f_r(r)dr \end{aligned} \tag{7.39}$$

and

$$R_{erg}^{UL} = \int_0^{\infty}\int_0^{\infty} e^{-\frac{\mu\gamma_a\sigma_a^2}{(1-\rho_0)a_0}r^{\alpha}} \exp\left(-\frac{\pi\lambda r^{2-\alpha}}{\mu(-2+\alpha)}\ {}_2F_1\left(\left[1,\frac{-2+\alpha}{\alpha}\right];2-\frac{2}{\alpha};-\gamma_a\frac{(1-\rho_i)a_i}{(1-\rho_0)a_0}\right)\right) f_r(r)drdt. \tag{7.40}$$

Therefore, the total throughput and the system energy efficiency can be computed as

$$R(\tau_B,\rho) = R_{erg}^{DL} + R_{erg}^{UL} \tag{7.41a}$$

$$\eta = \frac{R_{tot}}{\tau_B(P_c^D + \zeta P_a) + (1-\tau_B)P_c^U} \tag{7.41b}$$

7.4 WP-Cellular Network with Uplink mm-Wave

In order to increase spectral efficiency, mm-wave is considered as one of promising solution for the ever increasing demand of bandwidth in Internet-of-Things (IoT) where billions of devices will get data connectivity. With this motivation, we assumed that randomly distributed APs can broadcast the energy-bearing signal to the nearby UEs on the unlicensed frequency band, but these users send their data uplink to the corresponding serving APs using mm-wave frequency band. In such a case, the channel modeling for the uplink information transfer experiences different characteristics since the wave length of GHz signals is so small that the mm-wave signals are very sensitive to the blockage effects [72]. Hence, the wireless link between the UEs and APs could be either line-of-sight (LOS) or non line-of-sight (NLOS). According to channel measurements for the LOS/NLOS propagation characteristics, the probability function for being LOS/NLOS can be modeled as exponential function such that $p(r) = e^{-\beta r}$ where β is a constant which depends on the channel characteristics and r is the Euclidean distance for the link between AP and UE. Intuitively, the larger the distance, the lesser the probability to establish LOS link. In fact, the geometry of the surrounding and the presence of blockage materials, e.g., buildings, have also significant impact on this probability. Furthermore, the distance-dependent path loss in both scenarios will be different, and they

are defined as $v_L(r) = K_L r^{-\alpha_L}$ and $v_{NL}(r) = K_{NL} r^{-\alpha_{NL}}$ for the LOS and NLOS, respectively. Note that α_L and α_{NL} are the corresponding path loss exponents, and it is expected that $\alpha_{NL} > \alpha_L$. We assume that the typical UE and generic AP adjust their antenna steering orientations to maximize the directivity gain, and hence UE_0 establishes LOS link with the serving AP. However, the interfering links could be either in LOS or NLOS. As noted in the literature, an equivalent LOS ball, which is an approximate model for the irregular shape of LOS region, is considered to simplify analysis, and in this section, we assume that the generic AP certainly has LOS link with the nearby the UEs located at a distance $r < R_B$ where R_B is the radius of the ball, and otherwise it forms NLOS link. In addition to the path loss, we assume that the every link between UE and AP experiences a small-scale fading, and u_i denotes the Gamma function for the channel gain assuming an independent Nakagami fading between a generic AP and UE in the i^{th} cell coverage area.

Assuming sectored antenna model, the array gains for the main lobe and side lobe are constant, and denoted by M_* and m_*, respectively. Note that the subscript $* \in \{u, a\}$ describes whether the antenna directivity gain is for the UE or AP. We assume that there is perfect beam alignment between a typical UE and generic AP, i.e., $G = M_u M_a$ where G is total antenna array again. Meanwhile, the beam direction of the interfering nodes is uniformly distributed on $[0, 2\pi]$, and the antenna gain for the link between the generic AP and the UE served by the interfering AP have a discrete probability which is defined as

$$\begin{aligned}
p_1 &= \left(\tfrac{\theta_a}{2\pi}\right)\left(\tfrac{\theta_u}{2\pi}\right) \quad \text{for the gain } G_1 = M_a M_a \\
p_2 &= \left(\tfrac{\theta_a}{2\pi}\right)\left(\tfrac{\bar{\theta}_u}{2\pi}\right) \quad \text{for the gain } G_2 = M_a m_u \\
p_3 &= \left(\tfrac{\bar{\theta}_a}{2\pi}\right)\left(\tfrac{\theta_u}{2\pi}\right) \quad \text{for the gain } G_3 = M_u m_a \\
p_4 &= \left(\tfrac{\bar{\theta}_a}{2\pi}\right)\left(\tfrac{\bar{\theta}_u}{2\pi}\right) \quad \text{for the gain } G_4 = m_a m_u
\end{aligned} \tag{7.42}$$

where θ_* and $\bar{\theta}_*$ for $* \in \{a, u\}$ denote the beam width of the main lobe and side lobe, respectively.

As mentioned above, we apply a new operation protocol, known as harvest-then-(mm-

W)transmit, in which downlink and uplink operations are carried out over different frequency bands, i.e, the UEs transmit information in mm-wave frequency band during uplink operation interval, but the downlink energy broadcasting is performed at lower frequencies. Hence, the harvested energy at the typical UE is given as

$$\begin{aligned} E_0^{hv} &= \tau_B \mathbb{E}\left\{ P_a G_0^{DL} h_0 g_0 + \sum_{i\in\Phi\setminus 0} \sum_{k=1}^{4} P_a h_i G_k^{DL} g_i \right\} \\ &= \tau_B \big(P_0 + P_I\big) \end{aligned} \tag{7.43}$$

where G_*^{DL} is the directivity gain of the antenna array between thel UE and associated AP. The explicit expressions for P_0 and P_I are as follow:

$$\begin{aligned} P_0^{DL} &= \mathbb{E}\Big\{ P_a G_0^{DL} h_0 g_0 \Big\} \\ &= \mu P_a G_0^{DL} \mathbb{E}_r \left\{ \big[\max(r,d) \big]^{-\alpha} \right\} \\ &= \mu P_a G_0^{DL} \left[\int_0^d d^{-\alpha} f_r(r) dr + \int_d^\infty r^{-\alpha} f_r(r) dr \right] \\ &= \frac{\mu P_a G_0^{DL}}{2} \left[d^{-\alpha} \Big(- e^{-Cd^2} + 1 \Big) + C^{\frac{\alpha}{2}} \Gamma\Big(\frac{-\alpha+2}{2}, Cd^2 \Big) \right] \end{aligned} \tag{7.44}$$

where $\Gamma(a,x)$ is the incomplete gamma function, and $C = 2\pi\lambda$. In addition, the second equality above uses the fact that $\mathbb{E}\{h_0\} = \mu$. Similarly,

$$\begin{aligned} P_I^{DL} &= \mathbb{E}\left\{ \sum_{i\in\Phi\setminus 0} \sum_{k=1}^{4} P_a G_k^{DL} h_i g_i \right\} \\ &= \sum_{k=1}^{4} \mathbb{E}\left\{ \sum_{i\in\Phi\setminus 0} P_a G_k^{DL} h_i \Big[\max(x_i, d) \Big]^{-\alpha} \right\} \\ &= \sum_{k=1}^{4} P_I^k \end{aligned} \tag{7.45}$$

where x_i is the distance between the typical user and an interfering AP, and indeed $x_i > r$. Applying Campbell's theorem, which states that $\mathbb{E}\Big\{ \sum_{x\in N} f(x) \Big\} = \lambda \int_{R^d} f(x) dx$ where

N denotes a stationary point process defined on the d-dimensional Euclidean space, (7.7) becomes

$$P_I^k = 2\pi\lambda\mu P_a G_k^{DL} \int_0^\infty \Big[\int_r^\infty \Big[\max(u,d) \Big]^{-\alpha} u du \Big] f_r(r) dr \tag{7.46}$$

which leads to

$$\begin{aligned} P_I^k &= 2\pi\lambda\mu P_a G_k^{DL} \left[\int_0^d \Big[.5d^{-\alpha+2} - 0.5d^{-\alpha} r^2 - \frac{d^{-\alpha+2}}{2-\alpha} \Big] f_r(r) dr + \int_d^\infty \frac{r^{-\alpha+2}}{\alpha-2} f_r(r) dr \right] \\ &= \mu P_a G_k^{DL} \left[\frac{d^{-\alpha+2}}{2} \Big(\frac{1}{2} - \frac{1}{2-\alpha} \Big) \Big(- e^{-Cd^2} + 1 \Big) + \frac{d^{-\alpha}}{4C} \Big[\big(Cd^2 + 1 \big) e^{-Cd^2} - 1 \Big] + \frac{C^{\frac{\alpha}{2}-1}}{2\alpha - 4} \Gamma \Big(\frac{-\alpha+4}{2}, Cd^2 \Big) \right]. \end{aligned} \tag{7.47}$$

During the uplink operation interval, the typical UE sends information-bearing signal to its serving AP uplink over mm-wave bandwidth, and the received SINR is given as

$$SINR_0^{mm-W} = \frac{P_1 p_1 G_1 u_0 v_0}{\sigma^2 + P_{int}} \tag{7.48}$$

where P_{int} is the total interference power, and u_0 and v_0 are denote fading power gain and path loss, respectively, in the presence of mm-wave propagation. From Lemma 1 in [72], we note that the probability density function for the distance to the nearest LOS AP given that the typical UE observes at least one LOS AP is expressed as

$$f(r) = \frac{2\pi r p(r)}{B_L} e^{-2\pi\lambda \int_0^r x p(x) dx} \tag{7.49}$$

where $B_L = 1 - e^{-2\pi\lambda \int_0^\infty x p(x) dx}$. According to our assumption, $p(r) = 1$ for $r < R_B$ and $p(r) = 0$ otherwise, and hence we have $B_L = 1$ and (7.49) becomes

$$f(r) = 2\pi x e^{-\pi\lambda r^2}. \tag{7.50}$$

Thus, the conditional coverage probability of a wireless-powered network that operates with harvest-then-mm-transmit protocol is given as

$$\begin{aligned} P_c(\gamma_T, \tau_B) &= \int_0^\infty \Pr\left\{ \frac{P_0 p_1 G_1 u_0 v_0}{\sigma^2 + P_{int}} > \gamma_T \right\} f(r) dr \\ &= \int_0^\infty \Pr\left\{ u_0 > \frac{\gamma_T r^{\alpha_L} (\sigma^2 + P_{int})}{P_0 K_L p_1 G_1} \right\} f(r) dr \end{aligned} \tag{7.51}$$

where $P_0 = \frac{E_{hv}^0}{1-\tau_B}\sigma^2$, and $|u_0|^2$ is a normalized gamma random variable with parameter N_L for the link between the typical UE and the generic AP. Based on the tight approximation given in Lemma 6 in [72], we have

$$\begin{aligned} \Pr\left\{ u_0 > \frac{\gamma_T r^{\alpha_L} (\sigma^2 + P_{int})}{P_0 K_L p_1 G_1} \right\} &= \sum_{n=1}^{N_L} (-1)^{n+1} \binom{N_L}{n} \mathbb{E}\left[e^{-\frac{n a \gamma_T r^{\alpha_L} (\sigma^2 + P_{int})}{P_0 K_L p_1 G_1}} \right] \\ &= \sum_{n=1}^{N_L} (-1)^{n+1} \binom{N_L}{n} e^{-\frac{n a \gamma_T r^{\alpha_L} \sigma^2}{P_0 p_1 G_1}} \mathbb{E}\left[e^{-\frac{n a \gamma_T r^{\alpha_L} P_{int}}{P_0 K_L p_1 G_1}} \right] \end{aligned} \tag{7.52}$$

where $a = N_L (N_L)^{-\frac{1}{N_L}}$. The term in the expectation is due to the interference signal, and it can be explicitly expressed considering the LOS and NLOS links as indicated below.

$$\mathbb{E}\left[e^{-\frac{n a \gamma_T r^{\alpha_L} P_{int}}{P_0 p_1 G_1}} \right] = \mathbb{E}\left[e^{-\frac{n a \gamma_T r^{\alpha_L} \sum_{k=1}^{4} \sum_{l \in \Phi_L / 0} v_l P_l p_k G_k r_l^{-\alpha_L}}{P_0 K_L p_1 G_1}} \right] \mathbb{E}\left[e^{-\frac{n a \gamma_T r^{\alpha_L} \sum_{k=1}^{4} \sum_{l \in \Phi_{NL} / 0} v_l P_l p_k G_k r_l^{-\alpha_L}}{P_0 K_L p_1 G_1}} \right] \tag{7.53}$$

where $\Phi = \Phi_L \cup \Phi_{NL}$, and Φ_L/Φ_{NL} denote the PPP in which the the AP is forms LOS/NLOS link with the UEs. The first expectation in (7.53) can be further simplified as follow

$$\mathbb{E}\left[e^{-\frac{na\gamma_T r^{\alpha_L}\sum_{k=1}^{4}\sum_{l\in\Phi/0} v_l P_l p_k G_k r_l^{-\alpha_L}}{P_0 K_L p_1 G_1}}\right] = \prod_{k=1}^{4} e^{-2\pi\lambda P_l p_k \int_r^{R_B}\left(1-\mathbb{E}\left[e^{-n\gamma_T n_L |u_l|^2 \frac{G_k}{P_0 G_1}(\frac{r}{t})^{\alpha_L}}\right]\right)p(t)tdt}$$
$$= \prod_{k=1}^{4} e^{-2\pi\lambda p_k \int_r^{R_B}\left(1-\frac{1}{\left(1+\frac{n\gamma_T n_L \frac{K_L}{K_L}\frac{P_l G_k}{P_1 G_1}(\frac{r}{t})^{\alpha_L}}{N_L}\right)^{N_L}}\right)p(t)tdt} \tag{7.54}$$

Similarly, for the NLOS link, we have

$$\mathbb{E}\left[e^{-\frac{na\gamma_T r^{\alpha_L}\sum_{k=1}^{4}\sum_{l\in\Phi/0} v_l P_l p_k G_k K_{NL} r_l^{-\alpha_{NL}}}{P_0 K_L p_1 G_1}}\right] = \prod_{k=1}^{4} e^{-2\pi\lambda p_k \int_r^{R_B}\left(1-\frac{1}{\left(1+\frac{n\gamma_T n_L \frac{K_{NL}}{K_L}\frac{P_l G_k}{P_1 G_1}(\frac{r}{t})^{\alpha_{NL}}}{N_L}\right)^{N_L}}\right)p(t)tdt} \tag{7.55}$$

Note that based on our assumption, $p(t) = 1$ inside the ball, and hence we can substitute in the above equations accordingly. Therefore, the achievable data rate for a wireless-powered networks operating at mmWave frequency band is given as

$$\begin{aligned}\mathcal{R} &= \int_0^{\infty}(1-\tau_B)\mathbb{E}\Big\{\log_2\left(1+SINR_0^{mm-W}\right)\Big\}f_r(r)dr \\ &= \int_0^{\infty}\left[\int_0^{\infty}\Pr\left\{SINR_0^{mm-W}>\gamma_b\right\}f_r(r)dr\right]dt \\ &= \int_0^{\infty}P_c(\gamma_b,\tau_B)dt\end{aligned} \tag{7.56}$$

where $\gamma_b = 2^{\frac{t}{1-\tau_B}-1}$, and $P_c(\gamma_b,\tau_B)$ is the coverage probability defined in (7.51).

On the other hand, the system energy efficiency for the wireless-powered network with

uplink mm-Wave can be computed using

$$\eta_{cell} = \frac{\mathcal{R}}{\tau_B P_T^D + (1-\tau_B)\lambda P_T^U} \tag{7.57}$$

7.5 Numerical Analysis

In this section, we provide numerical results on the performance analysis and optimal resource allocation strategies considering throughput maximization and energy efficiency maximization problems. In both cases, we assume that the uplink and downlink channels of a given UE have the same characteristics, and the channel gains are exponentially distributed with means β_1 and β_2, respectively.

Fig. 7.3a illustrates how the downlink/uplink operation intervals affect the network throughput. As can be observed from the figure, allocating more time for energy harvesting initially improves the uplink information transfer rate, but once it reaches an optimal point, each incremental harvesting time sacrifices data rate. Besides, the optimal point which maximizes the network throughput depends on the downlink transmit power level. As expected, transmitting energy-bearing signal at higher power level reduces time allocated for energy harvesting operation, for instant $\tau_B^* = 0.25$ for $P_a = 10$dB whereas $\tau_B^* = 0.16$ for $P_a = 20$dB. Furthermore, we observe that this benefits the uplink information transfer. On the other hand, Fig. 7.4b shows that SINR coverage probability improves with harvesting interval, but the characteristics of the curve change with the threshold. We observe that higher threshold forces the allocation of more time to energy harvesting in order to secure SINR coverage.

The impact of downlink transmitted power level on the maximum energy efficiency is shown in Fig. 7.4a. From the figure, we observe that broadcasting at higher power achieves better system energy efficiency, and this is because, more energy can be harvested with shorter downlink operation interval, and hence there will be less power consumption. In addition, this provides extra time for uplink information transfer. As can be seen from the

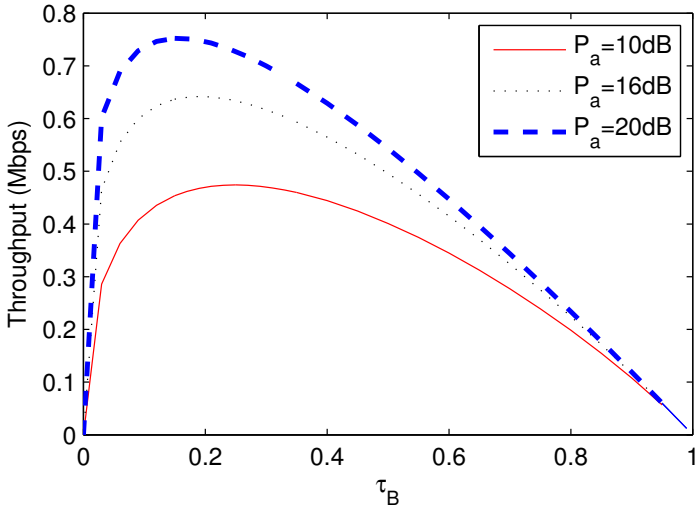

(a) Throughput vs. harvesting interval (Sec.)

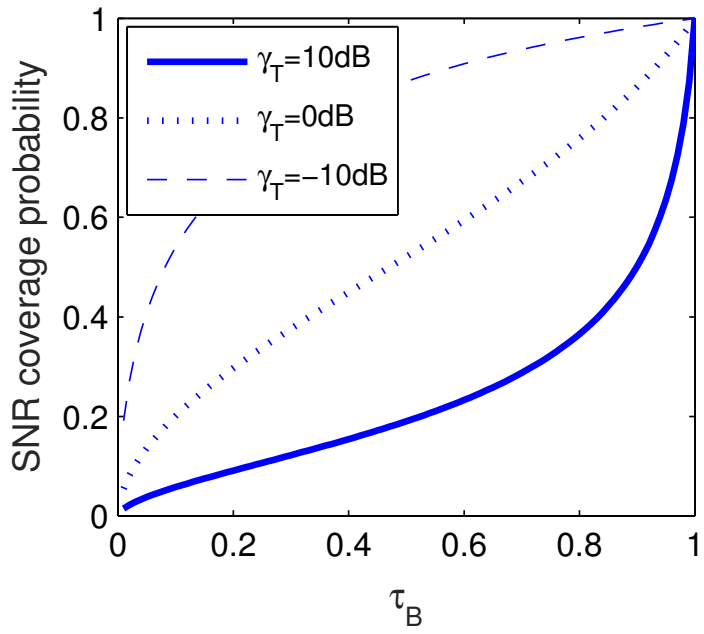

(b) SNR coverage probability vs. harvesting interval (Sec.)

Figure 7.3: Impact of downlink/uplink operating interval on the network performance

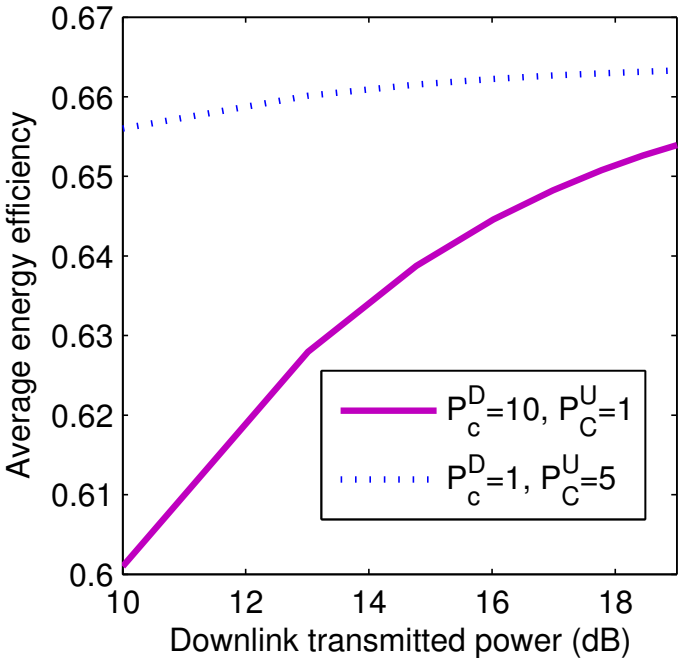

(a) Average EE (bpJ/Hz) vs. downlink transmit power at $\lambda = 10^{-2}$

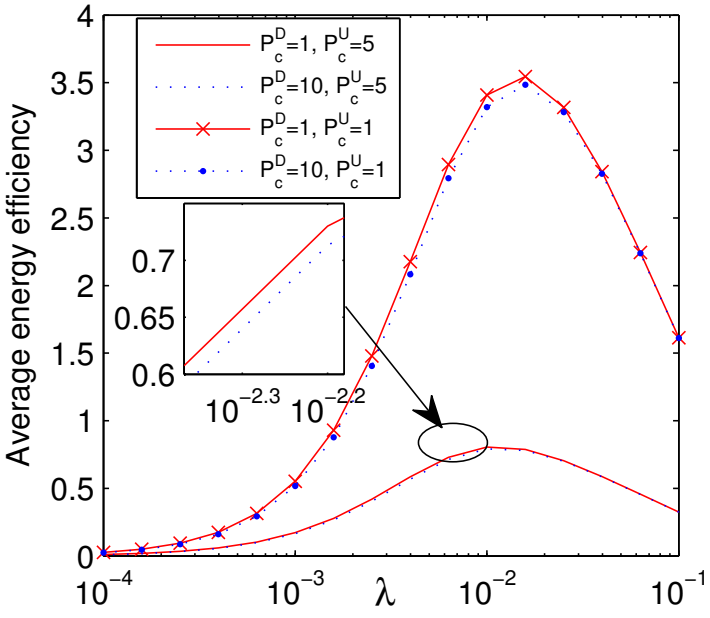

(b) Average EE (bpJ/Hz) vs. AP density at $P_a = 16dB$

Figure 7.4: Impact of downlink transmit power and AP density while maximizing system energy efficiency

figure, the energy efficiency increases significantly comparing at $P_a = 10$dB and $P_a = 20$dB if the circuit consumption is dominant, i.e., $P_c \gg P_a$. On the other hand, AP density also has an affect on the system energy efficiency as illustrated in Fig. 7.4b. It is interesting to observe that there is an optimal AP density at which maximum energy efficiency is obtained. In fact, when the APs are located more densely, the distance between UE and nearby serving AP is expected to reduce, and as a result more energy can be harvested over a given duration. This helps to improve the energy efficiency. However, these characteristics can not be achieved if λ exceeds a certain threshold. Furthermore, circuit power consumption determines the impact of AP density on the overall performance. As can be seen from the figure, the uplink consumption has significant effect on average energy efficiency compared with the downlink circuit power consumption. For instance, the maximum EE reaches close to 3.5 b/J for $P_c^U = 1$ whereas it is below 1b/J when the uplink consumption is increased five fold.

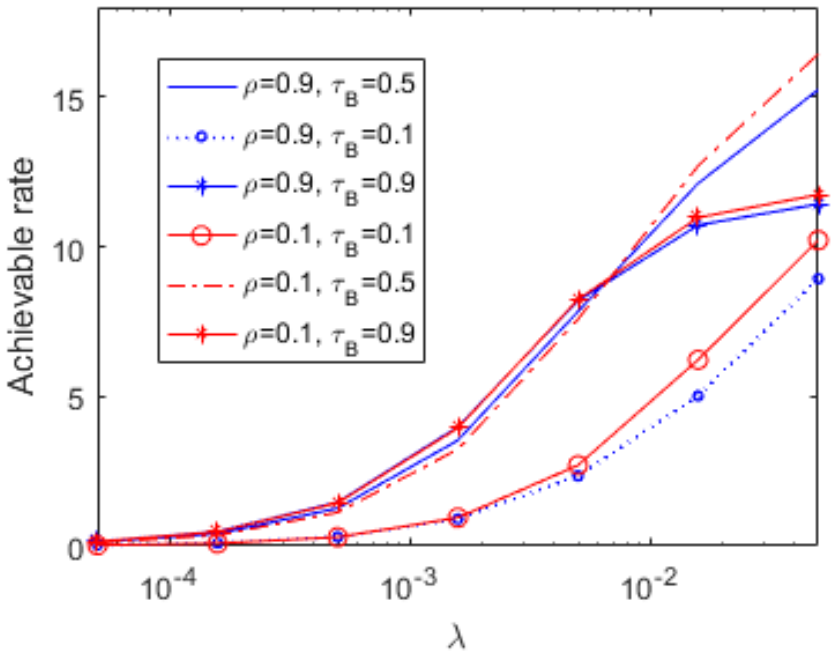

Figure 7.5: Impact of AP density and τ_B (Sec.) on the network throughput (bps/Hz)

In regard to downlink SWIPT with uplink information transfer for wireless-powered net-

work discussed in Section 7.3, Figure 7.5 and Fig. 7.6 illustrate impact of network parameters in the achievable data rate while maximizing the system energy efficiency. As can be seen from Fig. 7.5, when the AP are densely deployed, the network throughput improves. This is because the distance between the generic AP and typical user decreases, and this reduces the path loss significantly compared with the increase in the aggregate interference. Furthermore, the power splitting factor and the time allocated for the downlink operation affects the system performance, and we observe that allocating too small or too much time for the energy harvesting hurts the network throughput, especially when the density of AP is higher λ values.

Similarly, Fig. 7.6a and Fig.7.6b show that increasing the downlink transmit power level improves the network throughput, as expected, and for a given downlink operating interval, the point at which maximum achievable data rate is obtained changes accordingly. For instance, at $\tau_B = 0.9$, higher data rate is obtained for $P_a = 10$ when $\rho = 0.36$, but this changes to $\rho = 0.45$ for $P_a = 15$. In addition, comparing these two figures, we observe that the time allocated for energy harvesting has an impact on the network throughput, even for the same downlink transmit power level.

On the other hand Fig. 7.7 shows how the system energy efficiency changes in response to the AP density and the power splitting factor at the UE. It is interesting to observe that the energy efficiency improves when the APs are densely populated, and we claim that there exists an energy-efficient downlink/uplink interval given the harvested energy constraint at the UE. In addition, this energy demand has direct impact on the characteristics of the system energy efficiency curve, and more importantly the maximum achievable operating point.

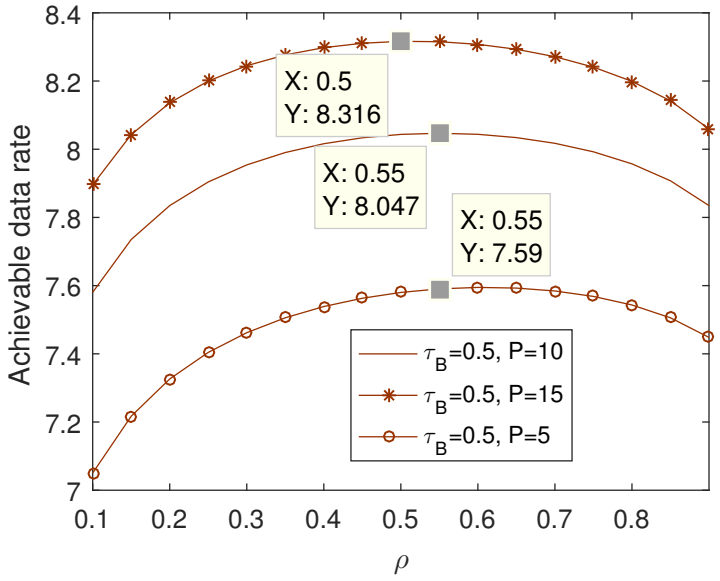

(a)

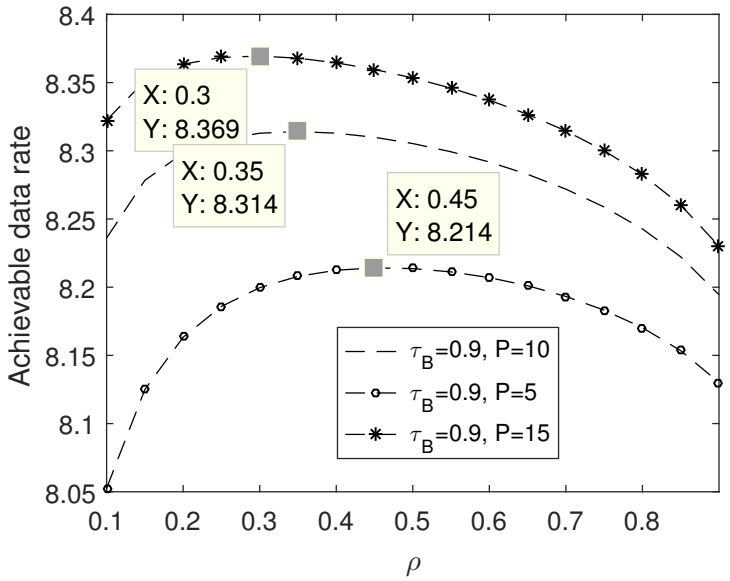

(b)

Figure 7.6: Impact of power splitting factor and downlink transmit power level on the throughput (bps/Hz)

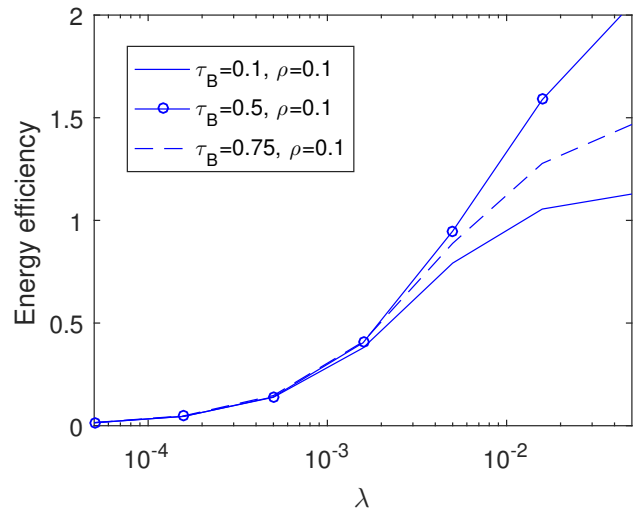

(a) Energy efficiency vs. density of AP

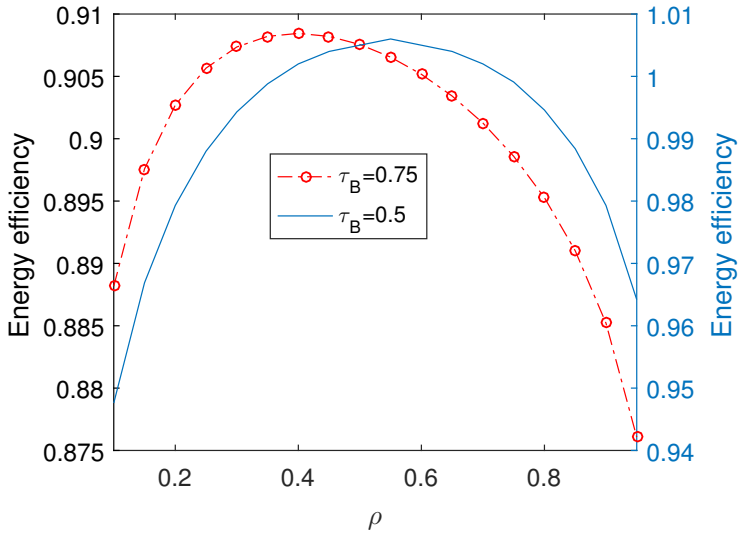

(b) Energy efficiency vs. power splitting factor

Figure 7.7: Impact of various parameters on the system energy efficiency (bpJ/Hz)

Chapter 8

NOMA-Based Energy-Efficient Wireless Powered Communications

In the previous chapters, we considered that multiple transmitting nodes transfer information employing either TDMA or MAC scheme. In this chapter, we study the significance of non-orthogonal transmission for wireless information and power transfer, and the system model is described in Section 8.1. Assuming delay-tolerant sources, optimization strategies are well investigated for half-duplex and asynchronous transmission in Section 8.2. Subsequently, energy-efficient time allocation for the above mentioned protocols are investigated in Section 8.3 for delay-sensitive sources. Despite the difficulty of obtaining analytical expressions for uplink and downlink operating intervals, optimal solution can be obtained numerically and algorithms are included to summarize the procedure.

8.1 System Model

We consider multiple energy harvesting nodes as shown in Fig. 8.1, which operate based on the harvest-then-transmit protocol. The wireless power transmitter (WPT) has an embedded power source, and it broadcasts a deterministic signal, denoted by W_a with power $P_a = |W_a|^2$, over the downlink channel to power the nearby UEs. We employ similar as-

sumptions as in [49] and [56] that each user fully utilizes the harvested energy to support data transmission and circuit power consumption in one cycle. Without loss of generality, we use a normalized unit for each cycle, i.e., $T = 1$.

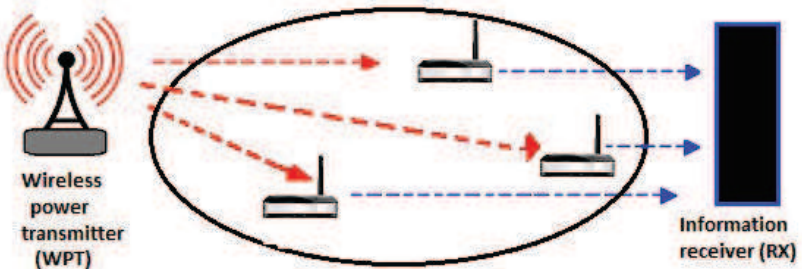

Figure 8.1: Network model

In regard to the harvest-then-transmit protocol, UEs first harvest energy from the dedicated source (i.e., WPT), and then transmit data uplink to the access point (AP) employing the NOMA scheme[1]. More explicitly, we consider two scenarios, namely half-duplex operation and asynchronous transmission, based on how downlink and uplink operations are coordinated.

Half-duplex operation:

Here, the downlink and uplink operations are carried out over non-overlapping time intervals, i.e., all the UEs harvest energy while WPT transfers power through the downlink wireless channel over a duration τ_0, and then they simultaneously transmit information-bearing signals to the AP for the rest of the period, i.e., $1 - \tau_0$, as shown in Fig. 8.2a. In such a case, the harvested energy at user $i \in \mathcal{S} = \{1, 2, \cdots, N\}$ in one cycle can be expressed as[2]

$$E_i^{hd} = \tau_0 g_i P_a \quad \text{(Joules)} \tag{8.1}$$

[1]Although the WPT and AP are depicted as separate nodes in Fig. 8.1, they can also be co-located or be the same node.

[2]Note that the formula for the harvested energy generally includes an energy harvesting efficiency factor, which we assume, without any loss of generality, to be equal to one.

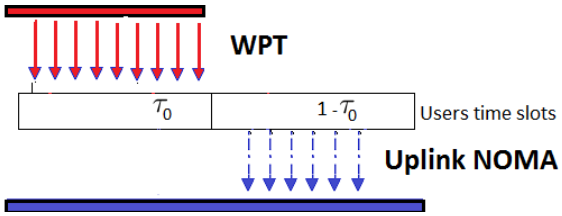

(a) Half-duplex operation

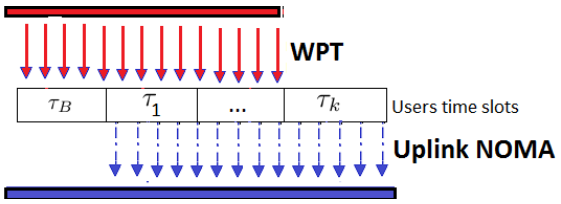

(b) Asynchronous transmission

Figure 8.2: WPCN uplink-downlink operation schemes

---

where τ_0 is the downlink energy harvesting interval which is allocated to all the users, and g_i denotes the fading coefficient between the i^{th} user and WPT, and hence $|g_i|^2$ is the channel power gain. We assume that the WPT-user links and user-AP links all experience frequency-flat fading, and uplink as well as downlink fading coefficients stay fixed in each frame duration. Thus, the received signal at the AP is expressed as

$$Y = \sum_{i=1}^{N} h_i X_i + N_{ap} \tag{8.2}$$

where h_i is fading coefficient capturing the effect of path loss as well as small scale fading for the wireless link between user i and AP, and $N_{ap} \sim \mathcal{CN}(0,1)$ is the circularly symmetric, complex Gaussian noise at the AP with unit variance. In addition, X_i for $i \in \mathcal{S}$ denotes the uplink signal from UE i transmitted with power P_i based on power domain NOMA scheme such that $P_i > P_j$ for $|h_i| < |h_j|$. Moreover, the AP decodes the information sent from the users in the reverse order of improving channel qualities, i.e., signal from the UE with the best channel condition is decoded last without any interference from the signals transmitted by other UEs, while the signal from UE with the worst channel is decoded first in the presence of interference from all other users.

If, without loss of generality, we assume that $|h_1| < |h_2| < \ldots < |h_N|$, then the achievable instantaneous information transfer rate of user i over an uplink operation interval of $1 - \tau_0$ is given as

$$R_i = (1 - \tau_0) \log_2 \left(1 + \frac{\gamma_i}{1 + \sum_{k=i+1}^{N} \gamma_k}\right) \text{ bps/Hz} \tag{8.3}$$

where $\gamma_i = |h_i|^2 P_i$ is the received SNR from user i. Therefore, the throughput or sum-rate capacity for the half-duplex scenario becomes

$$R_{sum} = \sum_{i=1}^{N} R_i = (1 - \tau_0) \log_2 \left(1 + \sum_{i=1}^{N} \gamma_i\right) \text{ bps/Hz.} \tag{8.4}$$

Asynchronous transmission

In this scenario, UEs start harvesting energy at the same time, but as the name implies, they begin transmitting data signals to the AP at different time instants, as depicted in Fig. 8.2b. The advantage of this approach is that it provides an opportunity for some UEs to harvest more energy while others are scheduled for uplink information transfer. Without loss of generality, we assume that UEs are ordered according to their uplink transmission starting sequence, i.e., UE 1 begins sending data first, then user 2 and so on. Hence, the harvested energy at the i^{th} UE is given as follows:

$$E_i^{at} = \left(\tau_0 + \sum_{j=1}^{i-1} \tau_j\right) |g_i|^2 P_a \quad \text{(Joules)} \tag{8.5}$$

where τ_i is the time interval between the uplink starting points of i^{th} and $(i+1)^{th}$ UEs such that

$$\sum_{i=1}^{N} \tau_i \leq 1 - \tau_0. \tag{8.6}$$

Once each UE has harvested the required energy, it transfers information to the AP until the end of the cycle. This implies that i number of UEs simultaneously carry out the uplink information transfer operation during the interval τ_i. Thus, the received signal at AP during

interval τ_i is expressed as

$$Y_i = \sum_{k=1}^{i} h_k X_k + N_{ap}. \tag{8.7}$$

In addition to the amount of harvested energy, each UE's transmit power level directly depends on the information decoding order applied at the AP. As noted above, we consider power domain NOMA scheme which encourages the UE with the best channel condition to transmit at the lowest power level as well as to be decoded without interference. As a result, the achievable information rate of UE $j \in \{1, 2, \cdots, i\}$ over the interval τ_i is given as

$$R_j = \tau_i \log_2 \left(1 + \frac{\gamma_j}{1 + \sum_{k=j+1}^{i} \gamma_k} \right) \quad \text{bps/Hz} \tag{8.8}$$

where $|h_j| < |h_k|$ for $k = j+1, j+2, \ldots, i$. Note that following each incremental operating interval, one or more UEs join the uplink operation, and hence the information decoding order at the receiving end is modified accordingly. Therefore, the total throughput becomes the sum of the sum-rate capacity of the system over each interval until the end of τ_N. Mathematically, we have

$$R_{sum} = \sum_{i=1}^{k} \tau_i \log_2 \left(1 + \sum_{j=1}^{i} \gamma_j \right). \tag{8.9}$$

8.2 Energy-Efficient Time Allocation without Statistical QoS Constraint

In this section, we analyze time allocation strategies for energy harvesting and data transmission phases, considering both half-duplex and asynchronous operations. No delay or buffer constraints are imposed initially. Delay-sensitive sources and statistical QoS constraints are introduced into the analysis in Section IV. We consider system energy efficiency which is defined as

$$\eta = \frac{\text{Throughput}}{\text{Total consumed energy}} \qquad \text{(bits/Joule)}, \tag{8.10}$$

and let P_{c_D} denote the circuit power consumption at WPT during downlink operation, and assume that it is independent of the transmitted power level for $P_a > 0$. However, if no wireless power is transferred, there is no consumption, i.e., $P_a = 0$ and $P_{c_D} = 0$. Hence, the total energy consumption during the entire downlink-uplink operation of a given cycle becomes

$$E_{tot} = \begin{cases} \tau_0 P_{DT} + (1-\tau_0) P_{c_U} & \text{Half-duplex} \\ \\ \left(\tau_0 + \sum_{i=1}^{N-1} \tau_i\right) P_{DT} + P_{c_U} \sum_{i=1}^{N} \tau_i & \text{Asynchronous} \end{cases} \tag{8.11}$$

where $P_{DT} = P_{c_D} + P_a$, and P_{c_U} is the power consumption at the receiver for decoding information during uplink operation.

8.2.1 Optimal Harvesting Interval in the Half-Duplex Protocol

Assuming that the harvesting interval depends on the fading state realizations, the uplink transmitted signal power level from the i^{th} user becomes

$$P_i = \xi_i |g_i|^2 P_a \frac{\tau_0}{1-\tau_0}. \tag{8.12}$$

Note that ξ_i denotes the fraction of harvested energy utilized for data transmission while the rest, i.e., the fraction of $1-\xi_i$, is consumed by the circuit to carry out the process. Then, substituting (8.12) into (8.3) and simplifying the expression, we get

$$\mathcal{R}_i(\tau_0) = (1-\tau_0) \log_2 \left(1 + \frac{\alpha_i \tau_0}{1-\tau_0 + \sum_{j=i+1}^{N} \alpha_j \tau_0}\right) \tag{8.13}$$

where $\alpha_i = \xi_i |g_i|^2 |h_i|^2 P_a$. We first have the following characterization.

Lemma 8.2.1 *The individual achievable rate of a wireless-powered UE operating in half-duplex mode with uplink NOMA strategy is concave in the harvesting interval τ_0.*

Proof: See Appendix R.

Note that the total throughput, i.e., the sum of individual achievable data rates, is given by

$$\begin{aligned}\mathcal{R}_{sum}(\tau_0) =& \sum_{i=1}^{N} \mathcal{R}_i(\tau_0) \\ =&(1-\tau_0)\log_2\left(1+\sum_{i=1}^{N}\alpha_i\frac{\tau_0}{1-\tau_0}\right).\end{aligned} \tag{8.14}$$

Therefore, the system energy efficiency (EE), which measures the numbers of bits of information reliably transmitted to the AP per consumed unit energy, is given as

$$\eta_{HD}(\tau_0) = \frac{(1-\tau_0)\log_2\left(1+\sum_{i=1}^{N}\alpha_i\frac{\tau_0}{1-\tau_0}\right)}{\tau_0\big(P_{c_D}+P_a-P_{c_U}\big)+P_{c_U}}. \tag{8.15}$$

Note that each UE's circuit power consumption is supported by the harvested energy, and hence it is not necessary to consider these explicitly while defining the total energy consumption of the system.

Proposition 8.2.1 *The system EE of a wireless-powered communication network given in (8.15) is a pseudo-concave function of the harvesting interval* τ_0.

Proof: See Appendix S.

Proposition 8.2.1 guarantees that there is a unique optimal time allocation strategy that maximizes the system EE such that the harvesting interval is within the feasible set. In order to obtain the optimal time allocation for downlink and uplink operations that maximizes the system energy efficiency, we formulate the following optimization problem:

$$\text{(PR:8.1)} \qquad \max_{\tau_0} \ \eta_{HD}(\tau_0) \tag{8.16a}$$

$$\text{subject to } \ \tau_0(1-\tau_0) > 0. \tag{8.16b}$$

The constraint in (8.16b) dictates that the optimizing parameter τ_0 is always within the feasible set, i.e., $0 \leq \tau_0 \leq 1$. Since this constraint is convex, and the objective function is the ratio of a concave function over an affine function, it is obvious that (PR:1) is a concave-linear fractional programming (CLFP) problem. As noted in [93], Dinkelbach's method can be used to solve concave-convex and concave-linear fractional programming problems, and we employ this method to identify the optimal solution. Thus, (PR:8.1) can be equivalently expressed as

$$\min_{\lambda} \left\{ \max_{\tau_0} \ \mathcal{L}(\tau_0) \right\} \tag{8.17a}$$

$$\text{subject to} \quad (8.16b) \tag{8.17b}$$

where $\mathcal{L}(\tau_0) = (1-\tau_0)\log_2\left(1+\frac{\alpha_T \tau_0}{1-\tau_0}\right) - \lambda\left(\tau_0 P_\Delta + P_{c_D}\right)$, $\alpha_T = \sum_{i=1}^{N} \alpha_i$ and $P_\Delta = P_{c_D} + P_a - P_{c_U}$. Since $\mathcal{L}(\tau_0)$ is a concave function and the constraint is convex, Karush-Kuhn-Tucker (KKT) conditions, i.e.,

$$\left.\frac{\partial \mathcal{L}}{\partial \tau_0}\right|_{\tau_0=\tau_0^*} = 0 \tag{8.18a}$$

$$\mu^*\left(\tau_0 - \tau_0^2\right) = 0, \qquad \kappa^* \tau_0^* = 0, \tag{8.18b}$$

are necessary and sufficient for the global optimality of the solution of the inner maximization problem. From the characteristics of the EE curve, when $\tau_0^* = 0$ or $\tau_0^* = 1$, we have $\eta_{HD}(\tau_0^*) = 0$ for $P_{c_D} \neq 0$. But, this cannot be the optimal value, which implies $0 < \tau_0^* < 1$. As a result, $\mu^* = 0$ and $\kappa^* = 0$ in order to satisfy the complementary slackness conditions given in (8.18b). Taking these into account, and applying the first order optimality criteria given in (8.18a), we obtain

$$\frac{\alpha_T}{1-\tau_0+\alpha_T\tau_0} - \ln\left(1+\alpha_T\frac{\tau_0}{1-\tau_0}\right) - \ln(2)\lambda P_\Delta = 0 \tag{8.19}$$

which leads to

$$z\ln(z) + \Omega z = \alpha' \tag{8.20}$$

or equivalently

$$e^{\ln(ze^{\Omega})}\ln(ze^{\Omega}) = \alpha' e^{\Omega} \tag{8.21}$$

where $z = 1 + \alpha_T \frac{\tau_0}{1-\tau_0}$, $\Omega = \ln(2)\lambda P_{\Delta} - 1$, and $\alpha' = \alpha_T - 1$. Mathematically, (8.21) has the form of $Xe^X = Y$ whose solution is given by the Lambert function, i.e., $X = \mathcal{W}(Y)$ for $Y \geq -\frac{1}{e}$. Thus, the solution to (8.21) can be analytically expressed as

$$z^* = \mathbf{e}^{\left[\mathcal{W}(\alpha'.\mathbf{e}^{\Omega}) - \Omega\right]}. \tag{8.22}$$

Therefore, the optimal harvesting time as a function of λ is

$$\tau_0^*(\lambda) = \frac{\alpha' - \mathcal{W}\Big(\alpha'.\mathbf{e}^{(\lambda P' - 1)}\Big)}{\alpha'\Big[1 + \mathcal{W}\Big(\alpha'.\mathbf{e}^{(\lambda P' - 1)}\Big)\Big]} \tag{8.23}$$

where $P' = \ln(2)P_{\Delta}$. The parameter λ is iteratively updated until the optimal solution satisfies $\mathcal{R}_{sum}(\tau^*) - \lambda^* E_{tot}(\tau^*) = 0$. We provide the complete procedure below in Algorithm 11.

Algorithm 11 EE maximization using Dinkelbach's algorithm

1: Given: ϵ, λ_0
2: $n \leftarrow 0$
3: **repeat**
4: Determine τ_0^* using (8.23)
5: $\mathcal{F}(\lambda_n, \tau_0^*) = \mathcal{R}_{sum}(\tau_0^*) - \lambda_n E_{tot}(\tau_0^*)$
6: $\lambda_{n+1} = \frac{\mathcal{R}_{sum}(\tau_0^*)}{E_{tot}(\tau_0^*)}$
7: $n \leftarrow n + 1$
8: **until** $|\mathcal{F}(\lambda_n, \tau_0^*)| < \epsilon$
9: Set $\tau_0^* = \tau_0^n$.

8.2.2 Energy-Efficient Intervals with Asynchronous Transmission

In this section, we consider overlapping and non-overlapping scenarios for the uplink operation as follow.

Overlapping uplink operation

As noted above in Section II, asynchronous transmission is defined in such a way that UEs do not necessarily begin sending information-bearing signals to the AP at the same time in each downlink-uplink operation cycle. However, if a UE has started transmission, it stays active until the end of the cycle. Assuming that UEs are ordered according to their uplink starting point as mentioned earlier, the transmitted signal power level from UE i is given as

$$\begin{aligned} P_i =& \xi_i \frac{E_i^{at}}{\sum_{k=i}^{N} \tau_k} \\ =& \xi_i |g_i|^2 P_a \left[\frac{\tau_0 + \sum_{j=1}^{i-1} \tau_j}{\sum_{k=i}^{N} \tau_k} \right] \end{aligned} \tag{8.24}$$

where E_i^{at} denotes the harvested energy by UE i in the asynchronous scheme, and ξ_i is the fraction of harvested energy utilized for data transmission while the rest, i.e., the fraction of $1 - \xi_i$, is consumed by the circuit to carry out the process.

Then, we substitute (8.24) into (8.8), and derive the expression for the sum-rate capacity (within the interval of duration τ_i in which i users are transmitting) as a function of the operating intervals as

$$\mathcal{R}_{sum}^{i}(\tau_0, \boldsymbol{\tau}_N) = \tau_i \log_2 \left(1 + \sum_{l=1}^{i} b_l \frac{\tau_0 + \sum_{j=1}^{l-1} \tau_j}{\sum_{k=l}^{N} \tau_k} \right) \tag{8.25}$$

which leads to

$$\mathcal{R}_{sum}^{i}(\tau_0, \boldsymbol{\tau}_N) = \tau_i \log_2 \left(a_i + \sum_{l=1}^{i} \frac{b_l}{\sum_{k=l}^{N} \tau_k} \right) \tag{8.26}$$

where $b_i = \xi_i |g_i|^2 P_a$, $a_i = 1 - \sum_{l=1}^{i} b_l$ and $\boldsymbol{\tau}_N = [\tau_1, \tau_2, \cdots, \tau_N]$.

Proposition 8.2.2 *The achievable sum-rate capacity for the two-user setting during the transmission interval of duration τ_i is jointly concave over the operating intervals (τ_0, τ_1, τ_2).*

Proof: See Appendix T.

From Proposition 8.2.2, we conclude that the system throughput is a jointly concave function since concavity is preserved under summation. Note that the total sum-rate capacity is given as

$$\mathcal{R}_{tot}(\boldsymbol{\tau}_N) = \sum_{i=1}^{2} \tau_i \log_2 \left(a_i + \sum_{l=1}^{i} \frac{b_l}{\sum_{k=l}^{2} \tau_k} \right). \tag{8.27}$$

Then, the system energy efficiency (EE) for asynchronous transmission scenario becomes

$$\eta_{AT}(\tau_0, \tau_1, \tau_2) = \frac{\tau_1 \log_2 \left(a_1 + \frac{b_1}{\tau_1 + \tau_2} \right) + \tau_2 \log_2 \left(a_2 + \frac{b_1}{\tau_1 + \tau_2} + \frac{b_2}{\tau_2} \right)}{P_{DT}\big(\tau_0 + \tau_1\big) + \big(\tau_1 P^1_{c_U} + \tau_2 P^2_{c_U}\big)} \tag{8.28}$$

where $P^i_{c_U}$ denotes the total uplink circuit power consumption during the interval τ_i.

Since the throughput is proved to be a concave function, and the total consumed power is an affine function of the operation intervals, the system EE given in (8.28) satisfies the criteria for pseudo-concavity based on Proposition 2.9 stated in [93]. Unlike the previous scenario where we had only one parameter to adjust, i.e., τ_0, to achieve maximum energy efficiency, now there are 3 optimizing parameters, i.e., τ_0, τ_1, τ_2, and hence obtaining the optimal time allocation strategy which maximizes the EE is a more challenging task. Thus, we formulate the following optimization problem:

$$\text{(PR:8.2)} \quad \max_{\tau_0, \boldsymbol{\tau}_N} \ \eta_{AT} \tag{8.29a}$$

$$\text{subject to} \ \sum_{i=1}^{N} \tau_i \leq 1 - \tau_0 \tag{8.29b}$$

$$\tau_i \geq 0, \qquad i \in \{0, 1, 2, \cdots, N\}. \tag{8.29c}$$

As noted above, the objective function in (8.29a) is pseudo-concave since the total achievable sum-rate capacity is jointly concave with respect to operating intervals (τ_0, τ_1, τ_2). In addition, the constraints (8.29b) and (8.29c), which define the feasible operating intervals, are convex. Thus, the optimization problem (PR:8.2) is also a concave-linear fractional programming problem, and hence it can be easily solved using Dinkelbach's algorithm following a similar procedure as in the earlier scenario, but we skip the details for brevity.

Non-overlapping uplink operation

In this subsection, we consider a special scenario where energy harvesting by a user can still occur concurrently with the data transmission of other users, but the uplink data transmission among users follows time-division multiple access instead of allowing the activated user to use the channel until the end of the block duration. Hence, data transmissions by the users occur over non-overlapping time intervals. In such a case, the system energy efficiency expression for N users is given by

$$\eta_{AT}(\tau_0, \boldsymbol{\tau}_N) = \frac{\sum_{i=1}^{N} \tau_i \log_2 \left(1 + b_i \frac{\sum_{k=0}^{i-1} \tau_k}{\tau_i}\right)}{P_{DT}\left(\tau_0 + \sum_{i=1}^{N-1} \tau_i\right) + P_{c_U} \sum_{i=1}^{N} \tau_i} \tag{8.30}$$

where P_{c_U} denotes the circuit power consumption of a UE assuming that each UE consumes the same amount. Therefore, the optimization problem is reformulated as follows:

$$\text{(PR:8.3)} \quad \max_{\tau_0, \boldsymbol{\tau}_N} \ \eta_{AT} \tag{8.31a}$$

$$\text{subject to} \ \sum_{i=1}^{N} \tau_i \leq 1 - \tau_0 \tag{8.31b}$$

$$\mathcal{R}_i(\tau_0, \boldsymbol{\tau}_i) \geq R_{min}^i \tag{8.31c}$$

where

$$\mathcal{R}_i(\tau_0, \boldsymbol{\tau}_i) = \tau_i \log_2 \left(1 + b_i \frac{\tau_0 + \sum_{j=1}^{i-1} \tau_j}{\tau_i}\right) \tag{8.32}$$

and $\boldsymbol{\tau}_i = [\tau_1, \cdots, \tau_i]$. The additional constraint given in (8.31c) is introduced in order to guarantee that each user's rate is above a certain minimum level when non-overlapping time slots are being allocated to the users. From Lemma 2 in [56], we know that $\mathcal{R}_i$ is a jointly concave function of downlink and uplink time intervals, i.e., τ_0 and $\boldsymbol{\tau}_i$. Thus, the above optimization problem is still a concave-linear fractional programming problem, and (PR:8.3) can be equivalently expressed as

$$\min_{\lambda,\mu} \left\{ \max_{\tau_0, \boldsymbol{\tau}_i} \ \mathcal{G}(\tau_0, \boldsymbol{\tau}_i) \right\} \tag{8.33a}$$

$$\text{subject to} \quad (8.31b) \ \text{ and } \ (8.31c) \tag{8.33b}$$

where $\mathcal{G}(\tau_0, \boldsymbol{\tau}_i) = \tau_i \log_2\Big(1 + b_i^{\frac{\tau_0 + \sum_{j=1}^{i-1} \tau_j}{\tau_i}}\Big) - \lambda\Big(P_{DT}\big(\tau_0 + \sum_{i=1}^{N-1} \tau_i\big) + P_{c_U} \sum_{i=1}^{N} \tau_i\Big)$, and $P_\Delta = P_{DT} - P_{c_U}$. Given λ, the objective function for the inner maximization problem $\mathcal{G}(\tau_0)$ is a concave function while the constraints are convex, and hence Karush-Kuhn-Tucker (KKT) conditions, i.e.,

$$\left.\frac{\partial \mathcal{L}}{\partial \tau_0}\right|_{\tau_0 = \tau_0^*} = 0, \qquad \left.\frac{\partial \mathcal{L}}{\partial \tau_i}\right|_{\tau_i = \tau_i^*} = 0 \tag{8.34a}$$

$$\zeta^*\Big(\sum_{i=0}^{N} \tau_i - 1) = 0, \qquad \kappa^*\Big(\mathcal{R}_i(\tau_0, \boldsymbol{\tau}_i) - R_{min}^i\Big) = 0, \tag{8.34b}$$

are necessary and sufficient for global optimality where the Lagrangian is given as

$$\mathcal{L} = \mathcal{G}(\tau_0, \boldsymbol{\tau}_i) + \beta\Big(\sum_{i=0}^{N} \tau_i - 1\Big) + \kappa\Big(\mathcal{R}_i(\tau_0, \boldsymbol{\tau}_i) - R_{min}^i\Big). \tag{8.35}$$

Applying the first order optimality criterion in (8.34a), we obtain

$$\frac{\partial \mathcal{L}}{\partial \tau_0} = \sum_{k=1}^{N} \frac{(1-\kappa_k) b_k}{\ln(2)\Big(1+ b_k \frac{\tau_0 + \sum_{j=1}^{i-1} \tau_j}{\tau_k}\Big)} - \lambda P_{DT} - \beta = 0 \tag{8.36a}$$

$$\frac{\partial \mathcal{L}}{\partial \tau_i} = \sum_{k>i}^{N} \frac{(1-\kappa_k) b_k}{\ln(2)\Big(1+ b_k \frac{\tau_0 + \sum_{j=1}^{i-1} \tau_j}{\tau_k}\Big)} + (1-\kappa_i) \log_2\Big(1+ b_i \frac{\tau_0 + \sum_{j=1}^{i-1} \tau_j}{\tau_i}\Big) - \frac{(1-\kappa_i) b_i \frac{\tau_0 + \sum_{j=1}^{i-1} \tau_j}{\tau_i}}{\ln(2)\Big(1+ b_i \frac{\tau_0 + \sum_{j=1}^{i-1} \tau_j}{\tau_i}\Big)} - Z = 0 \tag{8.36b}$$

$$\frac{\partial \mathcal{L}}{\partial \tau_N} = (1-\kappa_N) \log_2\Big(1 + b_i \frac{\tau_0 + \sum_{j=1}^{N-1} \tau_j}{\tau_N}\Big) - \frac{(1-\kappa_N) b_N \frac{\tau_0 + \sum_{j=1}^{N-1} \tau_j}{\tau_N}}{\ln(2)\Big(1 + b_N \frac{\tau_0 + \sum_{j=1}^{N-1} \tau_j}{\tau_N}\Big)} - \lambda P_{c_U} - \beta = 0 \tag{8.36c}$$

where $Z = \lambda(P_{DT} + P_{c_U}) - \beta$. Taking the difference of (8.36a) and (8.36b), we have

$$-\sum_{k=1}^{i} \frac{(1-\kappa_k) b_k}{1 + b_k z_k} + (1-k_i) \mathcal{Z}_i(z_i) + \lambda P_{c_U} \ln(2) = 0 \tag{8.37}$$

which leads to

$$\mathcal{Z}_i(z_i) - \frac{b_i}{1 + b_i z_i} = \frac{\lambda P_{c_U} \ln(2)}{1-\kappa_i} + \sum_{j=1}^{i-1} \frac{b_j}{1 + b_j z_j} \tag{8.38}$$

where $\mathcal{Z}_i(z_i) = \ln(1 + b_i z_i) - \frac{b_i z_i}{1 + b_i z_i}$ and $z_k = \frac{\tau_0 + \sum_{j=1}^{k-1} \tau_j}{\tau_k}$. Similarly, from (8.36c), we have

$$\mathcal{Z}_N(z_N) - \frac{b_N}{1 + b_N z_N} = \frac{\lambda(P_{DT} + P_{c_U}) \ln(2)}{1 - k_N} + \sum_{k=1}^{N-1} \frac{b_k}{1 + b_k z_k}. \tag{8.39}$$

Applying a similar approach as in [56], the optimal time allocations are given as

$$\tau_N^* = \frac{1}{1 + z_N} \tag{8.40a}$$

$$\tau_i^* = \frac{1 - \sum_{j=i+1}^{N} \tau_j^*}{1 + z_i} \tag{8.40b}$$

where

$$z_i = \frac{1}{b_i}\left[e^{\mathcal{W}\left(\frac{b_i-1}{e^{\phi_i+1}}\right)+\phi_i+1} - 1\right], \tag{8.41}$$

$\forall i \in \mathcal{S} = \{1, 2, \cdots, N\}$ with

$$\phi_i = \frac{\lambda P_{c_U} \ln(2)}{1-\kappa_i} + \sum_{j=1}^{i-1} \frac{b_j}{1+b_j z_j} \quad \text{and} \tag{8.42a}$$

$$\phi_N = \frac{\lambda\Big(P_{DT} + P_{c_U}\Big) \ln(2)}{1-k_N} + \sum_{k=1}^{N-1} \frac{b_k}{1+b_k z_k}. \tag{8.42b}$$

Hence, the optimal time interval, τ_0, becomes $\tau_0^* = 1 - \sum_{i=1}^{N} \tau_i^*$. From the above expressions, we observe that the energy-efficient time allocation depends on the minimum data rate constraint. For instance, if this constraint is inactive for all UEs, then $\kappa_i = 0\ \forall i$ due to complementary slackness conditions. However, if it is active for any UE, then the corresponding optimal solution will be changed in such a way that the constraint is satisfied while maximizing the system energy efficiency. Therefore, we first determine the best solution assuming all the rate constraints are satisfied with inequality, i.e., $\kappa_i = 0\ \forall i \in \mathcal{S}$ and then check if the optimal solution satisfies the rate constraint for each UE. For any constraint violation, the optimal time allocation policy will be updated taking into account all of the active constraints, and the detailed procedure is provided below in Algorithm 12.

8.3 Impact of Statistical Queuing Constraints

In this section, we analyze the impact of QoS constraints on the optimal time allocation strategies that target the maximization of the system energy efficiency. Since effective capacity describes the maximum constant data arrival rates, i.e. characterizes the throughput in the presence of delay-limited data sources, we focus on the effective-EE to determine the number arriving bits that can be supported per one joule of consumed energy by the system in the presence of statistical queuing constraints. Let us first address half-duplex opera-

Algorithm 12 Energy-efficient time allocation for non-overlapping scheme

Given: ϵ

Define: $\mathcal{F}(\boldsymbol{\tau}_N) = \mathbb{E}\left\{\tau_i \log_2\left(1+ b_i^{\frac{\tau_0+\sum_{j=1}^{i-1}\tau_j}{\tau_i}}\right)\right\}$

$$g(\boldsymbol{\tau}_N) = \left(\mathbb{E}\left\{(P_{c_D})\left(\tau_0+\sum_{i=1}^{N-1}\tau_i\right) + P_{c_U}\sum_{i=1}^{N}\tau_i\right\}\right)$$

$n \leftarrow 0$

Initialize λ, $\kappa_1 = \kappa_2 = \cdots = \kappa_N = 0$

repeat

  $r \leftarrow 0$

  repeat

    Determine z_i using (8.41)

    Update τ_i using (8.40)

    Update $\tau_0 = 1 - \sum_{i=1}^{N}\tau_i$

    $r \leftarrow r + 1$

    for i=1 to N **do**

      if $|\mathcal{R}_i - \mathcal{R}_{min}^i| > \epsilon$ **then**

        $\kappa_i \neq 0$

        Update k_i using gradient method

      end if

    end for

  until $|\mathcal{R}_i - \mathcal{R}_{min}^i| < \epsilon$

  Determine $\Delta_n = \mathcal{F}(\boldsymbol{\tau}_N) - \lambda_n g(\boldsymbol{\tau}_N)$

  $\lambda_{n+1} = \frac{\mathcal{F}(\boldsymbol{\tau}_N)}{g(\boldsymbol{\tau}_N)}$

  $n \leftarrow n + 1$

until $|\Delta_n| < \epsilon$

Set $\tau_0^* = \tau_0$ and $\tau_i^* = \tau_i$.

tion. Since UEs harvest energy simultaneously and send information-bearing signals to the AP using NOMA, harvesting time becomes the only parameter to optimize for maximum performance. In the case in which each user harvests energy to support data transfer with half-duplex operation, the corresponding effective capacity expression of user i given in (2.5) is modified by incorporating the additional parameter τ_0, i.e., the harvesting interval, as follows

$$C_i^e(\theta_i, \tau_0) = -\frac{1}{T\theta_i}\log\left(\mathbb{E}\left\{e^{-(1-\tau_0)\theta_i \log_2\left(1+\frac{\alpha_i\tau_0}{1+\omega_i\tau_0}\right)}\right\}\right). \tag{8.43}$$

The sum effective capacity of users transmitting through a multiple access channel can be determined by summing up the individual effective capacities:

$$C^e(\boldsymbol{\theta}, \tau_0) = \sum_{i=1}^{N} C_i^e(\theta_i, \tau_0) \tag{8.44}$$

where the vector of QoS exponents of different users is denoted as $\boldsymbol{\theta} = [\theta_1, \theta_2, \cdots, \theta_N]$. Now, the optimization problem for maximizing the effective-EE with half-duplex operation is formulated as follows:

$$\text{(PR:8.4a)} \quad \max_{\tau_0} \quad \frac{-\sum_{i=1}^{N} \log\left(\mathbb{E}\left\{e^{-(1-\tau_0)\theta_i \log_2\left(1+\frac{\alpha_i \tau_0}{1+\omega_i \tau_0}\right)}\right\}\right)}{T\theta_i \mathbb{E}\Big\{\tau_0 P_{DT} + P_{c_U}(1-\tau_0)\Big\}} \tag{8.45a}$$

$$\text{subject to} \;\; \tau_0(1-\tau_0) \leq 0 \tag{8.45b}$$

Note that in (8.45), the objective function is the system effective energy efficiency while the constraint specifies the feasible range of the harvesting interval.

Proposition 8.3.1 *The effective-EE of energy-harvesting UEs with half-duplex protocol is pseudo-concave with respect to the harvesting interval* τ_0.

Proof: See Appendix U.

Based on Proposition 8.3.1, the objective function of (PR:8.4a) is pseudo-concave and hence the problem is a concave-linear fractional problem, and the optimization procedure described in earlier sections can easily be applied to obtain the optimal solution. Similarly, for the asynchronous transmission scenario, we have

$$\text{(PR:8.5)} \quad \max_{\tau_0, \boldsymbol{\tau}} \quad \frac{\sum_{i=1}^{N} C_i^e(\theta_i, \tau_B)}{\mathbb{E}\Big\{P_{DT}\Big(\tau_0 + \sum_{i=1}^{N-1} \tau_i\Big) + P_{c_U} \sum_{i=1}^{N} \tau_i\Big\}} \tag{8.46a}$$

$$\text{subject to} \;\; \sum_{i=1}^{N} \tau_i \leq 1 - \tau_0 \tag{8.46b}$$

where

$$C_i^e(\theta_i, \tau_B) = -\frac{1}{T\theta_i} \log_2 \left(\mathbb{E}\left\{ e^{-\Phi_i \log\left(1+\frac{b_i p_i}{1+\sum_{l=1}^{i-1} b_l p_l}\right)} \right\} \right) \tag{8.47}$$

with $\boldsymbol{\theta} = [\theta_1, \theta_2, \cdots, \theta_N]$, $\Phi_i = \tau_i \theta_i$ and $p_i = \frac{\sum_{k=0}^{i-1} \tau_k}{\sum_{j=i}^{N} \tau_j}$. Again, similar algorithmic approaches can be employed to solve (PR:8.5).

8.4 Numerical Analysis

In this section, we provide numerical results considering two energy harvesting UEs communicating with an AP. We assume that the channel gain for the link between UE $i \in \{1, 2\}$ and the AP is exponentially distributed with mean β_i. In order to compare the performance gains, we consider three cases denoted by I, II and III. In the first case, we focus on energy efficient solutions that are obtained for both half-duplex and asynchronous transmissions using uplink NOMA, as discussed in this paper. In the second case, we determine the throughput maximizing time allocations for the same problems, and in the last case we apply energy-efficiency maximization for time-division multiple access (TDMA). Additionally, we consider two values, i.e., $P_{c_U} = 5dB$ and $P_{c_U} = 15dB$, for the uplink power consumption in order to capture its impact on the overall characteristics.

Fig. 8.3 illustrates the performance of WPCN operating in half duplex mode with uplink NOMA. According to Fig. 8.3a, we observe that broadcasting the downlink signal at a higher power level improves the system energy efficiency for case I. This is because, as P_a increases, more energy can be harvested over a smaller time duration τ_0 as shown in Fig. 8.3b, and hence the UEs get an opportunity to transfer information over a longer time period which in turn benefits the energy efficiency. Meanwhile, comparing case I and case II as shown in Fig. 8.3a, we notice that allocating the harvesting interval with the goal to maximize the throughput hurts the system energy efficiency, and the degradation becomes more sig-

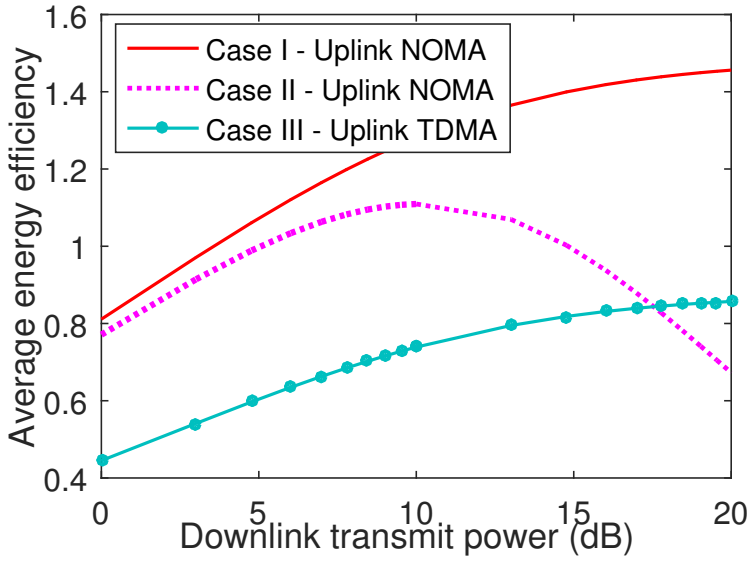

(a) Average energy efficiency η_{HD} (bpJ/Hz) vs. P_a

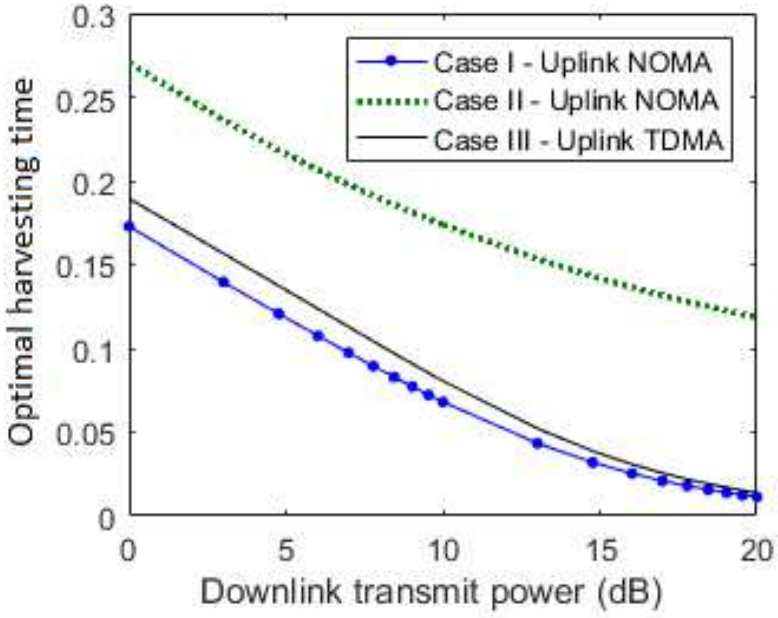

(b) Optimal harvesting time (sec.) vs. downlink power P_a

Figure 8.3: Impact of downlink transmit power level P_a with half-duplex downlink-uplink operation

---

nificant at higher values of the downlink transmit power level. Furthermore, comparing all the three cases, we observe that NOMA based uplink information transfer outperforms uplink TDMA. According to the figure, throughput maximizing time allocation strategy using

uplink NOMA is more energy-efficient than energy-efficiency maximizing policy for uplink TDMA. One reason for this could be that the latter approach requires more time for downlink operation, and this means more energy consumption over the interval τ_0. However, this is not necessarily the case for very high P_a values.

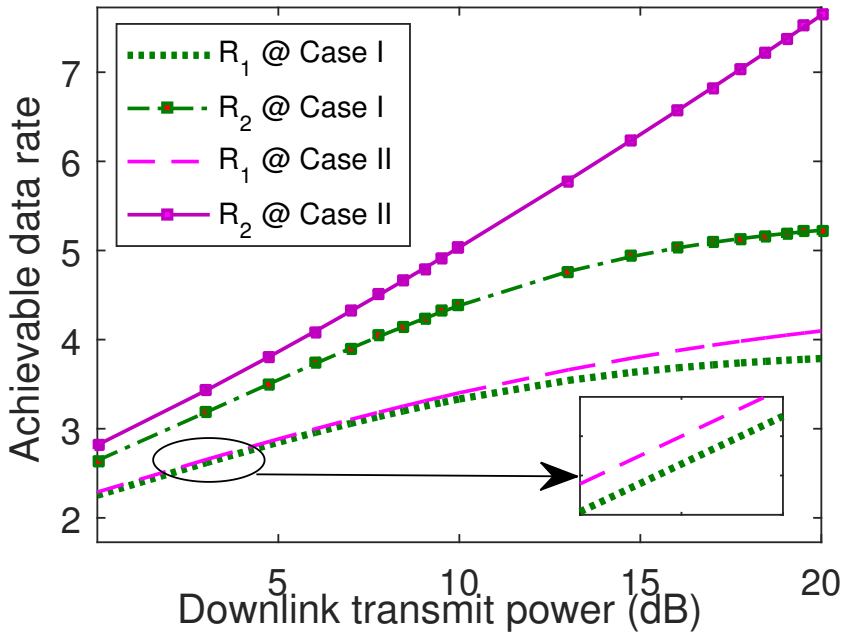

Figure 8.4: Achievable rates (bps/Hz) vs. P_a

In regard to the achievable data rates, intuitively we expect throughput in case II to be higher than that in case I, and Fig. 8.4 demonstrates this fact, i.e., R_i@ Case II $>$ R_i@ Case I $\forall P_a$ where $i \in \{1, 2\}$. As can be seen from the figure, the performance gain in terms of throughput is not significant at lower downlink transmit power levels, but this changes as P_a increases. Furthermore, comparing the individual data rates, UE 1 always achieves better channel capacity, but the gap is smaller for case II than case I and this reveals that uplink NOMA encourages fairness in data rate among UEs. It is also interesting to observe that the performance difference between uplink NOMA and uplink TDMA lies in the optimal time allocated to each UE to transmit data uplink to the receiver. As can be seen from Fig. 8.3b, energy-efficient downlink operating intervals for Case I and Case III are very close specially for higher P_a values, and hence the way uplink interval is allocated

determines the system performance.

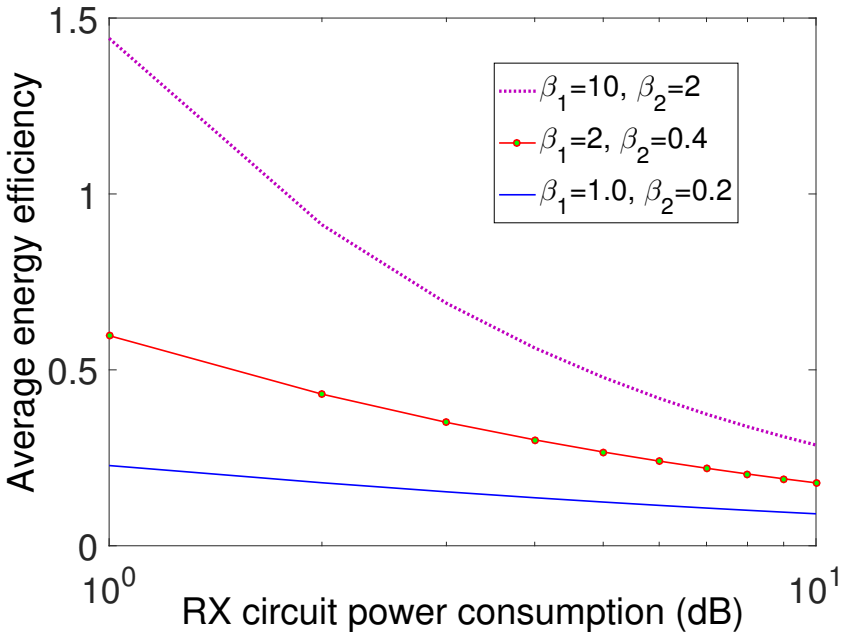

Figure 8.5: Average energy efficiency (bpJ/Hz) vs. P_{c_U}

Figs. 8.5 - 8.7 demonstrate the system performance and the corresponding optimal operating parameters when the UEs operate in the asynchronous transmission mode. As can be seen in Fig. 8.5, the system energy efficiency decreases with an increase in circuit power consumption at the receiving end, and this tradeoff characteristic depends on the wireless link power gain between each UE and the receiver. More specifically, when UEs have relatively favorable channel conditions, i.e., higher gains, each incremental circuit power hurts the EE significantly. This is because the energy efficient strategy dictates both users to harvest and to transmit synchronously, i.e, $\tau_1 = 0$ (as seen in the case with $\beta_1 = 10$ and $\beta_2 = 2$). Besides, more time is allocated to information transfer. On the other hand, worse channel characteristics lead to $\tau_1 \neq 0$, and the reduction in the average energy efficiency decreases as AP circuit power consumption increases. In such a case, more time is allocated to energy harvesting, and this in turn reduces throughput and system energy efficiency. Intuitively, the impact of WPT circuit power depends on the downlink transmit power level and for

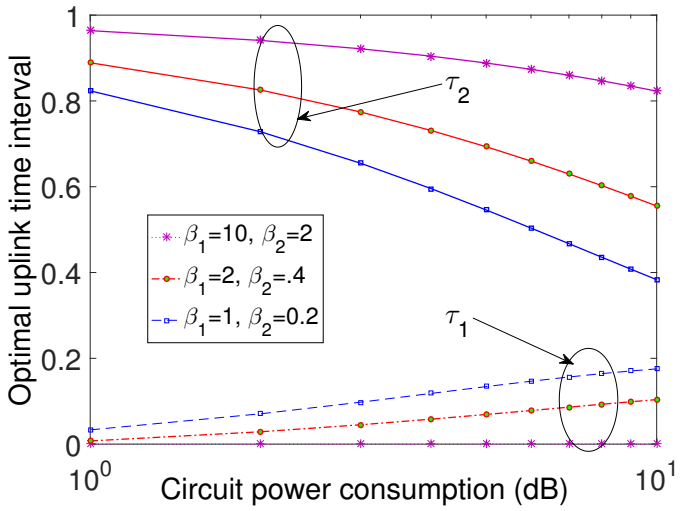

(a) Operating intervals (sec.) vs. P_{c_U}

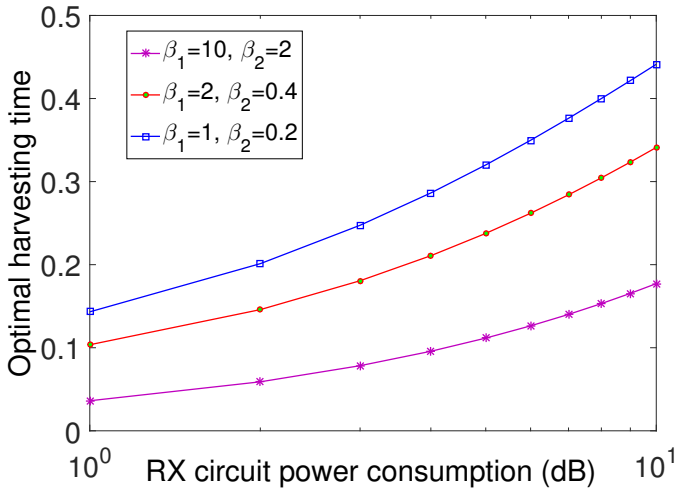

(b) Harvesting time (sec.) vs. P_{c_U}

Figure 8.6: Effect of uplink (receiver) circuit power consumption P_{c_U} on the performance with asynchronous transmission

---

higher values of P_a, i.e., when $P_a \gg P_{c_D}$, the change in EE along with P_{c_D} is expected to be small. Meanwhile, from Fig. 8.7, we observe that EE increases with downlink transmit power level (similarly as discussed earlier for the half-duplex operation) unless throughput maximization is the goal as in Case II. In addition, WPCN with uplink NOMA achieves better energy efficiency compared to case III in which TDMA is considered.

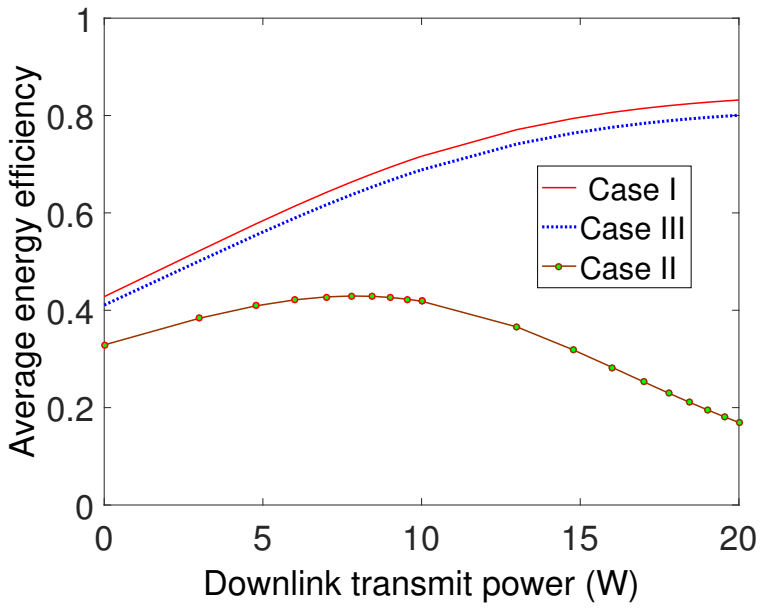

Figure 8.7: Performance gain of asynchronous transmission

The impact of QoS parameter on the optimal time allocation strategy and the corresponding system energy efficiency is illustrated in Figs. 8.8a and 8.8b. In general, stricter QoS constraint (i.e., higher value for the QoS exponent θ) degrades the system energy efficiency as can be seen from Fig. 8.8a, and higher circuit power consumption hurts the efficiency further as expected. In addition, we observe that uplink NOMA outperforms the TDMA approach regardless of the value of θ. However, the performance gain due to uplink NOMA diminishes with an increase in the aggregate circuit power consumption of UEs. In regard to the optimal time allocation strategy for TDMA, we observe that higher θ forces to allocate more time for energy harvesting, i.e., leads to increased τ_0, which in turn reduces the time for uplink information transfer.

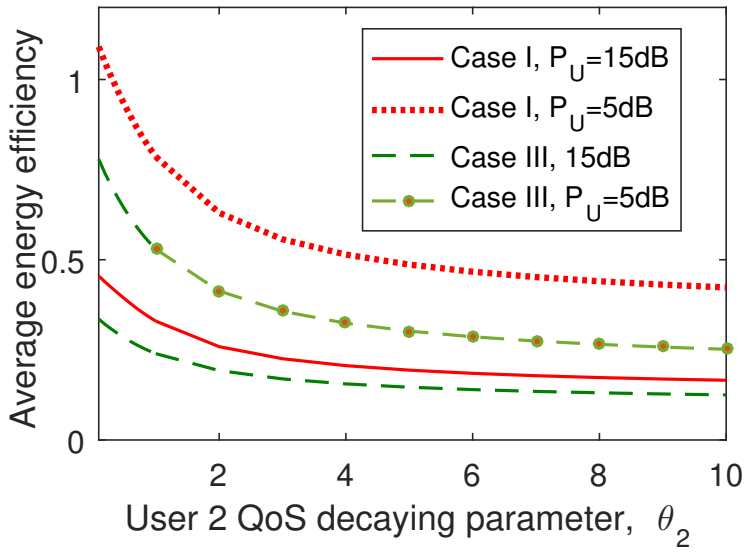

(a) Effective EE (bpJ/Hz) vs. user 2 QoS exponent θ_2

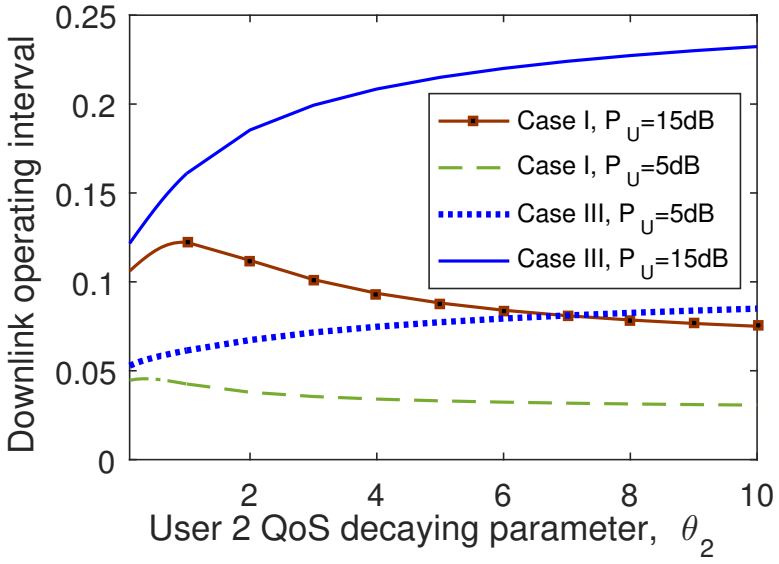

(b) Operating intervals (sec.) vs. θ_2

Figure 8.8: Impact of QoS parameter θ and circuit power consumption on the performance charactristics

Chapter 9

Conclusion

9.1 Summary

In this thesis, performance analysis of wireless information and power transfer in WPCNs has been studied in terms of network throughput and energy efficiency, and optimal resource allocation schemes for SWIPT with orthogonal and non-orthogonal MACs have been determined in the presence of delay-limited sources. Specifically, the contribution of this thesis are summarized below.

In Chapter 3, we studied SWIPT with finite-alphabets input focusing on the throughput for single user and multiple users settings. In this chapter, we introduced non-uniform probability distribution which assigns probability to each signal in the constellation space based on its energy level. This novel approach considers practically appealing finite signal constellations, and we investigated the significance of non-uniform probability assignment to these signals in order to improve the tradeoff in SWIPT. We explicitly defined two approaches, namely static slope and dynamic slope characteristics, to determine each alphabet probability according to the required harvested energy. In both single user and multiple user settings, we discussed that assigning higher probability to the signals with higher energy level allows to allocate more power to the ID component, assuming the receiver applies

power-splitting scheme to perform information-decoding and energy-harvesting operations. We formulated optimization problems that maximize information rates subject to harvested energy constraint and boundaries to the alphabets probabilities. Since obtaining closed form expression for the receiver power-splitting factor is difficult, we provided an algorithm to solve the optimization problem using standard numerical tools. Furthermore, we incorporated delay-sensitive sources and analyzed the impact of exponential decaying QoS exponent on SWIPT. In such a case, we provided explicit expression for the network throughput, i.e., effective capacity, as a function of power-splitting factor and signals probabilities. We considered time-division multiple access scheme for the transmitters, and operating time intervals, signal probabilities and receiver power-splitting factor are optimally adjusted according to the minimum harvested energy constraint such that the performance metric, i.e., effective capacity or system energy efficiency, is maximized. Theoretical formulations are justified using numerical results. According to the rate-energy tradeoff characteristics, we observed that non-uniform probability assignment improved the network throughput given the required harvested energy constraint. In addition, static slope characteristics has better performance compared to the dynamic scheme for lower energy demand. Furthermore, for looser QoS constraint, higher network throughput was attained.

In Chapter 4, we studied the optimal resource allocation strategies for MACs taking energy efficiency as the major performance metric. We provided energy-efficient node selection and power control policy by formulating an optimization problem which maximizes the system energy efficiency subject to peak power constraint. From the control policy, we noted that the node with the best link, i.e., with the highest channel gain, is selected to transmit while the rest nodes are kept silent. Activation of multiple UEs, for instance with the second highest channel gain, is possible when the mathematical solution for the optimal power of the activated UE exceeds its peak power constraint. Furthermore, we observed that the optimal transmitted power follows channel inversion approach, i.e., more power is required when the wireless link experiences very poor condition. Besides, an increase in the circuit power

consumption shifts the optimal transmit power level. On the other hand, we studied energy-efficient SWIPT in MAC considering two types of receiving architecture, namely separated antenna architecture and common antenna architecture. We formulated optimization problems in both scenarios to determine optimal policies, and we provided explicit expressions for the energy-efficient transmission strategies as well as the system energy efficiency. We noted that the node selection, i.e., activation of UEs, and the corresponding optimal transmit power level depend not only on the peak power level but also on the required harvested energy. In addition, the system energy efficiency is always a non-increasing function for the common antenna architecture, but for the separated architecture, there exists a constraint at which the system energy efficiency achieves the highest value. Numerical results justified the theoretical characterizations and impact of peak power constraint on the power allocation policy among the transmitting nodes. In addition, impact of circuit power consumption on the energy-efficient transmit power level and the optimal average energy efficiency were illustrated. We observed that the optimal splitting factor changes logarithmically when the transmitted power is below the peak power level, but once it reaches the peak, the factor linearly changes as the harvested energy increases.

In Chapter 5, we studied the performance of WPCNs in terms of throughput and energy efficiency under various wireless information and power transfer protocols, namely synchronous TDMA, synchronous MAC and asynchronous TDMA. In addition, we investigated the impact of statistical QoS constraints on the optimal harvesting time as well as overall performance of the networks in the presence of delay limited sources. For each operation protocol mentioned above, we formulated throughput maximizing and energy-efficiency maximizing optimization problems. Assuming that the harvesting interval is dependent of the fading state, we determined the KKT conditions to identify the optimal operating intervals. We provided analytical expressions for the operating time intervals in the synchronous MAC protocol, and suboptimal solution for the TDMA protocols. Also, because of the difficulty in obtaining closed-form solution in some cases, we proposed algorithms to solve the

problems numerically. Finally, several insightful observations were made through numerical results. We observed that asynchronous TDMA achieves highest throughput compared with other protocols, but synchronous MAC is an energy efficient protocol. In addition, as the exponential decaying component θ increases, more time will be allocated for the downlink operation, i.e., energy harvesting, and hence there is less time for information transfer which in turn hurts the sum effective capacity. Meanwhile, we observed that the QoS constraint can override the doubly near-far problem mentioned in the literature, i.e. UEs closer to the AP might not transmit at higher data rate when the distant UEs have loser constraint or lower buffer overflow probability. Furthermore, increasing the downlink transmit power level improves the system average energy efficiency of WPCNs. However, higher θ value still hurts EE.

In Chapter 6, we investigated the significance of introducing non-zero mean component on the information-bearing signal for full-duplex wireless information and power transfer. We modeled a hybrid system having energy harvesting and non-energy harvesting UEs, and formulated optimization problem subject to harvested energy and peak power constraints considering throughput and energy efficiency as the major performance metrics. In order to offset the channel phase shift and benefit the harvested energy, we applied pre-channel co-phasing to the transmitted signals by the AP and NEHU. Throughput-maximising power control strategies were identified, and an iterative algorithm was proposed to obtain optimal solution numerically. Furthermore, we derived energy efficient policies for two-users model taking various scenarios for the harvested energy constraint. According to the analytical expressions, signals transmitted from the NEHU with zero-mean were considered to be energy-efficient when the harvested energy constraint was not binding, i.e., for smaller demand. Furthermore, simulation results illustrated that introducing a non-zero mean information-bearing signal achieved higher energy efficiency compared with zero-mean based on the harvested energy constraint and channel characteristics. On the other hand, we observed that the optimal energy efficiency improved while the harvested energy demand increased

within certain boundaries. Any additional increment beyond the boundary hurts the EE.

In Chapter 7, we studied the impact of harvesting time interval, AP density, transmitted power level and related parameters on the overall performance of energy-harvesting cellular networks using stochastic geometry. We provided analytical framework to compute the SINR coverage probabilities, average data rate and energy efficiency for different types of downlink-uplink operation schemes that are categorized as WPT-WIT protocol, SWIPT-WIT protocol and WPT-WIT(mmWave) protocol. For the wireless-powered cellular network operating on lower frequency band with harvest-then-transmit protocol, i.e., WPT-WIT, we explicitly characterized coverage probabilities considering noise-limited and interference limited scenarios. We noted that SNR coverage probability is an increasing function of harvesting interval, but not achievable data rate. Meanwhile, in the case of SWIPT-WIT protocol, allocating more time for energy harvesting benefited the downlink data rate since the splitting factor became higher but the uplink data rate suffered from shorter duration for information transfer despite sufficient energy being harvested. On the other hand, we explicitly characterized average harvested energy and average throughput of cellular UEs when uplink information transfer is done on mmWave frequency band. Finally, several insightful observations have been made through numerical results. More specifically, densely deployed AP improves both the throughput and energy efficiency of WP cellular networks. In addition, transmitting the downlink WPT signal enhances the average energy efficiency. In the case of downlink SWIPT, there exists an optimal power-splitting factor that achieves maximum throughput or energy efficiency, and the downlink transmit power level and the harvesting time interval affects this optimal solution given the AP intensity.

In Chapter 8, we considered energy efficiency as a performance metric, and we investigated impact of uplink-NOMA on the overall performance of energy-harvesting communication networks. We took into account half-duplex and asynchronous transmission downlink-uplink operation modes, and formulated optimization problems in both cases focusing on the maximization of the system energy efficiency. Since these are concave-linear fractional pro-

gramming problems, Dinkelbach's method can be directly applied. With this, we obtained closed-form characterizations for the optimal time intervals and provided an algorithm to obtain the optimal solution for half duplex operation. Meanwhile, because of the difficulty in obtaining closed-form solutions for asynchronous transmission, we analyzed the optimal solution using standard numerical tools. Finally, several insightful observations were made through numerical results. According to the these results, we observed that downlink transmit power improved the system energy efficiency. In addition, circuit power consumption hurts EE, but this was dependent on the channel characteristics. Time intervals for energy harvesting and data transmission display intricate dependence on system parameters and operational modes. Finally, we noted that stricter delay constraints could lead to degradation in energy efficiency.

9.2 Future Research Directions

9.2.1 Analysis of SWIPT in MIMO Networks with Finite-Alphabet Inputs

In Chapter 3, we studied optimal resource allocation for SWIPT with finite-alphabet input assuming that the transmitter and receiver are equipped with single antenna. On the other hand, in the presence of multiple antennas at both ends, we can exploit more by introducing not only non-uniform probability distribution but also non-zero mean component. In such a case, channel co-phasing can be applied and constellation shifting can be designed so as to improve the overall performance.

9.2.2 NOMA-based SWIPT under Delay-Limited Sources

In Chapter 8, NOMA technique is well investigated for wireless-powered communication networks considering various harvest-then-transmit protocols. This work can be extended

taking into account of delay-limited sources as well as simultaneous transfer of information and power. Indeed, this introduces more variables to control and additional characteristics curves to analyze.

9.2.3 Optimal Resource Allocation for WPCNs with finite block-lenghth

In Chapter 5 and Chapter 8, we assumed that energy harvesting UEs transfer information uplink approximately without error , i.e. infinite block length. However, when finite block length is considered, each UEs uplink and donwlink operating interval, i.e., transmitting block length, will be affected and the overall performance changes accordingly.

Appendix A

Proof Theorem 3.1.1

We consider n being even and odd scenarios separately as follows.

I. Square Geometry: n-even

Under this assumption, let the constellation has $N_s \times N_s$ square configuration with (x, y) coordinates in a 2-dimensional space where $x, y \in \{-K, \ldots, -3, -1, 1, 3, \ldots K\}$, $K = \sqrt{M} - 1$ and $N_s = K + 1$. Assuming the constellation is centered at the origin, it can be divided into four $N_s/2 \times N_s/2$ symmetrical sub-squares in which the number of different energy levels in the constellation space, N, is the same as in one of the quadrants. Without loss of generality, considering the 1^{st} quadrant, x, $y \in \{1, 3, \ldots K\}$, we have

$$\mathcal{E}_s = \begin{vmatrix} \mathcal{E}_{11} & \mathcal{E}_{13} & \ldots & \mathcal{E}_{1K} \\ \mathcal{E}_{31} & \mathcal{E}_{33} & \ldots & \mathcal{E}_{3K} \\ \ldots & \ldots & \ldots & \ldots \\ \mathcal{E}_{K1} & \mathcal{E}_{K3} & \ldots & \mathcal{E}_{KK} \end{vmatrix}$$

where $\mathcal{E}_s$ is a matrix consisting of each signal energy level, $\mathcal{E}_{ij} = |X_{(i,j)}|^2$, at constellation coordinate point (i, j) in the square QAM constellation. For $E_{ij} = E_{ji}$, it is optimal to have $p_{ij} = p_{ji}$, where p_{ij} is the probability of the signal located at (i, j). Let Q be a vector having only different energy levels, i.e., $Q = \{\mathcal{E}_{11}, \ldots, \mathcal{E}_{KK}\}$ for $i, j = \{1, 3, \ldots K\}$ with $i < j$. Note

that $\mathcal{E}_s$ is symmetrical, and hence the number of different energy levels in this quadrant, $N^1 = |Q|$, can be determined using either upper or lower diagonal matrix of $\mathcal{E}_s$ as follows

$$\begin{aligned} N^1 &= \left[\left(\frac{N_s}{2}-1\right)+\cdots+\left(\frac{N_s}{2}-\left(\frac{N_s}{2}-1\right)\right)\right]+\frac{N_s}{2} \\ &= \sum_{i=0}^{\frac{N_s}{2}-1}\left(\frac{N_s}{2}-i\right). \end{aligned} \tag{A.1}$$

Therefore, based on the fact that $N = N^1$, the total number of different energy levels can be expressed as in (3.31a).

II. Rectangular geometry: n-odd

In this case, let each signal coordinate be denoted as (x, y) where $x \in \{-K_a, \cdots, -3, -1, 1, 3, \cdots K_a\}$, $K_a = \sqrt{M/2} - 1$ and $y \in \{-K_b, \ldots, -3, -1, 1, 3, \ldots K_b\}$, $K_b = \sqrt{2M} - 1$. The constellation has $N_a \times N_b$ rectangular configuration with $N_a = K_a + 1$ and $N_b = K_b + 1$, and using similar arguments as stated above, we consider the 1^{st} quadrant to determine the number of different energy levels. Hence, we have

$$\mathcal{E}_r = \begin{vmatrix} \mathcal{E}_{11} & \mathcal{E}_{13} & \ldots & \mathcal{E}_{1K_b} \\ \mathcal{E}_{31} & \mathcal{E}_{33} & \ldots & \mathcal{E}_{1K_b} \\ \ldots & \ldots & \ldots & \ldots \\ \mathcal{E}_{K_a1} & \mathcal{E}_{K_a3} & \ldots & \mathcal{E}_{K_aK_b} \end{vmatrix}$$

where $\mathcal{E}_r$ is a matrix consisting of each signal's energy level in the rectangular constellation. Since $N_a/2 < N_b/2$, $\mathcal{E}_r$ can be partitioned into two sub-matrices $\mathcal{E}_r^{aa} = N_a/2 \times N_a/2$ and $\mathcal{E}_r^{ab} = N_a/2 \times (N_b/2 - N_a/2)$ whose numbers of different energy levels are denoted as N^{aa} and $N^{a(b-a)}$, respectively. Since $\mathcal{E}_r^{aa}$ has square configuration, N^{aa} can be easily determined using (A.1), whereas in the case of $\mathcal{E}_R^{ab}$, it is obvious that each coordinate has a unique energy level. Hence,

$$N^{aa} = \sum_{i=0}^{\frac{N_a}{2}-1} \left(\frac{N_a}{2} - i \right) \tag{A.2a}$$

$$N^{a(b-a)} = \frac{N_a}{2} \left(\frac{N_b}{2} - \frac{N_a}{2} \right). \tag{A.2b}$$

Therefore, the total number of different energy levels in $N_a \times N_b$ constellation space becomes $N = N^{aa} + N^{a(b-a)}$, which is the same as given in (3.31b) after a minor substitution.

Appendix B

Proof of Proposition 3.1.1

As noted in Theorem 3.1.1, signals are grouped based on energy levels so that it is possible to adjust their probabilities in such a way that the subset with the highest energy level signals, $\mathcal{S}_N \in \mathcal{S}_{sc}$, gets high priority for transmission as the minimum required harvested energy level increases. Considering the boundaries, when $\mathcal{X} = 0$ input is uniformly distributed with $p_j = \frac{1}{|\mathcal{S}|}$, $\forall X_j \in \mathcal{S}$ according to Remark 3.1.1, whereas when $\mathcal{X} = E_{mx}$, only highest energy signals are chosen, i.e., $p_j = 0$, $\forall X_j \notin \mathcal{S}_N$. In the latter case, assuming $|\mathcal{S}_N| \neq 1$, the transmitted signal can be either among these signals that are equiprobable, $p_j = \frac{1}{|\mathcal{S}_N|}$, or one of them almost a surely, i.e, $\{X_a, X_b\} \in \mathcal{S}_N$ with $\Pr\{X = X_a\} = 1$ but $\Pr\{X = X_b\} = 0$, $\forall b = \{1, 2, \ldots, |\mathcal{S}_N|\}$ and $b \neq a$. In both cases, the same amount of energy is harvested; however, equpiprobable assignment benefits information transfer under opportunistic or ideal harvesting/decoding scheme.

Appendix C

Proof of Proposition 3.1.2

First, let us re-write the achievable rate expression given in 3.19 as follows:

$$R(\rho) = -\sum_{k=1}^{M} \frac{p_k}{\pi N_0} \int_{-\infty}^{\infty} \int_{-\infty}^{\infty} e^{-|v|^2} f_k(\rho) dv_1 dv_2 \tag{C.1}$$

where

$$f(\rho) = \log \left[\sum_{j=1}^{M} p_j e^{a_i \rho} \right] \tag{C.2}$$

and $a_i = -|v+\gamma_d|^2 + |v|^2$. Since non-negative weighted summation and integration preserves convexity, it is necessary and sufficient to show the convexity of the function $f(\rho)$ in order to verify that $R(\rho)$ is concave in ρ. Thus, applying second-order derivative, we get

$$\frac{\partial^2 f(\rho)}{\partial \rho^2} = \frac{\sum_i p_i a_i^2 e^{a_i \rho}}{\sum_i p_i e^{a_i \rho}} - \frac{\left(\sum_i p_i a_i e^{a_i \rho} \right) \left(\sum_i p_i a_i e^{a_i \rho} \right)}{\left(\sum_i p_i e^{a_i \rho} \right)^2} \tag{C.3}$$

$$
\begin{aligned}
&= \frac{1}{\Big(\sum_i p_i e^{a_i\rho}\Big)^2}\left[\Big(\sum_i p_i a_i^2 e^{a_i\rho}\Big)\Big(\sum_i p_i e^{a_i\rho}\Big) - \Big(\sum_i p_i a_i e^{a_i\rho}\Big)^2\right] \\
&= \frac{1}{\Big(\sum_i p_i e^{a_i\rho}\Big)^2}\left[\Big(\sum_i p_i^2 a_i^2\Big)\Big(\sum_i e^{2a_i\rho}\Big) - \Big(\sum_i p_i a_i e^{a_i\rho}\Big)^2\right] \\
&= \frac{1}{\Big(\sum_i p_i e^{a_i\rho}\Big)^2}\left[\big(z^T z\big)\big(v^T v\big) - \big(z^T v\big)\right]
\end{aligned}
\tag{C.4}
$$

where $z = [p_1 a_1, p_2 a_2, \cdots, p_n a_n]$ and $v = [e^{a_1\rho}, e^{a_2\rho}, \cdots, e^{a_n\rho}]$. From the Cauchy-Schwarz inequality, we know that

$$
|\langle \boldsymbol{X}, \boldsymbol{Y}\rangle|^2 \le \langle \boldsymbol{X}, \boldsymbol{X}\rangle \cdot \langle \boldsymbol{Y}, \boldsymbol{Y}\rangle \tag{C.5}
$$

where $\boldsymbol{X}$ and $\boldsymbol{Y}$ are vectors, and $\langle\cdot,\cdot\rangle$ is the inner product. Hence, we claim that $\big(z^T z\big)\big(v^T v\big) \ge \big(z^T v\big)$, and this guarantees $\frac{\partial^2 f(\rho)}{\partial \rho^2} \ge 0$. Therefore, $f(\rho)$ is a convex function of ρ.

Appendix D

Proof of Theorem 4.2.1

Without loss of generality, we assume that $h_1 < h_2 < \cdots < h_N$. The Lagrangian of (PR:3.1) is

$$\mathcal{L} = \frac{\log_2\left(1+\sum_{i=1}^{N}\gamma_i\right)}{P_C+\sum_{i=1}^{N}P_i} - \sum_{i=1}^{N}\phi_i P_i(P_i - P_i^{mx}) \tag{D.1}$$

where ϕ_is are the Lagrange multipliers associated with the power constraints. Hence, the corresponding KKT conditions are

$$\frac{\partial \mathcal{L}}{\partial P_i} = 0, \qquad \phi_i P_i\big(P_i - P_i^{mx}\big) = 0 \tag{D.2}$$

where $i \in \mathcal{S}$. Based on the complementary slackness condition, $\phi_i = 0$ for $0 < P_i < P_i^{mx}$, and the boundary conditions $P_i = P_i^{mx}$ will be considered later. Now, the first order optimality criterion is given by

$$\frac{\partial \eta}{\partial P_i} = \frac{h_i}{\ln(2)\Big(1+\sum_{i=1}^{N}\gamma_i\Big)\Big(P_C+\sum_{i=1}^{N}P_i\Big)} - \frac{\log_2\Big(1+\sum_{i=1}^{N}\gamma_i\Big)}{\Big(P_C+\sum_{i=1}^{N}P_i\Big)^2} = 0 \tag{D.3}$$

By rearranging the terms, we can rewrite (D.3) as

$$\omega\ln(\omega) - \omega = \Gamma_N \tag{D.4}$$

which can be further expressed as

$$e^{\ln(\frac{\omega}{e})}\ln\left(\frac{\omega}{e}\right)=\frac{\Gamma_N}{e} \tag{D.5}$$

where $\Gamma_N=\sum_{j=1}^{N-1}(h_N-h_j)P_j-1+h_NP_C$ and $\omega=1+\sum_{i=1}^{N}\gamma_i$. Mathematically, (D.5) has the functional form of $Xe^X=Y$ whose solution is given by the Lambert function $\mathcal{W}$, i.e., $X=\mathcal{W}(Y)$ for $Y\geq-\frac{1}{e}$. Thus, the solution to (D.5) can be analytically expressed as

$$\omega^*=e^{\mathcal{W}\left(\frac{\Gamma_N}{e}\right)+1},\qquad \Gamma_N\geq-1. \tag{D.6}$$

Given P_j^* for $j=1,\ldots,N-1$, the optimal transmit power level from node N becomes

$$\tilde{P}_N=\frac{\omega^*-1-\sum_{j=1}^{N-1}\gamma_j}{h_N}. \tag{D.7}$$

Substituting (D.6) and (D.7) into (4.6), we have

$$\eta(\Gamma_N)=c\frac{\mathcal{W}(\frac{\Gamma_N}{e})+1}{(\Gamma_N+e^{\mathcal{W}(\frac{\Gamma_N}{e})+1})} \tag{D.8}$$

where $c=\frac{h_N}{\ln(2)}$. Thus, the optimal efficiency depends on Γ_N, and considering its slope characteristics using $W'(x)=\frac{\mathcal{W}(x)}{x+x\mathcal{W}(x)}$, we obtain

$$\frac{\partial\eta}{\partial\Gamma_N}=-c\left[\frac{\mathcal{W}(\frac{\Gamma_N}{e})+1}{(\Gamma_N+e^{\mathcal{W}(\frac{\Gamma_N}{e})+1})^2}\right]\leq 0. \tag{D.9}$$

This implies that energy efficiency is a decreasing function of Γ_N, and hence the maximum energy efficiency is achieved at the lowest value of Γ_N. This occurs when $P_j=0$ for all $h_j<h_N$ and $j\in\{1,2,\cdots,N-1\}$. Therefore, the user with the highest channel gain will be active, and its optimal transmit power is given as

$$\tilde{P}_N=\left.\frac{e^{\mathcal{W}(\frac{\Gamma_N}{e})+1}-1}{h_N}\right|_{\forall P_j=0,P_C=P_c}. \tag{D.10}$$

However, if $\tilde{P}_N$ exceeds the peak, then node N operates at $P_N^* = P_N^{mx}$. In such a case, other nodes could be allowed to transmit based on the corresponding optimal strategy. Let us assume that the nodes $N, N-1, \ldots, k+1$ are transmitting at their peak power levels, i.e., $P_N^* = P_N^{mx}, \cdots, P_{k+1}^* = P_{k+1}^{mx}$. Then, the transmit power for node k, under the assumption $h_N > \cdots > h_{k+1} > h_k$, needs to be determined in such a way that the system energy efficiency

$$\eta = \frac{\log_2(1 + \gamma_k + \sum_{j=k+1}^{N} h_j P_j^{mx})}{P_c^k + \sum_{j=k+1}^{N} P_j^{mx} + P_k} \tag{D.11}$$

is maximized. Applying the optimality criteria and following a similar procedure as noted earlier, we get

$$\tilde{P}_k = \frac{e^{\mathcal{W}(\frac{\Gamma_k}{e})+1} - 1 - \sum_{j=k+1}^{N} h_j P_j^{mx}}{h_k} \tag{D.12}$$

where $\Gamma_k = \sum_{j=k+1}^{N} (h_k - h_j) P_j^{mx} - 1 + h_k P_c^k$. Note again that unless $\tilde{P}_k$ exceeds the peak power level, we again have to set $P_i^* = 0$ for $i = 1, \ldots, k-1$ in order to maximize the energy efficiency.

Appendix E

Proof of Theorem 4.3.1

Without loss of generality, we again assume that $h_1 < h_2 < \cdots < h_N$. The Lagrangian for problem (PR:4.2a) is expressed as

$$\mathcal{L} = \frac{\log_2\left(1+\sum_{i=1}^{N}\gamma_i\right)}{\kappa+\sum_{i=1}^{N}P_i} - \sum_{i=1}^{N}\phi_i P_i(P_i - P_i^{mx}) \tag{E.1}$$

where $\{\phi_i\}$ are the Lagrange multipliers associated with the power constraints. The complementary slackness condition is the same as stated in (D.2), and KKT conditions for the first order optimality are

$$\frac{\partial \eta_s}{\partial P_i} = \frac{h_i}{\ln(2)\Big(1+\sum_{i=1}^{N}\gamma_i\Big)\Big(P_C+\sum_{i=1}^{N}(1-g_i)P_i\Big)} - \frac{(1-g_i)\log_2\Big(1+\sum_{i=1}^{N}\gamma_i\Big)}{\Big(P_C+\sum_{i=1}^{N}(1-g_i)P_i\Big)^2} = 0, \quad \text{for } B > \chi \tag{E.2a}$$

$$\frac{\partial \eta_s}{\partial P_i} = \frac{h_i}{\ln(2)\Big(1+\sum_{i=1}^{N}\gamma_i\Big)\Big(P_C+\sum_{i=1}^{N}P_i-\chi\Big)} - \frac{\log_2\Big(1+\sum_{i=1}^{N}\gamma_i\Big)}{\Big(P_C+\sum_{i=1}^{N}P_i-\chi\Big)^2} = 0, \qquad B = \chi \tag{E.2b}$$

i) $B > \chi$: When the additional harvested energy beyond the demand can be stored, we have (E.2a) and this can be expressed as

$$\omega \ln(\omega) - \omega = \Gamma_i \tag{E.3}$$

where $\omega = 1 + \sum_{i=1}^{N} \gamma_i$ and $\Gamma_i = \sum_{j=1, j\neq i}^{N} (h_i - h_j)P_j - 1 + h_i \frac{P_C}{1-g_i}$. Based on (E.3), the problem is feasible if

$$\Gamma_i = \Gamma_j \tag{E.4}$$

when nodes i and j are transmitting. Following a similar procedure as in the proof of Theorem 4.2.1, we conclude that η is a decreasing function of Γ_i and hence energy efficiency is maximized at the lowest possible value of the corresponding Γ_i. As a result, we have

$$\Gamma_N = -1 + h_N \frac{P_c}{1 - g_N} \tag{E.5a}$$

assuming $P_j = 0, \forall j \in \{1, ...N-1\}$, and

$$\Gamma_{N-k} = -1 + h_{N-k} \frac{P_c^k}{1 - g_{N-k}} + \sum_{j=0}^{k-1} \Big(h_{N-k} - h_{N-j}\Big) P_{N-j} \tag{E.5b}$$

for $k = 1, 2, \cdots, N-1$, assuming $P_j = 0, \forall j \in \{1, ...N-k-1\}$. It seems there are N different node selection strategies, but we show by contradiction that the one with the best channel link should be active for maximum energy efficiency. For instance, let us consider Γ_{N-1}, and in this case, both $P_N \neq 0$ and $P_{N-1} \neq 0$ implying node N and node $N-1$ are active. This leads to $\Gamma_{N-1} > \Gamma'_N = -1 + h_N \frac{P_c}{1-g_N} + (h_N - h_{N-1})P_{N-1}$ for $P_c^{N-1} > P_c$, but $\Gamma'_N > \Gamma_N$ which contradicts the optimality condition in (E.4). Therefore, $P_j = 0, \forall j \in \{1, ...N-1\}$ and

$$\tilde{P}_N = \frac{e^{\mathcal{W}\left(\frac{h_N \frac{P_c}{1-g_N} - 1}{e}\right) + 1}}{h_N} - 1. \tag{E.6}$$

ii) $B = \chi$: In case there is a limited capacity to store harvested energy, i.e., $B = \chi$, the optimality condition given in (E.2b) is similar to (D.3) except the additional term χ. Hence, applying the same procedure as in the proof of Theorem 4.3.1, we get $P_j = 0 \ \forall h_j < h_N$ and

$$\tilde{P}_N = \frac{e^{\mathcal{W}\left(\frac{h_N(P_c-\chi)}{e}\right)+1} - 1}{h_N}. \tag{E.7}$$

In both cases above, when the optimal solution $\tilde{P}_N$ exceeds the peak power constraint, the transmitted power level from node N is kept at P_N^{mx}, and similar steps can be followed as in Appendix D to determine $\tilde{P}_{N-1}$ and iteratively the other power levels if peak power constraints become active. Furthermore, the threshold at which the harvested energy constraint becomes active can be determined, for instance, by substituting $\tilde{P}_N = \frac{\chi^*}{\beta g_N}$ into (E.6) or (E.7) and solving for χ^*. Thus, we have

$$W\Big(\frac{h_N\Phi - 1}{e}\Big) + 1 = \ln\Big(1 + \frac{h_N}{g_N}\chi^*\Big) \tag{E.8}$$

where

$$\Phi = \begin{cases} \dfrac{P_c}{1 - g_i} & B > \chi \quad \text{(E.9a)} \\ P_c - \chi & B = \chi. \quad \text{(E.9b)} \end{cases}$$

It is difficult to get a closed-form expression for χ^* from this equation, which, nevertheless, can be easily solved using numerical tools.

Appendix F

Proof of Proposition 4.3.1

Without loss of generality, we assume that $h_i > h_j$ for $i, j \in \{1, 2\}$, and the conditions in (4.26) are explicitly expressed as

$$\begin{aligned} \frac{h_i}{\ln(2)\Big(1+\sum_{i=1}^{N}\gamma_i\Big)\Big(P_C+\sum_{i=1}^{N}P_i-\chi\Big)} - \frac{\log_2\Big(1+\sum_{i=1}^{N}\gamma_i\Big)}{\Big(P_C+\sum_{i=1}^{N}P_i-\chi\Big)^2} &= \mu g_i \\ \frac{h_j}{\ln(2)\Big(1+\sum_{i=1}^{N}\gamma_i\Big)\Big(P_C+\sum_{i=1}^{N}P_i-\chi\Big)} - \frac{\log_2\Big(1+\sum_{i=1}^{N}\gamma_i\Big)}{\Big(P_C+\sum_{i=1}^{N}P_i-\chi\Big)^2} &= \mu g_j, \end{aligned} \tag{F.1}$$

assuming the two-user setup. Accordingly, there are two possible conditions that need to be addressed independently.

(a) $h_i > h_j$ and $g_i > g_j$: When user i has higher power gains with the ID and EH components than user j, (F.1) holds true if either $P_i = 0$ or $P_j = 0$. Since user j achieves a lower EE for the same transmit power, it is better to keep user j in silent mode and let user i to transmit. The maximum energy that can be harvested from user i is $\chi_a' = g_i P_i^{mx}$. When the demand exceeds this, user j begins transmission to satisfy the extra energy demand $\Delta\chi = \chi - \chi_a'$.

(b) $h_i > h_j$ but $g_i < g_j$: In this case, (F.1) can be satisfied with $P_i \neq 0$ and $P_j \neq 0$. Now, we have

$$\left(\frac{h_i}{g_i} - \frac{h_j}{g_j}\right)\frac{1}{\big(1+\sum_i \gamma_i\big)} = \left(\frac{1}{g_i} - \frac{1}{g_j}\right)\frac{\ln\big(1+\sum_i \gamma_i\big)}{\big(P_c + P_i + P_j - \chi\big)} \tag{F.2}$$

which leads to

$$A = z\ln(z) - z \tag{F.3}$$

where $A = P_c\Big(\frac{h_i g_j - h_j g_i}{g_j - g_i}\Big) + \chi\Big(\frac{1-g_j}{g_j}\big(\frac{h_i g_j - h_j g_i}{g_j - g_i}\big) - \frac{h_j}{g_j}\Big) - 1$ and $z = 1 + \chi\frac{h_j}{g_j} + P_i\Big(h_i - \frac{h_j g_i}{g_j}\Big)$. Hence, solving for P_i, we obtain

$$P_i^* = \frac{g_j e^{\mathcal{W}(\frac{A}{e})+1} - g_j - h_j\chi}{g_j h_i - g_i h_j} \tag{F.4}$$

and substituting this into $g_j P_j^* = \chi - g_i P_i^*$, we get

$$P_j^* = \frac{-g_i e^{\mathcal{W}(\frac{A}{e})+1} + g_i + h_i\chi}{g_j h_i - g_i h_j}. \tag{F.5}$$

Then, the maximum energy χ_b' that can be harvested from user i while user j is silent can be obtained by setting $P_j^* = 0$ and $\chi = \chi_b'$ in (F.5). This results in

$$\ln\Big(\frac{h_i}{g_i}\chi_b' + 1\Big) = \mathcal{W}\left(\frac{A}{e}\right)\Big|_{\chi=\chi_b'} + 1, \tag{F.6}$$

which can be solved numerically. Thus, user j becomes active when $\chi > \chi_b'$, and this continues until $P_j = P_j^{mx}$ which occurs at $\chi = \chi''$. Any additional demand $\Delta\chi = \chi - \chi''$ will be satisfied by user i until it reaches its peak.

Appendix G

Proof of Theorem 4.3.2

The Lagrangian of (PR:4.3) is given by

$$\mathcal{L} = \eta_c - \sum_{i=1}^{N} \kappa_i (P_i - P_i^{mx}) + \sum_{i=1}^{N} \phi_i P_i. \tag{G.1}$$

Applying similar procedure as in proof of Theorem 4.2.1, the first order criteria, which is given as

$$\frac{\partial \eta_c}{\partial P_i} = \frac{h_i}{\ln(2)\Big(1 + \sum_{i=1}^{N} \gamma_i - \chi\Big)\Big(P_C + \sum_{i=1}^{N} P_i - \chi\Big)} - \frac{\log_2\Big(1 + \sum_{i=1}^{N} \gamma_i - \chi\Big)}{\Big(P_C + \sum_{i=1}^{N} P_i - \chi\Big)^2} = 0, \tag{G.2}$$

can not be satisfied, i.e., $\frac{\partial \eta_c}{\partial P_i} \neq \frac{\partial \eta_c}{\partial P_j}$ for $h_i \neq h_j$, unless a single node is active at a time while the rest silent. Since the energy-efficient approach is to let the node with the highest channel gain transmit, from (G.2) we have

$$\phi \ln \phi - \phi = \Omega_N \tag{G.3}$$

where $\Omega_N = h_N P_c - 1 + \chi(1 - h_N)$ and $\phi = 1 + \gamma_N - \chi$, and the corresponding optimal transmit power becomes

$$P_N^* = \frac{e^{\mathcal{W}(\frac{\Omega}{e})+1} + \chi - 1}{h_N}. \tag{G.4}$$

An increment in harvested energy requires transmission at a higher power level, and eventually this leads to transmission at the peak power. Hence, the maximum demand χ_N^{mx} that can be satisfied by node N is obtained by solving

$$h_N P_N^{mx} + 1 = e^{W\left(\frac{h_N P_c - 1 + \chi_N^{mx}(1-h_N)}{e}\right)+1} + \chi_N^{mx} \tag{G.5}$$

which is derived from (G.4). The threshold at which node $N-1$ becomes active depends on its the impact on the optimal energy efficiency. For $\chi > \chi_N^{mx}$, we have

$$\eta_c = \frac{\log_2\left(1 + h_N P_N^{mx} + h_{N-1} P_{N-1} - \chi\right)}{P_c^1 + P_N^{mx} + P_{N-1} - \chi}, \tag{G.6}$$

and following the same procedure as in the previous cases, the transmitted power level from node $N-1$ becomes

$$P_{N-1}^* = \frac{e^{W\left(\frac{h_{N-1} b_1 - a_1}{e}\right)+1} - a_1}{h_{N-1}} \tag{G.7}$$

where $a_1 = 1 + h_N P_N^{mx} - \chi$ and $b_1 = P_c^1 + P_N^{mx} - \chi$. Mathematically, P_{N-1}^* can take any value, but note that it is feasible only for $P_{N-1}^* \geq 0$. Hence, the maximum demand at which node $N-1$ is still silent can be computed by substituting $P_{N-1}^* = 0$ in (G.7), and this results in

$$W\left(\frac{c_{N-1} + d_{N-1}\chi}{e}\right)\Big|_{\chi=\chi_{N-1}^{mn}} + 1 = \ln\left(1 + h_N P_N^{mx} - \chi\right)\Big|_{\chi=\chi_{N-1}^{mn}} \tag{G.8}$$

where $c_{N-1} = h_{N-1} P_c + \left(h_{N-1} - h_N\right) P_N^{mx} - 1$ and $d_{N-1} = 1 - h_{N-1}$. Therefore, for $\chi_{N-1}^{mn} > \chi > \chi_N^{mx}$ the optimal strategy dictates node $N-1$ to be silent while node N transmits at its peak. Beyond this threshold, node $N-1$ operates based on (G.7) until $P_{N-1}^* = P_{N-1}^{mx}$. In

general, for node $N-k$, its transmitted signal power level is determined as follows:

$$P^*_{N-k} = \frac{e^{W\left(\frac{h_{N-k}b_k - a_k}{e}\right)+1} - a_k}{h_{N-k}} \tag{G.9}$$

where $a_k = 1+\sum_{j=k}^{N} h_j P_j^{mx} - \chi$ and $b_k = P_c^k + \sum_{j=k}^{N} P_j^{mx} - \chi$. Correspondingly, the minimum and maximum demand, i.e., χ_k^{mn} and χ_k^{mx}, for which node k operates within the boundaries can be obtained by substituting $P^*_{N-k} = 0$ and $P^*_{N-k} = P^{mx}_{N-k}$ into (G.9) and solving for χ.

Appendix H

Proof of Proposition 5.1.1

Applying second-order derivative criterion to the instantaneous service rate of user i, we get

$$\ln(2)\frac{\partial R_i(\tau_B)}{\partial \tau_B} = -\ln\left(1+\frac{a_i\tau_B}{(1-\tau_B)+\tau_B a_*}\right)+(1-\tau_B)\frac{a_i}{\Big(1+\tau_B(a_i+a_*-1)\Big)\Big(1-\tau_B+a_*\tau_B\Big)}$$

$$\ln(2)\frac{\partial^2 R_i(\tau_B)}{\partial \tau_B^2} = -\left[\frac{\Big(1-\tau_B\Big)\Big(2a_ia_*+a_i^2\Big)+2a_ia_*\tau_B\Big(a_*+a_i\Big)}{\Big(1-\tau_B+a_*\tau_B\Big)^2\Big(1-\tau_B+a_i\tau_B+a_*\tau_B\Big)^2}\right]. \tag{H.1}$$

Hence, it can be inferred from (H.1) that $\frac{\partial^2 R_i}{\partial \tau_B^2} < 0$ for all $\tau_B \in (0,1)$, and hence the instantaneous service rate is concave in the domain set. This completes the proof.

Appendix I

Proof of Proposition 5.1.2

First, let us consider that the downlink and uplink operating intervals, i.e., $\tau_B, \tau_1, \cdots, \tau_N$, are non-overlapping. Let $\mathbf{H}_i$ denote the Hessian of $R_i(\tau_B, \boldsymbol{\tau}_i)$ with respect to τ_B and τ_i where $i \in \mathcal{S}$. Thus, the diagonal and off-diagonal entries given in [56] are modified as:

$$d_{m,m}^{(i)} = \begin{cases} -\dfrac{a_m^i \tau_i}{(\tau_i + a_B^i \tau_B + \sum_{j=1}^{i-1} a_j \tau_j)^2}, & m < i \\ -\dfrac{(a_B^i \tau_B + \sum_{j=1}^{i-1} a_j \tau_j)^2}{\tau_i (\tau_i + a_B^i \tau_B + \sum_{j=1}^{i-1} a_j \tau_j)^2}, & m = i \\ 0 & \text{otherwise} \end{cases} \tag{I.1}$$

$$d_{m,n}^{(i)} = \begin{cases} -\dfrac{a_m^i a_n^i \tau_i}{(\tau_i + a_B^i \tau_B + \sum_{j=1}^{i-1} a_j \tau_j)^2}, & m < i \text{ and } n < i \\ \dfrac{a_m (a_B^i \tau_B + \sum_{j=1}^{i-1} a_j \tau_j)}{(\tau_i + a_B^i \tau_B + \sum_{j=1}^{i-1} a_j \tau_j)^2}, & m < i \text{ and } n = i \\ 0 & \text{otherwise} \end{cases} \tag{I.2}$$

Hence, for every non-zero column vector denoted by $\mathbf{z} = [z_1, z_2, \cdots, z_{i-1}]^T$, we have

$$\mathbf{z}^T H_i \mathbf{z} = -\frac{1}{\tau_i (\tau_i + \beta_i)^2} \left(\tau_i \sum_{m=1}^{i-1} z_m a_m - z_i \beta^i \right)^2 \leq 0 \tag{I.3}$$

where $\beta^i = a_B^i \tau_B + \sum_{j=1}^{i-1} a_j \tau_j$. This shows that $\mathbf{H}_i$ is a negative semi-definite matrix, and hence based on Theorem 21.5 given in [97], $R_i(\boldsymbol{\tau}_i)$ is a concave function of operation intervals, and this completes the proof.

Appendix J

Proof of Theorem 5.2.1

First, let $h_i(\tau_B) = (1-\tau_B)\log\left(1+\frac{a_i^k\tau_B}{1+\left(a_*^k-1\right)\tau_B}\right)$ and $H_i(\tau_B) = -\frac{1}{\theta_i}\log\left(\mathbb{E}\{e^{-\theta_i h_i(\tau_B)}\}\right)$ where θ_i's are assumed to be known. Earlier from (U.1), we observed that $h_i(\tau_B)$ is concave or $-h_i(\tau_B)$ is convex in the domain set. Applying the second-order derivative criterion to $h_i(\tau_B)$, we get

$$\ln(2)\frac{\partial h(\tau_B)}{\partial \tau_B} = -\log\left(1+\frac{a_i\tau_B}{(1-\tau_B)+\tau_B a_*}\right) + (1-\tau_B)\frac{a_i}{\Big(1+\tau_B(a_i+a_*-1)\Big)\Big(1-\tau_B+a_*\tau_B\Big)}$$

$$\ln(2)\frac{\partial^2 h(\tau_B)}{\partial \tau_B^2} = -\left[\frac{\Big(1-\tau_B\Big)\Big(2a_ia_*+a_i^2\Big)+2a_ia_*\tau_B\Big(a_*+a_i\Big)}{\Big(1-\tau_B+a_*\tau_B\Big)^2\Big(1-\tau_B+a_i\tau_B+a_*\tau_B\Big)^2}\right]. \tag{J.1}$$

It can be inferred from (U.1) that $\frac{\partial^2 h_i(\tau_B)}{\partial \tau_B^2} < 0$ for all $\tau_B \in (0,1)$, and hence $h_i(\tau_B)$ is concave or $-h_i(\tau_B)$ is convex in the domain set. This implies that $e^{-h(\tau_B)}$ is log-convex, and $\mathbb{E}\{e^{-h(\tau_B)}\}$ is log-convex as well, as log-convexity is preserved under sums. Noting that $\log(g(\cdot))$ is convex for log-convex $g(\cdot)$ [98], clearly $H(\tau_B)$ is a concave function of τ_B for $0 < \tau_B < 1$. Meanwhile, the sum effective capacity can be re-written as

$$C^e(\tau_B) = \frac{H_{sm}(\tau_B)}{T} \tag{J.2}$$

where $H_{sm} = \sum_{i=1}^{2} H_i(\tau_B, \theta_i)$. Since convexity/concavity is preserved under sums, it is obvious that H_{sm} is also a concave function. Thus, $C^e(\tau_B)$, is a concave function. Theorem 5.2.1 is then proved.

Appendix K

Proof of Proposition 5.2.1

First, the Lagrangian of (PR:5.1) is

$$\mathcal{L} = -\frac{1}{T\theta_1} \log \left(\mathbb{E} \left\{ e^{-\theta_1 \mathcal{R}_1} \right\} \right) + \lambda(\tau_B(1-\tau_B)). \tag{K.1}$$

Since the problem is convex, KKT conditions are necessary and sufficient for optimality, and they are given as

$$\frac{\partial \mathcal{L}}{\partial \tau_B} = 0 \tag{K.2a}$$

$$\lambda^*(\tau_B^* - {\tau_B^*}^2) = 0. \tag{K.2b}$$

In regard to the complementary slackness condition given in (K.2b), we have $\lambda^* \neq 0$ provided $\tau^* = 0$ or $\tau^* = 1$. However, in both cases it is not possible to transfer a single bit of information. Hence, the optimal solution lies $0 < \tau_B^* < 1$, and this implies $\lambda^* = 0$. Thus, we have

$$\frac{e^{-\theta_1 \mathcal{R}_1}}{T\mathbb{E}\{e^{-\theta_1 \mathcal{R}_1}\}} \frac{\partial \mathcal{R}_1}{\partial \tau_B} = 0 \tag{K.3}$$

which leads to

$$\ln\left(1+\frac{a_1\tau_B}{1-\tau_B}\right)-\frac{a_1}{1-\tau_B+a_1\tau_B}=0. \tag{K.4}$$

After several manipulations, we get

$$e^{\ln(\frac{\omega}{e})}\ln\left(\frac{\omega}{e}\right)=\frac{A}{e} \tag{K.5}$$

where $A=a_1-1$ and $\omega=1+\frac{a_1\tau_B}{1-\tau_B}$. The above equation has the form of $Xe^X=Y$ whose solution is given by the Lambert function, i.e., $X=\mathcal{W}(Y)$ for $Y\geq-\frac{1}{e}$. Thus, the solution to (K.5) can be analytically expressed as

$$z^*=\begin{cases} e^{\mathcal{W}\left(\frac{A}{e}\right)+1}, & A\geq -1 \quad \text{(K.6a)} \\ e^{\mathcal{W}_{-1}\left(\frac{A}{e}\right)+1} & -1\leq A\leq 0. \quad \text{(K.6b)} \end{cases}$$

Hence, the optimal harvesting time interval during k^{th} fading state is determined by

$$\tau_B^*=\frac{z^*-1}{z^*-1+a_1}. \tag{K.7}$$

Accordingly, τ_B^* has two mathematical solutions when $-1\leq\Gamma\leq 0$, but only one of them is the solution as will be noted later. Using the fact that τ_B is neither negative nor zero, i.e., $\tau_B>0$, we have

$$z^*>1 \tag{K.8}$$

Substituting (K.6a) and (K.6b) into (K.8), it results

$$\mathcal{W}\left(\frac{A}{e}\right)>-1 \tag{K.9a}$$

$$\mathcal{W}_{-1}\left(\frac{A}{e}\right)>-1 \tag{K.9b}$$

Nevertheless, (K.9a) cannot be satisfied with strict inequality as $\mathcal{W}_{-1}(A/e) < -1$ for $-1 < A < 0$, whereas (K.9b) is always feasible based on its definition. Therefore, the solution becomes

$$z^* = e^{\mathcal{W}(\frac{A}{e})+1}. \tag{K.10}$$

The harvesting interval is independent of the exponential decay component, and this completes the proof.

Appendix L

Proof of Proposition 5.2.2

Knowing that service rates of wireless-powered users are concave function of operating intervals for TDMA scheme as stated in Section II, we claim that each user effective capacity, and the total throughput, preserves concavity for the same argument given in the proof of Theorem 5.2.1.

Appendix M

Proof of Lemma 6.1.1

Assuming that $f(x)$ and $g(y)$ are convex function, their sum $h(x,y) = f(x) + g(y)$ will be convex if

$$h(\lambda x_1 + (1-\lambda)x_2, \lambda y_1 + (1-\lambda)y_2) \leq \lambda h(x_1, y_1) + (1-\lambda)h(x_2, y_2). \tag{M.1}$$

In order to compare, let us simplify the LHS and RHS as follow:

$$h(\lambda x_1 + (1-\lambda)x_2, \lambda y_1 + (1-\lambda)y_2) = f(\lambda x_1 + (1-\lambda)x_2) + g(\lambda y_1 + (1-\lambda)y_2) \tag{M.2}$$

$$\lambda h(x_1, y_1) + (1-\lambda)h(x_2, y_2) = \lambda f(x_1) + (1-\lambda)f(x_2) + \lambda g(y_1) + (1-\lambda)g(y_2) \tag{M.3}$$

which leads to

$$\begin{gathered} f(\lambda x_1 + (1-\lambda)x_2) + g(\lambda y_1 + (1-\lambda)y_2) \leq \lambda f(x_1) + (1-\lambda)f(x_2) + \lambda g(y_1) + (1-\lambda)g(y_2) \\ f_\Delta + g_\Delta \leq 0 \end{gathered} \tag{M.4}$$

where $f_\Delta = f(\lambda x_1 + (1-\lambda)x_2) - \lambda f(x_1) + (1-\lambda)f(x_2)$ and $g_\Delta = g(\lambda y_1 + (1-\lambda)y_2) - \lambda g(y_1) + (1-\lambda)g(y_2)$. Based on the fact that $f(x)$ and $g(y)$ are convex, we claim that $f_\Delta \leq 0$ and $g_\Delta \leq 0$. Therefore, $f_\Delta + g_\Delta \leq 0$ which guarantees that $g(x,y)$ is convex.

Appendix N

Proof of Proposition 6.1.1

First of all, it is obvious that $f(\boldsymbol{\sigma}^2)$ is an affine function of σ_i^2, and hence it is convex/concave. Then, let $g(\boldsymbol{\Phi}) = \sum_{i=1}^{N} h_i(\Phi_i)$ where $h_i = z_i\Phi_i^2 + \alpha_i\phi_i + C_i$ and $C_i = \frac{C}{N}$. Here also, we can see that h_i is a quadratic function, and hence it is convex since $z_i > 0$. According to Lemma 6.1.1, $g(\boldsymbol{\Phi})$ is also a convex function of $\Phi_1, \Phi_2, \cdots, \Phi_N$. Therefore, again Lemma 6.1.1 guarantees that the harvested energy function $\mathcal{E}_{hv}$ is also jointly convex since both $f(\boldsymbol{\sigma}^2)$ and $g(\boldsymbol{\Phi})$ are convex.

Appendix O

Proof of Proposition 6.3.1

First, let us express $\eta_{EE} = \frac{q(\cdot)}{p(\cdot)}$. According to Proposition 2.9 stated in [93], η_{EE} is a pseudo-concave provided that $q(\cdot)$ and $p(\cdot)$ are concave and convex, respectively. In addition, both should be differentiable, and non-negative. In this case, it is obvious that $q(\sigma^2) = \log_2\left(1 + r\sigma^2\right)$ is a concave function as $\frac{\partial^2 q(\cdot)}{\partial(\sigma^2)^2} \leq 0$. Meanwhile, the denominator can be equivalently expressed as $p(\sigma^2, \phi) = P_k + \sigma^2 + \phi^2$ where $P_k = P_c + P_A - \chi$ is a constant for a given harvested energy demand. In order to check convexity, we determine the Hessian matrix

$$M = \begin{bmatrix} M_{11} & M_{12} \\ M_{21} & M_{22} \end{bmatrix}.$$

for which we have

$$M^T \nabla^2 p(\cdot) M = 2M_{22}^2 \geq 0 \tag{O.1}$$

This implies $p(\cdot)$ is a convex function. Hence, η_{EE} is a pseudo-concave function.

Appendix P

Proof of Corollary 6.3.1

Substituting $\gamma = 0$ and $\phi = 0$ into (6.17), we have

$$\frac{\frac{h_d}{\ln(2)}}{(1+h_d\sigma^2)(K+\sigma^2)} - \frac{\log_2(1+h_d\sigma^2)}{(K+\sigma^2)^2} + \lambda = 0. \tag{P.1}$$

Based on the slackness conditions given in (6.16b), we know that $\lambda \neq 0$ only when $\sigma^2 = P^{pk}$. Otherwise, $\lambda = 0$ and (P.1) is simplified as

$$\begin{aligned} h_d(K+\sigma^2) &= (1+h_d\sigma^2)\ln(1+h_d\sigma^2) \\ \Omega &= z\ln(z) - z \end{aligned} \tag{P.2}$$

where $\Omega = h_d K - 1$ and $z = 1 + h_d\sigma^2$. The above equation has the form of $Xe^X = Y$ whose solution is given by the Lambert function, i.e., $X = \mathcal{W}(Y)$ for $Y \geq -\frac{1}{e}$. After several steps, the solution becomes

$$z^* = e^{\mathcal{W}\left(\frac{\Omega}{e}\right)+1}. \tag{P.3}$$

Therefore,

$$\sigma^2 = \frac{z^* - 1}{h_d}. \tag{P.4}$$

Appendix Q

Proof of Proposition 7.2.1

When the interference signals from energy harvesting UEs are assumed to be insignificant compared with the thermal noise, the signal-to-noise (SNR) coverage probability becomes

$$\Pr_{c} = \int_0^\infty e^{-l\mathcal{G}(\tau_B)} f_r(r) dr \tag{Q.1}$$

where $\mathcal{G}(\tau_B) = \frac{1-\tau_B}{\tau_B}$ and $l = \frac{\gamma_T \mu \sigma^2 r^\alpha}{a_0}$. Applying the first order derivative to $\mathcal{G}(\tau_B)$, we get $-\frac{1}{\tau_B^2}$, and this shows that $\mathcal{G}$ is a decreasing function of $\tau_B \in [0, 1]$. Since exponential functions are monotonic, we immediately observe that $e^{-l\mathcal{G}}$ is an increasing function. Furthermore, noting that $e^{-l\mathcal{G}}$ is monotonically increasing function and integration preserves monotonicity for nonnegative measurable functions [99], we have, $\Pr_c$ is an increasing function of τ_B.

Appendix R

Proof of Proposition 8.2.1

The expression given in (8.13) can be re-written as

$$\mathcal{R}_i(\tau_0) = (1-\tau_0)\log_2\left(1+\frac{\alpha_i\tau_0}{1+\omega_i\tau_0}\right) \tag{R.1}$$

where $\omega_i = -1+\sum_{j=i+1}^{N}\alpha_j$. Hence, applying the second order derivative criteria to (R.1), we have

$$\frac{\partial^2 R_i(\tau_0)}{\partial\tau_0^2} = -\alpha_i\left[\frac{\alpha_i((2\omega_i+1)\tau_0+1)+2(\omega_i+1)(\omega_i\tau_0+1)}{(\omega_i\tau_0)^2(\alpha_i\tau_0+\omega_i\tau_0+1)^2}\right] \tag{R.2}$$

Knowing $\omega_i \geq -1$ and $0<\tau_0<1$, it is obvious that $(2\omega_i+1)\tau_0 \leq 1$ if $\omega_i<0$, otherwise $(2\omega_i+1)\tau_0>1$. This guarantees $\frac{\partial^2 R_i(\tau_0)}{\partial\tau_0^2}<0$ for any $\alpha_i\neq 0$, and hence R_i is a concave function.

Appendix S

Proof of Proposition 8.2.1

Proof: Since the system EE in (8.15) is a fractional function, it will satisfy pseudo-concavity according to Proposition 2.9 stated in [93] if the numerator is concave and denominator is convex. In this case, the denominator is an affine function, and hence we only need to show that the throughput, i.e., the numerator, is concave with respect to τ_0. Using the fact that concavity is preserved under summation and $R_i(\tau_0)$ is a concave function of τ_0 based on Lemma 1, we conclude that $\mathcal{R}_{sum}$, i.e., the throughput, is concave as well.

Appendix T

Proof of Proposition 8.2.2

For the case of two users, we have τ_1 and τ_2, and hence we show that the throughput in each interval is jointly concave with respect to the opeating intervals:

(i) During τ_1: In this case, only UE 1 transmits information uplink to the access point, i.e.,

$$R^1_{sum} = \tau_1 \log_2 \left(a_1 + \frac{b_1}{\tau_1 + \tau_2} \right). \tag{T.1}$$

Let $\mathbf{F}^i$ denote the Hessian matrix of R^i_{sum} with respect to τ_1 and τ_2. Then, applying the second-order derivatives, we get

$$\begin{aligned} F^1_{11} &= \frac{\partial^2 R^1_{sum}}{\partial \tau_1^2} = -\frac{b_1(2a_1\tau_2(\tau_2+\tau_1)) + b_1(2\tau_2+\tau_1)}{(\tau_1+\tau_2)^2(a_1(\tau_1+\tau_2)+b_1)^2} \\ F^1_{22} &= \frac{\partial^2 R^1_{sum}}{\partial \tau_2^2} = \frac{b_1\tau_1(2a_1(\tau_2+\tau_1)) + b_1}{(\tau_1+\tau_2)^2(a_1(\tau_1+\tau_2)+b_1)^2} \\ F^1_{12} &= \frac{\partial^2 R^1_{sum}}{\partial \tau_1 \partial \tau_2} = -\frac{b_1(a_1(\tau_2-\tau_1)(\tau_2+\tau_1) + b_1\tau_2)}{(\tau_1+\tau_2)^2(a_1(\tau_1+\tau_2)+b_1)^2}. \end{aligned} \tag{T.2}$$

Since $F^1_{11}F^1_{22} - (F^1_{12})^2 \leq 0$, the Hessian $\mathbf{F}$ is a negative semi-definite matrix. Based on Theorem 21.5 given in [97], R^1_{sum} is a jointly concave function of τ_1 and τ_2.

(ii) During τ_2: Here, both UE 1 and UE 2 are transmitting, and the corresponding achievable

sum-rate capacity is given as

$$R_{sum}^2 = \tau_2 \log_2 \left(a_2 + \frac{b_1}{\tau_1 + \tau_2} + \frac{b_2}{\tau_2} \right), \tag{T.3}$$

and applying the second order derivative, we get

$$\begin{aligned} F_{11}^2 &= \frac{\partial^2 R_{sum}^2}{\partial \tau_1^2} = \frac{2b_1(\tau_1+\tau_2)(a_2+\frac{b_2}{\tau_2}) + b_1^2}{(\tau_1+\tau_2)^4(a_2+\frac{b_1}{\tau_1+\tau_2}+\frac{b_2}{\tau_2})^2} \\ F_{22}^2 &= \frac{\partial^2 R_{sum}^2}{\partial \tau_2^2} = -\frac{\frac{2b_1 y}{(\tau_1+\tau_2)^3}}{a_2+\frac{b_1}{\tau_1+\tau_2}+\frac{b_2}{\tau_2}} - \frac{\tau_1(-\frac{b_2}{\tau_2^2}-\frac{b_1}{(\tau_1+\tau_2)^2})^2}{(a_2+\frac{b_1}{\tau_1+\tau_2}+\frac{b_2}{\tau_2})^2} \\ F_{12}^2 &= \frac{\partial^2 R_{sum}^2}{\partial \tau_1 \partial \tau_2} = -\frac{b_1\tau_2(a_2\tau_2(\tau_1-\tau_2)+\tau_1(2b_2+b_1\frac{\tau_2}{\tau_1+\tau_2}))}{(\tau_1+\tau_2)^3(\tau_2(a_2+\frac{b_1}{\tau_1+\tau_2})+b_2)^2}. \end{aligned} \tag{T.4}$$

It is obvious that $F_{11}^2 F_{22}^2 - (F_{12}^2)^2 \leq 0$ and hence R_{sum}^2 is also a jointly concave function of the operating intervals using a similar argument as stated above.

Appendix U

Proof of Proposition 8.3.1

First, let $h_i(\tau_B) = (1-\tau_B)\log_2\left(1+\frac{a_i\tau_B}{1+\left(a_*-1\right)\tau_B}\right)$ and $H_i(\tau_B) = -\frac{1}{\theta_i}\log\left(\mathbb{E}\{e^{-\theta_i h_i(\tau_B)}\}\right)$ where θ_i's are assumed to be known. Applying the second-order derivative criterion to $h_i(\tau_B)$, we get

$$\begin{aligned}
\ln(2)\frac{\partial h(\tau_B)}{\partial \tau_B} &= -\log\left(1+\frac{a_i\tau_B}{(1-\tau_B)+\tau_B a_*}\right) + (1-\tau_B)\frac{a_i}{\Big(1+\tau_B(a_i+a_*-1)\Big)\Big(1-\tau_B+a_*\tau_B\Big)} \\
\ln(2)\frac{\partial^2 h(\tau_B)}{\partial \tau_B^2} &= -\left[\frac{\Big(1-\tau_B\Big)\Big(2a_ia_*+a_i^2\Big)+2a_ia_*\tau_B\Big(a_*+a_i\Big)}{\Big(1-\tau_B+a_*\tau_B\Big)^2\Big(1-\tau_B+a_i\tau_B+a_*\tau_B\Big)^2}\right]
\end{aligned} \tag{U.1}$$

, and it can be inferred from (U.1) that $\frac{\partial^2 h_i(\tau_B)}{\partial \tau_B^2} < 0$ for all $\tau_B \in (0,1)$, and hence $h_i(\tau_B)$ is concave or $-h_i(\tau_B)$ is convex in the domain set. This implies that $e^{-h(\tau_B)}$ is log-convex, and $\mathbb{E}\{e^{-h(\tau_B)}\}$ is log-convex as well, as log-convexity is preserved under sums. Noting that $\log(g(\cdot))$ is convex for log-convex $g(\cdot)$ [98], clearly $H(\tau_B)$ is a concave function of τ_B for $0 < \tau_B < 1$. Meanwhile, the sum effective capacity can be re-written as

$$C^e(\tau_B) = \frac{H_{sm}(\tau_B)}{T} \tag{U.2}$$

where $H_{sm} = \sum_{i=1}^{N} H_i(\tau_B, \theta_i)$. Since convexity/concavity is preserved under sums, it is obvious that H_{sm} is also a concave function. Thus, $C^e(\tau_B)$, is a concave function, completing the proof.

Bibliography

[1] H. Dinis, I. Comiais, P. M. Mendes, " A multiantenna approach to maximize wireless power transfered to implantable devices," *Inter. Applied Computational Electromagnetics Society Symposium - (ACES)*, Italy, Mar. 26-30, 2017.

[2] K. Agarwal, R. Jegadeesan, Y.X Guo, and N. V. Thakor, "Wireless power transfer strategies for implantable bioelectronics: Methodological review," *IEEE Reviews in Biomedical Engineering*, 2017.

[3] Z. chen, H. Sun, and W. Geyi, "Maximum wireless power tranfer to the implantable device in the radiative near-field," *IEEE Antennas and Wireless Propagation Letts.*, 2017.

[4] O. H. Murphy, A. Borghi, M. R. Bahmanyar, C. N. McLeod, M. Navaratnarajah, M. Yacoub, and C. Toumazou, "RF communication with implantable wireless device: effects of beating heart on performance of miniature antenna," *Healthcare Technology Letts.*, pp. 51-55, vol.1, no. 2, 2014.

[5] Y. Jang, J. K. Han, S. Y. Cho, G. W Moon, J. M. Kim, and H. Sohn, "Wireless power and data transfer system for smart bridge sensors," *Applied Power Electronics Conference and Exposition (APEC)*, Long Beach, CA, Mar. 20-24, 2016.

[6] L. R. Varshney, "Transporting information and energy simultaneously," *IEEE Int. Symp. Info. Theory*, pp 1612-1616, Jul. 2008.

[7] P. Grover and A. Sahai, "Shannon meets Tesla: Wireless information and power transfer," *IEEE Int. Symp. Info. Theory*, pp. 2363-2367, Jun. 2010.

[8] H. Ju, R. Zhang, "Optimal Resource Allocation in Full-duplex wireless-powered communication network," *IEEE Trans. Commun.*, vol. 62 no. 10, pp. 3528-3540, Oct. 2014.

[9] A. M. Fouladgar, O. Simeone, "On the transfer of information and energy in multi-user systems," *IEEE Commun. Lett.* vol. 16 no.11, Nov. 2012.

[10] J. Park, B. Clerckx, "Joint wireless information and energy transfer in a two-user MIMO interference channel," *IEEE Trans. Wireless Commun.*, vol. 12 no. 8, pp. 4210-4221, Aug. 2013.

[11] X. Zhou, R. Zhang, and C. K. Ho, "Wireless information and power transfer: architecture design and rate-energy tradeoff," *IEEE Trans. Commun.*, vol. 61. no. 11, pp. 4754-4767, Nov. 2013.

[12] L. Liu, R. Zhang, K. C. Chua, "Wireless information and power transfer: a dynamic power splitting approach," *IEEE Trans. Commun.*, vol. 61, pp. 3990-4001, September 2013.

[13] K. Hang and E. G. Larsson, "Simultaneous information and power transfer for broadband wireless systems," *IEEE Trans. Signal Process.*, vol. 61 No. 23, pp. 5972-5986, Dec. 2013.

[14] R. Zhang, C. K. Ho, "MIMO boadcasting for simultaneous wireless information and power transfer," *IEEE Trans. Wireless Commun.*, vol. 12 no. 5, pp. 1989-2001, May 2013.

[15] J. Xu, L. Liu, and R. Zhang, "Multiuser MISO beamforming for simultaneous wireless information and power transfer," *IEEE Trans. Signal Process.*, vol. 62, no. 18, pp. 4798-4810, Sep. 12, 2014.

[16] F. Yuan, S. Jin, J. Zhao, and H.b. Zhu, "Wireless information and power transfer design for energy cooperation distributed antenna systems," to appear on *IEEE Access*, 2017.

[17] G. Saleh, C. E. Koksal, and N. B. Shroff, "Optimal SINR based resource allocation for simultaneous energy and infomraiton transfer," *Proc. of IEEE GlobalSIP*, pp. 391-394, 2013.

[18] Z. Ding, S. M. Perlaza, I. Esnaola, and H. C. Poor, "Simultaneous information and power transfer in wireless cooperative networks," *Proc. of* 8^{th} *CHINACOM*, pp. 252-255, 2013.

[19] Z. Fang, X. Yuan, and X. Wang, "Distributed enregy beamforming and information transfer: a case study for multiway relay channels," *Proc. of IEEE ICCC*, pp. 670-675, June 2014.

[20] W. Lu, Y. Gong, J. Wu, H. Peng, and J. Hua, "Simultaneous wireless information and power transfer based on joint subcarrier and power allocation in OFDMA systems," *IEEE Acess*, pp. 2763-2770, vol. 5, Feb. 2017.

[21] A. M. Fouladgar, O. Simeone, "On the transfer of information and energy in multi-user systems," *IEEE Commun. Lett.* vol. 16 no.11, Nov. 2012.

[22] X. Lu, W. Xu, S. Li, Z. Liu, and J. Lin, "Simultaneous wireless information and power transfer for cognitive two-way relaying networks," *Proc. of IEEE PIMRC Symp.*, pp. 748-752, Sep. 2014.

[23] J. Shin, and D. Kim, "Simultaneous wireless information and power transfer for cognitive radio systems with average energy harvesting constraint," *Proc. of IEEE CCNC Conf.*, pp. 156-157, Jan. 2015.

[24] X. Lu, W. Xu, S. Li, J. Lin, and Z. He, "Simultaneous information and power transfer for relay-assisted cognitive radio networks," *Proc. of IEEE ICC*, pp. 331-336, June 2014.

[25] I. Krikidis, "Simultaneous information and energy transfer in large-scale networks with/without relaying," *IEEE Trans. Commun.*, vol. 62, no. 3, pp. 900-912, Mar. 2014.

[26] D. S. Michalopoulos, H. A. Suraweera, R. Schober, "Relay selection for simultaneous information transmission and wireless energy transfer: a tradeoff perspective," *IEEE Jou. Sel. Area Commun.*, vol. 33, no. 8, pp. 1578-1594, Aug. 2015.

[27] C.S. Chang and T. Zajic, "Effective bandwidths of departure processes from queues with time varying capacities, *Proc. IEEE Infocom.*, pp. 1001-1009, 1995.

[28] D. Wu, and R. Negi, "Effective capacity: a wireless link model for support of quality of service," *IEEE Trans. Wirless Commun.*, vol. 2, no. 4, pp. 630-643, July 2003.

[29] "Quality-of-Servie driven power and rate adaptation over wireless links," *IEEE Trans. Wireless Commun.*, vol. 6, no. 8, pp. 3058-3068, Aug. 2007.

[30] D. Qiao, M. C. Gursoy, and S. Velipasalar, "Effective capacity of two-hop wireless communication systems," *IEEE Trans. Info. Theory*, vol. 59, no. 2, pp. 873-885, Feb. 2013.

[31] M. Ozmen, and M. C. Gursoy, "Wireless throughput and energy efficiency with random arrivals and statistical queuing constraints," *IEEE Trans. Info. Theory*, vol. 62, no. 3, pp. 1375-1395, Mar. 2016.

[32] D. Qiao, M. C. Gursoy, S. Velipasalar, "Transmission strategies in multiple-access fading channels with statistical QoS constraints," *IEEE Trans. Inform. Theory* vol. 58, no. 3, March 2012.

[33] M. C. Gursoy, D. Qiao, and S. Velipasalar, "Analysis of energy efficiency in fading channels under QoS constraints", *IEEE Trans. Wireless Commun.*, vol. 8, no. 8, pp.4252-4263, Aug. 2009.

[34] M. S. Obaidat, A. Anpalagan, I. Woungang, *Handbook of Green Information and Communication Systems*, Waltham, USA:, Elsevier Academic Press, 2013.

[35] J. Joung, and S. Sun, "EMA: Energy-efficiency-aware multiple access," *IEEE Commun. Lett.*, vol. 18, no. 6, pp. 1071-1074, June 2014.

[36] G. Yu, and Y. Jiang, "Energy-efficiency region for multiple access channels," *IEEE Electronic Lett.*, vol. 50, no. 13, pp.959-961, June 2014.

[37] C. Zhou, J. Li, and L. J. Cimini, "Energy efficiency region for Gaussian multiple access channels under different power consumption models," *Proc. of CISS*, Mar. 18-20, 2015.

[38] Y. Cui, E. M. Yeh, and S. V. Hanly, "Energy-efficiency data transmission over multiple-access channels with QoS constraints," *Proc. of IEEE ISIT*, pp. 441-445, July 2014.

[39] M. M. Butt, E. A. Jorswieck, and B. Ottersten, "Maximizing energy efficiency in multiple access channels by exploiting packet dropping and transmitter buffering," *IEEE Trans. Wireless. Commun.*, vol. 14, no. 8, pp. 4129-4141, Aug. 2015.

[40] S. Mishra, and C. S. R. Murthy, "Increasing energy efciency via transmit power spreading in dense femto cell networks," *IEEE Systems Journal*, 2016. DOI:10.1109/JSYST.2016.2573845

[41] W. Cheng, X. Zhang, H. Zhang "Statistical-QoS driven energy-efficiency optimization over green 5G mobile wireless networks," *IEEE Jou. Sel. Area Commun.*, vol. 34, no. 12, pp. 3092-3107, Dec. 2016.

[42] D. W. Kwan Ng, E. S. Lo, and R. Schober, "Wireless information and power transfer: energy efficiency optimization in OFDMA systems," *IEEE Trans. Wireless Commun.*, vol. 12, no. 12, Dec. 2013.

[43] C. Zhang, H. Zhao, W. Li, K. Zheng, J. Yang, "Energy efficiency optimization of simultaneous wireless information and power transfer system with power splitting receiver,"

IEEE 25th Annual Int. Sympo. Personal, Indoor, and Mobile Commun., pp. 2135-2139, Sep. 2014.

[44] C. Xiong L. Lu, G.Y. Li, "Energy efficiency tradeoff in downlink and uplink TDD OFDMA with simultaneous wireless information and power transfer," *Proc. IEEE ICC*, pp. 5383-5388, Jun. 2014.

[45] Q. Sun, L. Li, and J. Mao,"Simultaneous information and power transfer scheme for energy-efficient MIMO Systems," *IEEE Commun. Lettr.*, vol. 18, no. 4, pp 600-603, April 2014.

[46] S. Leng, D. W. Kwan Ng, N. Zlatanov, and R. Schober, "Multi-objective beamforming for energy-efficient SWIPT systems," http://arxiv.org/pdf/1509.05959v1.pdf, Sep. 20, 2015.

[47] S. Bi, C. Ho, and R. Zhang, "Wireless powered communication: opportunities and challenges," *IEEE Commun. Mag.*, vol. 53, no. 4, pp. 117-125, Apr. 2015.

[48] S. Bi, C. K. Ho, and R. Zhang, "Recent advances in joint wireless energy and information transfer," *Proc. IEEE Info. Theory Workshop*, pp. 341-345, 2014.

[49] H. Ju, R. Zhang, "Throughput maximization in wireless powered communication networks," *IEEE Trans. on Wireless Commun.*, vol. 13, no. 1, pp. 418-428, Jan, 2014.

[50] F. Zhao, L. Wei, and H. Chen, "Optimal time allocation for wireless information and power transfer in wireless powered communication systems," DOI: 10.1109/TVT.2015.2416272

[51] Y. L. Che, L. Duan, and R. Zhang, "Spatial throughput maximization of wireless powered communication networks," *IEEE J. Sel. Areas Commun.*, vol. 33, no. 8, pp. 1534-1548, Aug. 2015.

[52] Q. Sun, G. Zhu, C. Shen, X. Li, and Z. Zhong, "Joint beamforming design and time allocation for wireless powered communication networks," *IEEE Commun. Letts.*, vol. 18, no. 10, pp. 1783-1786, Oct. 2014.

[53] W. Huang, H. Chen, Y. Li, and B. Vucetic, "On the performance of multi-antenna wireless-powered communications with energy beamforming," *IEEE Trans. Vehic. Tech.*, vol. PP. no. 99, 2015.

[54] D. Hwang, D. I. Kim, and T. J. Lee, "Throughput maximization for multiuser MIMO wireless powered communication networks," DOI: 10.1109/TVT.2015.2453206.

[55] L. Liu, R. Zhang, and K. C.Chua, "Multi-antenna wireless powered communication with energy beamforming," *IEEE Trans. Commun.*, vol. 62, no. 12, pp. 4349-4361, Dec. 2014.

[56] X. Kang, C. K. Ho, and S. Sun, "Full-Duplex Wireless-Powered communication Network With energy causality," *IEEE Trans. Wireless Commun.*, vo. 14, no. 10, pp. 5539-5551, Dec. Oct. 2015.

[57] H. Ju, and R. Zhang, "Optimal resource allocation in full-duplex wireless-powered communication network," *IEEE Trans. Commun.*, vol. 62, no. 10, pp. 3528-3540, Oct. 2014.

[58] Y. Zeng, and R. Zhang, "Full-duplex wireless-powered relay with self-energy recycling," *IEEE Wireless Commun. Letts.*, vol. 4, no. 2, pp. 201-204, Apr. 2015.

[59] Q. Wu, M. Tao, D. W. Ng, W. Chen, and R. Schober, "Energy-efficient resource allocation for wireless powered communication networks," *IEEE Trans. Wireless Commun.*, vol. 15, no. 3, pp. 2312-2327, Mar. 2016.

[60] M. D. Renzo, and W. Lu, "System-level analysis and optimization of cellular networks cellular networks with simultaneous wireless information and power transfer: Stochastic geometry modeling," *IEEE Trans. Veh. Tech.*, vol. 66, no. 3, pp. 2251-2275, Mar. 2017.

[61] T. L. Thanh, M. D. Renzo, and J. P. Coon, "MIMO cellular networks with simultaneous wireless information and power transfer," *Proc. of Signal Processing Advances in Wireless Communications (SPAWC)*, July 2016.

[62] W. Lu, M. D. Renzo, and T. Q. Duong, "On stochastic geometry analysis and optimization of wireless-powered cellular networks," *Proc. IEEE Global Commun. Conference (GlobeCom)*, 2015.

[63] T. T. Lam, M. D. Renzo, J. P. Coon, "System-level analysis of receiver diversity in SWIPT-enabled cellular networks," *Jour. Commun. and Networks*, vol. 18, no. 6, pp. 926-937, Dec. 2016.

[64] S. Akbar, Y. Deng, A. Nallanathan, M. Elkashlan, and A. H. Aghvami, "Simultaneous wireless information and power transfer in k-tier heterogeneous cellular networks," *IEEE Trans. Wireless Commun.*, vol. 15, no. 8, pp. 5804-5818, Aug. 2016.

[65] Y. Deng, L. Wang, M. Elkashlan, M. D. Renzo, and J. Yuan, "Modeling and analysis of wireless power transfer in heterogeneous cellular networks," *IEEE Trans. Commun.*, vol. 64, no. 12, pp.5290-5303, Dec. 2016.

[66] S. Lohani, R. A. Loodaricheh, E. Hossain, and V. K. Bhargava, "On multiuser resource allocation in relay-based wireless-powered uplink cellular network," *IEEE Trans. Wireless Commun.*, vol. 15, no. 3, pp. 1851-1865, Mar. 2016.

[67] A. H. Sakr, E. Hossain, "Analysis of K-tier uplink cellular networks with ambient RF energy harvesting," *IEEE Jour. Sel. Areas in Commun.*, vol. 33, no. 10, pp. 2226-2238, Oct. 2015.

[68] Y. Liao, J. Zhang, Y. Zhang, M. Chen, Q. Li, and T. Han, "Performance analysis of K-tier cellular networks with time-switching energy harvesting," *Proc. of IEEE PIMRC Workshop*, pp. 1-5, 2016.

[69] M. Sheng, L. Wang, X. Wang, Y. Zhang, C. Xu, and J. Li, "Energy-efficient beamforming in MISO heterogeneous cellular networks with MIMO cellular networks with wireless Information and Power Transfer," *IEEE Jour. Sel. Areas Commun.*, pp. 954-968, vol. 34, no. 4, Apr. 2016.

[70] E. Turgut, and M. C. Gursoy,"Energy efficiency in relay-assisted mmWave cellular networks," *Proc. IEEE* 84^{th} *Vehicular Technology Conf.*, 2016.

[71] O. Georgiou, "Simultaneous wireless information and power transfer in cellular networks with directional antennas," *IEEE Commun. Letts.*, pp. 885-888, vol. 21, no. 4, Apr. 2017.

[72] T. Bai, R. W. Heath, "Coverage and rate analysis for mimimeter-wave cellular networks," *IEEE Trans. on Wireless Commun.*, vol. 14, no. 2, pp. 1100-1114, Feb. 2015.

[73] X. Yu, J. Zhang, M. Haenggi, K. B. Letaief, "Coverage analysis for milimeter wave networks: The impact of directional antenna arrays," *IEEE Jour. Sel. Areas in Commun.*, vol. 35, no. 7, pp. 1498-1512, July 2017.

[74] M. A. Abana, M. Peng, Z. Zhao, L. A. Plawoyin, "Coverage and rate analysis in heterogenous cloud radio access networks with device-to-device communication," *IEEE Acess*, vol. 4, pp. 2357-2370, 2016.

[75] M. O. Al-Kadri, Y, Deng, A. Aijaz, A. Nallanathan, "Full-duplex small cells for next generation heterogenous cellular networks: A case study of outage and rate coverage analysis," *IEEE Access*, vol. 5, pp. 8025-8038, 2017.

[76] T. A. Khan, A. Alkhateeb, and R. W. Heath, "Milimeter wave energy harvesting," *IEEE Trans. on Wireless Commun.*, vol. 15, no. 9, pp. 6048-6062, Sep. 2016.

[77] L. Wang, M. Elkashlan, R. W. Health, M. R. Renzo, and K. Wong, "Milimeter wave power transfer and information transmission," *Proc. Global Commun. Conf. (GlobeCom*, Dec. 2015.

[78] L.T. Tu and M. D. Renzo, " Analysis of millimeter wave cellular networks with simultaneous wireless information and power transfer," *Proc. of Intern. Conf. on Recent Advances in Signal Processing, Telecommunicaitons, ad Computing (SigTelCom)*, pp. 39-43, 2017.

[79] L. Dai, B. Wang, Y. Yuan, S. Han, C.L I, and Z. Wang, "Non-orthogonal multiple access for 5G: Solutions, challenges, opportunities, and future research trends," *IEEE Commun. Mag.*, vol. 53, no. 9, pp. 74-91, Sep. 2015.

[80] S. R. Islam, N. Avazov, O. A. Dobre, and K.S. Kwak, "Power-domain non-orthogonal multiple access (NOMA) in 5G systems: potentials and challenges," https://arxiv.org/abs/1609.06261, DOI: 10.1109/COMST.2016.2621116,

[81] S. N. Datta, and S. Kalyanasundaram, "Optimal power allocation and user selection in non-orthogonal multiple access systems," *Proc. of IEEE WCNC*, Apr. 2016.

[82] L. Lei, D. Yuan, C. K. Ho, and S. Sun, "Power and channel allocation for non-orthogonal multiple access in 5G systems: tractability and computation," *IEEE Trans. Commun.*, pp. 8580 - 8594, vol. 15, no. 12, Dec. 2016.

[83] W. Han, Y. Zhang, X. Wang, J. Li, M. Sheng, and X. Ma, "Orthogonal power division multiple access: A green communicaiton prespective," *IEEE Jour. Sel. Area Commun.*, vol. 34, no. 12, pp. 3828-3842, Dec. 2016.

[84] S. Buzzi, C. L. I, T. E. Klein, H. V. Poor, C. Yang, and A. Zappone, "Survey of energy-efficient techniques for 5G networks and challenges ahead," *IEEE J. Sel. Areas Commun.*, vol. 34, no. 4, pp. 697-709, 2016.

[85] Q. T. Vien, T. A. Le, B. Barn, C. V. Phan, "Optimising energy efficiency of non-orthogonal multiple access for wireless backhaul in heterogenous cloud radio access network," *IET Commun.*, 2016.

[86] H. Q. Tran, P. Q. Truong, C. V. Phan, Q. T. Vien, "On the energy efficiency of NOMA for wireless backhaul in multi-tier heterogenous CRAN," *Proc. of Intern. Conf. Recent Advances in SigTelCom*, 2017.

[87] F. Fang, H. Zhang, J. Cheng, V. C.M. Leung,"Energy-efficient resource allocation for downlink non-orthogonal multiple access network," *IEEE Tran. Commun.*, vol. 64, no. 9, pp. 3722-3732, Sep. 2016.

[88] Q. Sun, S. Han, C.L. I, Z. Pan, "Energy efficeincy optimization for fading MIMO non-orthogonal multiple access system,"*Proc. IEEE ICC*, 2015.

[89] P. D. Diamantoulakis, K. N. Pappi, Z. Ding, and G. K. Karagiannidis, "Wireless powered communications with non-orthogonal multiple access," *IEEE Trans. Wireless Commun.*, pp. 8422 - 8436, vol. 15, no. 12, Dec. 2016.

[90] Y. Yaun, Z. Ding, "The application of non-orthogonal multiple access in wireless powered communication networks," *Proc. IEEE SPAWC*, pp. 1-5, Jul. 2016.

[91] H. Chingoska, Z. Hadzi-Velkov, I. Nikoloska, and N. Zlatanov, "Resource allocation in wireless powered communication networks with non-orthogonal multiple access," *IEEE Wireless Commun. Letts.*, pp. 684 - 687, vo. 5, no. 6, Dec. 2016.

[92] T. C. Cover and J. A. Thomas, *Elements of Information Theory*, 2^{nd} edition, John Wiley and Sons, Inc., 2006.

[93] A. Zappone, and E. Jorswieck, "Energy efficiency in wireless network via fractional programming theory," *Found. Trends® in Commun. Inform. Theory*, vol. 11, no. 3-4, pp. 185-396, 2015.

[94] P. Zabihi, M. F. Sabahi, K. Shahtalebi, "Power allocation game considering QoS and interference for fading multiple access channels," *7^{th} International Sympo. on Telecom. (IST)*, pp.1166-1171, 2014.

[95] Z. Fang, X. Yuan, and X. Wang, "Distributed energy beamforming for simultaneous wireless information and power transfer in the two-way relay channel," *IEEE Sig. Process. Letters*, vol. 22, no.6, pp. 656-660, June 2015.

[96] F. Baccelli, and B. Blaszezyszyn, *Stochastic Geometry and Wireless Networks: Volume 1: Theory*, Now Publishers Inc, 2009, vol 1.

[97] C. P. Simon and L. Blume, *Mathematics for Economists*, W. W. Norton & Company Inc., New York, NY, 1994.

[98] S. Boyd, and L. Vandenberghe, *Convex Optimization*, Cambridge, U.K.:, Cambridge Univ. Press, Mar. 2004.

[99] F. Burk, *Lebesgue Measure and Integration: An Introduction* A Wiley-Interscience Publication John Wiley & Sons, Inc, New York, USA, 1998.

[100] J.G. Proakis, M.Salehi, *Digital Communications*, 5^{th} edition, McGraw-Hill, Inc., 2008.

VITA

TEWODROS AKLILU ZEWDE: He received the B.Sc. degree in Electrical Engineering and M.Sc. degree in Electrical Power Engineering from Bahir Dar University and Addis Ababa University, Ethiopia in 2004 and 2009, respectively. He has been a Ph.D. student at Syracuse University since 2012. He received the Outstanding Teaching Assistant Award from Syracuse University in April, 2017. In addition, He participated in the Future Professorate Program (FPP) which is organized by the Graduate School Program of Syracuse University every year, and he received the Certificate of University Teaching in April 2017. His research interests include wireless communications, wireless information and power transfer, energy-ecient protocols, statistical signal processing, wireless powered communication networks, smart grid communication, distributed generation, and integration of renewable resources.